TEXT FLY WITHIN
THE BOOK ONLY

UNIVERSAL
LIBRARY
OU_160814
UNIVERSAL
LIBRARY

OSMANIA UNIVERSITY LIBRARY

Call No. 523.01 L725 Accession No. 49588

Author Liller, William, ed.

Title Space astrophysics. 1961.

This book should be returned on or before the date last marked below.

SPACE ASTROPHYSICS

The University of Michigan
Institute of Science and Technology Series

ALLEN · *Molecular Control of Cellular Activity*
LILLER · *Space Astrophysics*

SPACE ASTROPHYSICS

Edited by

William Liller

Professor of Astronomy

Harvard University

McGraw-Hill Book Company, Inc.

New York Toronto London

1961

SPACE ASTROPHYSICS

Copyright © 1961 by the McGraw-Hill Book Company, Inc. Printed in the United States of America. All rights reserved. This book, or parts thereof, may not be reproduced in any form without permission of the publishers.
Library of Congress Catalog Card Number 61-8657.

37859

Preface

During the 1959-1960 academic year, the University of Michigan Department of Astronomy, with financial assistance from the University's Institute of Science and Technology, presented a series of lectures on those aspects of astronomy and astrophysics which were either concerned with or could only be studied from outer space. The purpose of these lectures, which have now been gathered together in the following pages, was twofold: first, to bring to Ann Arbor leading space scientists and have them describe to the students and staff the work in which they were currently engaged; and second, to give members of space projects at the University an opportunity to ask questions of these often more experienced researchers.

With the publishing of this volume, these lectures plus two additional ones now become available to students, scientists, and engineers everywhere. Every effort has been made to keep the time required for publication to a minimum; indeed, many of the results are presented here well in advance of their appearance in periodical scientific journals.

At the time the lectures were delivered, Dr. R. R. White was Director of the Institute of Science and Technology, Mr. Joseph A. Diana was his administrative assistant, and Professor Leo Goldberg was Director of the University of Michigan Observatory. To all three go my sincere thanks for their assistance in arranging the lectures and this volume. Above all, as editor I wish to thank each of the contributors for his part in making this volume possible.

William Liller

Contents

Preface v
William Liller

Chapter SECTION I: THE EXPERIMENTS

1. Ultraviolet Spectroscopy of the Sun 1
R. Tousey

2. Solar Ultraviolet Research 17
W. Rense

3. Telemetering Monochromator Measurements of Extreme Ultraviolet Radiation 34
H. E. Hinteregger

4. Telemetering Monochromator Measurements of Extreme Ultraviolet Radiation (continued) 74
H. E. Hinteregger

5. Some Plans for Experiments in Space 96
B. Rossi

6. X-ray and Ultraviolet Radiation Measurements from Rockets 107
H. Friedman

7. Ultraviolet Astronomical Photometry from Rockets 121
A. B. Boggess III

SECTION II: THE THEORY

8. The Solar Corona and Interplanetary Gas 133
S. Chapman

9. The Solar Wind and the Interplanetary Media 150
L. Bierman

10. The Solar Wind 157
E. N. Parker

11. The Moon 171
T. Gold

12. The Electric Universe 179
H. Bondi

SECTION III: THE INSTRUMENTATION

13. Astrostats for Astrophysical Research in Space 185
R. A. Nidey

14. Attitude Control of Artificial Satellites 205
R. B. Kershner and R. R. Newton

15. Choice of Grating Mountings Suitable for a Monochromator in a Space Telescope 228
T. Namioka

Index 269

Section I. The Experiments

1. ULTRAVIOLET SPECTROSCOPY OF THE SUN

R. Tousey
U. S. Naval Research Laboratory

INTRODUCTION

The extreme ultraviolet spectrum of the sun first became accessible to astronomers in 1946, thanks to the availability of captured V-2 rockets. Almost the first attempt to photograph the spectrum was a success. On October 10, 1946, the U. S. Naval Research Laboratory (NRL) obtained spectra (Baum, et al (1946)) showing that as far as 2200 A the spectrum of the sun is similar in nature to the near ultraviolet and visible; a continuum, of intensity decreasing to short wavelengths, with Fraunhofer lines in great abundance. The most striking of the Fraunhofer lines within this region are the pair produced by Mg II at 2802.698, 2795.523 A, corresponding to the H and K lines of ionized calcium.

PENETRATION OF SOLAR RADIATION

These first results were a powerful stimulus to laboratory work on the absorption by atmospheric gases. From the work of G. L. Weissler's group at the University of Southern California, R. W. Ditchburn and associates at the University of Reading, K. Watanabe and co-workers at the Air Force Cambridge Research Center and now at the University of Hawaii, and a number of others, a considerable amount of exact information is available. This field has been reviewed by Weissler (1956), and by Watanabe(1958).

From the laboratory absorption coefficients and available data on the density and composition of the upper atmosphere it is possible to calculate the attenuation of the different spectral radiations as they enter the upper atmosphere. In Fig. 1 and Fig. 2 there are shown plots of the altitude to which 1/e of the incident solar intensity penetrates as a function of wavelength. These calculations must still be regarded as tentative because further work in the laboratory and a more complete knowledge of the profiles of solar emission lines are necessary before the exact penetration of the various emissions can be calculated.

Between 3000 and 2000 A incoming solar radiation is attenuated by

PENETRATION TO 1/e OF SOLAR
ULTRAVIOLET AND PHOTOCHEMICAL EFFECTS

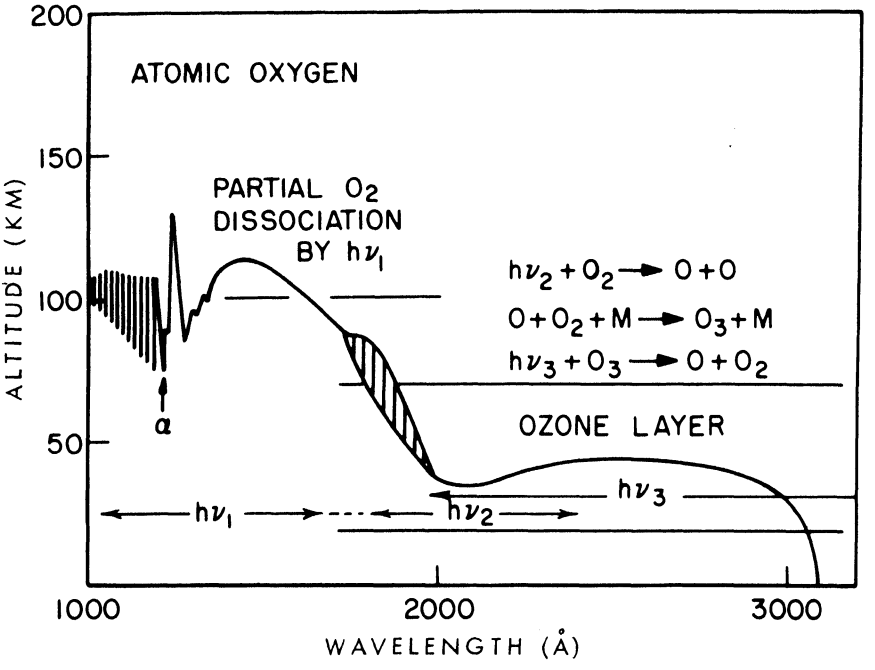


Fig. 1. The depth to which 1/e of the incident solar intensity penetrates, for 1000 to 3000 A.

the ozone layer, centered at approximately 25 km above the earth's surface, and extending as high as 70 km (Johnson, et al (1952)). The ozone layer is governed principally by the three reactions noted in Fig. 1; molecular oxygen is dissociated by the absorption of radiation from about 2400 A to shorter wavelengths; the atomic oxygen so produced collides with an oxygen molecule and a second body to form ozone, which, in turn, is dissociated photochemically by absorption of radiation in the wavelength range 2000 to 3000 A.

Below 2000 A, the absorption is produced principally by O_2, first in the Schumann-Runge bands, and then in a continuum extending beyond the convergence limit at 1750 A. The absorption is continuous and smooth to approximately 1350 A. To shorter wavelengths the absorption spectrum becomes extremely irregular; below Lyman-α the curve of Fig. 1 is intended only to suggest the fact that there are many windows, and is not quantitatively correct. The Lyman-α line of hydrogen happens to lie in the deepest window, and penetrates to 75 km, approximately, before it is attenuated by 1/e.

Below approximately 1000 A, molecular nitrogen is the principal absorber. Its spectrum is extremely complicated, and consists of

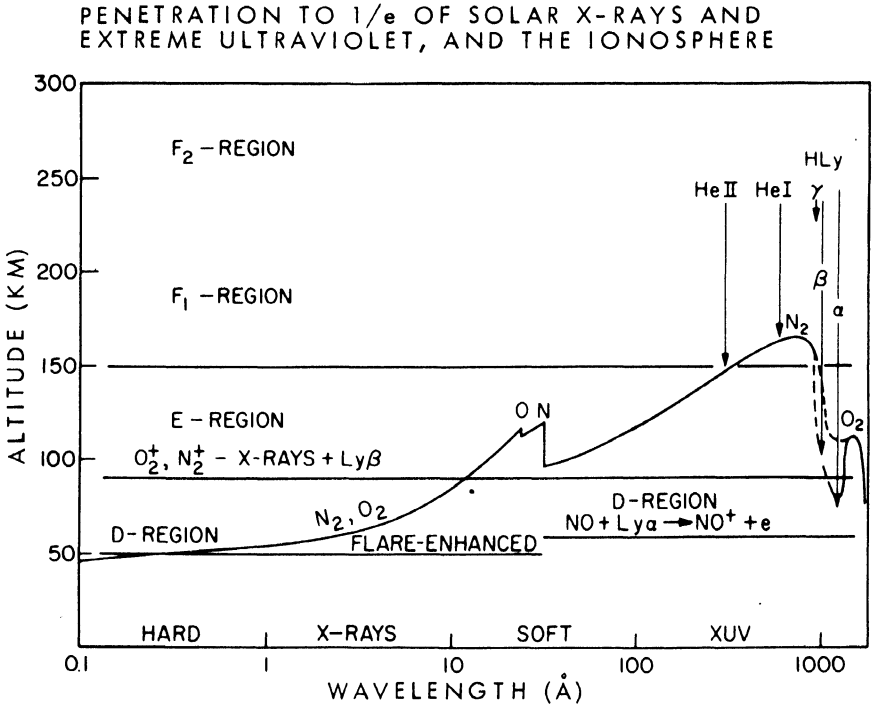


Fig. 2. The depth to which 1/e of the incident solar intensity penetrates, for 0.1 to 1000 A.

a series of strong bands which overlie an ionization continuum that extends below 800 A. The depth of penetration varies greatly with wavelength. In Fig. 2 there is indicated only a very approximate estimate of the depth of penetration. The absorption edges of N and O at 31 and 23 A, respectively, limit the penetration of soft x-rays. The effect of the L edges, lying near 180 and 120 A, is small and is not shown.

The various layers of the ionosphere are attributed, largely, to photoionization by these radiations. Lyman-α penetrates to the altitude range of the D-layer, but is unable to ionize O_2. It is assumed, though not yet established, that there is present in this region a small quantity of NO, which is ionized by wavelengths shorter than 1350 A. Sufficient Lyman-α radiation can be absorbed by this constituent to produce the D-layer ionization.

The ionization of the E-region is produced principally by x-rays in the wavelength range greater than about 10 A. However, Lyman-β, the rest of the Lyman series and the Lyman continuum are able to ionize O_2 whose ionization limit lies at 1027 A. Therefore they may contribute to the ionization of the E-region. The F-region is produced mainly by the absorption of the 304 A line of He II and the 584 A line of He I. Other radiations in this wavelength range con-

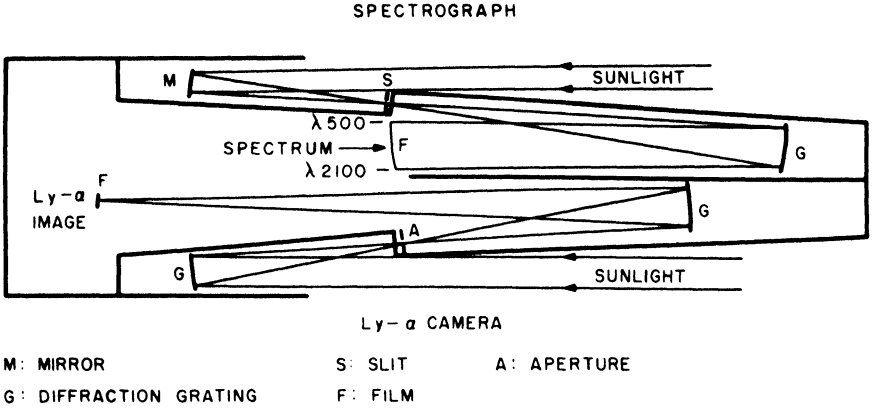


Fig. 3. An extreme ultraviolet spectrograph and Lyman-α disc camera flown by the U. S. Naval Research Laboratory.

tribute, as do all wavelengths shorter than 850 and 800 A, the ionization limits of N and N_2, respectively.

INSTRUMENTATION

The basic spectrograph used by the Naval Research Laboratory on March 13, 1959 is shown schematically in Fig. 3. Within the single housing there are two separate instruments, a spectrograph, and a Lyman-α disc camera. Each employs 600 groove/mm, 40 cm radius of curvature diffraction gratings in the first order. Both instruments operate near normal incidence. The spectrograph covers the wavelength range 500 to 2100 A. Light from the sun is imaged on the slit with a concave mirror. The mirror is distorted mechanically in such a way as to neutralize the astigmatism of this system (Purcell and Tousey (1957)) so that the density along each solar line is a measure of its intensity variation from center to limb.

The Lyman-α disc camera was designed to photograph the disc of the sun in the light of the Lyman-α line itself. The instrument comprises a double-dispersing grating monochromator operating at normal incidence. The first grating produces an image of the sun in Lyman-α. Because this line is far more intense than neighboring lines, it was possible to pass the entire solar image through a diaphragm which excluded the spectrum outside the range 1195 to 1245 A. In the position occupied by the disc camera, various other instruments have been flown, for example, a high dispersion profile spectrograph for study of the profile of the Lyman-α line.

The whole spectrograph unit is directed at the sun during flight by means of the biaxial pointing control developed by the University of Colorado group (Stacey, et al (1954)), now directed by F. Wilshusen.

This servo-system, employing photoelectric sensors which are extremely sensitive to the sun in angle, forces the spectrograph unit to remain directed at the sun to within one or two minutes of arc during the entire rocket flight.

Until recently the limitation in studying the extreme ultraviolet spectrum of the sun has been set by instrumental stray light. Because the solar spectrum is from five to six orders of magnitude more intense in the visible than near 1000 A, instrumental stray light must be almost completely removed in order to reveal the spectrum at the shortest wavelength. In a flight on April 19, 1960, this was accomplished by NRL (C. R. Detwiler, J. D. Purcell, and R. Tousey). The method was to predisperse the sun's image by means of a diffraction grating used in place of the collector mirror shown in Fig. 3. This grating dispersed the solar spectrum along the entrance slit. The second grating produced the principal dispersion in the direction perpendicular to the slit, as usual. Spectra obtained with this instrument are shown in Fig. 5. Because of the action of the predisperser, the spectrum lay in a diagonal position, and it was necessary to use a curved slit. For the first time, however, everything that can be seen in the spectrum is uncontaminated extreme ultraviolet radiation.

THE SOLAR SPECTRUM

In Fig. 4, the solar spectrum is shown from 2400 to 1800 A. In the region to long wavelengths of approximately 2100 A the spectrum is similar in nature to the visible and near ultraviolet, a photospheric continuum with densely packed Fraunhofer lines. The intensity decreases to short wavelengths and at 2100 A has reached approximately the level for a 5200°K black body. At 2085 A the spectrum changes suddenly in character; the intensity drops to a level close to the bottoms of the Fraunhofer lines and almost no detail remains.

The cause for the change in character below 2085 A has not been established. Three possible explanations have been proposed. The first is absorption by aluminum and calcium beyond their ionization limits which are indicated in Fig. 4. It is known that Al absorption is strong in the sun because the broad double absorption lines that occur between 1930 and 1940 A, and which are visible in the densitometer trace in Fig. 4, are produced by the autoinization of Al I. The second suggestion, made by L. Goldberg (Goldberg and Pierce (1959)), is that the absorption is first produced by nitric oxide and to shorter wavelengths by carbon monoxide. The third possibility, proposed by G. Herzberg, is the charge transfer continuum of H_2^+. This has its maximum near 1200 A (Herzberg (1950)), but the continuous absorption produced by it may well extend several hundred angstroms to longer wavelengths.

To shorter wavelengths, the character of the spectrum changes

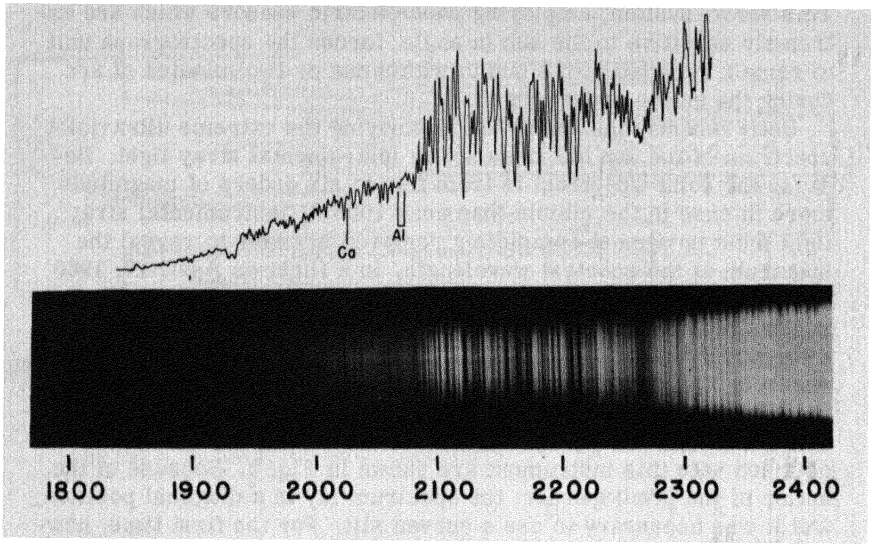


Fig. 4. The solar spectrum from 2400 to 1800 A, by the U. S. Naval Research Laboratory.

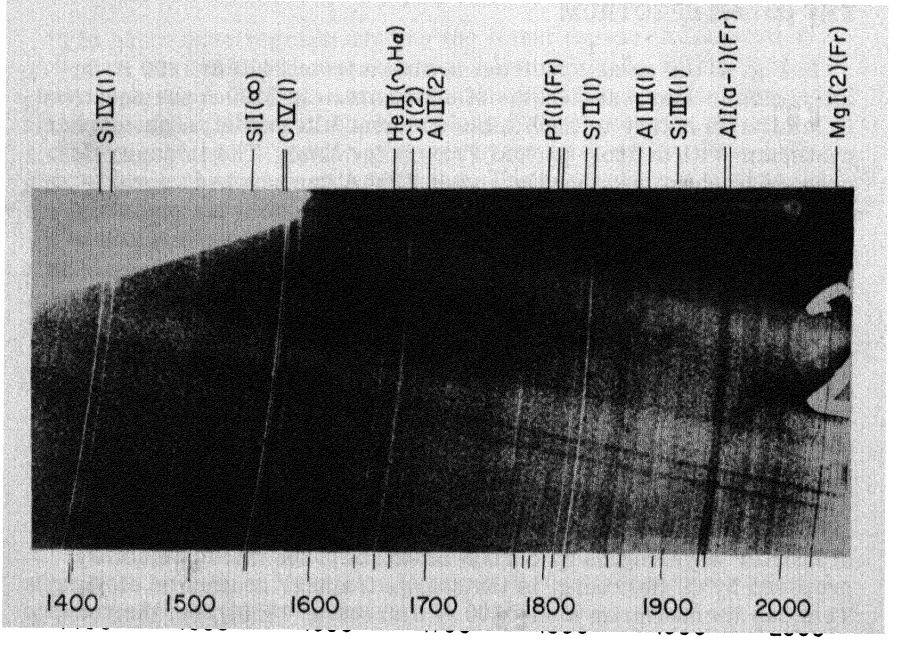


Fig. 5 (a). Solar spectra obtained by the U. S. Naval Research Laboratory on April 19, 1960. Altitude 220 to 200 km, exposure 60 sec SC-4 film. Slit illuminated by stray light from the first grating.

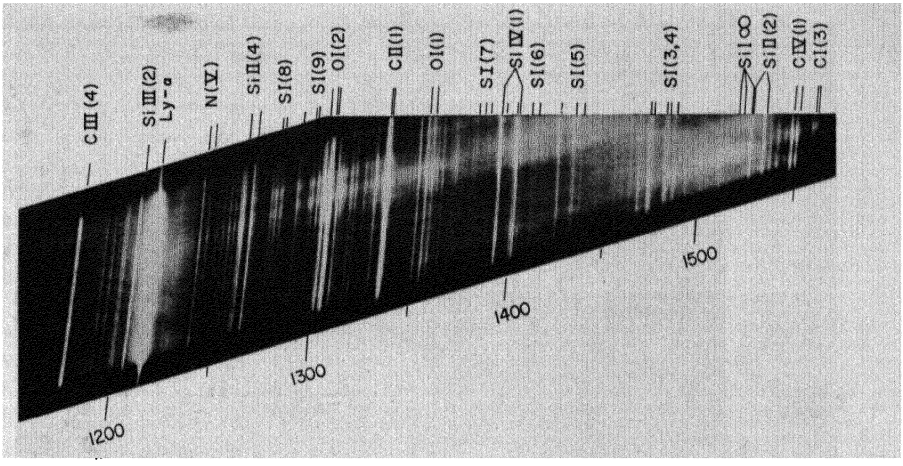


Fig. 5(b). Solar spectra obtained by the U. S. Naval Research Laboratory on April 19, 1960. Altitude 125 to 141 km, exposure 13 sec SWR-C film. Slit illuminated by predispersed solar image.

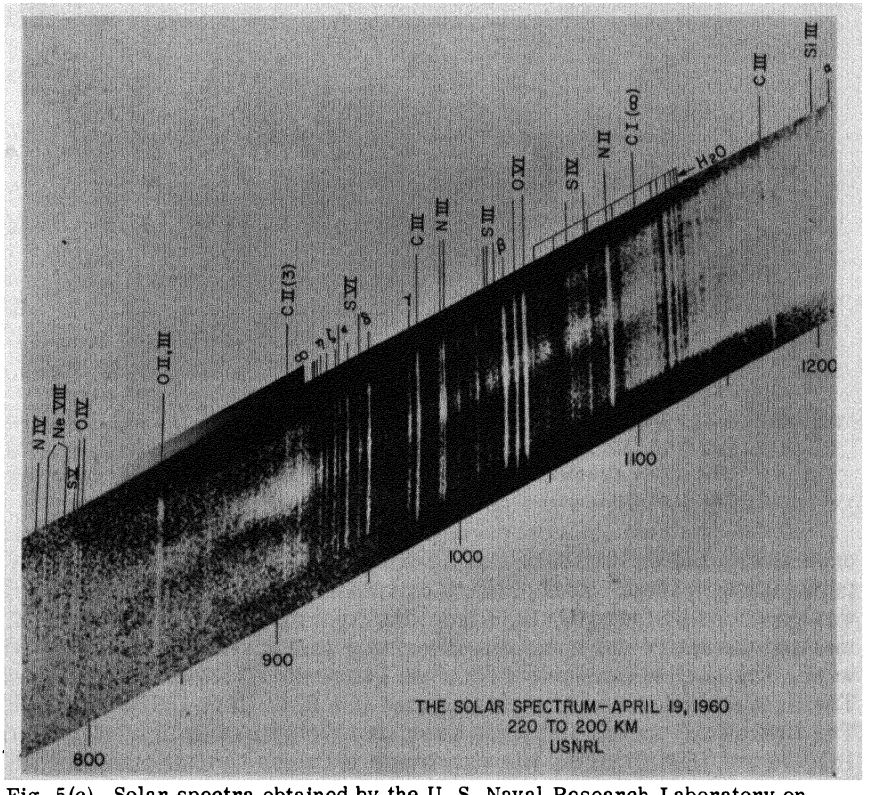


Fig. 5(c). Solar spectra obtained by the U. S. Naval Research Laboratory on April 19, 1960. Altitude 220 to 200 km, exposure 60 sec SC-4 film. Slit illuminated by predispersed solar image.

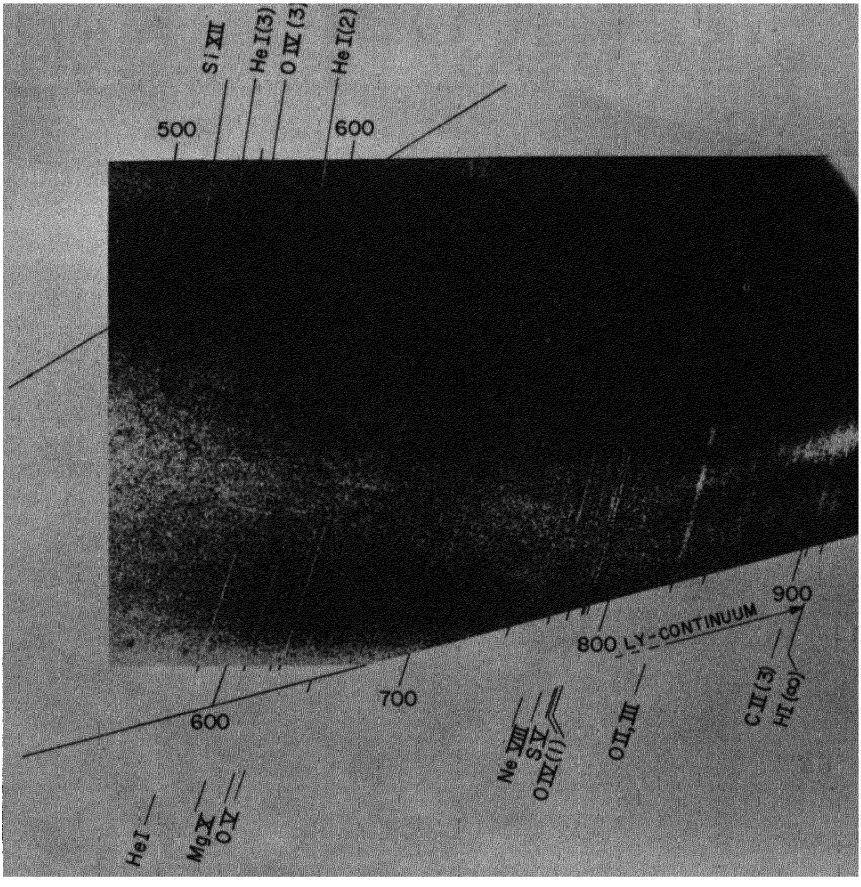


Fig. 5(d). Solar spectra obtained by the U. S. Naval Research Laboratory on April 19, 1960. Altitude 220 to 200 km, exposure 60 sec SC-4 film. The upper spectrum is produced by the second order image from the first grating.

once more. Below 1900 A in Fig. 5 we see the first appearance of pure emission lines. Most of the spectrum reproduced in Fig. 5(a) was produced by the stray light from the first grating which illuminated the entire entrance slit. Therefore this portion is relatively weak. The autoionization doublet of Al I is seen at 1930 to 1940 A. The first emission line is the resonance line of Si III at 1892.03 A. The first really strong lines, however, are the pair of Si II at 1816.94 and 1808.01 A. As the wavelength becomes shorter the continuum decreases in intensity, and the detail continues to fade out.

Figures 5(b) and (c) were obtained with the predispersed solar image illuminating the slit. Below 1525 A, the continuum can be

seen extending smoothly, with no Fraunhofer lines at all, as far as 1000 A, approximately. Preliminary intensity measurements place the level of this continuum at about 5000° K in the neighborhood of Lyman-α. Superimposed upon the continuum are many intense emission lines. Most conspicuous are the Lyman series of hydrogen. Lyman-α at 1215.67 A is greatly over-exposed, and all the higher members through Lyman-λ are present. Below 918 A the unresolved higher members of the series cause the background to rise, reaching a maximum at 912 A, from which the Lyman continuum can be seen extending to the neighborhood of 800 A.

The intensity of Lyman-γ is of considerable interest because its wavelength, 972.54 A, is just within a strong absorption band of N_2 with head at 972.1 A. As a result, in spectra photographed at 200 km, Lyman-γ is almost completely absorbed, and for spectra obtained below this altitude it is altogether missing (Purcell, Packer, and Tousey (1960)). At 220 km, where Fig. 5 was photographed, its intensity is sufficient for it to be recorded, but it is still greatly attenuated and only as intense as the fifth line in the series.

Within the Lyman continuum other absorption effects produced by N_2 can be seen, producing irregular intensity variations. Much of the structure which appears to be emission lines actually is the continuum showing brightly between the absorption bands of N_2.

Most of the nearly 200 emission lines visible in this spectrum have been identified. They come from the abundant elements from hydrogen through sulfur. They are the resonance lines and the low excitation potential lines of various stages of ionization. In Table I is presented a list of the resonance lines which occur within the region observed by NRL, arranged in isoelectronic sequences. The entries without brackets are the lines which have been observed in the sun. He I, 303.78 A lies outside the range of the Table, but has been observed (Rense (1959)).

The most complete isoelectronic sequence is the lithium-like spectrum. In Fig. 5 there can be seen the resonance line pairs produced by C IV, N V, O VI, Ne VIII, Mg X, and Si XII. Missing are the lines from B II, F VII, Na IX, and Al XI. Boron and fluorine are not at all abundant in the sun.

Within the lithium-like sequence, the energy required to produce the particular state of ionization increases rapidly, reaching 207.2, 327.9, and 476.0 ev for Ne VIII, Mg X, and Si XII, respectively. Therefore, the lines originate farther and farther out in the atmosphere of the sun until, finally, the line pairs, from Ne VIII, Mg X, Si XII are truly from the corona. They are permitted lines whereas the coronal lines that have been identified in the visible are from forbidden transitions.

Employing a grazing incidence spectrograph (Violett and Rense (1959)) have photographed the spectrum from 1216 A to very short wavelengths, and report lines extending to wavelengths as short as 84 A. These results do not agree well with the spectrum shown in Fig. 5. For example, from 975 to 912 A, nine members of the Lyman

TABLE I

SOLAR RESONANCE LINES FOR λ > 500 A,

[ ] = Not observed

Ground State	$1s\ ^2P$	$1s^2\ ^1S$	$2s\ ^2S$	$2s\ ^1S$	$2p\ ^2P^0$	$2p^2\ ^3$	$2p^3\ ^4S^0$	$2p^4\ ^3P$	$2p^5\ ^2P^0$
Atomic Number									
1	H I								
2	He II								
3			Li I						
4			Be II	Be I					
5			[B III]	[B II]	[B I]				
6			C IV	C III	C II	C I			
7			N V	N IV	N III	N II	N I		
8			O VI	O V	O IV	O III	O II	O I	
9			[F VII]	[F VI]	[F V]	[F IV]	[F III]	[F II]	[F I]
10			Ne VIII		[Ne VI]	[Ne V]	[Ne IV]		
11			[Na IX]						
12			Mg X						
13			[Al XI]						
14			Si XII						
15									
16									
17									
18									
19									
20									
21									

series of hydrogen can be seen, with Lyman-γ weaker than δ and ε. Also visible are the resonance lines of S VI. Over this same region, Violett and Rense list none of these lines except Lyman-γ, but their list includes ten lines, which are not present in our spectrum; only two of these are identified. Since the new spectra obtained on April 19, 1960 confirm the spectra obtained by NRL on March 13, 1959, it is necessary to explain these unidentified lines as higher orders of shorter wavelength lines. One would expect, therefore, to find these lines present in lower orders, but they are not listed.

SPECIAL STUDIES OF THE LYMAN-ALPHA LINE

Lyman-α is by far the most intense solar emission line in the extreme ultraviolet. In recent years during the sun-spot maximum, its intensity measured by means of ionization chambers, has been 5 to 6 ergs/cm^2 sec (Byram, et al. (1954)). The profile of the Lyman-α line and the appearance of the disc as photographed in the Lyman-α line have been studied by the Naval Research Laboratory.

A number of solar images were obtained with the Lyman-α disc camera, shown in Fig. 3. One of these is reproduced in Fig. 6. Included also are spectroheliograms made from ground at the same time in CaK and Hydrogen-α, and also a white light photograph.

The Lyman-α image is most like the CaK spectroheliogram, but

AND SEQUENCES THROUGH ARGON

in the sun.

$2p^6\ ^1S$	$3s\ ^2S$	$3s^2\ ^1S$	$3p^2\ P^0$	$3p^2\ ^3P$	$3p^3\ ^4S^0$	$3p^4\ ^3P$	$3p^5\ ^2P^0$	$3p^6\ ^1S$	Ground State
									Atomic Number
									1
									2
									3
									4
									5
									6
									7
									8
									9
[Ne I]									10
	Na I								11
	Mg II	Mg I							12
	Al III	Al II	Al I						13
	Si IV	Si III	Si II	Si I					14
	[P V]	[P IV]	[P III]	[P II]	P I				15
	S VI	S V	S IV	S III	S II	S I			16
	[Cl VII]	[Cl VI]	[Cl V]	[Cl IV]	[Cl III]	[Cl II]	[Cl I]		17
	[A VIII]	[A VII]	[A VI]	[A V]	[A IV]	[A III]	[A II]	[A I]	18
	[K IX]	[K VIII]	[K VII]	[K VI]	[K V]		[K III]	[K II]	19
	[Ca X]		[Ca VIII]	[Ca VII]	[Ca VI]				20
	[Sc XI]		[Sc IX]		[Sc VII]				21

shows less detail and higher contrast between plage regions and the quiet background. Comparing intensities, the ratio between the brightest and darkest regions is approximately twice greater than for CaK, and the plage regions seem to cover a larger fraction of the solar disc. The resolution of the Lyman-α camera was of the order of one-third of a minute of arc, but the finest Lyman-α detail visible in the sun is only one-half minute.

Dark filaments show conspicuously in hydrogen-α and CaK. Most of these can also be seen in Lyman-α. There is, however, one dark feature in Lyman-α that cannot be seen at all in Hydrogen-α and that is only suggested in CaK. This is a great dark rift in the Southern Hemisphere extending down from close to the equator in the west, at an angle of 30°, through about 70° in longitude. Also visible in the Lyman-α image are several indistinct dark bands parallel to the equator near the poles. Two bands can be seen in the Southern Hemisphere, and the pole itself seems dark. In the North, they are confused by plage regions, and the North Pole itself cannot be seen because the sun was tipped slightly away at the time, however, two of the dark bands are still suggested.

Qualitatively, it is possible to say that these three images represent maps of the solar atmosphere at different altitudes. Hydrogen-α originates from the photosphere, CaK from a somewhat higher level, and Lyman-α from a still higher level in the region where the temperature is rising with altitude.

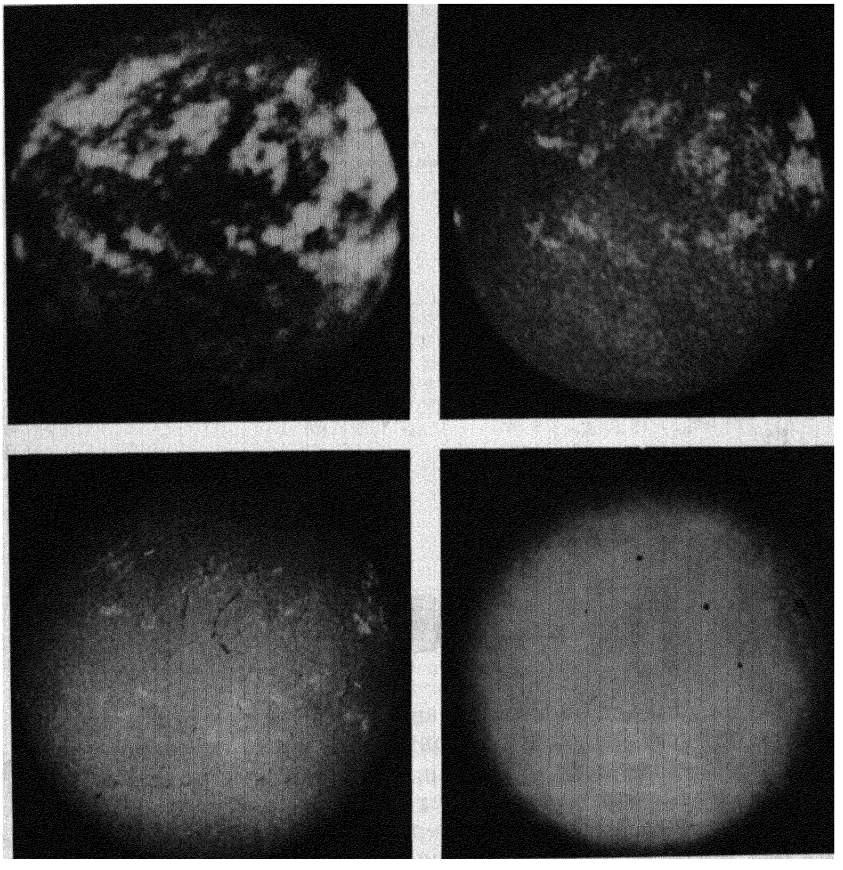


Fig. 6. Images of the sun on March 13, 1959:—
Upper left: Lyman-α from the Aerobee-Hi rocket obtained by U. S. Naval Research Laboratory.
Upper right: Calcium $K_{2,3,2}$, spectroheliogram (obtained by McMath-Hulbert Observatory).
Lower left: Hydrogen-α with 0.7 A monochromatic filter (obtained by U. S. Naval Research Laboratory).
Lower right: White light (obtained by U. S. Naval Observatory).

In another experiment, the profile of the Lyman-α line was determined on July 21, 1959 (Purcell and Tousey (1960)). The spectrograph employed a 30,000 line/inch, 50 cm radius diffraction grating in the 13th order, together with a similar grating in the 1st order as predisperser. An astigmatic image of the sun was obtained. In Fig. 7 is shown one of the nine images secured during the first flight together with a densitometer tracing of the densest region of the image. The variations along the line are produced by different regions on the sun, and plages.

It can be seen that the Lyman-α line is very broad. Its wings extend to one or more angstroms on either side of center. The central region of the line is strongly absorbed. First, there is a broad central absorption that is produced in the atmosphere of the sun. Second, there is a deep narrow absorption core produced by absorption by neutral hydrogen lying between the earth and the sun.

Analysis of the central absorption core shows that its width at half-maximum lies between 0.025 and 0.04 A. Therefore, the hydrogen producing this absorption is largely at a temperature between 1000 and 2000°K. This is the range which includes the best estimates of the temperature in the outermost atmosphere of the earth. The spectra obtained at different altitudes were analyzed. From the depth of the absorption core and the total vertical hydrogen was determined. The value for 92 km was 3×10^{12} atoms cm^2 column; the value for 197 km was 1.5×10^{12}. New spectra, obtained on April 19,

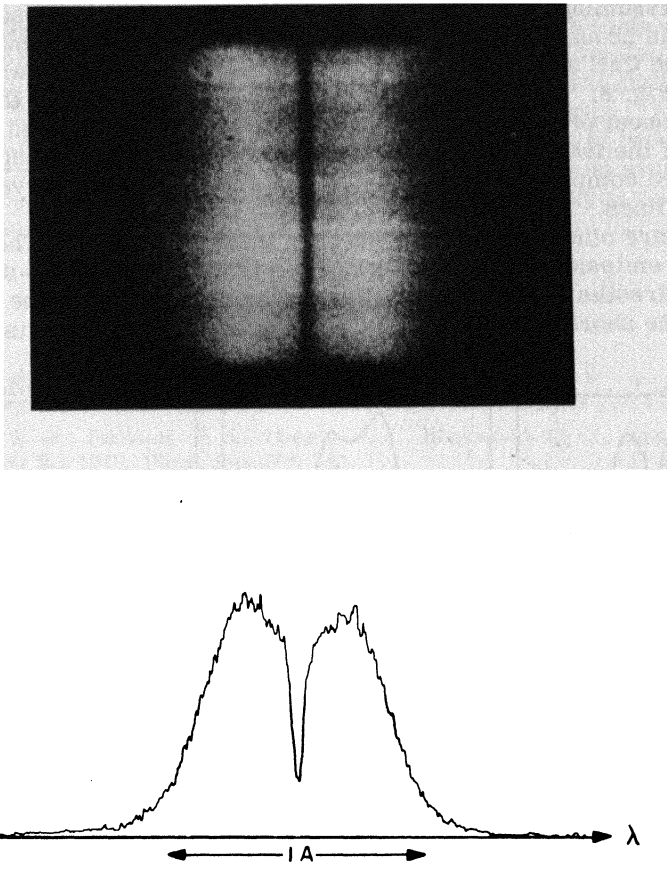


Fig. 7. Lyman-α profile photographed between 134 and 163 km altitude, July 21, 1959, by the U. S. Naval Research Laboratory.

1960 and not yet reduced indicate a less change with altitude. However, it appears certain that a large portion of the neutral hydrogen lies in the atmosphere of the earth.

The absorption measurements are in qualitative agreement with the Lyman-α fluorescence observed by NRL (Kupperian, et al (1959)) in the night sky from the very high atmosphere, which is still illuminated by sunlight. The absorption core was found to remove approximately 0.1 erg/cm^2 sec of the solar radiation. When reradiated by fluorescence this produces a Lyman-α luminescence of the order of 0.001 erg/cm^{2}sec ster-radian. This is the order of magnitude of the luminescence observed by means of rocket-borne ion chambers.

The solar portion of the absorption has been studied by Morton and Widing (1961). They have computed the profile on the basis of the Jeffries and Thomas Theory, in which the effect is produced by noncoherent scattering and Doppler broadening. It was found that the shape of the portion of the Lyman-α line between the maxima can be fitted by assuming that the line is emitted from a region whose temperature is about 90,000°K. In shape the Lyman-α line resembles closely the CaH and K and the Mg II resonance lines. These are compared in Fig. 8. The Lyman-α emission line corresponds to the second component of the H and K lines and the emission observed at the centers of the two Mg II lines. The central depression corresponds to the third component of the H and K lines and is also observed in the Mg II lines.

There are other similarities between these three lines. The Lyman-α emission line in most places in the sun is Doppler-shifted a few hundredths of an angstrom to short wavelengths, and the maximum on the short wavelength side is the greater. The same is true

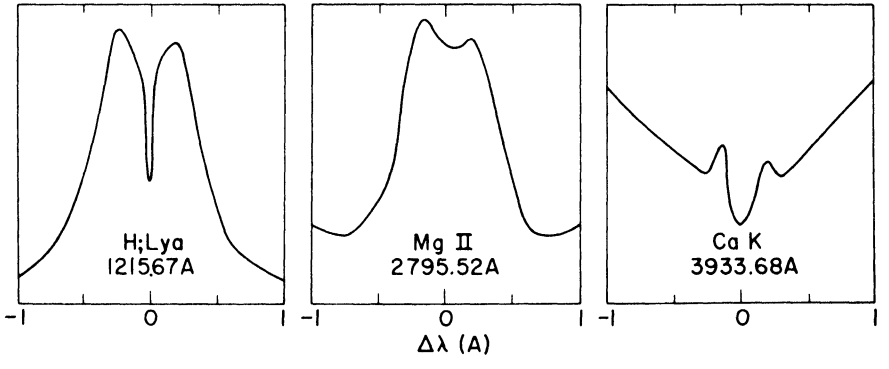


Fig. 8. Typical profiles:
(a) H. Lyman-α; U. S. Naval Research Laboratory (Purcell and Tousey, 1960).
(b) Mg II; U. S. Naval Research Laboratory (Boggess, Purcell and Tousey, 1958).
(c) Calcium K; McMath-Hulbert Observatory (Goldberg, Mohler and Müller, 1959).

of CaH and K, and the Mg II lines. The separation between the maxima is greater than at the center, and for non-plage regions as against plages, just as in the case of CaH and K. It is thought, therefore, that the same basic theory should apply to all three lines and that the physical processes which produce the asymmetry must be similar.

CONCLUSION

There is a great deal of room for further research on the extreme ultraviolet spectrum of the sun. The spectrum from 500 to 1 A is still almost completely unexplored, except in large wavelength bands. Changes in line intensities with altitude require detailed investigation: The scanning photoelectric monochromator of Hinteregger (1960) is well adapted for this work. Much of this can be best accomplished from rockets.

Satellites, however, have two great advantages over rockets. The first is the providing of a long observing period, so as to detect time variations in the solar spectrum. The second is the complete freedom from contaminating gases carried by the equipment and the vehicle, which a few days in orbit should serve to outgas. This is especially important in view of the recent observation of water vapor absorption bands, appearing in the spectra of Fig. 5, and probably caused by outgassing of the rocket. These two advantages may well compensate for the far greater difficulties of satellite instrumentation.

REFERENCES

Baum, W. A., Johnson, F. S., Oberly, J. J., Rockwood, C. C., Strain, C.,V., and Tousey, R., 1946, Phys. Rev. **70**, 781.

Weissler, G. L., 1956, Handbuch der Physik Vol. XXI, pp. 304-382. Springer-Verlag, Berlin, Ed. S. Flügge.

Watanabe, K., 1959, Advances in Geophysics 5, 155-210. Edited by H. E. Landsberg and J. Van Miegham, published by Academic Press Inc., New York, N. Y.

Johnson, F. S., Malitson, H. H., Purcell, J. D., and Tousey, R., 1959, Ap. J. **127**, 80.

Purcell, J. D., and Tousey, R., 1957, J. Opt. Soc. Am. **47**, 1057.

Stacey, D. S., Stith, G. A., Nidey, R. A., and Pietenpol, W. B., 1954, Electronics **27**, 149.

Herzberg, G., 1950, Molecular Spectra and Molecular Structure, Vol. I, "Spectra of Diatomic Molecules," 2nd Ed. D. Van Nostrand, Princeton, N. J.

Purcell, J. D., Packer, D. M., and Tousey, R., 1960, Proceedings of the First International Space Science Symposium, pp. 581-589, North Holland Pub. Co., Amsterdam.

Johnson, F. S., Purcell, J. D., Tousey, R., Watanabe, K., 1952, J. Geophys. Res. **57**, 157.

Violett, R., and Rense, W. A., 1959, Astrophys. **130**, 954.

Byram, E. T., Chubb, T. A., Friedman, H., and Kupperian, J. E., Jr., 1956, Astrophys. J. **124**, 480.

Purcell, J. D., Packer, D. M., and Tousey, R., 1959, Nature, **184**, 8.

Purcell, J. D., and Tousey, R., 1960, J. Geophys. Res. **65**, 370.

Kupperian, J. E. Jr., Byram, E. T., Chubb, T. A., and Friedman, H., 1959, Planet Space Sc. **1**, 3.

Morton, D. C., and Widing, K. G., 1961, Astron. J. (to be published).

Goldberg, L. and Pierce, A. K., 1959, Handbuch der Physik Vol. LII, Ed. S. Flügge, Springer-Verlag, Berlin.

Hinteregger, H. E., 1960, Proceedings of the First International Space Science Symposium, pp. 615-627, North Holland Pub. Co., Amsterdam.

Boggess, A. B., III, Purcell, J. D., and Tousey, R., 1958, "A High Resolution Ultraviolet Spectrogram of the Sun," IGY Rocket Report Series No. 1, 198-200.

Goldberg, L., Mohler, O. C., and Müller, E. A., 1959, Astrophys. J. **129**, 119.

2. SOLAR ULTRAVIOLET RESEARCH

William A. Rense
Upper Air Laboratory Physics Department
University of Colorado

INTRODUCTION

Since 1948 the Physics Department of the University of Colorado has been engaged in research concerned with the study of solar ultraviolet radiation as observed from rockets. Several organizations have sponsored the research, namely, Air Force Cambridge Research Center, Naval Research Laboratory, National Academy of Science (IGY) and the National Aeronautics and Space Administration (NASA). The program included the design and construction of a biaxial electronic rocket pointing control; the design and construction of laboratory facilities for the study of ultraviolet radiation and related phenomena; the design and construction of rocket spectrographs and cameras for detecting and measuring solar ultraviolet radiation; the performance of basic research helpful in completing the objective of the program; the flying of rocket instruments and the analysis of data obtained; and the theoretical work involving the application of data. The following pages will be devoted to a discussion of some of the more specialized aspects of the design of rocket spectrographs and cameras, to the presentation of data obtained, and to the interpretation of the data.

ROCKET INSTRUMENTS FOR MEASURING SOLAR ULTRAVIOLET RADIATION

A rocket instrument must be adapted to the environment of the upper atmosphere and to the exigencies of rocket acceleration, flight and recovery. These restrictions limit the size of the instrument, the kinds of mounts used for the more delicate optical parts, the type of evacuation baffles, and the method of storage of detector items such as film. Another important consideration has to do with the intense visible light from the sun. Since the intensity of visible light is a factor of the order of a million above that of the ultraviolet light to be detected, the instrument must be designed so that scattered light is reduced to a minimum. The detection of the near ultraviolet spectrum of the sun does not call for special optics beyond that of the use of reflection gratings and quartz prisms. However as one goes to shorter wavelengths transmission optics becomes unfeasible and one

must rely entirely upon mirrors and gratings. An exception occurs in the region between 2000 and 1000 A; here lithium fluoride prims and lenses are somewhat satisfactory. Even reflection optics becomes inadequate as you go to extremely short wavelengths unless special precautions are taken. The reason for the difficulty lies in the low reflectivity of most materials in the far ultraviolet. Special films have been successfully used to enhance reflectivity down to about 800 A when normal incidence optics in employed.[1] For the extreme ultraviolet (wavelengths less than 800 A) one must at present resort to optics involving grazing-incidence angles. Such a procedure is appropriate only when the severe aberrations associated with grazing-incidence have been reduced by suitable methods.

A typical grating rocket spectrograph will be described to illustrate how some of the difficulties mentioned above can be partially overcome. The basic unit of our hypothetical rocket spectrograph will be a Rowland circle type spectrograph with the reflection concave grating set for grazing incidence (Fig. 1). Light from the source passes through the slit on to the grating and then on to the film placed along the Rowland circle. The spectrum is formed along the latter.[2] It is a characteristic for such an instrument that the spectrum lines are elongated by astigmatism. The reason for this defect lies in the fact that the concave grating forms two images, one of the slit in horizontal focus at the Rowland circle and one of the source in vertical focus beyond the Rowland circle. Referring to the figure one can write the following two equations for the location of these two images:

$$r/R = \cos\alpha, \quad r'/R = \cos\beta \tag{1}$$

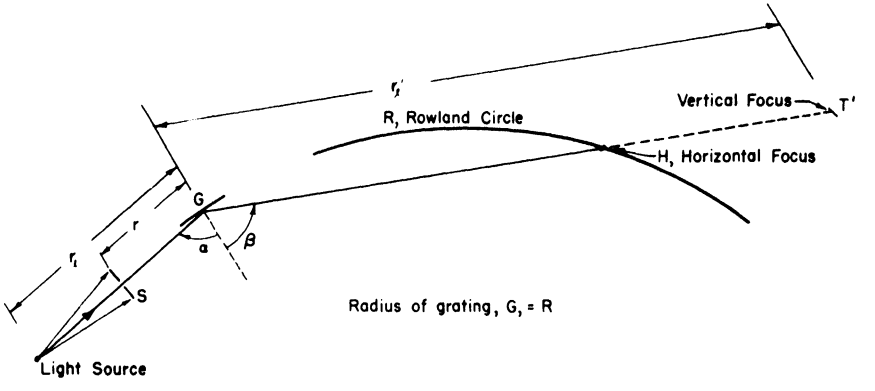


Fig. 1. The essential optical elements of the grazing incidence type, Rowland circle mounting, grating spectrograph. The slit, the concave grating and the film holder all lie on the Rowland circle whose diameter is equal to the radius of the grating. The H focus, on the circle, is an image of the slit in horizontal focus, whereas the T′ focus is an image of the source seen through the slit, and is in vertical focus. The fact that the two images do not both fall on the Rowland circle gives rise to considerable lengthening of the lines of the spectrum, and hence loss of sensitivity.

$$r/r_l - \cos\alpha/R + 1/r_l' - \cos\beta/R = 0 \qquad (2)$$

Here r' is the distance GH. The elongation of a spectral line on the Rowland circle results from the fact that the (vertical focus) image of the source is well beyond the circle. No choice of parameters can assure that the vertical focus fall on the Rowland circle unless grazing incidence angles are abandoned in the optical set-up. In particular it is possible to effect a coincidence of the images for a given ultraviolet wavelength when the source is at the slit for an angle of incidence of 0° (normal incidence). Of course for normal incidence one runs into the problem of low reflectivity for λ's less than 800 A; so serious is this defect that the elimination of the astigmatism does not compensate for it, so that one is forced to reconsider grazing-incidence optics.

Referring to Eqs. 1 and 2 one notes that the source must be a virtual source in order that its vertical focus fall on the Rowland circle. In other words, the light passing through the slit must be converging instead of diverging. Thus, for the sun (source distance equal to infinity) and for a grating of constant 6000 lines/cm and radius 50 cm, the image distance for vertical focus turns out to be −11 cm when the angle of incidence is 85° and when the wavelength is 300 A. To get around this difficulty another mirror may be placed in front of the slit as shown in Fig. 2. The mirror, also set at grazing incidence in order to assure high reflectivity, is so located and has such a radius that the horizontal focus for the sun at the slit and the vertical focus for the sun is at precisely the correct distance behind the circle to assure the coincidence on the Rowland circle of the two images formed by the grating. In addition to eliminating astigmatism for one wavelength the first mirror also increases the effective aperture. A rocket instrument designed along these principals[3] showed the expected high speed in the extreme ultraviolet and suceeded in recording chromospheric and coronal emission lines in the extreme ultraviolet region.

Up to the present time Eastman-Kodak short wave radiation (SWR)

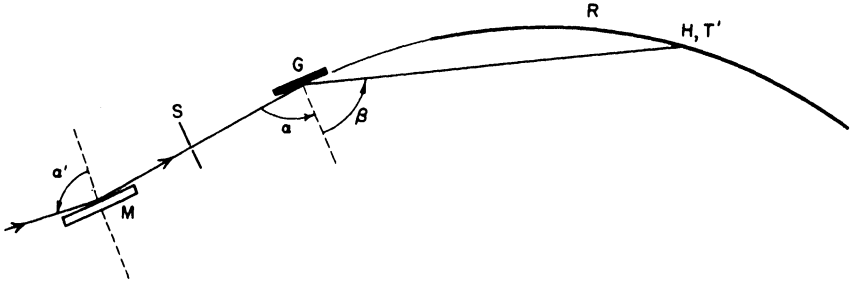


Fig. 2. The grazing incidence concave grating spectrograph equipped with a pre-focussing toroidal mirror. The latter forms the first of its astigmatic images on the slit, and the second beyond the grating at just such a point that the grating focusses both images on the Rowland circle. The mirror increases the speed of the spectrograph by increasing the aperture and reducing astigmatism.

film has been employed for photographing the sun's ultraviolet spectrum. The film is of the Schuman type containing a low gelatin content, is extremely sensitive to abrasions and does not have a satisfactory characteristic curve for photometric work. It does, however, exhibit good resolving power and relatively high speed. Eastman-Pathe in France has developed a similar film with considerable more speed but with less resolving power.

For some rocket spectrographs the film is pulled along the Rowland circle into a cassette by sprocket and gear devices; the motor which accomplishes the movement is activated automatically by a timer. The exposures are controled by a solenoid-regulated shutter behind the slit. In other instances strips of film are mounted on a drum and are brought into the Rowland circle position for each exposure. The former method has the disadvantage of introducing abrasions on the film but has the advantage of simplicity of focusing and better safety during recovery since it can be wound into a compact steel cassette. The drum type calls for more elaborate machine work since each film strip must be on its own Rowland circle, but reduces the chances of abrasion. Another disadvantage of the roll type over the drum type has to do with the tendency of SWR to crack in a direction parallel to the spectrum lines when it stays in rolled form in a vacuum for an extended period.

The resolving power of rocket spectrographs is determined mainly by two facts, the slit width and the film characteristics. It has been found desirable to make the slit width about 5 to 12 microns. Smaller widths lead to the danger of a clogged slit during flight, whereas larger slit widths introduce additional scattered visible light. The film restricts the sharpness of focus, first because of its intrinsic resolving power, second because of the difficulty in getting it to lie exactly along the Rowland circle, and third because of a property known as film creep. The latter refers to a tendency for the emulsion to creep slightly during exposure if it has not been completely dehydrated. Until smaller slit widths and better film can be used the resolving power of the grating itself will probably not be fully realized.[2] Incidentally, for grazing incidence, the optimum resolving power of a grating calls for a small grating width and hence reduced aperture.

When the rocket is ascending air must leave the spectrograph in order to assure that the pressure in the spectrograph is comparable to the low pressure outside the spectrograph at high rocket heights. Suitable light-tight baffled channels having low impedence to air movement are incorporated into the spectrograph to provide the needed outlets. Sometimes a spectrograph is initially filled with a gas, such as helium, which procedure clears the spectrograph of air and replaces it with a gas that has low absorptivity in the far ultraviolet.

We will next consider another kind of solar ultraviolet rocket instrument, namely the monochromatic camera. One may be interested in the possibility of photographing the sun in a given wavelength in the

ultraviolet. Here intensity is a very important factor. Concentrating on the hydrogen Lyman-α line, which is one of the most intense emitted by the sun in the ultraviolet, several types of cameras are feasible. Two have been successfully flown.[4,5] Because coatings are available which give high reflectivity at 1216 A mirror optics are to be preferred over lithium fluoride optics until such a time as better techniques for grinding and polishing lithium fluoride have been developed. For a grating monochromatic camera light from the sun strikes the concave grating which forms an image of the sun in hydrogen Lyman-α. The image is relatively free of astigmatism because of the mounting employed which is of the Wadsworth-type. A second grating neutralizes the dispersion of the grating and forms a final image of the sun. The second grating must be ellipsoidal. The shape may easily be achieved by suitable mechanical stresses exerted by the grating mount. The quality of the image can be quite satisfactory though resolving powers associated with monochromatic cameras for visible light probably cannot be duplicated. If the gratings are coated with magnesium flouride film and if they are suitably blazed, the speed of the camera is sufficiently great so that photographs of the sun may be effected in a fraction of a second, thus cutting down on the blurring effect of pointing control motion. When one considers the possibility of photographing the sun in the extreme ultraviolet, for example at the 303.8 A radiation of ionized helium, then grazing incidence optics is desirable in order to maintain high reflectivity of the optical parts. With this restriction, however, special care must be taken to reduce aberrations, especially astigmatism. Considerable sacrifice of resolving power may have to be made.

ABSOLUTE CALIBRATION IN THE FAR ULTRAVIOLET

The determination of both relative and absolute intensities of solar spectral lines in the far ultraviolet is an important but difficult task. Some experience has been obtained in both instances, but much more work needs to be done before accurate results will be forthcoming.

The method used for obtaining relative intensities at a given ultraviolet wavelength when SWR Eastman Kodak film is employed is a straightforward one similar to methods appropriate for the visible spectrum. The objective is to obtain the characteristic curve for the film at a particular wavelength. The curve is a plot of density versus log of exposure and covers a range sufficiently great so that the saturation part of the characteristic curve is reached. Such curves give relative values for a given wavelength only. Exposures can be made with a Geissler tube capillary discharge source. In such a source hydrogen gas may be used at a pressure of about one mm of Hg, and with a discharge current of 100 ma, D.C. The source can be run for several hours at an intensity (of the Lyman-α line) that remains constant to within 5 to 10% (as measured by photomultiplier tube tests). For constant intensity of Lyman-α one can obtain a series

of exposures of the Lyman-α line by placing an adjustable sector disk next to the film. The sector disk is timed so that the flicker effect is negligible. A good rule for this is that the sector speed should be such that each exposure is divided into at least one hundred parts. The average exposure times are made to be compatible with those of the rocket flight in order to minimize reciprocity failure. For such a set-up relative exposures and later, after the film has been developed and micro-densitometered, densities corresponding to the exposures may readily be found. When helium gas is used in the source characteristic curves may be obtained for wavelengths down to 304 A.

It is clear that a set of characteristic curves such as those described above is all that is needed to trace the change in intensity of a given solar ultraviolet line as a function of rocket altitude. Data of this nature are helpful in determining atmospheric constituents. However, the much more desirable information concerning the ralative intensities of lines of appreciably different wavelengths is not available unless more data concerning film sensitivity as a function of wavelength are accumulated by further laboratory experimentation. In essence one must establish for several wavelengths in the ultraviolet the relative film sensitivity, that is, the relative intensities of the lines when they produce the same density on the film. One method of establishing the relative intensities of spectral lines emitted by a given source (assuming the latter to be stable and to give unchanging intensity for all wavelengths over a period of time) makes use of a vacuum thermopile which presumably is a black body receiver for the ultraviolet. The output of such a thermopile is believed to depend upon the total energy regardless of wavelength. If, while the source is on, the thermopile is made to scan the ultraviolet spectrum along the Rowland circle the response of the thermopile may be found for several wavelengths. Such data establish the relative intensities of the lines. Moreover, if the thermopile has been calibrated for absolute intensities of incident radiation by illumination with radiation of known intensity, one can obtain absolute intensities of the source lines as well. The thermopile may be checked in this way with the aid of a standard lamp calibrated at the National Bureau of Standards.

Although the above procedure has actually been applied to rocket spectrograms, the results are still questionable for several reasons. First, little is really known about the faithfulness of the thermopile in responding to incident radiation over a wide range of wavelengths. Although the flakes of the thermopile may absorb like a black body other effects such as photoemission may influence the response. Another source of error lies in the low sensitivity of the thermopile in relation to the rather weak ultraviolet laboratory spectra produced by currently known sources such as the capillary source described above. Only for the very intense lines such as the Lyman-α line is the response seen to be accurately measureable. The technique which has been adopted for getting around the latter difficulty is based on the assumption that the sodium salicylate phosphor has constant quantum efficiency over a long range into the far ultraviolet. A photomultiplier

tube coated with this phosphor can give data leading to the calculation of relative intensities when it is swept over the Rowland circle. If the tube is calibrated at the known Lyman-α line, one can tie in these results so as to obtain absolute intensities.

Other pitfalls that prevent accuracy of results in the photometry of rocket spectrograms have to do with the effect of strong visible scattered light background superimposed on the lines, and the problems associated with the densitometry of narrow lines.

Of course calibrating the film is only half of the problem; the instrument transmission constant must be established. This constant may be defined as the ratio of the total energy striking the slit at a particular wavelength to that striking the film at the spectrum line for that wavelength. When this constant is known the absolute calibration procedure consists of measuring the energy striking the film (utilizing the film calibration data) and then correcting the result by the factor of the instrument's transmission constant. The instrument constant may be directly established for a given wavelength by placing the rocket spectrograph in the large laboratory spectrograph vacuum chamber so that it receives the radiation of a line whose absolute intensity has been measured by the thermopile. The spectrum line as photographed along the Rowland circle of the instrument is then measured and from the film constants the total energy that strikes the film is determined. Thus the constant may be established. It will also be seen that one can by-pass the film calibration for absolute intensity by referring directly to data obtained with the above mentioned set-up whereby absolute intensity at the slit is correlated directly with density on the film for a given wavelength.

ABSOLUTE INTENSITY OF SOLAR ULTRAVIOLET EMISSION LINES

The techniques for determining absolute intensities were applied to spectrograms obtained during a rocket flight[6] on August 6th, 1957.

TABLE I
Intensities of Emission Lines

Identification	Wavelength (A)	Intensity (ergs/cm^2/sec)	Identification	Wavelength (A)	Intensity (ergs/cm^2/sec)
Si III	1206.5	0.23	Si II.	1526.7	0.03
HL a	1215.7	3.43	Si II.	1533.4	0.06
He II	1215.1	0.17	C IV.	1548.2	0.55
Si II.	1265.0	0.02	C IV.	1550.8	0.31
O I.	1302.2	0.04	C I	1560.3	0.04
O I	1304.9	0.04	C I	1561.4	0.08
O I	1306.0	0.04	He II	1640.4	0.27
Si II.	1309.3	0.04	C I	1656.3	0.28
C II	1334.5	0.31	C I	1658.1	0.20
C II	1335.7	0.33	Fe II	1670.8	0.21
Si IV.	1393.7	0.24	Si II.	1808.0	1.05
Si IV.	1402.7	0.17	Si II.	1816.0	1.65

The instrument was a concave grating spectrograph with the grating set at the angle of incidence of about 49°. The exposures were made at altitudes between 95 and 150 km. About 30 emission lines were studied. The results are shown in Table I. The value for Lyman-α is a little less than that (5.5 ergs/cm^2/sec) established by photoelectric and photoionization methods. Since the data represent the first attempt to measure absolute intensities for large numbers of solar emission lines, including fainter ones, they must not be regarded as being very accurate. However, it is felt that the order of magnitude is correct.

MEASUREMENT OF LINE PROFILES

The main obstacle in obtaining satisfactory measurements of line profiles lies in the low resolving power and dispersion of most rocket instruments. Nevertheless it is of astrophysical significance to know simply whether a line is broad or not broad; it is even better to know approximate values of the half-widths of broad lines. Attempts were made to determine which of the 30 or so emission lines studied on the spectrograms of the 6 August 1957 flight were definitely broad lines.[7] The procedure consisted in measuring the half-widths on the assumption that there is no instrument broadening. Of course in all cases these "half-widths" were appreciable. Two lines were distinctly broader than the others, namely the Lyman-α line at 1215.7 A and the helium II line at 1640.4 A. The half-widths were measured on rocket spectrograms corresponding to various exposures. As expected the half-widths depended on exposure times. One chooses the minimum of these for a given line as the starting value in the steps to be described. In this way effects introduced by over-long exposures or film creep were reduced. The next step was to correct the half-widths for an

TABLE II
Half-widths

Wavelength (A) (1)	89-Sec. Exp. (A) (2)	28-Sec. Exp. (A) (3)	12-Sec. Exp. (A) (4)	5-Sec. Exp. (A) (5)	Uncorrected Half-width (A) (6)	Half-width (A) (7)
1206.5	0.57	0.47	....	....	0.47	0
1215.7	1.65	1.28	1.25	....	1.25	0.80
1334.5	0.60	0.42	.....	....	0.42	0
1335.7	0.74	0.51	0.42	....	0.42	0
1393.7	0.69	....	....	....	0.69	0
1402.7	0.82	....	....	....	0.82	0
1526.7	0.63	....	....	....	0.63	0
1548.2	0.89	0.58	....	....	0.58	0
1550.8	0.76	0.53	0.47	....	0.47	0
1640.4	1.10	....	....	....	1.10	0.30
1670.8	0.70	0.83	....	....	0.70	0
1808.0	0.68	0.85	....	0.36	0.36	0

instrumental broadening. The latter was determined from laboratory spectrograms and amounted to about 0.3 A. The final step in establishing the half-width consisted in subtracting from a given half-width the average value of the half-widths of the emission lines in the immediate vicinity of the line in question. The validity of this procedure rests on the assumption that most of the lines are intrinsically narrow and that their half-widths measure instrumental and film creep broadening. Table II gives the result of measurements of the August 6, 1957 spectrograms.

Attempts were made to establish a rough profile of the Lyman-α hydrogen line. The results (uncorrected) are shown as the full line in Fig. 3. The theory of instrumental broadening indicates that for a flat profile of this kind the instrument effects do not alter the half-width appreciably. One notes that the profile half-width 0.9 A, compares favorably with the one shown in Table II. It is also interesting to com-

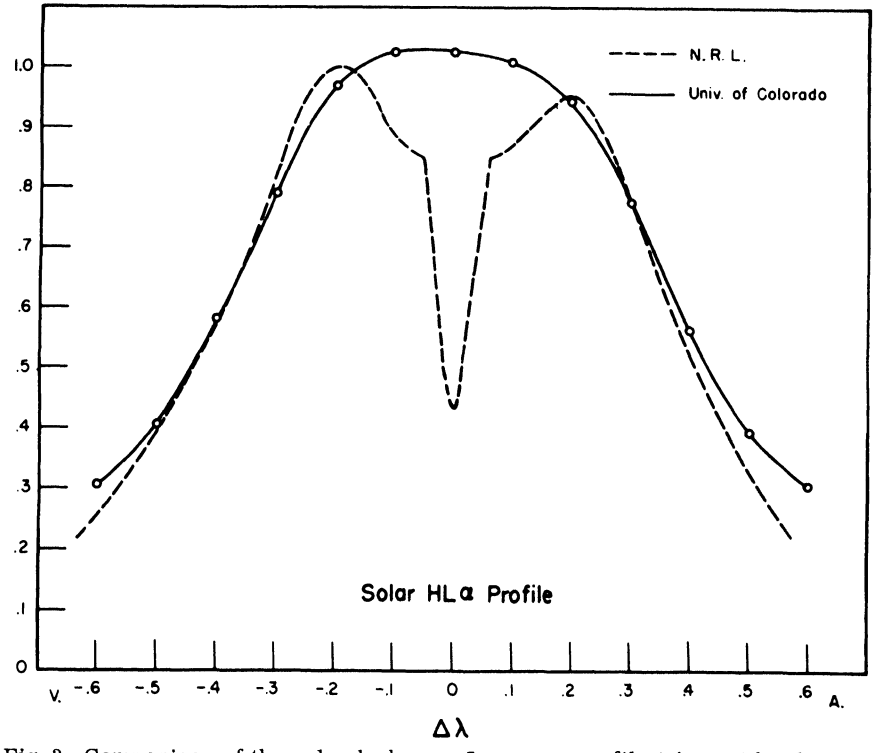


Fig. 3. Comparison of the solar hydrogen Lyman-α profile taken with a low resolving power and low dispersion instrument (University of Colorado) with one taken with high resolving power and high dispersion (N.R.L.). Both give about the same half-width, but the central absorption dip is completely absent from the low dispersion profile, although the flattened top is an indication of its presence. Relative intensities are plotted against wavelength intervals in A units from the center point of the line. The short wavelength side is to the left.

pare this profile with that obtained by a NRL group[8] (dotted line in Fig. 3) using an instrument at very high dispersion and resolving power. The half-width of the low resolution profile of Fig. 3 checks favorably with that of the NRL profile, but the absorption dip details are missing.

PHOTOGRAPHS OF THE SUN'S DISK IN HYDROGEN LYMAN-ALPHA LINE

A monochromatic camera employing lithium fluoride optics was designed and constructed for photographing the sun's disk in the light of the hydrogen Lyman-α line. Light passes thru a lithium fluoride prism which separates the hydrogen Lyman-α radiation from the intense visible radiation and directs the former to another prism which neutralizes the dispersion. The resulting beam is focused by a convex lens onto SWR film to give the final image of the sun. A photograph was obtained with an exposure of about 2 seconds.[9]

The images were very faint and of relatively poor quality. Scattered light background was at a high level. Nevertheless the greater intensity of Lyman-α radiation in the plage areas was clearly indicated. Comparison with photographs of the solar disk in the light of the visible hydrogen-α line and the calcium II lines verified the location of the plage areas. The enhancement in the plage areas was measured to be about a factor of 2 to 3 over surrounding areas. These conclusions were verified by excellent photographs taken by an NRL group.[5]

LIMB DARKENING IN SOLAR HYDROGEN LYMAN-ALPHA LIGHT

Solar limb darkening in hydrogen Lyman-α radiation was measured on spectrograms obtained during an Aerobee flight of December 15, 1955.[10] The grating had a radius of 39 cm, a constant of 6000 lines per cm and was set for an angle of incidence (49°) to eliminate astigmatism at hydrogen Lyman-α. The slit width was 12 microns. The procedure used for measuring limb darkening was based on the densitometry of the hydrogen Lyman-α spectrum line. Three densitometer tracings were made on each spectrogram. A given tracing was made along the length of the line down the center covering a width of about 1.2 A of the line. Background effects were eliminated by making two similar tracings, parallel to the first, outside the line. From the appropriate characteristic curves for the film in both visible light (corresponding to the scattered light background) and hydrogen Lyman-α light, relative intensities along the line could be found. These data were utilized in computing limb darkening. The intensity of any point on the spectrum line depends upon the integrated intensity over a thin section across the face of the sun perpendicular to the slit. By means of the proper transforms it is possible to express the

intensity at a point on the sun in terms of this integrated intensity along the line if one can assume circular symmetry. The following equation in the customary notation expressed the averaged results for the spectrograms considered:

$$I = 1 - (0.06 \pm 0.32) \cos \theta.$$

Apparently there is very little limb darkening insofar as this average result is concerned. However more decided effects existed for the individual spectrograms. These were readily accounted for by peaks of intensity in the densitometer tracings corresponding to plage areas on the sun's disk. Indeed this investigation was the first evidence of enhanced hydrogen Lyman-α radiation in plage areas and anticipated the results of the disk photograph mentioned in the previous section.

SOLAR EMISSION LINES IN THE EXTREME ULTRAVIOLET

On June 4, 1958 and March 30, 1959 solar ultraviolet spectrograms were obtained from Aerobee-Hi rockets flown at Holloman Air Force Base, N.M. The same instrument was employed in both cases except for a change of gratings; the instrument design was patterned after the spectrograph described in a previous section above, namely a grazing-incidence type with a toroidal focusing mirror also set at grazing-incidence. The film was SWR (Eastman-Kodak Co.). On the second flight, which produced the better spectrograms, a resolving power of about 4800 was achieved at Lyman-α. However, the latter spectrograms had numerous scratches and cracks which made the emission line analysis difficult. Two spectrograms from each flight were measured and only those lines were considered which appeared on all four spectrograms to a measurement accuracy equivalent to 0.5 of an Angstrom. An outstanding feature of the solar ultraviolet spectrum in the extreme ultraviolet is the intense He II emission line at 303.8 A.[11] The He I emission line at 585 A was much less intense at the altitude reached by the rockets (around 200 km). Numerous lines of ionized oxygen, nitrogen and carbon were readily identified. In Table III are shown wavelenths of lines which were identified with the aid of Charlotte Moore's tables. In addition to these identifications some tentative ones have been made such as the Ne VIII line at 83.9 A. The lines of Table III are to be compared with those obtained by an NRL group. About one-half of the measured lines were not identified. Many of the lines represent higher grating orders of one line. It was characteristic of both gratings that for the corresponding region 0 to 1200 A, the first, second and third orders of lines in the extreme ultraviolet appeared with about equal intensity. Further spectrograms, free of scattered light and with better exposures, are desired before much more identification work can be done in the extreme ultraviolet. The intensity of the 303.8 A He II line was measured in a semi-quantitative way. The speed of the spectrograph was assumed to be the same at this line as at Lyman-α and film sensitiv-

TABLE III
Identified Solar Emission Lines Below 1216 A, as Obtained from Rocket Data

Observed Wave Length	Estimated Intensity	Possible Emitter	Laboratory Wave Length
1215.7.....	1000	H	1215.7
1206.5.....	75	Si III	1206.5
1200.2.....	10	N I	1200.2
1195.0.....	10	C I	1194.5
1192.9.....	10	C I	1193.0
1189.8.....	5	C I	1189.7
1176.2.....	5	C III	1176.0
1169.1.....	10	N I	1168.5
1167.7.....	25	N I	1167.4
1158.1.....	5	C I	1158.1
1134.4.....	20	N I	1134.4
1085.1.....	10	N II	1085.7
1040.9.....	5	O I	1040.9
1038.2.....	40	O VI	1037.6
1032.2.....	30	O VI	1031.9
1025.7.....	60	H	1025.7
.....	.....	O I	1025.8
1009.8.....	10	C II	1010.7
990.0.....	15	N III	989.8
997.0.....	30	C III	977.0
972.9.....	10	H	972.5
964.5.....	10	N I	964.6
943.7.....	10	S VI?	944.5
932.2.....	10	S VI?	933.4
916.0.....	10	N II	916.0
913.0.....	10	S II	912.71
911.4.....	100	He II	.....
905.5.....	5	S II?	906.9
902.9.....	5	C II	903.6
858.2.....	10	C II	858.1
835.2.....	5	O III	835.3
834.0.....	5	O III	833.7
.....	.....	O II	834.5
791.2.....	5	O IV	790.2
779.4.....	5	O IV	779.8
764.5.....	10	N III	764.4
703.3.....	20	O III	702.9
687.3.....	15	C II	687.4
651.5.....	10	C II	651.3
644.9.....	20	N II	644.8
630.3.....	20	O V	629.7
625.1.....	5	O IV	625.1
611.4.....	5	O III	610.9
609.8.....	5	O III	609.7
.....	.....	O IV	609.8
.....	.....	Mg X	610
608.5.....	5	O IV	608.4
607.6.....	50	He II	.....

TABLE III (CONTINUED)

Wave Length	Estimated Intensity	Possible Emitter	Laboratory Wave Length
599.2.....	5	O III	599.6
597.9.....	5	O III	597.8
584.7.....	10	He I	584.3
553.7.....	10	O IV	554.1
539.2.....	5	O II	539.1
538.8.....	5	C III	538.3
.....	.....	O II	539.1
.....	.....	O II	538.3
536.5.....	5	He I	537.0
525.8.....	15	O III	525.8
463.8.....	10	S VI?	464.7
435.1.....	25	O III	434.9
430.7.....	10	O II	430.2
419.4.....	10	C IV	419.5
373.6.....	15	O III	374.1
.....	.....	N III	374.2
372.2.....	10	C III	371.7
344.7.....	20	O III	345.3
310.1.....	10	C III	310.2
303.8.....	30	He II	303.8
280.0.....	5	O IV	279.9
260.0.....	5	O IV	260.4
257.1.....	20	He II	256.3
243.3.....	10	He II	243.0
238.5.....	5	O IV	238.6
237.1.....	10	He II	237.3
234.6.....	5	He II	234.3
184.7.....	5	O VI	184.1
172.7.....	5	O VI	172.9
171.9.....	5	O V	172.2
150.0.....	10	O VI	150.1
83.9.....	30	Ne VIII?	85

ity relative to the latter line was estimated by assuming constant photon efficiency for the film. The intensity was measured relative to the hydrogen Lyman-α line. The results are shown in Table IV. It will be observed that both flights give comparable results. At the time of the first flight there was considerable solar activity with intense plage areas dominating the sunspot regions. During the second flight solar activity, though above average, was at a lower level than for the first flight. The intensity measurements were in line with those made by H. Hinteregger[12] who used a different technique.

It is evident that most of the solar ultraviolet lines that have been measured and identified arise in the chromosphere of the sun. Some however must arise in the corona where the temperatures are very much higher. A likely example is O VI. It is believed that the numerous lines of this ion are excited by recombination with electrons of O VII ions in the corona.[13]

SOURCE OF IONIZATION IN THE F-LAYER

The high intensity of the He II line at 303.8 A calls attention to the possibility that the ionization of the earth's atmosphere in the F-layer may be brought about by photoionization of atoms and molecules in that region. The He II line itself is of sufficient intensity to contribute significantly to this process. Other lines, though much less intense, when taken in total, must produce appreciable additional contribution.

TABLE IV
Solar He II 303.8 A Line Intensities

Date	Zenith Angle of Sun	Altitude (km)	Intensity erg/cm^2/sec
June 4, 1958	80°	140	0.04
March 30, 1959	60°	175	0.20
March 30, 1959	60°	195	0.40
June 4, 1958	80°	212	0.80

Assuming that the 303.8 A line is the sole cause of ionization in the F-layer, and that the ionization mechanism is only that of the ionization of the oxygen atom, one can account in part for the observed electron densities in the F-layer.[14] The basic equation is for $\lambda = 304$ A, and for a given height:

$$N = [(1/\alpha)\ (q - dN/dt)]^{\frac{1}{2}} \qquad (3)$$

where N is the electron density,

α is the recombination coefficient (electrons and oxygen),

q is the number of electrons produced per cm^3/sec, and is proportional to the oxygen atom density and the incident photon flux.

When reasonable values of the constants are substituted, the results are quite in line with observed densities. Observed and calculated values of electron densities at several altitudes based on data from two independent rocket flights[14,15] are shown in Table V. The observed electron densities were in most cases reduced ionograms taken at White Sands, New Mexico at the times of the flights.

Although the computed electron densities are less than the observed ones, this fact is to be expected because ionization radiation other than the helium 303.8 A line cannot be ignored and must contribute something to the ionization. For example, the 584 A line of neutral helium and numerous other emission lines in the extreme ultraviolet combine their effects. Until more quantitative data on these intensities, and until better values of the approximate coefficients are known, as well as the composition of the upper air in the F-layer region, the problem cannot be completly resolved.

THE SOLAR SPECTRUM IN THE REGION 2200 TO 1800 A

An atlas of the solar spectrum covering the range 2200 to 1800 A has been prepared from rocket spectrograms obtained during an

aerobee flight of Aug. 6, 1957. The spectrograms exhibited excellent focus; the resolving power was of the order of 6000 and the dispersion 0.045mm/A. An elaborate program of wavelength determination and identification was undertaken.[18] To aid in the measurement the rocket spectra were compared with the spectrum of iron taken in the laboratory with the rocket instrument. Several hundred Fraunhofer lines were identified. The solar spectrum between 3000 and 1800 A is reproduced in Fig. 4. Enlarged partions of the solar ultraviolet spectrum are shown in Fig. 5.

TABLE V
Electron Density Predictions in F-Layer

(km)	Date of Flight	Quanta/cm/sec (303.8 A line)	Predicted N (electrons/cm^3)	Observed N (electrons/cm^3)
140	4 June 1958	$.7 \times 10^8$	3.6×10^5	1.05×10^5
175	30 March 1959	3.2×10^9	7.6×10^5	2.3×10^5
195	30 March 1959	6.4×10^9	8.1×10^5	3.8×10^5
212	4 June 1958	1.3×10^{10}	4.5×10^5	2.21×10^5

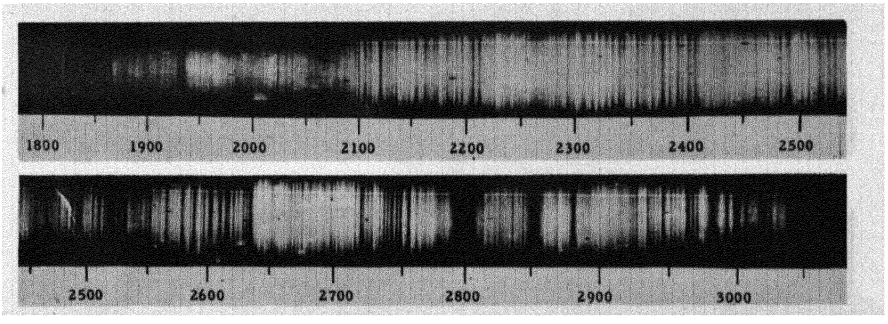
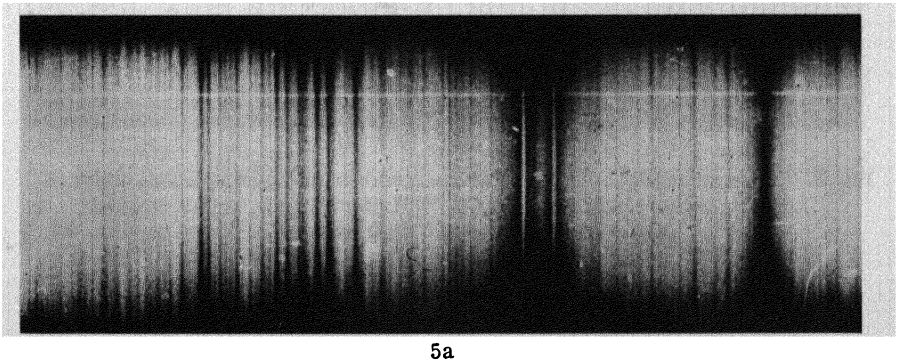


Fig. 4. Solar spectra from a rocket flight of August 6, 1957. Upper spectrum: 1800-2500 A taken at an altitude of approximately 140 km; exposure time 12.1 seconds. Lower spectrum: 2500-3000 A taken at an altitude of approximately 110 km; exposure time 5.2 seconds.



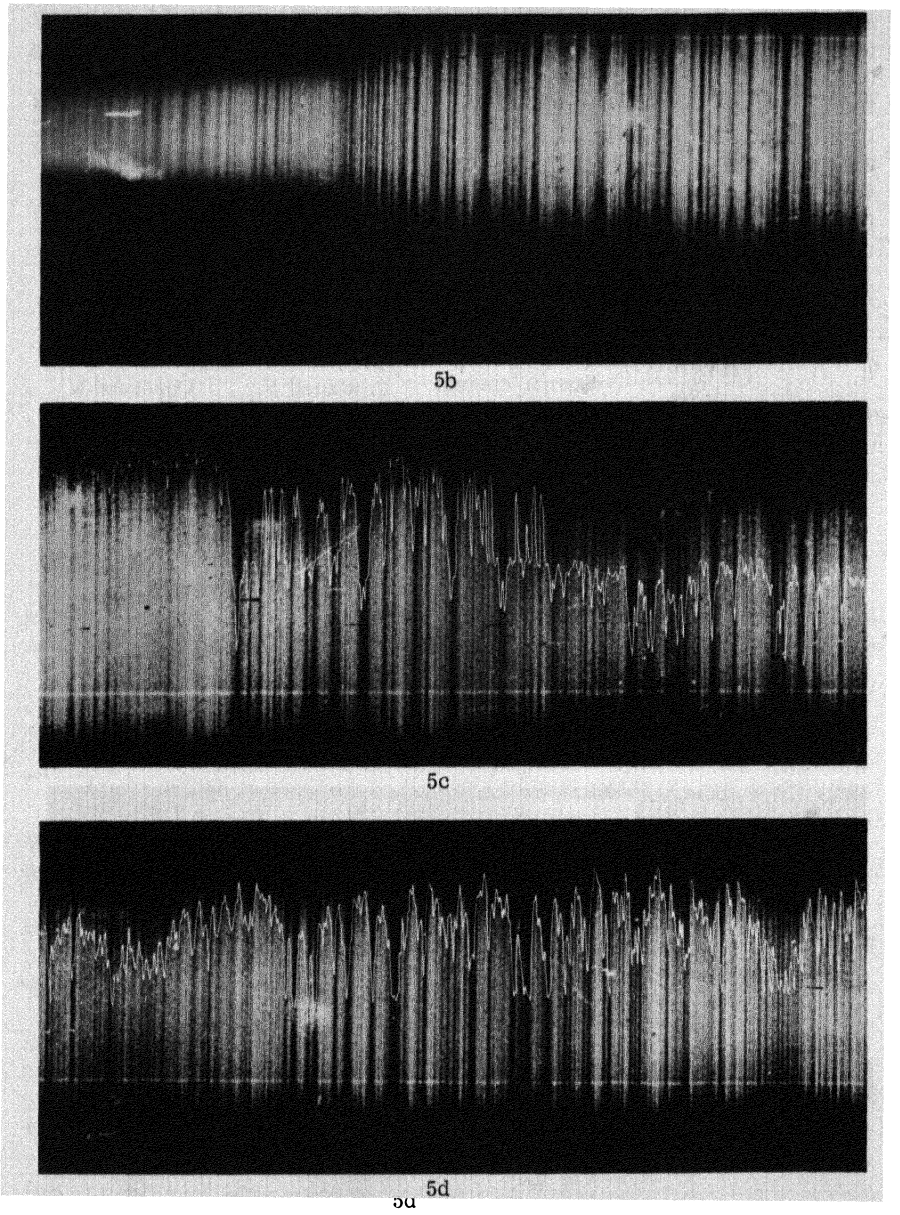


Fig. 5. Enlarged sections of the solar spectrum from spectrograms obtained during rocket flight of August 6, 1957. Section (a), region around 2800 A showing emission cores of Mg II absorption lines. Section (b), region around 2100 A showing the abrupt drop in intensity of the solar spectrum at about 2075 A. Sections (c) and (d) are of regions 2462-2672 and 2237-2470 A, respectively, and have microdensitometer tracings superimposed. The short wavelength side is to the left in all cases.

REFERENCES

[1]Hass, G. and Tousey, R., "Reflection Coatings for the Extreme Ultraviolet," J. Opt. Soc. Amer., vol. 49, no. 6, 1959, pp. 593-602.

[2]Beutler, H. G., "The Theory of the Concave Grating," Review of Modern Physics, vol. 35, no. 5, 1945, pp. 311-350.

[3]Rense, W. A. and Violett, T., "Method of Increasing the Speed of a Grazing-Incidence Spectrograph," J. Opt. Soc. Amer., vol. 49, no. 2, 1959, pp. 139-141.

[4]Behring, W. E., Jackson, J. M., Miller, S. C. and Rense, W. A., "Monochromatic Camera for Photography in the Far Ultraviolet," J. Opt. Soc. Amer., vol. 44, no. 3, 1954, pp. 229-231.

[5]Purcell, J. D., Packer, D. M. and Tousey, R., "Lyman-Alpha Photographs of the Sun," Nature, London, vol. 184, 1959, pp. 8-10.

[6]Aboud, A., Behring, W. E. and Rense, W. A., "Emission-Line Intensities in the Solar Ultraviolet," Ap. J., vol. 130, no. 2, 1959, pp. 381-383.

[7]Behring, W. E., McAllister, H., and Rense, W. A., "Ultraviolet Emission Lines in the Solar Spectrum," Astrophysical J., vol. 127, no. 3, 1958, pp. 676-679.

[8]Tousey, R., "Ultraviolet Spectroscopy of the Sun," p. 13, this volume. Research to be published.

[9]Mercure, R., Miller, S. C., Rense, W. A. and Stuart, F., "The Sun's Disk in Lyman-Alpha Radiation," J. Geophys. Res., vol. 61, 1956, pp. 571-573.

[10]Miller, S. C., Mercure, R. and Rense, W. A., "Lyman-Alpha Intensity and Solar Limb Darkening from Rocket Spectrograms," Astrophys. J., vol. 124, no. 3, 1956, pp. 580-585.

[11]Violett, T. and Rense, W. A., "Solar Emission Lines in the Extreme Ultraviolet," Astrophys. J., vol. 130, no. 3, 1959, pp. 954-960.

[12]Hinteregger, H. E., "Telemetering Monochromator Measurements of Extreme Ultraviolet Radiation," p. 78, this volume.

[13]Varsavsky, C., "Some Atomic Parameters for Ultraviolet Lines." Research to be published.

[14]Rees, M. H. and Rense, W. A., "Note on the Cause of Ionization in the F-Region," J. Geop. Res., vol. 64, no. 9, 1959, pp. 1251-1255.

[15]Violett, T., Thesis, "Solar Spectrum in Extreme Ultraviolet," 1959, Univ. of Colorado.

[16]McAllister, H., Thesis, "Solar Ultraviolet Spectrum, 1800 A to 2200 A," 1959, Univ. of Colorado.

3. TELEMETERING MONOCHROMATOR MEASUREMENTS OF EXTREME ULTRAVIOLET RADIATION
PART I: Introduction and Technology

H. E. Hinteregger
Geophysics Research Directorate
Air Force Research Division
Bedford, Massachusetts

1. INTRODUCTION

Solar extreme ultraviolet radiations (EUV) and soft x-rays are known to be absorbed very strongly in the upper parts of the terrestrial atmosphere (e.g. see Goldberg (1954); Watanabe (1958)). Therefore, their measurement requires experimentation at altitudes high above the earth's surface. The specific altitude at which the optical depth of the atmosphere above becomes less than a certain value, say unity, depends not only on the wavelength and the solar zenith angle but also on many other physical parameters. A quantitative description of all these parameters requires a considerable improvement in the existing knowledge of diurnal, seasonal, latitudinal, and other variations in the structure of the upper atmosphere. Indeed measurements of solar EUV absorption in the atmosphere are an invaluable source of such information (see II; 1).

If the prime interest is that of solar physics and not that of terrestrial aeronomy, the absorption by the terrestrial atmosphere (i.e. the part above the point of observation), is merely an undesirable effect, which one must overcome experimentally by going to sufficiently high altitudes, or at least take into account theoretically by corrections based on the current knowledge of the absorption characteristics of the upper atmosphere.

To this date, solar EUV spectrographs (U. Colorado, NRL, GRD) and telemetering monochromators (GRD) have been operated on vehicles with maximum altitudes no greater than about 220 km. At this altitude the atmospheric absorption is not completely negligible, at least not for all the wavelengths investigated. In fact, there are many important solar emission lines (e.g. He I 584 A; Mg X 610, 625 A; O VI 790 A; Ne VIII 770, 780 A; H Ly-γ 972 A) for which a point of observation as high as 220 km is probably still optically rather deep in the earth's atmosphere. Therefore, the need to extend rocket experiments with EUV monochromators to much higher altitudes is quite obvious. The

achievement of higher altitudes alone, however, will solve but one experimental problem of solar EUV spectrophotometry. This problem is to make sure that the solar EUV fluxes $\Phi(\lambda, h)$ actually measured at some altitude h in the terrestrial atmosphere would not be significantly different from the "incident" fluxes, $\Phi_0(\lambda)$, defined as those fluxes "on top of the earth's atmosphere" in the interplanetary space.

Another important experimental problem arises from the relatively short time of actual data acquisition by a rocket-borne monochromator. This sets a rather low limit to the total amount of information that can be acquired with any given instrument in one flight. Much of this limitation is of a basic nature (see I; 3.3., 4.4.) so that improvements in technology alone can never substitute fully for a longer time allotted for a specific measurement. Therefore, even the most advanced telemetering monochromators will not be capable of fulfilling simultaneously the different desirable experimental conditions, as would be possible were it permissible to ignore all *considerations of time*. These considerations must cover not only the *experimental periods of time* alloted for various procedures of measurement, but also any *physically significant periods of time*, during which changes may occur in the natural conditions. Such changes are of importance not only with respect to the phenomena to be investigated, but also to all those which can affect directly or indirectly the instrumental detection and measurement of the desired quantities.

The foregoing remark leads to an area of experimental problems which deserves the most serious attention. The whole problem of *backgrounds* and the *stability of all important instrumental parameters* for a largely unknown environment will have to be studied for some time experimentally until we can judge reliably which specific experiments can be considered practical in terms of existing technology and resources. Measurements of EUV and x-ray fluxes of different origins (direct solar, scattered solar, planetary, interplanetary, stellar, or interstellar) appear to be desirable for many different scientific purposes that impose vastly different requirements on spectral resolution, detectivity, absolute accuracy, response time, and accuracy of pointing in space.

These divergent requirements of many equally important fields of research suggest strongly that, at the time of this writing and for the near future, it would be quite impractical to design and construct one *universal instrument* attempting to fulfill the divergent requirements of the different disciplines of research. Another, though not technical, objection against such an approach would be the following. It appears that it would require a radical centralization of the various groups of researchers with all their rightfully diverging specific interests, simply because no individual, and not even any existing individual group, could conceivably develop such a universal instrument within a foreseeable period of time. During the same time, much more real progress would probably be made by combining the results of the essentially independent work of the individual groups. Even though some coordination will be essential and occasionally mandatory, the co-

operation will probably be most effective if it can remain on an informal, self-generated, and flexible basis. In the alternative approach of a more stringent centralization, the possible gain in economical and technological efficiency per individual or per group would probably be more than offset by the loss in depth and the loss of productive freedom. Even a considerable amount of "duplication" appears to be not only "excusable" but actually necessary for reasonably fast progress. Obviously, these remarks express the author's strictly personal viewpoint on a problem which does not belong to experimental physics. Problems of this type are of course common with any research activity. The contemplated future work in EUV and x-ray spectrophotometry, however, requires such advanced and costly space vehicles, that problems of coordination and organization assume an unusually high degree of importance. This is mentioned here, because actual progress in the new experimental field of EUV spectrometry appears to depend on the solution of this organizational problem as much as on the solution of the truly experimental work.

The goal of the early work by the author and his co-workers at the Geophysics Research Directorate (GRD) was primarily to demonstrate that solar EUV monochromators with wavelength scanning and photoelectric detection of the dispersed radiation (Hinteregger, Damon, Heroux, and Hall (1960)) could operate satisfactorily on a rocket. An obvious motive for this work was the desire to achieve direct telemetry, so that one could receive the spectrophotometric information on the ground without having to recover the instrument or a part of it from the rocket. The GRD instrument was designed to work with the same type of solar pointing control* that was developed some time ago by the University of Colorado (e.g. see Stacey, Stith, Nidey, and Pietenpol (1954)). This device has been used with good success for many rocket experiments involving photographic spectrometry of solar radiation in the past (e.g. Rense (1953); Jursa, LeBlanc, and Tanaka (1955); Johnson, Malitson, Purcell, and Tousey (1958)).

On March 12, 1959, the first successful performance of a telemetering solar EUV rocket spectrometer (scanning the wavelength range from 250 to 1300 A within about ten seconds per scan and resolving about 12 A) was recorded (loc. cit.). Since then, two more rocket monochromators (one for the same wavelength range from 250 to 1300 A, the other for the range from 60 to 320 A) have been flown successfully. The photon flux measurements obtained in these first flights have already been of considerable interest for terrestrial aeronomy and solar physics (see Part II). The most important results from a technological viewpoint, however, were the acquisition and subsequent augmentation of the practical information on details of the new techniques and on the performance of vital parts of the instrument, such as the photoelectric detector (Heroux and Hinteregger (1960); Hall and Hinteregger (1960)), that had never been flown before.

* Device designed to keep the optical entrance axis of the spectrometer in the direction to the sun.

Some of this experience will be described in the empirical part of the following discussions.

This discussion of techniques of EUV monochromator measurements will be far from complete. Auxiliary technologies such as those concerned with the general rocketry, power supply, telemetry, and the achievement of the necessary orientation of the optical instrument or at least its entrance axis in space, will not be discussed at all. Nevertheless, it should be emphasized that proper progress in these areas will be for some time among the most crucial limiting factors in the overall progress of extra-terrestrial experimental spectrometry of those wavelengths not accessible to terrestrial techniques, including measurements from balloons. Techniques of more or less monochromatic EUV or x-ray image formations, filter pinhole camera [Friedman], special optics of stigmatic monochromators [Tousey], zone plates for EUV [Baez, etc.] will be omitted, too, and non-dispersive techniques of EUV spectrophotometry will be discussed only briefly.

In general the reader should be aware of the author's experimental background; this has been limited to measurements of relatively strong EUV photon fluxes of solar origin, primarily in the interest of terrestrial aeronomy. These measurements required neither spatial resolution of the solar disk (in fact such resolution would have been undesirable) nor any spectral resolution of line shapes. Scanning speed and luminosity, however, have been quite important, because reasonably good resolution of the vertical attenuation profiles of monochromatic fluxes, $\Phi(\lambda, h)$ versus h, has been essential for the determination of the local atmospheric extinction coefficients, absorption rate densities, and the derivation of atmospheric scale heights (II; 1.) No artificial attempt has been made to eliminate the influence of this special interest (i.e. aeronomy) from the present article. Even the terminology (I;3.1.) and the schematic theory (I;3.1., 3.2., 3.3.) are likely to show some preference and possibly prejudice in favor of applications to the specific field of aeronomy. The author hopes, however, that colleagues interested mainly in fields other than that of aeronomy will still find much useful information, that may be directly applicable to some of their own experimental problems.

2. TYPICAL METHODS

2.1. Conventional Spectrophotometry

In the past, rocket measurements of solar EUV have been carried out by photographic detection techniques almost exclusively. (Rense, Tousey, and others, loc. cit.). Although the identification of specific solar emission lines from photographic spectrograms is very convenient, a quantitative determination of intensities from such records is well known to be difficult. For the wavelength range above about 500 A Tousey and his co-workers at the Naval Research Laboratory (NRL) have recently succeeded in improving the photographic techniques to a

remarkable degree. (See other article in this book.) This was made possible primarily by their successful suppression of the stray-light background by using two successive dispersions with gratings near normal incidence. For the wavelength range below about 500 A, however, it is necessary to use gratings in grazing incidence where the problem of scattered light is much worse. In fact, the photographic rocket spectrograms obtained so far in grazing incidence (Violett and Rense (1959)) are hardly adequate for any reliable densitometry. The background blackening of the photographic film in these grazing incidence spectrograms is serious even above 500 A and increases quite rapidly toward the central image (i.e. toward shorter wavelengths). Therefore, even the strongest emission lines from these spectrograms can be evaluated only crudely in terms of intensity.

Photographic measurements of absolute continuum intensities or absolute integral intensities for certain wavelengths bands of the solar EUV spectrum do not appear to be practicable.

The disadvantages of photographic detection techniques for rocket measurements of solar EUV are (a) the apparently inevitable sensitivity to stray light of longer wavelengths, (b) the need to recover the exposed film from the rocket vehicle, and (c) the cumulative background blackening due to any penetrating radiations. In the past, the latter (c) was no real problem because of the relatively short life of rocket experiments. The same effects would be far more serious, however, were photographic techniques used on satellite vehicles (particularly, if the orbit were to pass through regions of strong Van Allen belt radiation). The film recovery problem and the desire for direct data telemetry were probably the strongest stimuli for the development of non-photographic and even non-optical methods of measuring solar EUV photon fluxes in the upper atmosphere.

2.2. Dispersive Photoelectric Techniques

Photoelectric techniques of solar EUV spectrophotometry not only allow direct telemetry of the data, but also can be made so that the instrumental sensitivity to all stray light of longer wavelengths is virtually eliminated. Furthermore, for a photoelectric detector there is no accumulation of background due to penetrating radiations.

The development of telemetering solar EUV monochromators by the author and his co-workers of the Geophysics Research Directorate (GRD) has led to three successful flight experiments in 1959 and early 1960. These flights have confirmed the anticipated advantages of the new technique (see I;4.4.) and demonstrated the practicability of future experiments of this type for the physics of the solar system in general and the terrestrial atmosphere in particular (see part II). As research in the latter direction was the prime objective of the work at GRD, it is clear that the specific choice of instrumental parameters reflects this orientation. Many aspects of the instrumentation, however, will be useful also for applications other than those of terrestrial aeronomy. Therefore, a discussion of some important details of the rocket

instruments, the calibration procedures, and associated laboratory equipment has been included in this article (I; 4.).

2.3. Non-dispersive Techniques

Spectrographs as well as telemetering monochromators for solar EUV measurements require a pointing control, which must keep the optical entrance axis of the instrument in sufficiently accurate alignment with the incident solar rays. In the present stage of development, this pointing control alone requires about five times the weight and power of the completely equipped monochromator itself. The elimination of the need for a pointing control, however, was not the only motive for the development of non-dispersive techniques for EUV radiation measurements.

Other motives have been the desire to use much larger areas and solid angles for the interception of EUV radiation and to avoid the intensity loss inherent in optical dispersion. The pioneer work in rocket experiments of the non-dispersive type was started about ten years ago by Friedman's group of the Naval Research Laboratory (NRL). Since then, their measurements with gas-filled counters and ionization chambers with appropriately selected windows have led to a wealth of new information on integrated intensities over various regions of the solar EUV and x-ray emission spectrum. These measurements were not limited to the detection of direct solar radiation, but included successful investigations of scattered solar EUV as well as EUV of stellar origin (see another article in this book). Techniques and results have appeared in various publications and symposium reports, which are sufficiently well-known so that they need not be described here (see another article in this book). Friedman's experiments have demonstrated that the photoionization techniques are clearly superior to photographic techniques as far as the measurement of absolute intensities of solar EUV is concerned; particularly, the measurement of integral intensities over certain spectral sections.

It is known that gas-filled detectors with windows are not useful between about 1050 and 100 A. Fortunately, this gap does not exist for direct photoelectric emission analysis, carried out in vacuo. In fact, the aforementioned gap coincides essentially with the range of wavelengths for which high photoelectric yields can be obtained readily with materials which are at the same time conveniently insensitive to any visible or near ultraviolet radiation (Hinteregger and Watanabe (1953); Wainfan, Walker, and Weissler (1953); Walker, Wainfan, and Weissler (1955); Hinteregger (1954)).

The first estimates of solar EUV intensities from photoelectron retardation measurements were based on a rocket experiment of August 1958 (Hinteregger, Damon, and Hall (1959)). Since then, the techniques have been improved considerably (Hinteregger (1960)). The retardation analysis of photoelectric emission represents a truly "non-optical" type of spectrophotometry. As an experimental laboratory technique, it is actually older than grazing incidence grating

spectrometry and was used extensively in the early period of x-ray experimentation.

The photoelectric analysis used in rocket experiments until now has been of the simplest type (i.e. telemetry of the unmodified current voltage diagrams). Various other versions of purely electronic spectrophotometry, however, are also of interest for rocket and satellite experiments. As an example, one may use electronic differentiation of the photoelectric current-voltage curve before telemetry. In the case of a parallel plane geometry of the retarding potential analyzer, single differentiation then gives directly the so-called normal energy distribution of the emitted photoelectrons. This method is still straightforward and no uncertain assumptions are required to justify its principle of operation.

Unfortunately the same is not true for the scheme of double differentiation described by Sziklay and Schroeder (1946) and the scheme of triple differentiation described by Shinoda, Suzuki, and Kato (1956). These schemes suffer mainly from the fact that their principles of operation depend critically on the applicability of the well-known Fowler-Du Bridge model of photoelectric emission. This model is a good one only for wavelengths relatively close to the threshold of the ordinary photoelectric surface effect, but not for the much shorter wavelengths of the EUV. In the EUV range, this theoretical picture is quite incompatible with the actual energy distribution of the emitted photoelectrons. A more detailed discussion of this topic, however, is not within the scope of this article.

3. SCHEMATIC DESCRIPTION OF MONOCHROMATOR MEASUREMENTS

3.1. Terminology

To discuss the characteristics of telemetering monochromator measurements of solar EUV fluxes some explanation of the terminology used is required. It is convenient here, to introduce the essential quantities with the fairly narrow definitions listed below, so that lengthy qualifying remarks may be omitted from the discussion without much danger of confusion.

λ designates the correct wavelength setting of the monochromator, that is the setting "peaked" for maximum dispersed intensity signal when the instrument is illuminated with monochromatic radiation of true wavelength $\lambda_0 = \lambda$. We may use the same notation, λ, for both monochromator setting (nominal wavelength) and true wavelength of the dispersed radiation, whenever the meaning is clear.

$\dot{\lambda} \equiv d\lambda/dt$ designates the wavelength scaning speed of the monochromator. For a chosen bandwidth $\Delta\lambda$, this speed determines the time of measurement, Δt, of some narrow emission line ($\delta\lambda_0 \ll \Delta\lambda$) within each complete wavelength scan of the instrument ($\Delta t = \Delta\lambda/\dot{\lambda}$).

$\Delta\lambda$ designates the instrumental bandwidth, defined as the range of

λ-settings over which a significant dispersed intensity signal (first order diffraction unless otherwise stated) is produced, when the monochromator is illuminated with monochromatic radiation. In our present instruments (GRD) this bandwidth $\Delta\lambda$ is determined by the widths of the entrance and exit slit and not by the resolving limit of the diffraction grating.

The geometrical slit widths, W_{ent} and W_{ex}, are given as actual dimensions in the plane of dispersion, measured in the directions perpendicular to the entrance axis and the centerline of the diffracted beam respectively. For a given instrument, these slit widths correspond to a certain entrance bandwidth $(\Delta\lambda)_{ent}$ or exit bandwidth $(\Delta\lambda)_{ex}$, defined as the bandwidth which the instrument would have, if the exit slit or entrance slit respectively were narrowed to a negligible width. The "height" of a slit is always given as its length, L, in the direction perpendicular to the plane of dispersion.

$S(\lambda)$ designates the dispersed intensity signal due to that part of the incident radiation which is of wavelength $\lambda_0 = \lambda \pm \frac{1}{2}\Delta\lambda$. This intensity signal is measured by recording a certain number of counts, ΔN_S, within the time of measurement, Δt. Unless stated otherwise, it is assumed that $S(\lambda)$ is the corrected counting rate. This correction implies the discarding of background counts of all types, ΔN_B. It will be noted separately whether or not this correction also implies an elimination of counts due to radiation dispersed in higher orders of diffraction. Whenever a higher order diffraction is considered to be the interesting part of the observation, a modified notation will be used. For instance we may write $S(2 \times 584\ A)$ for the counting rate due to incident 584 A radiation recorded with a monochromator setting of 1168 A.

$B(\lambda)$ designates the total background counting rate obtained from the monochromator in a given wavelength setting under the actual conditions of the experiment. Two rather different contributions should be distinguished. There is a basic background B_0 that would persist even if the entrance slit were completely closed.* Besides the basic background B_0, there is also a background $B_{st}(\lambda)$ which is due to any stray light from the grating. Naturally, the value of B_{st} is a function of the monochromator setting λ. Its magnitude is essentially proportional to $(\Delta\lambda)_{ent}$ and proportional to $(\Delta\lambda)_{ex}$, i.e. proportional to $(\Delta\lambda)^2$ for the case of matched slits. The basic background B_0, however, depends neither on the wavelength setting nor the specific choice of slit widths. As the counting rate B_{st} depends only on that part of the total stray light from the grating for which the photon energies are higher than the photoelectric threshold of the detector, the ratio of signal to

*As a consequence of instrumental improvements, B_0 in the 29 January 1960 flight was close to the limit expected to be due to cosmic rays. In principle, this limit could be further decreased by an anti-coincidence arrangement of cosmic ray counters around the detector. For large sensitive detector areas, this step may have to be taken to obtain significant signals for measurements with higher resolution. A simpler solution, of course, is to make the detector smaller, as long as this is compatible with the experiment.

stray light background, $S(\lambda)/B_{st}(\lambda)$, can be made higher by several orders of magnitude than the corresponding contrast that could be achieved in photographic measurements of the solar EUV or x-ray spectrum.

$\varepsilon(\lambda)$ designates the overall spectral photon counting efficiency of the monochromator, as illustrated in Fig. 1, and is defined as the probability of recording one signal count for one incident photon of wavelength $\lambda_0 \pm \delta\lambda_0$ passing through the entrance slit, when the monochromator is set to this wavelength ($\lambda = \lambda_0$). To be more specific, it is assumed that the incident photons are sufficiently monochromatic with respect to the instrumental bandwidth, $\delta\lambda_0 \ll \Delta\lambda$, and that the directions of incidence are within a certain, relatively small angle measured with respect to the optical entrance axis (e.g. 0.02 radian)

$\Phi(\lambda)$ designates the flux density (abb. "flux") of photons of wavelengths $\lambda \pm \frac{1}{2}\Delta\lambda$ with directions of incidence within a certain angle measured with respect to the instrumental entrance axis. Unless otherwise stated, this axis is assumed to be parallel to the central solar ray and the limiting acceptance angle is assumed to be about 0.02 radian. This monochromatic flux is measured as

$$\Phi(\lambda) = \frac{S(\lambda)}{A\,\varepsilon(\lambda)} \tag{1}$$

where $\varepsilon(\lambda)$ is the spectral photon counting efficiency of the monochromator explained above and A is the area of radiation collection measured in a plane perpendicular to the central solar ray. For the GRD monochromators, the area A is equal to the product WL (width $\times$ height of entrance slit).

The so-defined flux Φ is expressed in units of photons per cm^2 per second and should be distinguished clearly from the differential spectral flux Φ_λ [ph $cm^2 sec^{-1} A^{-1}$], where A is the Angstrom unit. The latter is a differential quantity whereas the flux $\Phi(\lambda)$ is a practically more convenient quantity, which represents the integral flux within the instrumental wavelength bandwidth,

$$\Phi(\lambda) = \int_{\lambda - \frac{1}{2}\Delta\lambda}^{\lambda + \frac{1}{2}\Delta\lambda} \Phi_\lambda d\lambda \tag{2}$$

For solar emission lines that are narrow with respect to the instrument bandwidth, the quantity $I(\lambda) \equiv h\nu\Phi(\lambda)$ therefore represents the integral line intensity in terms of energy flux density [erg cm^{-2} sec^{-1}], provided of course that the integral of the spectral continuum flux over $\Delta\lambda$ is negligible. On the other hand, if there are no emission lines within the band $\Delta\lambda$ around wavelength λ, the differential continuum flux, Φ_λ, is simply given by the expression $\Phi(\lambda, \Delta\lambda)/\Delta\lambda$, as long as Φ_λ is sufficiently slowly variable over the instrument bandwidth. The differential continuum intensity, measured in [erg cm^{-2} sec^{-1} A^{-1}], is given as $I_\lambda \equiv h\nu\Phi_\lambda$ (cont.). The same formal relationship as that for the continuum should be used for the evaluation of the shape of solar emission lines, which may be measured with monochromators of con-

siderably greater resolving power than that chosen for the present GRD instruments. The choice for the latter was dictated by a number of practical reasons discussed later in this paper.

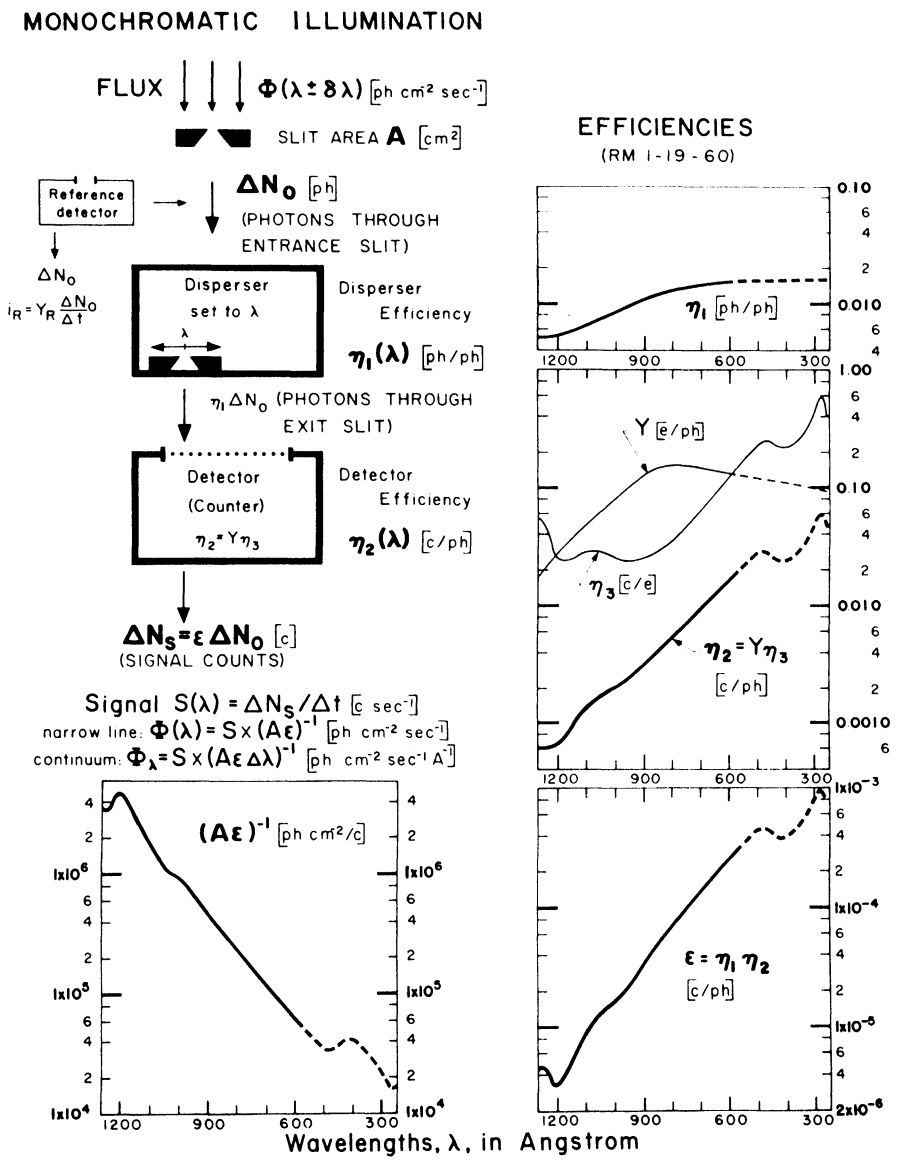


Fig. 1. Schematic diagram explaining solar monochromator measurements, spectral calibration, and individual efficiencies. Numerical values refer to the rocket instrument flown on January 19, 1960.

3.2. Spectral Calibration

The experimental determination of the spectral photon counting efficiency $\varepsilon(\lambda)$ over the entire wavelength range of a telemetering monochromator is the ultimate goal of preflight calibration work in the laboratory. Although considerable progress has been achieved toward this goal, much more remains to be done, particularly in the wavelength range below about 300 A.

In the calibration method used for the GRD monochromators, the counting rate $S(\lambda)$ is observed under monochromatic illumination of the entrance slit and compared with the photoelectric saturation current $i_R(\lambda)$ from a reference cathode that can be placed between entrance slit and grating of the rocket instrument (see I; 4. Fig. 8). The ratio $eS/i_R \equiv \eta(\lambda)$, where e is the electronic charge, then expresses a spectral efficiency of the instrument in terms of recorded counts per unit number of photoelectrons that would be emitted from the reference cathode if it intercepted the admitted beam for the same length of time as the counts are recorded. As long as the reference cathode can be moved in and out without disturbing the monochromatic illuminating conditions, little error is introduced by the fact that $S(\lambda)$ and $i_R(\lambda)$ are not really measured simultaneously. Then, the overall spectral photon counting efficiency $\varepsilon(\lambda)$ as defined in this paper is simply given as the product $\eta(\lambda)Y_R(\lambda)$, where $Y_R(\lambda)$ designates the yield of the reference detector. This yield $Y_R(\lambda)$ is defined as the probability of one photoelectron's being emitted from the reference cathode for one incident photon of wavelength λ. In the future, the expression "spectral photon counting efficiency" will be reserved for the quantity $\varepsilon(\lambda)$ as defined here and our previous use (loc. cit.) of essentially the same name for the quantity $\eta(\lambda)$ should be abandoned. Whenever a verbal expression for $\eta(\lambda)$ is desired, we shall use a different name such as relative efficiency or calibration factor η.

In the region of wavelengths from about 500 to 60 A (short wavelength limit of GRD instrument) the accuracy of the determination of $\varepsilon(\lambda)$ falls off significantly towards the shorter wavelengths. This is due to the combined uncertainties in the knowledge of absolute photoelectric yields of the reference detector, $Y_R(\lambda)$, and the calibration factor $\eta(\lambda)$. These uncertainties lead to a possible error in $\varepsilon(\lambda)$, which increases from about 30% at 500 A to an estimated factor of 2 at 300 A. Below 300 A, a quantitative estimate of the error in $\varepsilon(\lambda)$ seems premature, because laboratory techniques for converting observed counting rates $S(\lambda)$ into absolute fluxes $\Phi(\lambda)$ are still in their infancy. Experimental laboratory work now in progress is expected to extend the absolute determination of $\varepsilon(\lambda)$ to at least 60 A with an error of less than a factor of 2 in the near future. A significant improvement of the situation is expected from the introduction of a large windowless ion-chamber (with differential pumping) to be used instead of the tungsten cathode (loc. cit.) as the reference detector (see Fig. 1) for laboratory calibrations. Much more progress, though, may be achieved by a completely different approach to absolute spectral calibrations as sketched below.

The need to work with already monochromatized EUV radiation for laboratory calibrations of rocket monochromators (see Fig. 1) arises from the lack of conventional laboratory sources of sufficiently well-known absolute (or even relative) spectral intensity distribution for this wavelength range. Fortunately a very efficient though unconventional "light source" is in fact available in the form of electron synchrotrons. The classical acceleration radiation of the orbiting electrons (Schwinger (1949); Tomboulian and Hartman (1956)) seems to offer a nearly ideal solution of the urgent experimental need for "standards" for quantitative calibrations in the EUV and x-ray region. Naturally a number of practically important details remain to be worked out, before this simpler and more direct calibration method may become a practical one. We may hope that it will eliminate both the need to use two monochromators in series and the need to depend on reference detectors of poorly known absolute efficiency below about 300 A.

3.3. Limitations and Compromises

The basic operation in measuring solar photon fluxes with rocket or satellite monochromators can be described as the counting of a certain number of signal pulses within a certain time, Δt. The number of counts measured between time t and time $t + \Delta t$ with a constant monochromator setting λ,

$$\Delta N = \Delta N_S + \Delta N_{B_0} + \Delta N_{B_{st}}, \tag{3}$$

can be separated in the convenient form

$$\Delta N = [S(t) + B_0(t) + B_{st}(t)]\,\Delta t, \tag{4}$$

only under certain conditions. These conditions deserve a detailed discussion, because some of them are in fact incompatible for various cases of practical importance.

The separation in Eq. 4 is obviously justified, if the physical causes for both signal and background counts remain constant during the time Δt, and furthermore, if Δt is sufficiently large so that the *statistical fluctuations* are smaller than a certain chosen percentage. Unfortunately, the choice of a long time Δt is not in favor of the first essential assumption of constancy of the physical causes of the observed counts. In particular, one is concerned with the constancy not only of the emission intensity but also of the absorption along the path between instrument and source, which determine the photon flux density at the point of observation. Furthermore, one has to consider the relative constancy of the causes of background counts, such as scattered light, thermionic emission, cosmic or solar penetrating radiation, Van Allen belt radiations, and any primary or secondary effects of environmental charged particles.

To give a realistic illustration of this situation, let us discuss the actual order of magnitude for a specific example. For this, we assume for the moment, that the background counting rates are negligi-

ble, that the flux $\Phi_0(\lambda)$ outside the significantly absorbing part of the terrestrial atmosphere is constant within the time of measurement, that the flux $\Phi(\lambda, h)$ at the point of observation at altitudes h above a certain geographical location is relatively high, say of the order of magnitude of 10^8 ph cm^{-2} sec^{-1}, that the instrumental efficiency ε is about 10^{-3}c ph^{-1}, and that the entrance slit is 25 microns wide and 4 mm high ($A = 10^{-3}$ cm^2). Even though the standard statistical fluctuation of Φ itself is only 0.01 percent for a time of measurement $\Delta t = 0.1$ sec., the number of observed signal counts for this time is very small ($\Delta N_S \approx 100$), so that the standard statistical error in the actual determination of the photon flux from such a monochromator measurement would be about 10 percent.

This error is of a fundamental nature, because all the physical processes involved in the monochromator measurement constitute essentially a random sampling of random events. Therefore *this error can be reduced only by increasing the number of signal counts*, ΔN_S, from which the counting rate $S(\lambda)$ is determined.

The standard statistical error of a photon flux measurement may be stated as

$$\frac{\delta\Phi}{\Phi} \approx \frac{1}{\sqrt{\Delta N_S}} \approx \begin{cases} (\Phi A \varepsilon \Delta t)^{-\frac{1}{2}} \text{ (narrow line)} & \text{(5a)} \\ (\Phi_\lambda \Delta\lambda \; A\varepsilon \; \Delta t)^{-\frac{1}{2}} \text{ (continuum)} & \text{(5b)} \end{cases}$$

where $\delta\Phi$ designates the standard statistical absolute deviation of the "measured flux," $\Phi_{meas.} = (\Delta N_S/\Delta t)(A\varepsilon)^{-1}$, from the "true" value Φ that is understood as the average of the photon flux density over a large area and not too small a time. At the right side of Eq. (5), the expected number of signal counts has been expressed by the instrument parameters and the true flux. More specifically, Φ is the integral flux of a narrow line and Φ_λ is the differential flux of a continuum emission or that in a part of an instrumentally well-resolved line.

This formula can be applied to *scanning monochromators*, if the time of measurement is expressed by the instrumental scanning speed and bandwidth, $\Delta t \approx \Delta\lambda/\dot{\lambda}$. To simplify the discussion, let us assume matched slits, $(\Delta\lambda)_{ent} = (\Delta\lambda)_{ex} = \Delta\lambda$, and that $\Delta\lambda$ and A are not independent but essentially proportional. This is quite reasonable, if one compares instruments with the same slit height and a resolution not too close to the limit set by the diffraction grating. Then we may consider the quantity $A' = A/\Delta\lambda$ as being independent of the specific choice of scanning speed and slit width for a given type of monochromator. With these assumptions, the general relationship (5) can be expressed in the instructive form

$$\frac{\delta\Phi}{\Phi} \approx \frac{1}{\sqrt{\Phi A' \varepsilon}} \sqrt{\frac{\dot{\lambda}}{(\Delta\lambda)^2}} \qquad \text{(6a)}$$

for narrow lines, or

$$\frac{\delta \Phi_\lambda}{\Phi_\lambda} \approx \frac{1}{\sqrt{\Phi_\lambda A' \varepsilon}} \sqrt{\frac{\dot{\lambda}}{(\Delta\lambda)^3}} \tag{6b}$$

for a continuum.

These relations establish a convenient guide to a reasonable compromise in the practical choice of scanning speeds and bandwidths for a monochromator of a given type that is supposed to measure photon fluxes of a certain order of magnitude with a standard statistical error that is no more than a certain chosen value. For instance, a tenfold increase of spectral resolution requires a reduction of scanning speed by a factor of 100 or 1000 for monochromator measurements of the intensity of the same narrow emission line or differential continuum intensity with the same statistical accuracy.

It is also interesting to note the instrumental detectivity limits, Φ_{min} or $(\Phi_\lambda)_{min}$ for a given set of instrumental parameters (λ, $\Delta\lambda$, A,). These limits follow from the same relation (6), if one agrees on a certain maximum tolerable statistical error. Its acceptance is equivalent to the agreement that measurements based on signal counts totaling less than a certain number $(\Delta N_S)_{min}$ are not considered to give significant information about the true photon flux. If one agrees not to tolerate a standard statistical error above about 30%, $(\Delta N_S)_{min}$ equals 10 and the smallest photon fluxes considered to be "measurable" are then

$$\Phi_{min} \approx \frac{10}{A\varepsilon} \frac{\dot{\lambda}}{\Delta\lambda} \tag{7a}$$

for narrow lines, or

$$(\Phi_\lambda)_{min} \approx \frac{10}{A\varepsilon} \frac{\dot{\lambda}}{(\Delta\lambda)^2} \tag{7b}$$

for a continuum.

Application of these formulae to the GRD instrument flown on 19 January, 1960 ($\dot{\lambda} \approx 120$ A sec^{-1}, $\Delta\lambda \approx 12$ A) gives values of Φ_{min} and $(\Phi_\lambda)_{min}$ ranging from about 4×10^8 ph/cm^2-sec and 3×10^7 ph/cm^2-sec-A around 1200 A to 2×10^6 ph/cm^2-sec and 1.5×10^5 ph/cm^2-sec-A around 300 A. This relatively low sensitivity is due almost equally to the relatively low spectral photon counting efficiency (see plot of ε in Fig. 1) and the small area of radiation collection ($A \approx 0.064$ cm^2). It is true that both ε and A can be increased significantly, but an increase by several orders of magnitude will certainly represent a difficult problem for the development of future instruments in the measurement of very small EUV or x-ray photon fluxes. Suppose for the moment that the instrumental efficiency ε can be increased by a factor of 100 and that a collimator can be constructed to increase the equivalent value of A (see Rense and Violett (1959)) also by a factor of 100 (e.g. by the use of a collimating mirror of 1000 times larger collection area and an EUV reflectivity of 10%). If we are satisfied with the same rather poor resolution ($\Delta\lambda \approx 12$ A) we may

then expect to measure photon fluxes (of unresolved lines) as low as 4×10^4 and 200 ph/cm^2-sec near 1200 and 300 A respectively without having to slow down the speed of wavelength scanning. The detection of photon fluxes of the order of 1 ph/cm^2-sec, however, would require a reduction in scanning speed by a factor between 200 and 4×10^4, in addition to the foregoing improvements. A complete wavelength scan from 1300 to 300 A then would take up to 100 hours and the time Δt spent on the measurement of a single line emission would be as much as 1 hour per scan. Naturally, experiments of this type could not be conducted from the relatively short-lived rockets now in use for monochromator measurements of solar radiation. The realization of such experiments aboard satellites, however, appears to be quite possible, if one assumes of course that the effects of the inevitable disturbing backgrounds such as those due to other radiations in space can be reduced to the required minimum. A more detailed discussion of specific anticipated technical problems and possible solutions related to this challenging experimental task would suffer from considerable lack of factual knowledge and shall not be attempted here.

4. THE GRD-INSTRUMENT

4.1. Description of Rocket Monochromator

In the photograph of the rocket monochromator presented in Fig. 2, the more important parts are indicated by numbered arrows. Various recent improvements (see I; 4.4.) are not shown in this picture. A pho-

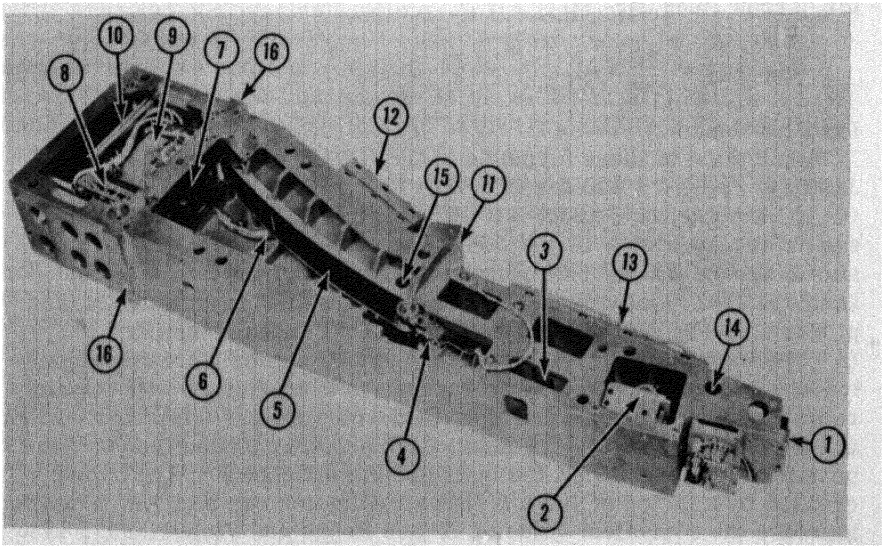


Fig. 2. Photograph of first flight model of GRD rocket monochromator. The numbered arrows point at the location of the more important parts explained in the text.

tograph of the first flight model was chosen for this illustration because it gives a simpler view of the main parts of the structure. These have remained essentially the same for the two models flown in January 1960, as well as the next three models prepared for rocket flights in the near future (I; 4.4.).

The over-all length of the instrument is about 1 meter, the largest cross-section (near arrow #16) is about 8 in. × 4 in., and the total weight (including all electronics except the telemetry transmitter) is 23 pounds. The monochromator operates on 28 volt D.C. (unregulated ± 5 volts) and draws a total power of about 14 watts. About half this power is required for the wavelength scanning mechanism which consists of a motor and gear (located below the point of arrow #4) that drives a thin continuous steel belt (#5) along a Rowland circle. This continuous steel belt is provided with 4 equidistant exit slit cut-outs (one of these, #6, has been made visible for the photograph by a piece of white paper). As there is no reversal of directions, the period of time, within which any given wavelength setting is repeated, is the same for all wavelengths.

The instrument is designed to accept gratings ruled on interchangeable blanks of 2 meter radius of curvature (nominal). These blanks are precision faced and centered. A photograph of these blanks is shown as Fig. 3. The ruling with 7500, 15,000, or 30,000 lines per inch provides a convenient choice of the instrumental scanning range of wavelengths from 1300 to 250 A, 650 to 125 A, or 325 to 62 A, respectively. The grating is held rigidly in fixed mount (arrow #2) for grazing incidence at an angle of 86°. The entrance slit (#1 in Fig. 2) is also mounted rigidly and made to be interchangeable with a series of

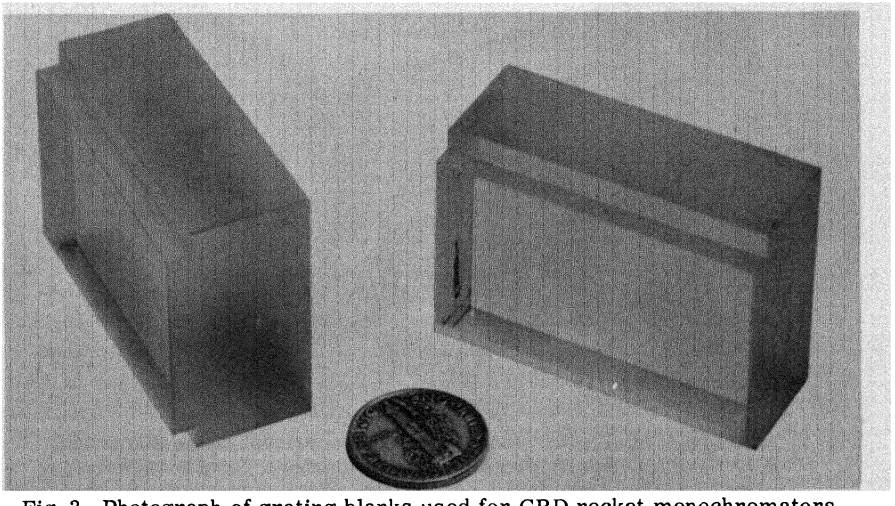


Fig. 3. Photograph of grating blanks used for GRD rocket monochromators. The precision faced and centered blanks are ruled exactly parallel to a reference side. These gratings are used interchangeably in the same rigid grating mount of the rocket monochromator. The nominal radius of curvature is 2 meters

slits of different widths. The slit height (dimension perpendicular to the plane of dispersion) can be established independently by the choice of different limiters that screw onto the slit mounts. In any case, the grating intercepts all direct solar radiation admitted through the entrance slit as long as the solar pointing control operates within the required accuracy of about 10 minutes of arc. The photo-electric eye assembly of this pointing control (not shown in the photograph) is mounted on a surface (#11) machined to be accurately perpendicular to the optical entrance axis, i.e., an axis through the center of the entrance slit and the pole of the grating. The part of the monochromator structure which bolts to the yoke of the solar pointing control is indicated by the arrows #16.

The spectral intensity measurements made with this instrument are characteristic of the total flux that arrives from all parts of the solar disk. There is no intentional image formation, nor an inadvertent one, at least not to any significant degree. If image formation were required for otherwise similar experiments, it would be advisable to consider major changes in the over-all optical scheme and to change the design considerably with respect to the present GRD instrument.

The dispersed radiation that passes through the exit slit at any position of the latter during its scan along the Rowland circle is intercepted by the large cathode (1 in. × 3.5 in.) of a special photomultiplier which is allowed to remain in a fixed position. A photograph of this

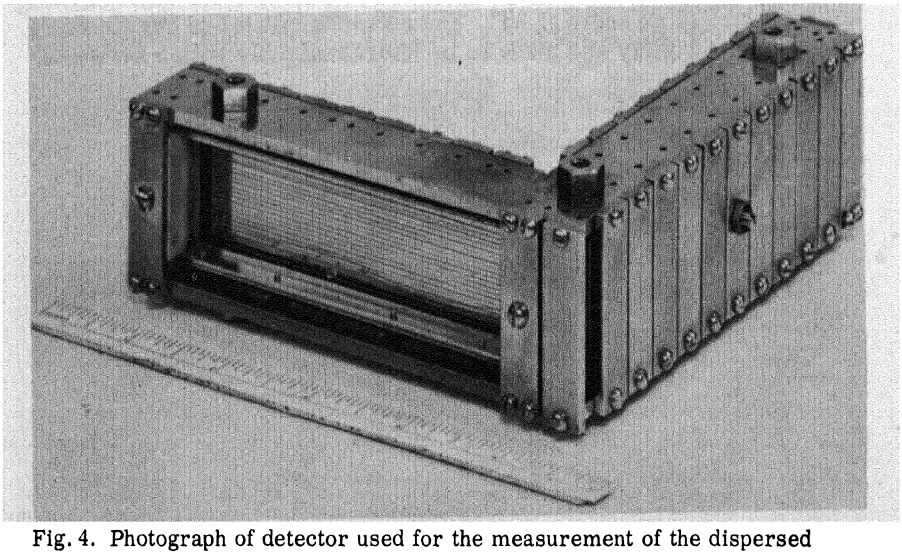


Fig. 4. Photograph of detector used for the measurement of the dispersed EUV fluxes in the GRD rocket monochromator. The 3.5-inch long tungsten cathode can be seen through the grid wires in the foreground of the picture. For schematic diagram, see Fig. 7.

detector is shown in Fig. 4. In Fig. 2, the cathode section and the multiplication section of this detector are indicated by the arrows #7 and #8, whereas arrows #10, #12, and #13 point at the locations of a transistorized pulse amplifier (and shaper), and two independent banks of binary scalers, one of 5 stages and the other of 10 stages. Arrow #9 points at the location of a transistorized regulated high voltage supply for the detector. The construction and performance characteristics of this detector will be described in more detail below (I; 4.2.).

The electronic operation of the rocket monochromator is outlined in the block diagram of Fig. 5. The output pulses of the photo-electron counter (see I; 4.2.) are fed into a pulse shaper and amplifier which is connected to two independent banks of binary scalers. Each of these scalers is combined with a resistor network which converts the events of subsequent photo-electron counts into a staircase voltage, i.e. 32 equal "steps" forming a complete "staircase" of 5 volts nominal input to one of the sub-carrier oscillators of the FM-FM telemetry system. This is indicated schematically in the lower part of Fig. 5, which also shows the type of signal (Channel III) which indicates the momentary position of the exit slit along the Rowland circle (wavelength indication). This signal has a step voltage superimposed in addition whenever a new complete wavelength scan is started. Between the end of any wavelength scan and the beginning of the subsequent one, there is a period of time of about 0.8 second, during which the field of vision from the photomultiplier to the grating is completely obscured. The counting rate recorded during this time therefore is characteristic for the basic background (see B_0 in I; 3.1.), free of any contributions by scattered light from the grating.

A copy of an actual telemetry record of the staircase presentation of photo-electron counting events is shown in Fig. 6. In the right-hand sections a and b, the hardly resolved steps in the record of the low-intensity channel have been connected with continuous lines in ink, merely to show the amusing resemblance with a conventional photographic spectrum. This illustration also shows the specific wavelengths that have been marked at the places where the leading edges of the wavelength scanning pulses (not shown) appeared in the original record. The notation "1 photo-electron" in the left side of Fig. 6 refers only to those photo-electrons which really cause a recorded output pulse of the multiplier. The number of these recorded pulses represents only a certain fraction (η_3) of the number of photo-electrons that are actually emitted from a certain place on the cathode. As the location of this place is a function of the monochromator setting, the efficiency η_3 (see Fig. 1) exhibits a wavelength dependence which is purely instrumental in nature, not involving any truly wavelength-dependent phenomenon such as the photo-electric emission yield.

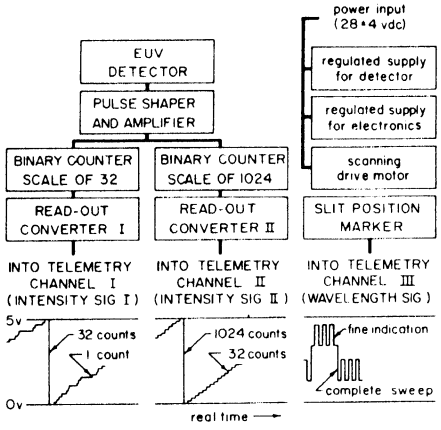


Fig. 5 Block diagram of over-all electronic operation of telemetering monochromator shown in Fig. 2.

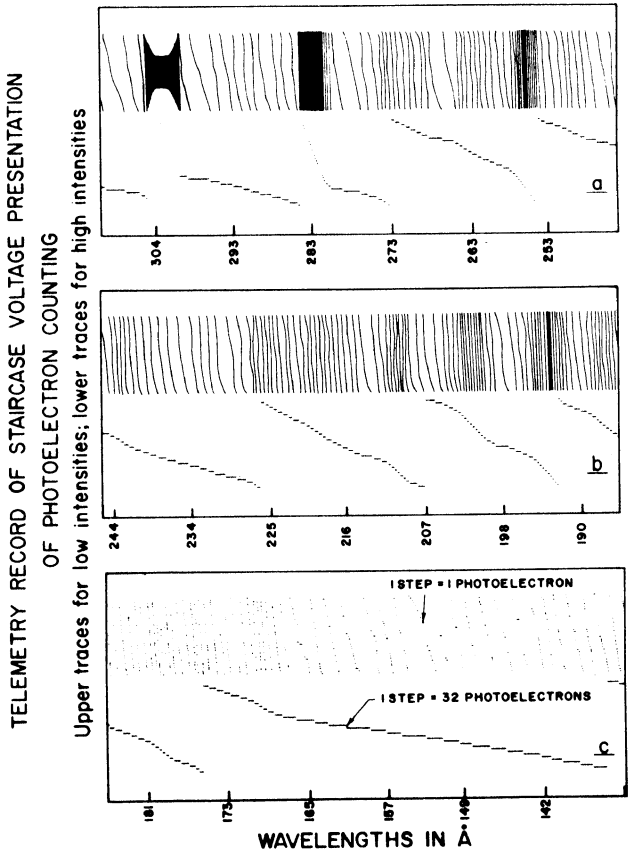


Fig. 6. Sample of telemetry record obtained from a GRD monochromator that was flown successfully on January 29, 1960 on an Aerobee Hi rocket reaching an altitude of 225 km over White Sands, New Mexico.

4.2 The EUV Detector

The intensity of the dispersed radiation passing through the exit slit of the monochromator (see Figs. 1 and 2) is measured with a photo-electric detector (see Fig. 4). The primary photo-electrons ejected from the cathode are guided into a secondary electron multiplier with a gain sufficiently high for convenient use of counting techniques. As the properties of photo-electric emission from solids in the extreme ultra-violet range of the spectrum are known only from rather preliminary studies, some of which have not been presented as formal publications; an introductory discussion of EUV photo-electric emission is probably in order here. However, there seems to be no need to discuss the much better known general aspects of secondary electron emission. To clarify the topic, it should be added that the name "photo-electric detectors" of EUV radiation or x-rays is commonly used for two distinctly different groups of sensing devices. One uses some luminescent material (e.g. Watanabe and Inn (1952)) to convert the EUV into longer wavelength radiation which can be transmitted through the glass envelopes of conventional phototubes or photomultipliers. The other group uses "windowless" photo-electric detectors, i.e. open structures in which the incident EUV radiation is the direct cause of the emission of photo-electrons from some conductive or semi-conductive cathode. Only the second group (i.e. the one involving true EUV photo-electric emission) will be discussed here. This group also has been chosen for all GRD rocket monochromators for solar EUV measurements. An important reason for this choice was the advantage of being able to combine a high efficiency of photo-electric EUV detection with a practically negligible sensitivity to longer wavelengths, say above 1500 or 2000 A. The need for such a detector is particularly great in connection with the use of gratings with nearly grazing angles of incidence, where, as was pointed out earlier in this article, stray light of longer wavelengths scattered from the grating represents one of the most serious problems for photographic detection. The level of this disturbing background increases rather rapidly towards the central image on the Rowland circle (i.e. toward shorter wavelengths) thereby competing with the dispersed intensities of the strongest solar emission lines, even in the case of relatively narrow slits. This well-known disturbance is really not surprising if one appreciates the fact that there is about 10^5 times as much solar radiation energy in the wavelength range above 1300 A than there is in all the EUV and x-rays below 1300 A combined.

The practical advantages of photo-electric EUV detectors of the direct type, (i.e. windowless structures) indicated in the foregoing paragraph, is due to the fact that practically all materials exhibit a rapid increase of photo-electric yields toward shorter wavelengths, starting around 1400 A, as a result of the onset of the *volume photo-electric effect.* The aspects of this photo-electric emission in the EUV are distinctly different from the well-known ones of the ordinary surface photo-electric effect. Around 1000 A the efficiencies of this

volume effect rise far above those known to be characteristic for the ordinary surface effect on elemental cathodes, even for alkali metals at the peak of their sensitivity in the visible or near ultra violet region of the spectrum. Photo-electric detectors for the range of longer wavelengths are well-known to be extremely sensitive to the slightest contaminations of the cathode, which must be prepared with the utmost care and be kept inside sealed envelopes. Therefore, windowless open structures would be of no practical use as photo-electric detectors of near ultra-violet radiation. For the volume effect, however, which appears to contribute by far the greatest part of all photo-electric emission occurring in the EUV, the actual conditions of a cathode surface or the presence of some monomolecular layer of adsorbed gases play only a subordinate role. The same is true for the so-called "work function" (thermionic work function or photo-electric work function defined as the smallest photon energy at which photo-electric emission occurs, i.e. between about 2 and 6 electron volts for most materials). The specific value of the work function has no major correlation with the photo-electric emission yields in the EUV or soft x-ray region of the spectrum. Indeed, the EUV photo-electron emission phenomenon has, as a whole, many more observable aspects in common with those of secondary electron emissions than with those of the ordinary surface photo-electric effect. Even metals with the highest work functions are found to exhibit photo-electric yields in the EUV which are only insignificantly smaller and often even larger than those of materials of very low work functions. Consequently, it is not difficult to find suitable materials for highly efficient EUV cathodes that are at the same time conveniently insensitive to radiation of longer wavelength. Due to their high work function, these cathodes have extremely low thermal noise, so that counting techniques are practicable without any cooling of the cathode, even for the measurement of extremely low photo-electron counting rates, and for large cathode areas, such as that used for the GRD rocket monochromator.

The photo-electric yield, Y, expressed in terms of the fractional number of emitted photo-electrons per incident photon as a function of wavelength, is shown in the diagram of efficiencies in Fig. 1. This curve refers specifically to commercially pure tungsten, but it should be noted that the differences in yield in the EUV from one material to another one, are relatively small (in all cases observed, much less than an order of magnitude).

The existence of a photo-electric volume effect has been postulated in 1931 on theoretical grounds (Tamm and Schubin (1931)) and again in 1945 with considerably clearer details (Fan (1945)). The first reliable experimental evidence of relatively high photo-electric yields of W, Ni and Mg in the EUV were obtained by Kenty in 1933 (Kenty (1933)) who investigated the emission from several cathodes that were subjected to the undispersed radiation from He, Ne, and A—discharges containing mainly the resonance radiations at 584, 740, and 1060 A, respectively. Measurements with dispersed radiation extending to a short wavelength limit of about 1050 A were made by Baker (Baker (1938)) who measured the yield of a cadmium cathode inside an argon-filled tube, which was illuminated

through a lithium fluoride window. These measurements have been taken as experimental evidence for the onset of the photo-electric volume effect that was predicted by Tamm and Schubin. The first quantitative measurements of EUV photo-electric emission yields for Ni, Pt, and W were reported by Hinteregger and Watanabe (loc. cit.). The general features of this effect for other materials have been indicated by Hinteregger (loc. cit.) and by Walker, Wainfan, and Weissler (loc. cit.) and have been reviewed recently by Weissler (Weissler (1956)). Preliminary measurements of EUV photo-electric yields of pyrex glass were reported at the 1955 M.I.T. Conference on Physical Electronics (Hinteregger, unpublished) and measurements on germanium were made by Weissler's group (Walker and Weissler (1954)). They have confirmed the prediction of high EUV photo-electric yields to be characteristic, not only of metals, but also of semi-conductors and insulators (Hinteregger (1954)). This prediction was based on preliminary observations with obviously oxidized magnesium, beryllium, and aluminum cathodes. To avoid misunderstandings in this connection, it should be mentioned that the expression "high yield" in the case of a relatively good insulator, refers to the "intrinsic yield" of the primary process of a photo-electron's being ejected before any local depletion of electrons or any local charge-up of the insulator-surface occurs. The latter prevents, of course, any continuous large-scale emission. There will be a rapid decrease in emission current so that the stationary photo-electron emission current associated with a relatively high photon flux density of EUV photons on an insulator corresponds to a yield (i.e. the inhibited stationary yield) that can be practically negligible even if the intrinsic yield is quite high (e.g. about 10% for pyrex glass at 584 A).

Kenty (loc. cit.) noted correctly that the photo-electric yield of oxidized tungsten appears to fall off toward the longer wavelengths around 1000 A more rapidly than that of the relatively pure tungsten which he obtained by heating to elevated temperatures. This observation was fully confirmed by the author's experiments leading to the practical conclusion that any commercially available tungsten sheet or ribbon, not subjected to any high temperature outgassing or annealing, makes very good EUV photo-cathodes with rather reproducible yields for wavelengths below about 1200 A after simple cleaning of the surface with organic solvents. The insensitivity to radiation of longer wavelengths is usually as good or even better than that of the purest platinum which exhibits the highest photo-electric work function known among all pure metals. To obtain platinum in this state, however, requires many hours of outgassing and annealing in the cleanest high vacuum. Otherwise this work function remains significantly below the value of 6.2 electron volts achieved in very well controlled experiments by DuBridge (DuBridge (1927; 1928)). To achieve such high work functions in an open structure to be launched in a rocket would impose rather serious experimental complications. Therefore, the opposite trend exhibited by tungsten, i.e. that it has its highest work function in the easily obtainable state of commercial tungsten sheet with its natural surface oxidation, represents a fortunate coincidence of desirable characteristics and technical convenience. It should be noted, however, that other metals could be found with equally good or even better properties as EUV cathodes. In conclusion to this brief survey, it should be noted that the steep drop of the photoelectric detection sensitivity of tungsten toward the longer wavelengths is, of course, not desirable for any instruments that may be designed to cover a wavelength range extending significantly beyond about 1300 A (e.g. up to 2000 or 3000 A). The discussion of such instruments, however, is not within the scope of this article.

After this brief discussion of photo-electric emission phenomena in the EUV, this section will conclude with a description of the actual EUV detector that has been flown successfully in the GRD rocket monochromators. The electrode arrangement of this detector is shown schematically in Fig. 7. The detector consists essentially of a cathode section and a SE-multiplication section. The latter is similar to a structure which was developed originally as an ion detector for a mass spectrometer by Wiley and Goodrich of the Bendix Aviation Corp., Research Laboratory Division (unpublished). The use of a multiplier of this type as a detector of extreme ultra violet radiation for the GRD rocket monochromator has been the result of the cooperative effort by Bendix and the author's group at GRD. All structural development was conducted by Bendix and the experimental exploration of the applicability and the necessary improvements for EUV photo-electron detection in rocket instruments was carried out at GRD. Detailed results of the preliminary studies have been described by Heroux and Hinteregger (loc. cit.) and the performance of a resistance strip magnetic multiplier of the type actually flown on the 1959 and January 1960 rocket monochromator is reported in detail by Hall and Hinteregger (loc. cit.). Therefore a rather brief description will suffice here. The EUV radiation emerging from the exit slit of the rocket monochromator is admitted onto the cathode (C) through a grid (G) of very high optical transmission. The wires forming this grid are stretched parallel to the plane of dispersion (i.e. perpendicular to the long dimension of the slit), so that they do not cause any possibly misleading signal variations as a function of the monochromator scanning position, which at the same time determines the position of the illuminated stripe on the cathode. This correlation between wavelength setting of the monochromator and location of the illuminated strip on the large cathode of the detector, is illustrated schematically in Fig. 8. If the SE-multiplier itself is operated so as to produce an output pulse for practically every electron guided into its input (i.e. at the "bend" in Fig. 7), the photo-electron counting efficiency η_3 must still be less than 100% as long as there is a significant chance that a primary photo-electron ejected from a certain place on the cathode may be lost toward the grid or toward the sides (i.e. parallel to the magnetic lines of force as indicated in Fig. 7). For the unipotential cathodes used until recently, the loss of primary photo-electrons due to recapture in the cathode itself, was very significant, leading to a rather rapid decrease of the actual detection sensitivity towards the far end of the cathode.

As this "transport efficiency" decreased from the bend towards the far end of the cathode by a factor of 15 and more, a significant increase of this instrumental efficiency was most important in order to improve the over-all spectral photon counting efficiency of the monochromator (ε in Fig. 1). Since the last rocket monochromator flights in January 1960, such an improvement has, in fact, been achieved by the use of a cathode of sufficiently high resistance so that a negative potential gradient can be maintained from the far end of the cathode

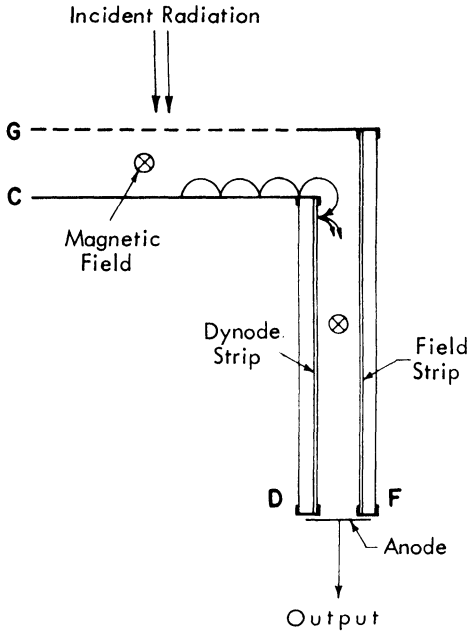


Fig. 7. Schematic drawing of EUV detector used in GRD rocket monochromators. The detector (see photograph of Fig. 4) consists of a cathode section and a SE multiplication section. Typical operating voltages for a gain of 10^8 are $V_C = -2200$ volts, $V_G = -2100$ volts, and $V_D = -100$ volts with respect to the anode and the end of the field strip (point F), which are run at the same potential.

toward the bend (see insert in Fig. 9). This negative potential gradient causes the equipotential surface for which the kinetic energy of the electrons becomes zero to lift away from the actual cathode surface as the electrons progress in their trochoid loops toward the multiplication section. This modification improves the over-all efficiency of the instrument considerably and also decreases the pronounced dependence of efficiency on wavelength setting, which in Fig. 1 is still shown for the instrument using a unipotential cathode. The new construction is being incorporated already in the rocket monochromators that are now prepared for the next flights. The remaining variation of instrumental sensitivity across the 3.5 inch long cathode measured on the first completed modified structure (Hall and Hinteregger (1960)) is reproduced here as Fig. 9. As one might suspect that the variations shown in this diagram could result from variations of the actual photoelectric yield along the cathode, it must be emphasized that this is not the case, at least not to any significant extent. Further improvements to give a smoother curve of η_3 versus position of illumination on the cathode are, of course, desirable, but may require much improvement of the uniformity, not only of the resistance cathode, but also of the magnetic field in the present construction. Whereas the magnetic field

within the SE-multiplication section is established by small permanent magnets mounted symmetrically over the field strip and dynode strip (see Fig. 7) respectively, the magnetic field in the cathode section is established by a much less symmetrical arrangement of permanent magnets (see Fig. 4) because of the obvious need to leave the entire grid structure without any obstructions.

Among the important experimental problems remaining to be investigated by systematic laboratory research, the improvement of absolute photo-electric emission yield determinations and the extension to wavelengths shorter than 300 A deserve the most serious emphasis. The difficulties involved in this task are known to be considerable, but they can hardly be considered to be unsurmountable. The absolute re-

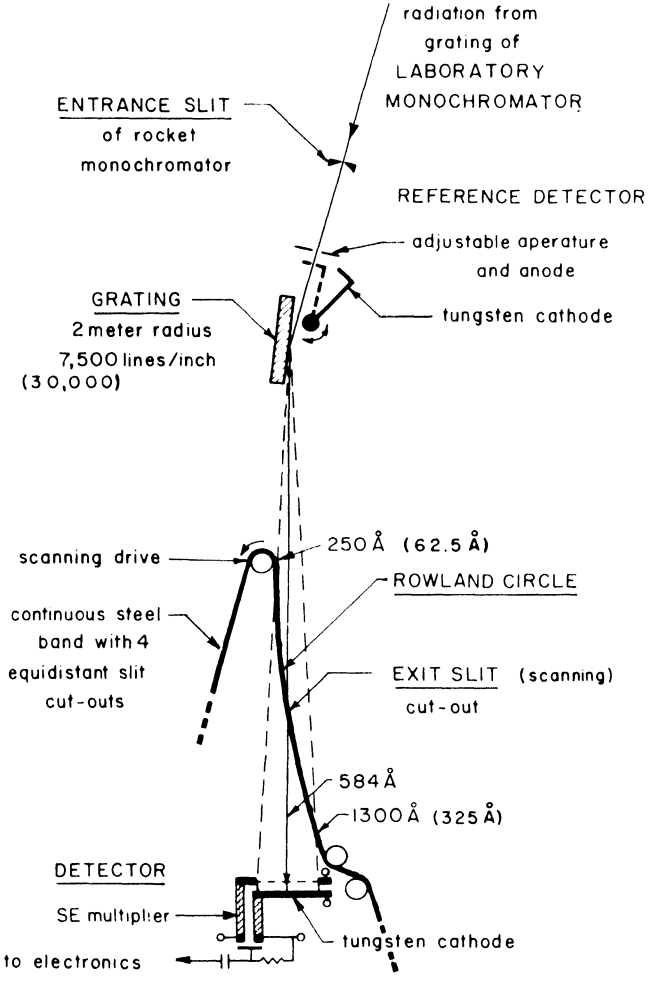


Fig. 8. Schematic illustration of optical lay-out of GRD rocket monochromator including auxiliary equipment for spectral calibration in the laboratory.

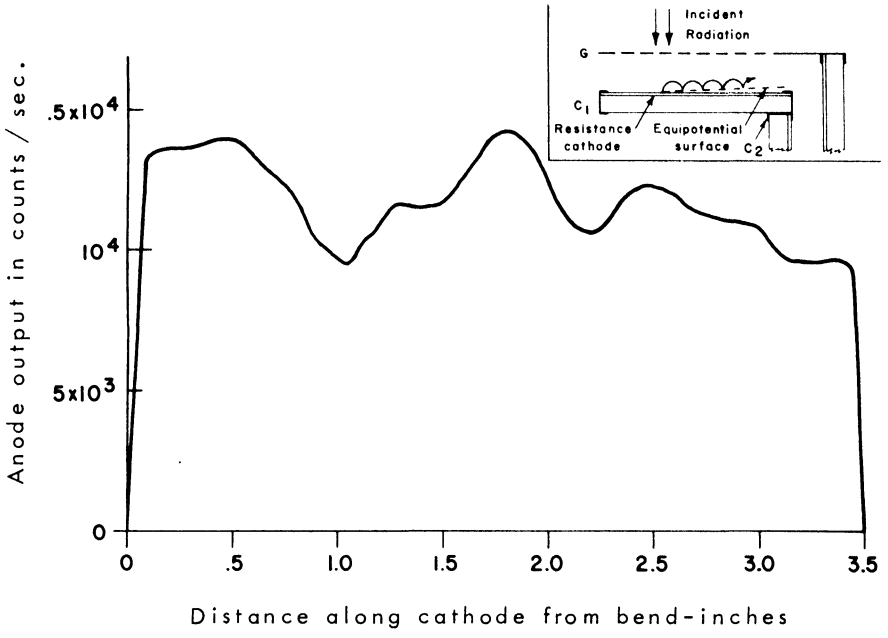


Fig. 9. Anode output of EUV detector (similar to that shown in Figs. 4 and 7) as a function of the position of illumination on a resistance cathode. The effect of maintaining a potential drop of 35 volts along this cathode is shown schematically in the inset.

liability in interpreting future rocket and satellite measurements of EUV photon fluxes, may soon depend on adequate progress of laboratory research in this direction more critically than the progress in general space vehicle technology.

4.3. Spectral Calibration

The spectral calibrations of the GRD rocket monochromators in the past have been achieved in a manner that is illustrated schematically in Fig. 8. The whole rocket monochromator is mounted inside a vacuum tank at the exit of a laboratory monochromator. Actually the rocket monochromator is mounted so that its entrance slit at the same time assumes the role of the exit slit of the laboratory monochromator. For the calibrations carried out in the past (extending to wavelengths no shorter than about 500 A) the laboratory monochromator was a grating instrument (one meter radius of curvature, 15,000 lines per inch) operated with a fixed position of the exit slit with respect to the center of the grating, that was simply turned about its axis for the purpose of wavelength scanning. This arrangement involved a slight defocusing as a function of the scanning position, but this effect was of no importance within the modest demands for resolution required. An advantage of this calibration set-up was the fact that the rocket mono-

chromator could remain fixed during changes of the wavelength setting of the laboratory monochromator. A precisely located and securely locked mounting plate (#4 in Fig. 10) is provided with bores matching the locating holes of the rocket monochromator (see #14 and #15 in Fig. 2). The latter are precisely located bores that actually serve as a reference during the machining of the optically important parts of the monochromator. The photograph in Fig. 10 shows the opened tank (#1 and #2) and exposes the monochromator (#3) already in proper location for a calibration. The whole tank assembly is provided with a separate pumping system and is connected to the dispersing unit of the laboratory monochromator with a gate valve (#6). The flanges #5 and #7 contain the necessary vacuum feed-throughs for electrical connections as well as the remote control of the movable parts inside the calibration tank. The top flange also holds two ionization gages, one connecting to the inside of the tank, the other to a gas inlet system (#8) that is used in conjunction with ion chamber tests and absorption measurements in the same tank. For such measurements, a plug-in slit unit then substitutes for the rocket monochromator, duplicating exactly the position of the entrance slit of the rocket monochromator.

The procedure of calibrating the rocket monochromator can be best explained following the schematic illustration of Fig. 8. The reference detector is turned into the beam of monochromatic radiation accepted by the entrance slit. The anode of this photo-electric detector at the same time serves as an optical aperture simulating the actual angular spread of solar radiation in the plane of dispersion (plane of drawing) in actual flight. The proper adjustment of the stops establishing this position whenever the reference detector is turned into the beam inside the vacuum chamber, naturally must be carried out prior to insertion of the rocket instrument into the tank. The "reference signal" i_R (see Fig. 1) is measured as the photo-electric saturation current leaving the tungsten cathode of the reference detector. After one has observed this signal the wavelength setting of the laboratory monochromator is adjusted to the desired wavelength (e.g. 584 A or any other line that can be produced with sufficient intensity with the available light source). Peaking of the reference signal serves as a control for the fine adjustment. The number of monochromatic photons admitted through the aperture per unit time then is equal to i_R/Y_R, if the current i_R is expressed in electrons per unit time and Y_R designates the photo-electric yield of the reference cathode at the known wavelength. Now, the aperture is left in place and the tungsten alone is rotated out of the beam, so that the same photon flux is now admitted to the grating. In this condition the rocket monochromator scanning position is also adjusted to the same wavelength in a reproducible manner that is best defined by peaking the counting rate of the flight detector. To check for possible drifts in the intensity emerging from the laboratory monochromator, the last step consists again of a measurement with the tungsten reference detector swung into the entrance beam. This procedure is subsequently repeated for all those

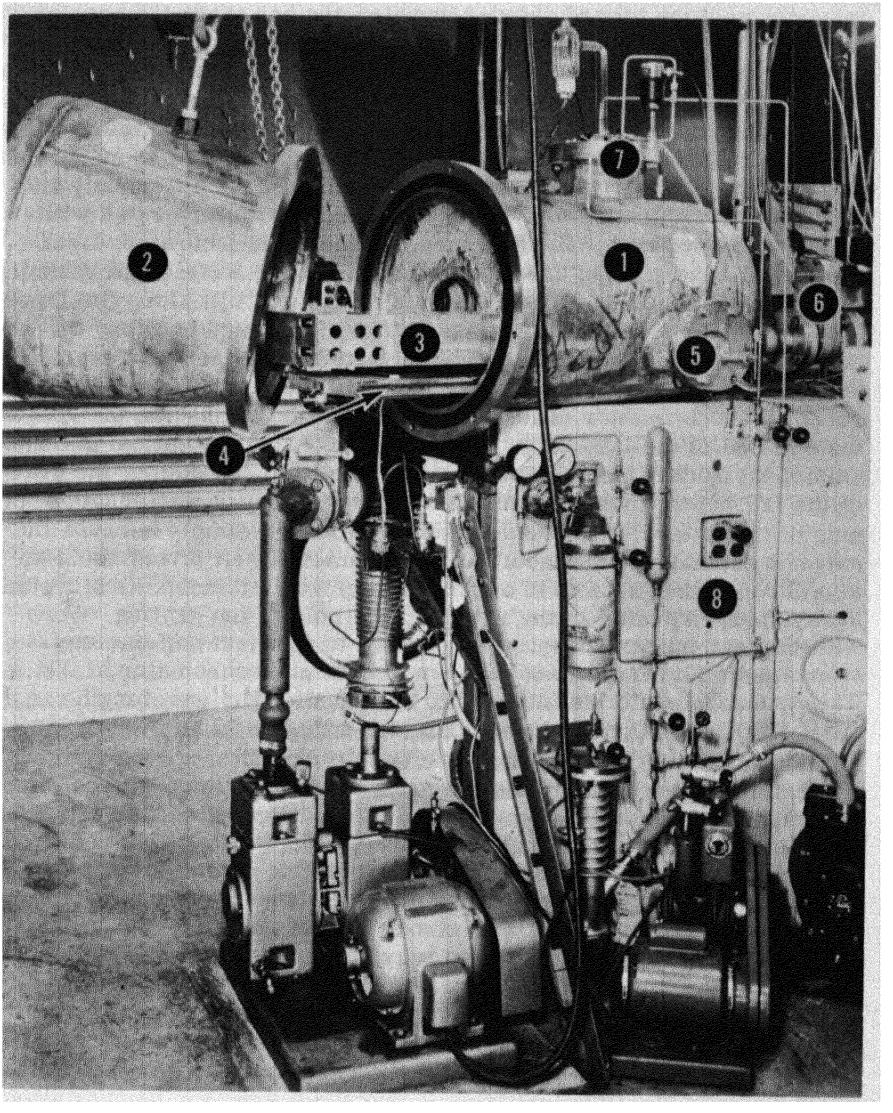


Fig. 10. Photograph of calibration set-up for GRD rocket monochromators as it was used for the wavelength range from 1300 to 500 A in connection with the exit part of a laboratory monochromator (1 meter grating, 45° incidence). Gate valve # 6 connects to the dispersion unit and light source of the latter (not shown).

wavelengths for which the laboratory monochromator-light source combination provides a sufficiently strong intensity so that a reliable measurement of the reference detector current can be achieved with a vibrating reed type of electrometer amplifier.

The need to extend calibrations of spectral transmissions of rocket

monochromators toward shorter wavelengths has made it necessary to work with another laboratory monochromator that is operated in nearly grazing incidence. Naturally this new facility no longer permits stationary mounting of the rocket instrument, because the exit slit of the new laboratory instrument is required to travel along the Rowland circle during the scaning operation. The new laboratory monochromator used for this purpose was built by the Jarrell-Ash Company and equipped with a grating of 3 meters radius of curvature ruled with 15,000 lines per inch. The entrance slit (near the laboratory light source) and the grating are mounted rigidly. The wavelength scanning is achieved by moving a carriage holding the exit slit along the Rowland circle. The exit slit carriage has been modified to carry the whole rocket monochromator on a mounting plate similar to that described before. The arrangement is such that again the entrance slit of the rocket monochromator is in the proper position to assume the role of the exit slit of the laboratory monochromator and the optical entrance axis of the rocket instrument remains pointed at the pole of the grating of the laboratory monochromator for all positions of wavelength scanning of the latter. This could be achieved rather simply because the exit slit carriage of the laboratory instrument itself pivots about an axis through the exit slit in such a manner so as to keep the slit plane always perpendicular to the ray from the pole of the grating. Work with this set-up has recently progressed to the first satisfactory transmission measurement of a new rocket monochromator at 304 A. This monochromator is intended to be flown for the wavelength range from 1300 to 250 A sometime during the summer 1960.

In conclusion to this section, the need for much more experimental laboratory research and development work toward improved calibration techniques should be emphasized. To a large extent the progress will depend on parallel developments concerned with EUV and soft x-ray light sources, as well as thermo-electric detection techniques. A radical improvement beyond the present state of affairs, however, may be expected only from the introduction of some reliable source of EUV and soft x-ray radiation that may be found to qualify as a "standard lamp" for this difficult but most interesting region of the spectrum. A systematic use of the so-called "classical acceleration radiation" from electron synchrotrons (Schwinger (1949)) appears to offer the best chance of progress in this direction (Tomboulian and Hartman (1956)).

4.4. Flight Tests and Subsequent Improvements

As soon as the various products of new developments had been integrated into a complete working model of a rocket monochromator, the latter was subjected to extensive tests in the laboratory. These tests very quickly confirmed the proper performance of all important parts under laboratory conditions, even though this resulted in numerous suggestions of desirable changes in certain details. These, however, were of relatively minor importance as compared with the re-

maining uncertainty related to questions that hardly could be clarified by laboratory experiments. Even the best available simulation of the actual rocket environment (i.e. not only simulation of the total environmental pressure, but also the photon and charged particle environment) is known to be far from being sufficiently representative. Therefore, two essentially identical instruments as shown in Fig. 2 were completed and prepared for flight on Aerobee Hi rockets. Both instruments were equipped with gratings of 7500 lines per inch (wavelength range from 1300 to 250 A), and their spectral efficiencies were determined with monochromatic EUV radiation as described in the foregoing paragraph.

The first monochromator was launched from Holloman Air Force Base, New Mexico, on February 27, 1959. The rocket trajectory was satisfactory and the telemetry record indicated proper behavior of all monitored functions of the equipment. The intensity signals, however, indicated a "saturated" counting rate of the detector for the entire period of time during which the high voltage supply was turned on. The recorded counting rate was exactly that at which the response of the transistorized counting circuit was known to level off in laboratory experiments. This behavior had been investigated for higher intensities in the laboratory, where the "true" counting rates calculated from the reference detector measurements would have corresponded to a value as high as 6×10^5 sec^{-1}. After discarding various tentative explanations, such as inadvertent generation of high frequency oscillations somewhere in the electronic circuitry, scattered light, or interference from the transmitter antenna, we were soon led to the conclusion, that only a part of the disturbing effect could have been due to insufficient shielding against scattered hydrogen Lyman-α radiation from the atmosphere, whereas the larger part of the disturbance must be laid to the interference of charged particles from the ionospheric environment. As it had been clear from the beginning that our detector would certainly count any positive ions (this was actually the original design purpose of the resistance strip magnetic multiplier by Bendix Aviation Corp.), the cathode of the detector had been kept at a positive voltage of +20 volts with respect to the vehicle, so that positive stray ions could hardly cause any harm. The problem of stray electrons of comparably low energies had been considered insignificant prior to the observation in this flight, mainly because the magnetic field prevents electrons of relatively small momentum from reaching the cathode, even if these electrons are aimed at the grid with an original kinetic energy of a few hundred electron volts. Even though this was borne out by laboratory experiments, no similar experiments had been attempted to check on possibilities of electrons leaking into the sensitive volume along the magnetic stray field lines. Our suspicion that we had seriously underestimated the possibility of a part of the stray electrons reaching the cathode was sufficiently strong, so that we decided to risk another rocket flight with a minor modification designed to answer this question experimentally. The modification consisted essentially in shifting the original cathode volt-

age from +20 volts to the new value of −20 volts with respect to skin (naturally with all other voltages following this shift so that the actual electric fields in the cathode section as well as the SE-multiplier section remained unchanged). To avoid impairing the protection against positive ions due to the negative potential at the cathode, the grid and all other metal structures around the cathode and resistance strip (the yokes and attached permanent magnets) were still left at a positive voltage with respect to the instrument body.

The Aerobee Hi rocket carrying this slightly modified instrument was launched on March 12, 1959, at 0844 hrs. MST, and reached an altitude of about 210 kilometers. Satisfactory telemetry signals were again received throughout the flight and all monitoring functions behaved properly. The instrument completed 17 full wavelength scans during the "on" period of the high voltage supply and produced intensity signals which at no time duplicated the saturation phenomenon that had been observed in the first flight. The subsequent evaluation of the telemetry records and rocket trajectory data showed that the 17 wavelength scans of this flight had been spread over the altitude range from about 140 kilometers to 210 kilometers. The " background counting rate" in this second flight had decreased to a value between 5000 and 8000 sec^{-1}. Even though this was still about 10,000 times as large as the background counting rate in the laboratory, it fortunately amounted to no more than about 5 percent of the highest intensity signal recorded at those times where the exit slit moved through the 304 A position on the Rowland circle (Lyman-α line of ionized solar helium). Therefore, the second flight test left no reasonable doubt regarding the practical value of the instrument in particular, as well as the use of the various new techniques for a systematic future rocket and satellite exploration of solar EUV and soft x-rays in general. Nevertheless, it was quite clear that the results of this flight merely reflected a first successful test of a new approach rather than the desirable systematic solar radiation "measurement" throughout the instrumental range from 1300 to 250 A. In particular, subsequent laboratory work with the same type of EUV detector revealed that the improvised change made in the field on the cathode section of the detector (for the purpose of rejecting environmental stray electrons from the cathode) was not completely successful. It resulted in a very serious lowering of the transport efficiency (see I; 4.2.) with which primary photo-electrons are guided into the SE-multiplication section of the detector. Even though this effect was quite negligible near the bend (i.e. the part of the cathode receiving the dispersed radiation between about 250 and 350 A), the efficiency must have dropped very rapidly towards the higher end of the cathode (i.e. towards the longer wavelengths). As soon as this was discovered it was clear that the already evaluated telemetry records from this flight (March 12, 1959) really contained no meaningful information on absolute intensities, at least not for any wavelengths above about 500 A. Therefore the only result of geophysical significance was the measurement of the solar 304 A line intensity throughout the interesting range of altitudes in the

upper atmosphere from about 150 km to 210 km. This range included the region of maximum ionization rate density associated with this monochromatic solar radiation. (Hinteregger, Damon, Heroux, and Hall (1960).)

The observed background counting rate during the second flight experiment of 12 March 1959 did not show any noticeable decrease during the 0.8 second long period between successive scans, when the grating was completely obscured with respect to the detector (see I; 4.1.). This observation safely excluded the possibility that more than about 200 counts per second could have been actually due to light scattered from the grating. Therefore, it had to be concluded that practically all of the observed background counting rate (5000 to 8000 sec^{-1}) was caused primarily by other interferences that would have to be suppressed much more efficiently before the light scattered from the grating could be noticed.

The next two rocket monochromators were launched in January 1960. In these instruments many minor details of both the mechanical structure and the electronics had been changed on the basis of the first flight experience and extended laboratory tests. Most of these details are not of sufficient interest to be mentioned here. One change, however, appears to warrant discussion in some detail.

The *pump-out* of the interior of the rocket monochromator in the 1959 flight model had been achieved by leaving a number of relatively large holes in the instrument housing. These holes offered no significant barrier against *charged particles* from the ionospheric environment. Also they appeared to admit an unnecessarily high amount of random *scattered light* from the atmosphere. Even though the contribution of the latter to the remaining background observed in the 12 March 1959 flight was believed to be much less than the part due to primary and secondary effects caused by charged particles, a simultaneous rejection of practically all ionospheric ions and electrons as well as a significant reduction in the total admission of scattered light from the atmosphere was of course most desirable. For the practical realization of this goal, however, it must be kept in mind, that the need to maintain a very high pump-out speed requires as much open area as one can possibly afford. This high pumping speed is required for the photo-electric rocket monochromator even more so than for a photographic spectrometer. For the latter a pressure of about 1 micron inside the instrument is probably small enough to avoid any undesirable absorption within the instrument. Satisfactory operation of the photoelectric detector of the GRD instrument, however, could not be expected unless the residual pressure inside the instrument is less than 0.1 micron (preferably 0.01 micron or less).

The structure eventually adopted for the practical solution of this combined problem (rejection of charged particles and suppression of scattered light, while maintaining a high pumping speed) is depicted in Fig. 11. This structure now replaces all the open holes used for pump-out in the 1959 models. The outer part of the opening is covered with a grid kept at a positive voltage of approximately 20 volts with

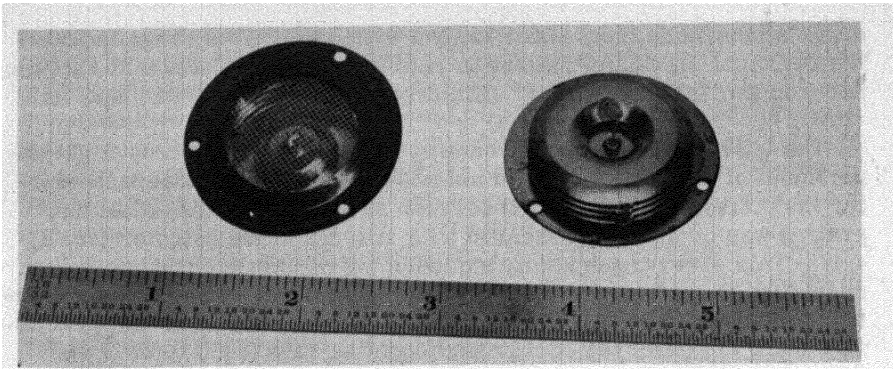


Fig. 11. Photograph of new pump-out plugs that afford protection against environmental charged particles and scattered light. These structures replace the plain pump-out holes which had been used in the first GRD rocket monochromators.

respect to the rocket body so that practically no positive ions can enter through the round openings of about 1 in. diameter. The inner part of the structure consists essentially of a set of equidistant conical shades which are conductively connected and kept at a negative voltage of about 20 volts with respect to the vehicle. This prevents any environmental electrons of energies less than 20 electron volts from entering the instrument. At the same time the conical shades reduce the amount of scattered light from the atmosphere quite appreciably without decreasing the effective pumping speed too much.

The effective suppression of scattered ultraviolet light is more effective than might be judged from considering visible radiation alone. In our case visible radiation is of no practical concern because of the complete insensitivity of the detector to such long wavelengths. A significant contribution to undesirable background counting rates, however, might be expected due to scattered hydrogen Lyman-α radiation. As the reflection coefficient of the conical shades is hardly higher than 10% at this wavelength, the amount of Lyman-α radiation reaching the interior of the instrument after multiple reflection corresponds to a fraction of the incident flux that is much smaller than that for visible light.

Two remaining problems not eliminated as yet are those of the additional extreme ultraviolet radiation caused by the electron capture at the positive outer grid (see Fig. 11) and the problem of rejection of charged particles of energies higher than the limits determined by the voltages at the outer grid and inner structure respectively. For experiments within the earth's ionosphere sufficiently below the Van Allen belt, these problems are probably not very important, at least for measurements with fairly modest resolution of relatively high photon fluxes of solar origin. Then the signal counting rates due to the dispersed radiation received by the EUV detector are sufficiently high.

No attempt at all has been made to suppress the expected disturb-

ing background counting rate due to penetrating radiations such as cosmic rays. Against these neither retarding grids nor the use of absorptive shielding offer any significant protection.

The next monochromator was launched in an Aerobee Hi rocket from White Sands, New Mexico, on January 19th, 1960 at 1117 hrs. MST. The rocket reached an altitude of about 215 km. Telemetry and all instrumental functions behaved properly with the exception of the solar pointing control, which could not lock on the sun for an appreciable part of the otherwise useful time of flight, because of excessive precession of the vehicle axis. The signal counting rates derived from the telemetry records are shown in Fig. 12 for two complete wavelength scans at different altitudes. Light scattered from the grating still did not contribute appreciably to the background counting rate, because the decrease of counting rate during the 0.8 sec. intervals, during which the detector did not see the grating at all, was still but a small fraction of the average observed background (not shown in Fig. 12). This was of the order of 3000 counts per second. At first glance there appears to be no remarkable improvement beyond the instrumental performance observed on March 12, 1959. To appreciate the actual improvement (by a factor of more than 20) one must take into account that in the 1959 flight only a small part of the cathode near the entrance to the SE-multiplier structure was effectively contributing to the recorded background. In fact, it must be concluded in retrospect that the relatively good signal to noise ratio in the detection of the 304 A line in the 1959 flight was merely a result of the accidental reduction of the electron transport efficiency at all farther parts of the cathode as has been discussed in a previous paragraph of this section. It should be noted though that a reduction of the background by considerably more than a factor of 20 had been expected, and the reason why this was not achieved is still not understood. As the vehicle was not recovered a post mortem analysis was unfortunately not possible. It appeared to be quite possible that the negative voltage to the environmental electron repellent shades may have been interrupted or shorted, at least at one of the traps in a critical position with respect to the EUV detector. If the inner conical shade then assumed accidentally a positive potential relative to the instrument (e.g. the potential of the outer grid) the device would have been much worse than a completely free opening, for it would then act as a funnel for environmental electrons. The idea that something of this type may have happened received some support by the observation of a much lower background (of the order of 100 counts per second) in the next flight with an instrument that appeared to have been baffled against charged particles from the environment only slightly more efficiently than would seem to be necessary to account for this remarkable reduction in the observed background counting rate.

The last rocket monochromator, also flown from White Sands, on January 29, 1960, 1152 hrs. MST, was the first one to be equipped with a grating with 30,000 lines per inch, so that the wavelength scanning range extended from about 320 to 60 A. A sample of the counting rates

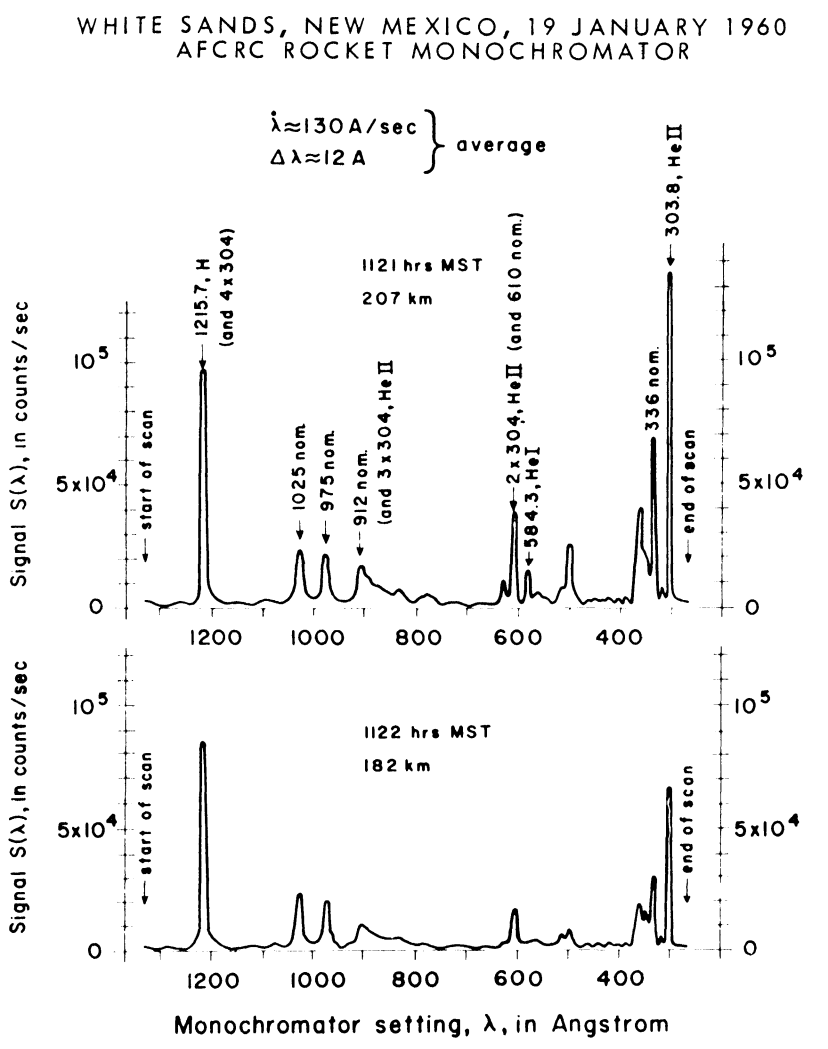


Fig. 12. Sample of monochromator signals from GRD rocket monochromator flown on January 19, 1960. The instrumental spectral photon counting efficiency of this monochromator decreases very rapidly towards longer wavelengths (see Fig. 1). A conversion of signal counting rates into actual photon fluxes is shown on the left of Fig. 16.

for several complete scans of this flight are presented in Fig. 13 and a sample of the actual telemetry record can be seen in Fig. 6. The records obtained from this flight showed for the first time, that the background counting rates due to causes other than that of scattered light from the grating had been reduced successfully to a sufficiently low level so that the actual contribution of scattered light of the grating had become observable.

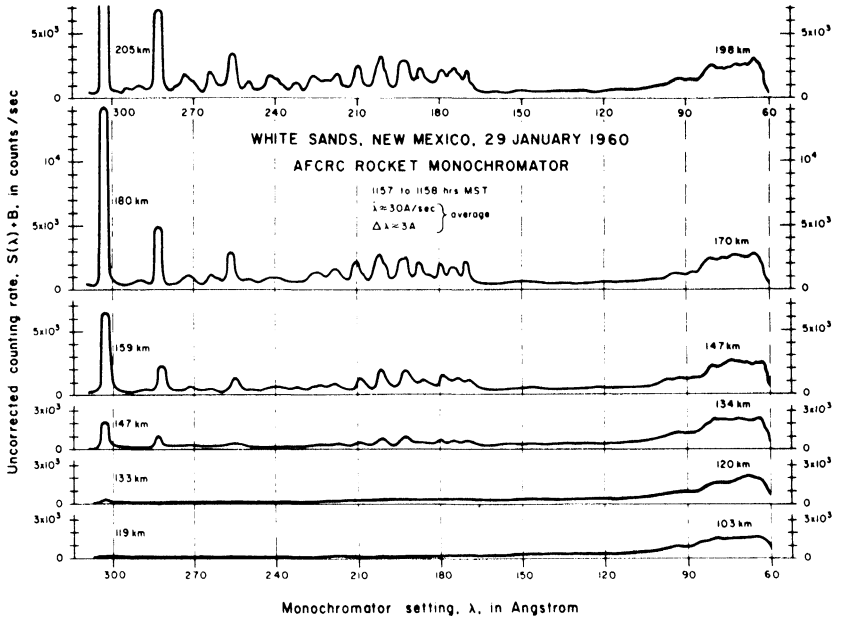


Fig. 13. Sample of monochromator signals from GRD rocket monochromator flown on January 29, 1960. A tentative conversion into actual photon fluxes is shown on the right of Fig. 16.

It seems reasonable at this stage of development to expect various minor and possibly some major improvements not only by a further decrease of background counting rates but also by increases in any one and hopefully in all the efficiencies indicated in Fig. 1.

The *wavelength scanning speed* of all rocket monochromators flown so far has been chosen so that the full wavelength range (from 1300 to 250 A or from 320 to 60 A) was covered within a time of about 10 seconds. In all cases the spectral resolution of the measurements was determined by the width of the exit and entrance slits. This *instrumental resolving power* was always rather far below the actual limiting resolving power of the gratings used. With the progress in suppressing the undesirable background counting rate and the progress in increasing the overall efficiency of the instrument, it will be possible to use smaller and smaller entrance slits (those used so far were about 0.4 mm wide) without a worsening in the signal to noise ratio.

As the background counting rate in the last flight of 29 January 1960 was already at a relatively low level, close to the expected background due to cosmic rays alone (the sensitive cathode area was about 20 cm^2), no further large improvements (leading to a decrease of background counting rate by a full factor of ten) can be expected with the present instrument. The more promising task appears to be that of improving the overall efficiencies and to explore the possibility

of using collimators in such a way that a reliable spectral intensity calibration of the overall instrument is still possible. The overall increase in the instrumental factor ε (see Fig. 1) resulting from such combined improvements, appears to be possible by much larger factors.

A truly significant reduction in the background counting rate, below that of the January 29 experiment, appears to be possible only by abandoning the present design based on the use of a large sensitive cathode in a fixed mount (see Figs. 2 and 8). An elimination of the background due to cosmic rays by means of surrounding the detector with cosmic ray counters in anti-coincidence circuit, at present appears to be less appealing than a more radical redesign of the overall instrument involving the development of EUV-detectors with a very small sensitive volume.

The next instrument now prepared for flight on an Aerobee Hi rocket in the near future is being equipped with a 7500 line per inch grating, a 0.1 mm wide entrance slit, and an EUV-detector of considerably improved average photo-electron counting efficiency (η_3). This time, the four exit slits in the steel band running along the Rowland circle will not be identical. Three of the slit cut-outs will be only slightly "over-matched" (i.e. the exit slit bandwidth is somewhat larger than the entrance slit bandwidth), whereas one of the slit cut-outs will be approximately 4 times as wide. This arrangement will afford a valuable help in the distinction of signal components due to merging spectral lines and overlapping continuum radiation.

4.5. Automatic Data Reduction

Even the records from a single relatively short-lived rocket monochromator flight (a sample is shown in Fig. 6) contain a sufficiently large amount of information, so that the conversion of this information into the most useful and intelligible form requires a very long time, if this evaluation is done by human hands. The three rocket monochromator flights that have provided geophysically significant information in the past have actually been evaluated that way. As it is not only technically possible but scientifically most desirable to fly many more vertical probing monochromators of improved performance (i.e. providing more information per flight), as well as to install similar instruments in satellite vehicles orbiting around the earth capable of more or less continuous data acquisition, strictly human evaluation of the expected enormously increased influx of recorded data can hardly be considered to be feasible.

Fortunately the records received on the ground are of a nature very conducive to automatic data reduction. Therefore, the fact that the physical information contained in the records of the past few flights has been extracted essentially by manual work, should not be taken as an indication of some major obstacles in the way of automatic data reduction. The need for human evaluation was simply caused by the fact that no significant effort had been devoted to the solution of

this technical problem until very recently. A first attempt made in this direction with the tape records from the January 1960 flights already gave very encouraging results. The composite FM/FM signal taken from magnetic tape was passed through the ground station discriminator for channel separation. The time of occurrence of each "staircase" was read and digitized at a rate up to and including 500 events per second. The time of the leading edge of the wavelength identification signal pulse was used as the digital reference. The wavelength values of all these signal edges (determined from laboratory calibrations for each monochromator) were furnished to the data reduction group at White Sands (Telecomputing Services, Inc.) to be used as the necessary information to correlate time and wavelength position. The counting rates were defined as the reciprocal of the elapsed time between "staircases." For each such intensity reading the corresponding wavelength was determined by linear interpolation between the neighboring two wavelength markers. The results were presented in both tabular form (time, wavelength position, counting rate) and in graphic form (plots of intensity vs. wavelength, one plot for each complete scan). In principle, this procedure worked very well. However, the limitations in the computational procedure resulted in much poorer accuracy than that extracted from the same record by manual evaluation. Since this first attempt, various other computational procedures have been considered. Discussion of the technical problems with various groups engaged in automatic data reduction have confirmed our hope that the need for human evaluation of rocket monochromator data will soon be completely eliminated. Also it is reasonable to hope that automatic data reduction will have reached a stage by the time of launching the first satellite monochromator, where the spectrophotometric information required by the instrument in orbit can be displayed on the ground and stored for future desirable correlations without much delay of time.

5. CONCLUSIONS

The practicability of telemetering spectrophotometry of solar EUV and x-rays, has been demonstrated experimentally for the case of rockets. The experience acquired from these first rocket flight tests leaves no doubt about the feasibility of future experiments of this type from artificial earth satellites, and even from future vehicles which may be sent far away from the earth to explore other regions of the inter-planetary space or the absorption characteristics of planetary atmospheres. The GRD instrument, in its present form, fills many important research requirements rather well. The specific requirements in the foreground during the design phase of this instrument were oriented primarily towards terrestrial aeronomy. The adoption of the same instrument design for other purposes, such as EUV or x-ray image formation of the sun, or stellar EUV and x-ray spectrophotometry is, of course, hardly advisable. Experimental develop-

ments in these directions may be expected to result in significantly different technical developments, each serving a specific purpose. The practicability of constructing a big universal instrument to serve all scientific purposes at the same time appears to be seriously questionable, and a major effort in this direction cannot be recommended, at least not at this time.

An important field other than that of terrestrial aeronomy, to which the present GRD instrument appears to be immediately applicable will be the study of monochromatic attenuations by planetary atmospheres (i.e. "Planetary Aeronomy") and possibly the study of any interplanetary absorption of solar radiation at certain wavelengths.

The question "grazing incidence" or "normal incidence" arising for future monochromator developments is not generally meaningful and an answer can be suggested only for certain specific cases. A comparison of the performance of the GRD monochromators (grazing incidence) with the photographic records obtained recently by Tousey's group, at the Naval Research Laboratory (Tousey (1960)) with gratings used in normal incidence leads to the conclusion that the construction of normal incidence monochromators for solar spectrophotometry above about 500 or 600 A will be much more profitable. For the range of shorter wavelengths, the use of grazing incidence appears to remain a practical necessity. The reason for the preference of normal incidence above 500 A is the well-known fact that this method eliminates automatically the appearance of significantly intense higher order diffractions of radiation of shorter wavelengths that may very inconveniently overlap with the first order spectrum between 500 and 1000 A. The problem of overlapping orders naturally exists also for measurements below 500 A, that is the domain of grazing incidence techniques. Some improvements may be expected from the use of a set of different instruments with different angles of incidence, corresponding to different short wavelength limits of instrumental response. A less costly approach appears to be that of equipping grazing incidence grating monochromators with suitable interchangeable filters of known soft x-ray transmission characteristics, so that the filter difference method can be used to separate, or at least to identify, overlapping orders. The additional use of retarding potential discrimination that may be incorporated in the photoelectric detector also deserves further consideration, even though an efficient discrimination of this type is not possible without a rather inconvenient decrease in the detection sensitivity for those wavelengths, against which one does not wish to discriminate.

A considerable amount of pure laboratory research related to the study of gratings, new optical systems, the problem of absolute intensity measurements in the EUV and soft x-ray region of the spectrum, and both broader and academically deeper study of photo-electric emission phenomena must be considered among the most crucial requirements for sound overall progress. One must conclude at this time that neglecting of these areas by too much diversion toward operational problems of vehicle instrumentation, would soon lead to a situ-

ation where the general rocket technology would be in a much better state than the actual physics that it enables us to do.

REFERENCES

Baker, R. F., 1938, J. Opt. Soc. Am. **28**, 60.

DuBridge, L. A., 1927, Phys. Rev. **29**, 451.

DuBridge, L. A., 1928, Phys. Rev. **31**, 236.

Ebert, H., 1889, Wiedemanns Ann. **38**, 489.

Fan, H. Y., 1945, Phys. Rev. **68**, 43.

Fastie, W. G., 1952, J. Opt. Soc. Am. **42**, 641.

Goldberg, L., 1954, "The Earth as a Planet," ed. G. P. Kuiper, Chap. 9.

Hall, L. A., and Hinteregger, H. E., 1960, in press.

Heroux, L., and Hinteregger, H. E., 1960, Rev. Sci. Instr. **31**, 280.

Hinteregger, H. E., 1954, Phys. Rev. **96**, 538.

Hinteregger, H. E., 1954, Fourteenth Annual Conf. on Physical Electronics, M.I.T.

Hinteregger, H. E., 1960, The First International Space Science Symposium, North Holland Publ. Co.

Hinteregger, H. E., Damon, K. R., and Hall, L. A., 1959, J. Geophys. Res. **64**, 961.

Hinteregger, H. E., Damon, K. R., Heroux, L., and Hall, L. A., 1960, The First International Space Science Symposium, North Holland Publ. Co.

Hinteregger, H. E., and Watanabe, K., 1953, J. Opt. Soc. Am. **43**, 604.

Jacchia, L. G., 1960, Smithsonian Astrophysical Observatory Report No. 39.

Johnson, F. S., Malitson, H. H., Purcell, J. D., and Tousey, R., 1958, Astrophys. J. **127**, 80.

Jursa, A., LeBlanc, F. J., and Tanaka, Y., 1955, J. Opt. Soc. Am. **45**, 1085.

Kenty, C., 1933, Phys. Rev. **44**, 896.

Rense, W. A., 1953, Phys. Rev. **91**, 229.

Rense, W. A., and Violett, T., 1959, J. Opt. Soc. Am. **49**, 139.

Schwinger, J., 1949, Phys. Rev. **75**, 1912.

Sziklay, G. C., and Schroeder, A. C., 1946, J. Appl. Phys. **17**, 763.

Shinoda, G., Suzuki, T., and Kato, S., 1956, J. Phys. Soc. Jap. **11**, 657.

Stacey, D. S., Stith, G. A., Nidey, R. A., and Pietenpol, W. A., 1954, Electronics **27**, 149.

Tamm, I. G., and Schubin, S., 1931, Zeitschr, F. Physik, **68**, 97.

Tomboulian, D. H., and Hartman, P. L., 1956, Phys. Rev. **102**, 1423.

Violett, T., and Rense, W. A., 1959, Astrophys. J. **130**, 954.

Wainfan, N., Walker, W. C., and Weissler, G. L., 1953, J. Appl. Phys. **24**, 1318.

Walker, W. C., Wainfan, N., and Weissler, G. L., 1955, J. Appl. Phys. **26**, 1366.

Walker, W. C., and Weissler, G. L., 1955, Phys. Rev. **97**, 1178.

Watanabe, K., and Inn, C. Y., 1952, J. Opt. Soc. Am. **43**, 32.

Watanabe, K., 1958, Adv. Geophys. **5**, 153.

Weissler, G. L., 1956, Encyclopedia of Physics, ed. S. Flügge, Vol. XXI.

4. TELEMETERING MONOCHROMATOR MEASUREMENTS OF EXTREME ULTRAVIOLET RADIATION
PART II: Physical Applications

H. E. Hinteregger
Geophysics Research Directorate
Air Force Research Division
Bedford, Massachusetts

1. TERRESTRIAL AERONOMY

1.1. General Discussion

It seems most appropriate first to summarize the existing preliminary data and discuss applications of EUV monochromator measurements with respect to the earth's atmosphere. As the primary interest of most of the readers of this article probably lies in other applications, this section is presented here mainly as an introductory illustration for future work in other fields, particularly the study of planetary atmospheres (II; 2). To date EUV monochromator measurements have been limited to terrestrial rocket experiments (see I; 4). Consequently, only this first section (II; 1) can be written on the basis of practical experience, whereas much of the discussion in the remaining sections will lack the desirable factual foundation. Therefore, these other sections will comprise no more than a selection of preliminary comments, that may have to be revised or revoked soon on the basis of more reliable factual evidence.

Measurements of a monochromatic flux of solar photons as a function of altitude contain much valuable information on the structure of the part of the atmosphere in which these measurements are made. This is indicated schematically in Fig. 14, where it is assumed that a rocket monochromator is kept pointing at the sun and transmits data on the spectral photon flux (see I; 3.1.), and that other information identifies the altitudes. Actually a vertical rocket trajectory is most desirable only if one suspects any unusually high horizontal variations of density and/or composition. Otherwise trajectories at angles considerably closer to the horizontal plane offer the practical advantage of a longer time spent in going through a given range of altitudes.

The determination of EUV absorption rate densities,

$$a(\lambda) = (d\Phi/dh) \cos Z$$

provides the necessary direct basis for a quantitative description of

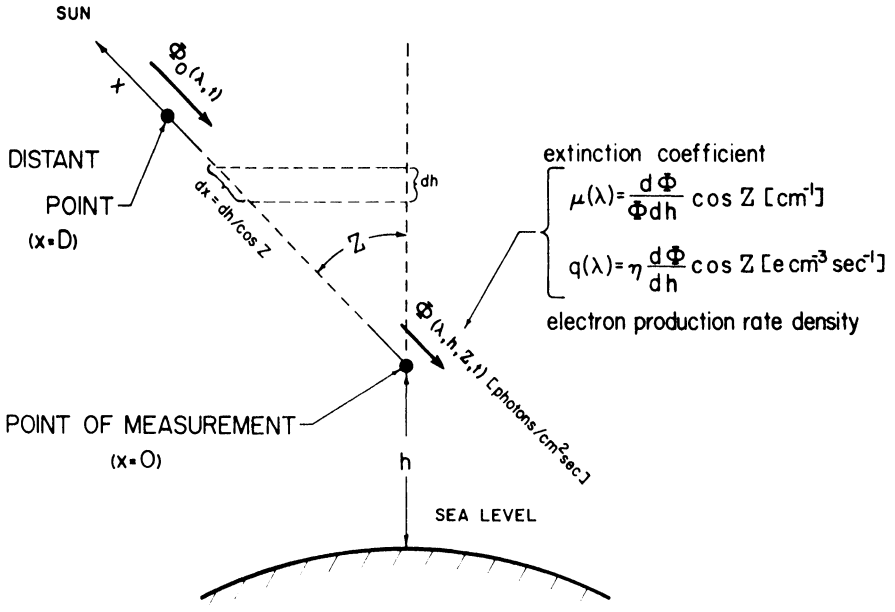


Fig. 14. Schematic illustration of solar EUV monochromator measurements in the upper terrestrial atmosphere or planetary atmospheres.

upper atmospheric heating and ionization (see Figs. 14 and 15).

The determination of monochromatic extinction coefficients,

$$\mu(\lambda,h) = (d \ln \Phi/dh) \cos Z$$

contains a wealth of information on upper atmospheric density and composition, even if the measurements are made for a few selected wavelengths only. As the extinction coefficient μ depends only on the ratio $d\Phi/\Phi$, even an instrument without any absolute intensity calibration gives accurate results on $\mu(\lambda, h)$ as long as it is linear in its response. Fortunately the achievement of excellent linearity hardly presents a problem for photo-electric detection techniques. The practical problem of absorption measurements for the purpose of deriving significant information on density, scale heights and composition is facilitated by the following natural circumstance. The solar emission in the EUV and soft x-ray region of the spectrum contains many sections of wavelengths within which the absorption cross sections of atmospheric constituents do not vary rapidly at all (ionization continua in regions of no superimposed line- or band-absorption). Where this is true, a useful absorption spectrometric analysis can be made with instruments of very modest resolution. This has not only the technological advantage of simplicity but also the physical advantage of much higher speed than that obtainable with any high resolution monochromator.

For any given wavelength, it is convenient to distinguish essentially

three regions: a "low attenuation region" at very high altitudes ($h > h_0$ in Fig. 15); the "main absorption region" with a maximum absorption rate density around some altitudes h^* (see Fig. 15); and a "base region" ($h < h_B$ in Fig. 15) that is the whole atmosphere below, where the specific monochromatic flux has dropped off to some practically negligible value. Naturally such a region does not exist if an appreciable amount of the radiation reaches the ground. However, for the wavelength range of solar radiation in EUV, say below 1300 A, practically complete extinction always occurs far above the ground.

EUV radiation measurements from rockets aid terrestrial aeronomy by three distinctly different types of experiments, namely:

(a) Experiments in which the *solar EUV* photon flux per se is the *object of investigation.* There, one wishes to measure the absolute spectral intensity distribution of the "incident fluxes" (i.e. those outside the significantly absorbing regions of the atmosphere), as well as their absolute dissipation rates in the various regions of the atmosphere.

(b) Experiments in which *solar EUV* radiation is merely used as a convenient *tool of probing* the upper atmospheric structure by the application of absorption spectroscopic analysis. These techniques are quite common and well-known as far as the general principles are concerned. The practical measurements in the upper atmosphere, however, require considerable additional developments, because the conventional techniques of absorption analysis have been established for

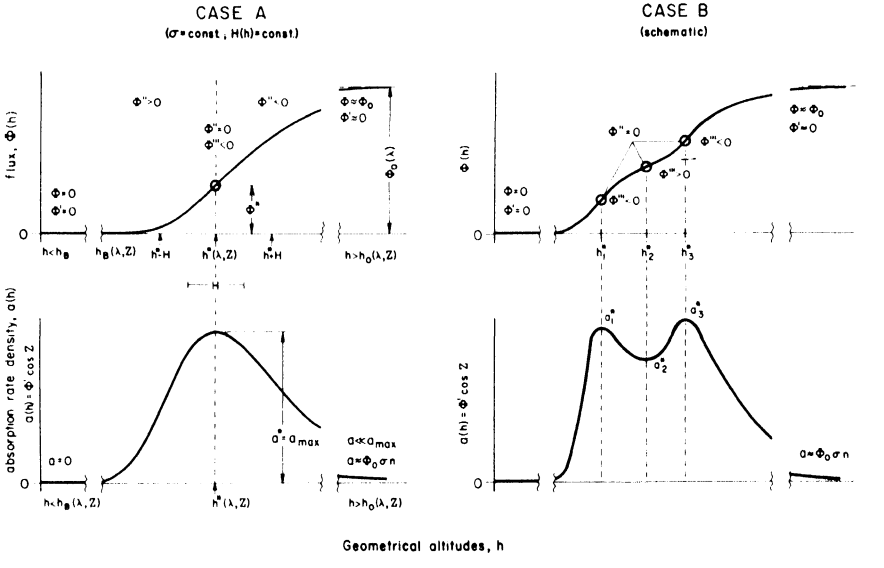


Fig. 15. Schematic illustration of the atmospheric attenuation of a monochromatic solar EUV photonflux, as a function of altitude, h. Case A represents the simplest type of a monochromatic Chapman-layer: case B indicates schematically some strong deviation from the idealized case A.

experimentation in the laboratory only. For the range of wavelengths below about 1100 A even these laboratory techniques leave much to be desired.

(c) Experiments in which *EUV radiation of atmospheric origin* is analyzed. Measurements of this type are extremely important and deserve a detailed discussion. Such a discussion, however, has not been included in this article.

In the present early stage of development of telemetering monochromators (see Part I), no instrumental specialization in the three directions (a), (b), and (c) has been carried through. It is quite obvious, however, that such a specialization is most desirable, because the specific instrumental requirements that are most important are not at all the same for the two groups of experiments.

It seems safe to predict that occasional *short-lived rocket experiments* will retain their value in a future systematic experimental program mainly as a probe of the vertical structure of the upper atmosphere, but not as the desirable means of acquiring accurate and complete knowledge of the flux of solar EUV photons incident upon the earth's atmosphere. A systematic study of the latter clearly demands the use of satellite vehicles. Some technical reasons for this requirement have been discussed in Part I (particularly I; 3.). The scientific reasons for this requirement (study of long and short term variations, correlations with ground observations of solar flares, magnetic storms, ionization measurements, measurements of solar radio emissions, upper atmospheric density variations, etc.) are truly obvious, so that they need not be discussed in detail here. The few experiments conducted in the past have revealed no more than an occasional glance at the solar EUV spectrum. It is true that a comparison of these few measurements supports the idea that no major changes occur in the intensities of certain important solar emission lines such as the Lyman-α lines of hydrogen (1216 A) and ionized helium (304 A). It would be quite wrong, however, to conclude from this meager evidence that there is probably no need for *continuous measurements* in time. At least for certain ranges of the solar emission spectrum most significant variations have already been determined experimentally by Friedman's group at the Naval Research Laboratory (see other article in this book).

The use of satellites rather than rockets also appears to be desirable for experiments of type (c) to make more or less continuous measurements of EUV radiation from aurorae and airglow.

1.2. The Incident Solar EUV Flux

The lack of continuity in time is but one defect in our present experimental knowledge of the incident solar EUV spectrum. The other defect lies in the insufficiently high altitudes to which all measurements have been limited in the past. Therefore our present knowledge of the absolute intensity distribution of the solar EUV photon flux, $\Phi_0(\lambda, t)$, that falls upon the earth's atmosphere, suffers not only from

instrumental inaccuracies (see Part I) but also, indirectly, from the existing uncertainties about the EUV absorption characteristics of the atmosphere above the highest point of observation reached so far. This is best illustrated by the practical example of combining the existing preliminary measurements of the spectral photon fluxes at altitudes of 210 and 225 km respectively (see Fig. 16) with partially hypothetical models of the spectral transmission, $\Phi(\lambda,h)/\Phi_0(\lambda)$, indicated in Fig. 17. To obtain the "incident" flux Φ_0, one has to multiply the true part of the flux values of Fig. 16 (i.e. the fluxes corrected for overlapping higher orders as well as non-diffracted background) with the reciprocal transmission of some adopted model (Fig. 17).

Consequently, any existing data of the incident fluxes on top of the earth's atmosphere reflect the combined errors of both the measurements and the assumed correction for atmospheric absorption. The first error, or group of errors, at present is still relatively high, particularly below 300 A, where a calculation of the "absolute" fluxes had to be based on extrapolated values of instrumental transmission and photo-electric yields. The other error, that is that of the calculated values of Φ/Φ_0 is more or less serious depending quite critically on the specific wavelength. At wavelengths at which the absorption cross sections of the major constituents (e.g. O and N_2) are relatively

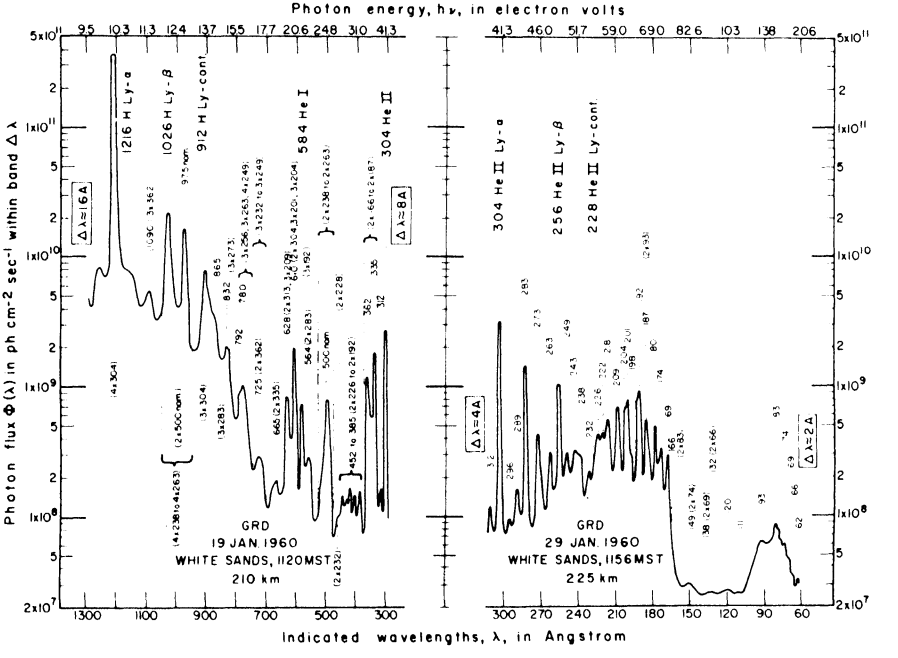


Fig. 16. Solar EUV photonfluxes in the upper atmosphere, as determined from two GRD rocket monochromator flights. Absolute values below 300 A are based on extrapolated instrument efficiencies that could be in error by as much as a factor of 10 towards the shorter wavelengths.

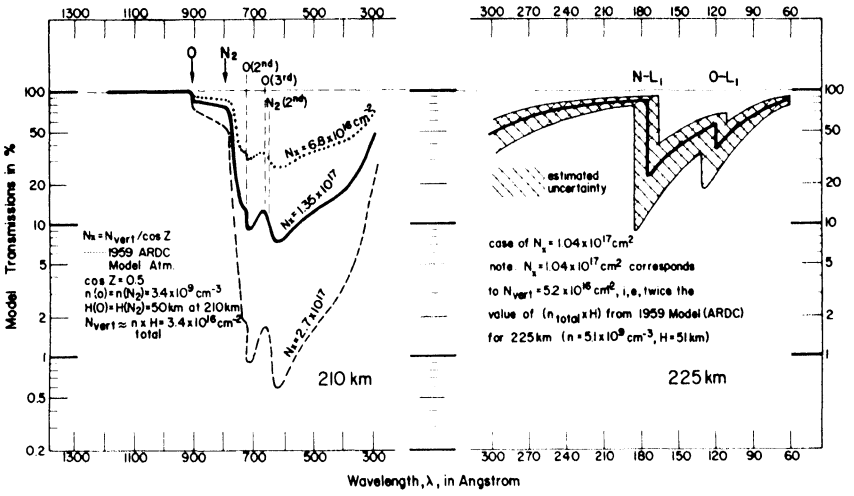


Fig. 17. Models of the EUV transmission of the atmosphere above the two points of observation. The curves are based only on the continuous absorption cross sections shown in Fig. 18.

small, say no higher than 2×10^{-18} cm^2, the transmission, Φ/Φ_0, is insensitive even to large variations in the specific values of densities, relative composition and scale heights that may be chosen for the calculation. The most significant quantities for this calculation are the number of particles contained in the slant column of unit cross section (N_x) and the "weighted mean absorption cross section" ($\sigma = \sum \sigma_j (n_j/n)$, where σ_j is the absolute cross section of a certain species of particles that are present with a number density n_j in the medium of total particle density n). Even though σ depends practically only on the relative composition and not on the absolute density or scale height, there are many regions of the spectrum for which accurate values of σ could not be calculated even for any exactly given composition, simply because the basic cross sections are known only approximately. Some pertinent experimental and theoretical data on cross sections (Bates and Seaton (1949); Weissler and Lee (1952)) are shown in Fig. 18. A weighted mean absorption cross section (dashed line) has been included in this diagram. It refers to the assumed case of a composition of 50% atomic oxygen and 50% molecular nitrogen. This simple case is certainly a rather poor approximation for the actual atmospheric composition above 210 or 225 km. If one considers all other sources of error, however, its adoption for a crude calculation at this time is probably permissible.

The main purpose of showing Fig. 17 here is not to express a preference for a specific model of the upper atmosphere, but to emphasize the extreme sensitivity of the atmospheric transmission correction Φ/Φ_0 to any change in the atmospheric structure above a point of observation around 200 km whenever the absorption cross sections are equal to or higher than about 1×10^{-17} cm^2. The dotted, fully drawn, and dashed curves represent the transmission of three models that progres-

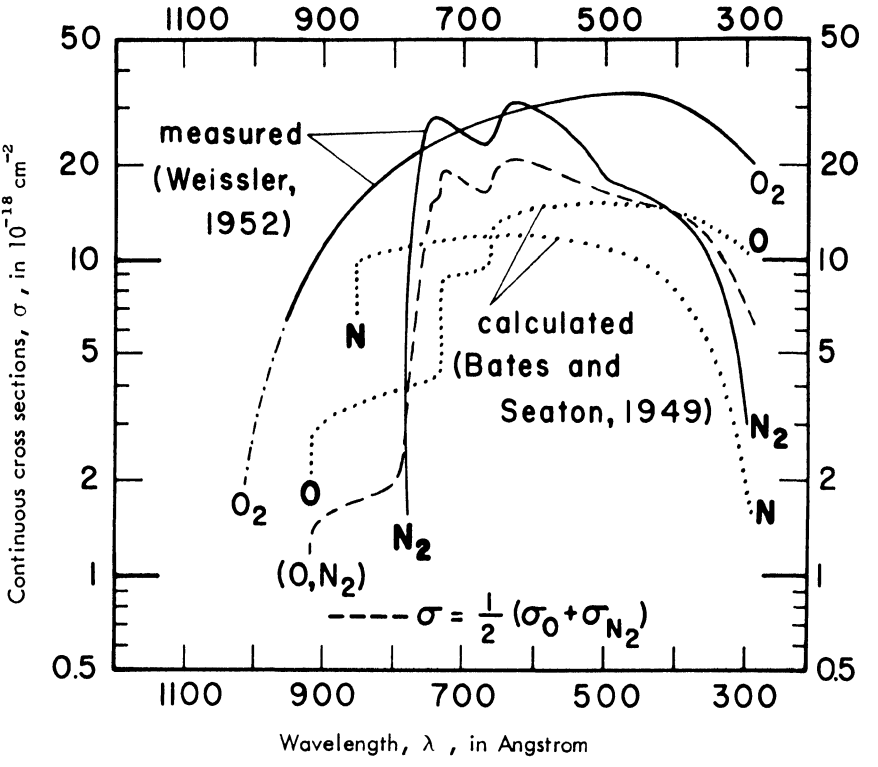


Fig. 18. Continuous absorption cross sections of the major atmospheric constituents, from experimental and theoretical work.

sively differ only by a factor of 2 with respect to the adopted number of particles in the slant column (i.e. the column in direction from the point of observation to the sun). The preference expressed by drawing one of the curves in Fig. 17 particularly thick, has probably only little geophysical significance. This choice merely shows an intention to take into account the special conditions of the rocket experiment (i.e. near local noon), for which the assumption of somewhat higher than average values for both the densities and the scale heights above the point of observation appears to be justified (Jacchia (1960); Priester and others (1960)).

The model transmissions shown in Fig. 17 take into account the absorption cross section of the ionization continua only, since line and band absorptions have been disregarded completely. This neglect is permissible in a crude picture only. This restriction is due mainly to the presence of molecular nitrogen, which is known to have both sharp absorption bands with rather high cross section maxima at certain wavelengths above 800 A and diffuse absorption bands below 800 A that contribute significantly to the total absorption cross section, at least at certain wavelengths. A striking example for the importance of nitrogen absorption can be observed around 972 A. There, the solar hydrogen

Lyman-γ line had been missing conspicuously in all spectrographic records from rockets in the past. This emission line could be identified only recently (Tousey, private communication (1960)) from a rocket experiment on April 19, 1960, in which altitudes above 200 km were reached with an instrument of particularly low stray-light background. But even then, Lyman-γ appeared with a much lower intensity than that of the subsequent members of the series. This is not surprising in view of recent quantitative absorption measurements made on N_2 in the laboratory by Watanabe (private communication (1960)), who worked with a monochromator provided with a hydrogen discharge as a source and achieved a wavelength resolution bandwidth of 0.1 A. In fact the very high value of the cross section obtained (over 10^{-16} cm^2) not only explains the missing of the Lyman-γ line observed in the earlier rocket experiments, but also leads to the conclusion that the hydrogen Lyman-γ emission from the sun itself must have a line breadth well in excess of 0.1 A, so that the effective cross section (averaged over the full breadth of the emission line) is again reduced to a much

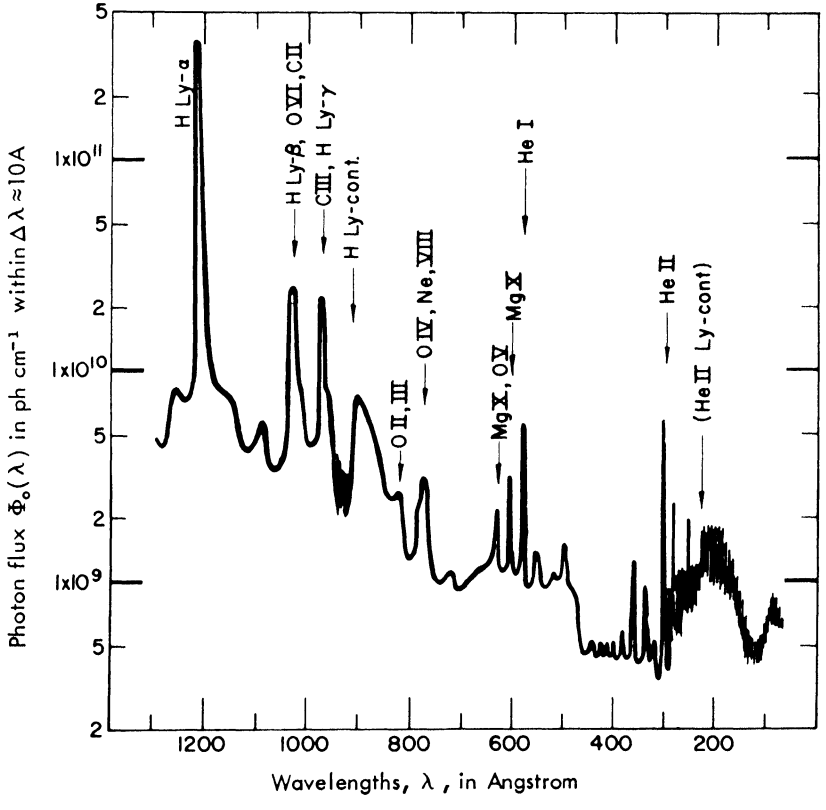


Fig. 19. Estimated solar EUV photonfluxes on top of the earth's atmosphere. The ordinates represent approximate photonflux densities for an assumed constant wavelength bandwith of 10 A.

smaller value than that measured by Watanabe. Otherwise one could not understand at all why the intensity of this line around 200 km could have been enough for detection even by the improved instrument flown on April 19, 1960.

From these considerations it is also clear that the "monochromatic" flux value measured with low resolution around 975 A as shown in Fig. 16 is practically exclusively due to the solar emission line of C III which falls within the instrumental bandwidth. It should also be noted that the flux shown in Fig. 16 for the wavelength of hydrogen Lyman-β includes the unresolved flux of the O VI and C II emission lines. Much of the spectrum of Fig. 16 between 900 and 300 A has no physical significance, because it is merely the instrumental result of radiation of shorter wavelengths appearing with relatively high intensities in second or third order of diffraction. This disturbance is a common consequence of using gratings in grazing incidence. Fortunately it is possible to obtain much information of value for the separation of the contribution of lines in higher order to the observed intensity signals of some interesting first order lines (e.g. 2×304 A overlapping with the Mg X line at 610 A) by a systematic evaluation of their different vertical absorption characteristics in the atmosphere. Nevertheless, there can be no doubt that a normal incidence grating monochromator would give a much "cleaner" spectrum in the wavelength range above about 500 A. In this range above about 500 A the use of grazing incidence is of course not necessary and has been chosen for the GRD instrument only because the construction of a single instrument for the whole wavelength range extending into the soft x-ray region was considered to be essential in this early phase of experimentation. Therefore, the simultaneous operation of two different types of monochromators (one being a grazing incidence instrument and the other working in normal incidence) would be a most desirable improvement.

As a GRD rocket monochromator of four times higher resolving power (I: 4.4.) has now been completed for a flight in the near future, only a somewhat superficial effort has been spent on the correction of the flux spectrum of Fig. 16. The elimination of overlapping orders of diffraction and the identification of specific lines were greatly aided by the invaluable comparison with densitometer traces of the much better resolved photographic spectrograms ($\Delta\lambda \approx 1$ A) obtained with a normal incidence instrument by Tousey's group for the region above 500 A. (Tousey (1960)). Due to the use of two reflections in nearly normal incidence these photographic records are completely free of the appearance of shorter wavelengths in higher order (no indication could be seen even for the second order of the very intense He II line of 304 A).

It was clear that even a preliminary and relatively crude determination of the absolute spectral EUV photon fluxes outside the earth's atmosphere was important for various fields, so that estimates on the basis of the already existing experimental material should be communicated without delay. To fill this requirement we have composed a graphical presentation (Fig. 19) of the photon fluxes $\Phi_0(\lambda)$ that one would expect to measure with an idealized photon flux meter of a con-

stant bandwidth of 10 A. In this plot the ordinates have the following meaning: the ordinates at the peaks of lines which are not merging with others (within the bandwidth of 10 A) and which are much stronger than the continuum background (integrated over this same bandwidth) represent the complete photon flux density (i.e. that of the line integrated over its whole breadth); where there are two or more lines within a band of 10 A, the ordinate at the peak refers to the sum; where the contribution of lines may be disregarded (e.g. for a curve drawn through adjoining valleys) the ordinates represent the integrated continuum flux for a bandwidth of 10 A. Naturally, the least certain value is that of the continuum intensities, the value of which in conventional units of ph cm^{-2} sec^{-1} A^{-1} equals the ordinate value in Fig. 19 divided by 10. It should be emphasized that the presentation of continuum fluxes other than the Lyman continuum at the present state of experimental knowledge remains quite tentative. Even the simple question, whether or not the qualitative shape of a curve through the valleys of Fig. 19, is significant, cannot be answered on an experimentally firm basis. On the other hand, the information of Fig. 19 with respect to the dominating solar emission lines and the hydrogen Lyman continuum is considered to be not only qualitatively significant but also quantitatively reliable within a factor of uncertainty that is estimated to be no higher than 2 to 5 above 300 A. For many specific wavelengths in this range the uncertainty factor is probably considerably less than 2, whereas below 300 A quoting a specific possible uncertainty is not warranted. Therefore, we add only the somewhat subjective comment, that an error of more than a factor of ten appears to be quite unlikely. A more detailed analysis of all possible sources of error in the existing preliminary data is not attempted. Further improved rocket experiments based on improved laboratory calibrations are expected to lead to a much more reliable evaluation in the near future.

1.3. Future Work

The future use of telemetering EUV monochromators for purposes of terrestrial aeronomy may be visualized rather clearly at this time. New instruments with different wavelength ranges and meeting the specific requirements of different types of measurements will need to be developed. Various versions of grating monochromators with photoelectric detection of the dispersed radiation will probably be the most important tools in this future work. Continued use of the GRD monochromator, essentially in its present rather well proven form, will probably remain profitable for some time, at least for the range of wavelengths below about 600 A.

For the range of wavelengths above about 600 A, however, new developments of rocket monochromators, based on the use of gratings with improved reflecting surfaces in nearly normal incidence and increased speed (by improved collimation techniques) should eliminate the need to continue work above 600 A with the existing GRD instrument (built for grazing incidence).

The most urgently needed future facility will be that of a "solar EUV radiation patrol," meaning a telemetering *satellite monochromator* (preferably a group of at least two or three instruments per vehicle). This instrument should transmit more or less continuously the spectral distribution of the "incident" solar photon flux, $\Phi_0(\lambda, t)$ for all wavelengths of interest. Measurements of this type, even in a preliminary form (e.g. mounting of the existing simple GRD instrument on a satellite), will be extremely valuable in many respects, as follows:

(a) The satellite measurements will fill the generally recognized need to observe the solar EUV emission spectrum on the *continuous basis* that is required for any systematic future studies of *solar-terrestrial relationships* in general, and for any attempt at systematic predictions of changes in the upper atmospheric structure (especially the ionization, etc.) in particular.

(b) Continuous measurements of the incident fluxes Φ_0 (see Fig. 14) will also increase appreciably the physical significance of any measurements with vertical probing monochromators. Even a very accurate determination of a monochromatic flux attenuation profile, $\Phi(\lambda, h)$ versus h, at present suffers from the fundamental doubt: "Is a certain structure in an observed curve of flux versus altitude really significant as an indication of specific conditions of the atmosphere at the time of the experiment, or is this structure merely the accidental result of essentially unknown fluctuations in the light source, i.e. the sun?" Even though this question may be answered in many instances qualitatively on other grounds now, the situation is basically unsatisfactory. For future quantitative studies of the atmospheric structure by means of vertical probing monochromators, a reliable knowledge of the *"reference flux,"* $\Phi_0(\lambda, t)$, for the duration of the vertical probing experiment therefore appears to be mandatory.

This section is concluded with two remarks. First, an apology is in order for the rather incomplete and occasionally quite subjective presentation. Second, the opinion is put forth rather strongly, that already existing technology permits more or less immediately practicable applications of EUV monochromator measurements within a much broader scope than one could have visualized only a few years ago. There is hope that more scientists and engineers will join in the effort of making the best possible use of this fortunate situation.

2. SOLAR PHYSICS

2.1. Change of Scientific Approach

The importance of reliable experimental determinations of the extreme ultraviolet and soft x-ray emission spectrum of the sun has been recognized by many solar physicists and astronomers in the past. Therefore, the advent of modern rocket technology, making possible the performance of complex experiments outside the earth's atmosphere, represents a major step in the history of solar physics. This step ap-

pears to lead to considerable revisions in the relative emphasis that may be put on the different types of scientific endeavor among researchers in the fields of solar physics and astronomy in general. Let us first review the past and then try to assess the present situation.

From inaccurate data on solar EUV (i.e. data that had to be extrapolated from observations at longer wavelengths) combined with inaccurate solar theory, working models of the solar EUV source- and opacity-functions have been constructed to be used for the prediction of the UV and EUV spectra of the sun. Another approach has been that of using existing observations and theories of the terrestrial ionosphere (both inaccurate) as the only available empirical adjustment parameters for various theoretical solar EUV radiation models, again primarily for the purpose of predicting the spectrum of the actual emitted solar radiation. Both the first and the second approach have been most fruitful. In fact, they constituted the only practicable techniques of acquiring any knowledge of the solar UV and EUV spectrum, because the latter was completely inaccessible to direct observation in the past.

Obviously, this situation no longer exists. In an introductory presentation with the title "The Prediction of the UV Spectra of the Stars and the Sun" by Pecker (Pecker (1960)) the present situation has been analyzed in considerable detail. Pecker's conclusion with respect to the most profitable approach for the present and future work appears to be sufficiently characteristic and free of prejudice so that the following liberal translation has a proper place in this article:

"Therefore, it seems that it would be more valuable to bring all efforts to bear on the observational study of the solar UV (EUV and x-rays) and to deduce from these observations a more precise model of the solar atmosphere (or an improved theory of the terrestrial ionosphere)."

2.2. Comments on Future Work

The present state of telemetering monochromator measurements of solar EUV and x-ray fluxes has been discussed under the preceding topic of terrestrial aeronomy. It may be noted though, that section II; 1.2., belongs also under the present topic of solar physics and actually represents the major part of all the factual information that the author can hope to present in this connection. Therefore the present section has been limited to comments on future more specific applications to solar physics per se, without any repetition of the general outlook on future monochromator experiments (presented in section II; 1.3. from a primarily aeronomical standpoint). Naturally, any future progress of telemetering EUV monochromator measurements achieved in the interest of terrestrial aeronomy will probably at the same time serve solar physics. Conversely, improvements conceived in the interest of solar physics will automatically be valuable for terrestrial aeronomy. Thus the historically long established theoretical ties between the two disciplines now have their experimental counterpart. In the present early phase of monochromator measurements, the experimental connec-

tion has been extremely close, and in fact the same instruments have been serving both disciplines. It seems unlikely, however, that the economically desirable use of essentially identical instruments for both fields of research can be maintained in the future. The largely diverging and partially conflicting requirements appear to demand a considerable branching-out into distinctly different instrument developments. The reader may be referred to part I; 1., where some general objections are raised against the idea of developing a large universal facility for common use by the various groups of researchers for all the different objectives. For best results, a team of physicists and engineers engaged in the preparation of new experiments and instrument developments for specific objectives of solar physics should not be hampered by the excessive technological and logistics coordination requirements or the many compromises that would be inevitable for a joint enterprise with another group of colleagues with primary interest in another field.

Among the first objectives of future monochromator measurements (in the interest of solar physics as well as terrestrial aeronomy) will be the improved determination of the absolute spectral distribution of the emitted solar EUV and x-ray photon fluxes. In the range of wavelengths for which experimental data are available now, the measurements should be repeated with many improvements. The transition from a few short-lived rocket experiments to more or less continuous operation from satellites will greatly facilitate the realization of many desirable instrument characteristics that could not possibly be achieved with a rocket instrument (see I; 3.3.).

It seems reasonable to visualize various generations of instruments with progressively advanced performance characteristics. The first generation may consist of grazing incidence grating monochromators similar to the present GRD instrument for the wavelength range from about 600 A to a short wavelength limit that may be extended to about 20 A. New normal incidence instruments should be built for a better coverage of the longer wavelengths. A desirable development in this direction would be that of converting Tousey's latest and most successful version of a normal incidence grating spectrograph (Tousey,(1960)) into a telemetering monochromator. This requires automatic wavelength scanning and photo-electric detection techniques. Another development of considerable promise for the region of longer wavelengths may be that of Ebert-type monochromators (Ebert (1889)). The construction of laboratory instruments of this type (Fastie (1952)) has been carried to a remarkable level by Fastie. The adaptation of Fastie's optical techniques for satellite experimentation (in connection with appropriate photo-electric detection) appears to be straightforward. A combination of instruments of the types listed here could be mounted simultaneously on a relatively simple solar pointing control on existing types of satellite vehicles. Without relying on any uncertain future improvements of grating efficiencies, detector efficiencies, or collimation efficiencies, one can expect that these experiments would cover the wavelength range from about 2000 A at least down to 60 A and hopefully to 20 A, that the measurements would be more or

less continuous and that the instruments would resolve a few tenths of an angstrom unit. A resolution of this order of magnitude appears to be ample for a detailed survey of the solar spectrum as a whole, even though it is of course not adequate for the study of line shapes. This whole *first generation of experiments* may be classified as "survey of the absolute spectral intensity distribution of solar radiation without spectral resolution of line shapes and without any spatial resolution of the solar disk."

Another generation of experiments may be designed to achieve high resolution spectrophotometry. A successful step in this direction with a photographic rocket instrument, for the case of the strong solar hydrogen Lyman- α line, has been achieved by Tousey (loc. cit.). The realization of similar measurements to be telemetered from outside the earth's atmosphere will be very desirable. Improvements in techniques should make it possible to study many other considerably weaker emission lines of the solar spectrum in high resolution. A discussion of these special techniques, however, is beyond the scope of this article.

A third generation of experiments may be designed to achieve both spectral resolution and image formation of the sun in a suitable form for telemetry. The well-known successful photographic rocket experiments with a monochromatic Lyman- α camera by Tousey's group (Purcell, Packer, and Tousey (1959)) and those with a crudely monochromatic x-ray camera (pin-hole camera with absorption filter) by Friedman's group (Friedman (1960)) appear to be the forerunners of future experiments with "monochromatic extreme ultra-violet television cameras." The ideal goal for the development of the latter generation of instruments would be the simultaneous achievement of a good spatial resolution of the sun, a narrow spectral bandwidth, and a sufficiently high F-number. In practice the achievement of high F-numbers may be of dominating importance, because without it the simultaneous use of high spectral resolution and high resolution of the solar disk in space would be impracticable.

The practical development of all these experiments will certainly overlap considerably. Therefore the foregoing order of numbered generations of experiments does not necessarily have a chronological meaning. The brevity of the treatment of the more advanced types of solar radiation experiments in this section does not imply any criticism of their practicability. This brevity has been merely due to the author's relative lack of experimental experience in these areas.

3. PLANETARY ATMOSPHERES

The solar energy flux contained in the extreme ultra-violet and soft x-ray part of the spectrum, say for all wavelengths below 1500 A, at present is known only with relatively poor accuracy (see II; 1.2.). Its order of magnitude, however, appears to be sufficiently well established as being 10 erg cm^{-2} sec^{-1}. As the energy flux of longer wavelengths is about 10^8 times higher, one could suspect that a more detailed knowl-

edge of the EUV and soft x-ray fluxes would have no value for the study of the heat balance of planets. However, this does not seem to be true. The amount of solar energy penetrating to a planet's surface is also a function of the structure of its atmosphere and this can be affected very significantly by solar EUV radiation, even though its intensity is a nearly negligible part of the solar constant.

Since planets without any significant atmosphere are the exception rather than the rule, the effect of photo-electric emission from planetary surfaces due to solar EUV radiation may be dismissed here with the simple comment that this radiation in general is practically completely absorbed by the planetary atmospheres. In fact, the absorption of all gasses in the EUV region of the spectrum is so strong that even extremely thin atmospheres, corresponding to pressures far below 1 micron at the planetary surface, are really rather opaque for these wavelengths. Therefore the restriction of this discussion to planetary atmospheres reflects a characteristic property of the EUV part of the spectrum.

The general effects of solar EUV radiation on planetary atmospheres may be summarized as follows:

(1) EUV contributes significantly to the heating of atmospheric regions that would not absorb any significant fraction of solar radiation of longer wavelengths,

(2) EUV is the major source of dissociation and photo-chemical reactions,

(3) Both phenomena (1) and (2) affect the atmospheric structure as well as the mechanism of escape of particles from planetary atmospheres into the inter-planetary space,

(4) EUV appears to be the major source of the formation of ionospheres. Indirectly, the photo-ionization of planetary atmospheres also affects their structure. The most significant secondary effect may be the influence on the escape rates from the exospheres (because ionized particles escape more readily than the corresponding neutral ones).

In contradistinction to the negligible role of EUV radiation in the direct heating of planetary surfaces, it is quite possible that solar EUV is not only a contributing but actually the dominating factor in the heating of "upper" planetary atmospheres such as that of the earth. In this connection, the expression "upper atmosphere" has been used freely implying the existence of some region starting at an altitude above which the atmospheric gas temperature may depend on EUV absorption and photo-chemistry more critically than on the temperature of the planetary surface. Recent evaluations of upper terrestrial atmospheric densities from satellite-drag observations have established beyond doubt the existence of systematic diurnal variations (Jacchia (1960); Priester, Martin, and Kramp (1960)). These variations are most logically associated with the absorption of solar EUV radiation. The existing observations of the earth's atmosphere suggest that a similarly close connection probably exists between solar EUV radiation and the upper atmospheres of other planets.

In principle, one may visualize a future experimental program of

EUV monochromator measurements for purposes of the physics of planetary atmospheres in more or less direct analogy with the existing program of technically much simpler applications of EUV measurements to terrestrial aeronomy (II; 1.). From a practical standpoint, however, one must appreciate the widely different degrees of technological difficulty associated with the vertical probing flight (see Fig. 14) of telemetering EUV monochromators in the atmosphere of the earth and in that of some planet respectively. Therefore, the value of the indicated analogy may be restricted to the planning of a future generation of experiments, and the question arises as to which type of immediately practicable experiments should be considered for an exploratory program. Some answers to this practical question are suggested below.

The acquisition of observational or at least partially observational data on the spectral distribution of the absolute EUV solar photon fluxes incident upon the planetary atmospheres seems to deserve priority, because it forms the fundamental basis required for any quantitative theory of planetary atmospheres. As the absorption of solar radiation by the interplanetary medium is probably insignificant for most wavelengths of the EUV spectrum (even over distances of several astronomical units), semi-empirical data on the fluxes incident upon a certain planet may be inferred from the existing and future better measurements of these fluxes outside the significantly absorbing regions of the earth's atmosphere. For this inference one would simply use the inverse-square law assuming that the variations from spherical symmetry in the solar emission can be neglected. This phase of work is well underway. One can also hope to obtain valuable experimental indications as to whether or not the foregoing two simplifying assumptions (insignificant interplanetary absorption and spherical symmetry of solar radiation) are really justified. This may be achieved much sooner than one may reach the technologically more demanding goal of reliable direct measurements in the vicinity of even the nearest planets.

Another group of experiments not yet requiring any actual vertical probing within a planetary atmosphere could be made from vehicles that have a reasonable chance of going through the umbra of a planet. It is true that one may not wish to devote a full effort to such a chance-experiment, but significant results may be obtained with nearly the same instrumentation that would be used for any experimental exploration of the solar EUV radiation fluxes throughout the inter-planetary space. If the vehicle really goes through the umbra of the planet, one should obtain some useful information on the EUV absorption characteristics of the planet's atmosphere, to be acquired during the time when the vehicle is approaching the umbra and before the pointing control loses hold of the sun. Depending both on the distance of the fly-by trajectory from the planet and on the instrumental speed with which the pointing control can again lock onto the sun, the exit from the umbra may be less valuable than the entry. Naturally it would be desirable to use the time spent within the umbra for some other experimental purpose (e.g. to switch to a completely different instrument of high sensitivity, relatively large field of vision, high scanning speeds

and necessarily low resolution; possibly non-optical photo-electric analyzers).

The last generation of planetary EUV experiments would be those requiring vertical probing vehicles within the planet's atmosphere. These experiments would probably in principle be the same as terrestrial atmospheric probing experiments. A repetition of their discussion *mutatis mutandis* here is not necessary as the reader may be referred to the section on terrestrial aeronomy (II; 1). The author wishes to admit, however, that this reference is caused primarily by the present lack of more pertinent experimental information. As work in this field progresses, the presently convenient working analogy may soon be broken down. In the future, the experimental differences and specific research needs should be treated in an increasingly specialized manner, probably separate with respect to any specific planet.

A separate discussion will be attempted here only for the case of the Moon. Naturally, the Moon is of considerable practical interest because of its technologically convenient vicinity. The main reason for its discussion here, however, is the "absence" of an "ordinary atmosphere." The Moon's inability to retain an atmosphere of substantial density is generally accepted and has been described in the standard literature (e.g. Urey (1952)). This does not of course mean that there is no lunar atmosphere at all. At least it is almost certain that the density in the lunar atmosphere exceeds considerably (and measurably) that of the interplanetary medium at greater distances. The problem whether or not the Moon may have retained significant amounts of heavy gases such as xenon as well as the whole problem of escape mechanisms have been considered in some detail by various authors. The applicability to the Moon of Spitzer's calculation of the escape rate of gases from a neutral isothermal exosphere (Spitzer (1952)) has been questioned on various grounds recently. Herring and Licht have discussed the effect of a "solar wind" (assumed to consist of a flux of about 10^{11} protons/cm^2-sec of energies around 10^4 electron volts). They concluded (Herring and Licht (1960)) that this effect would reduce the density of the lunar atmosphere to values many orders of magnitude smaller than those calculated for an idealized isothermal lunar atmosphere (Jeans (1954)). Another objection against the assumption is related to the effects of solar EUV radiation. Photoionization by solar EUV radiation has been mentioned as an additional reason (besides that of low gravitational potential) for the lack of a substantial lunar atmosphere by Urey (loc. cit.).

Most recently the role of ionizing solar EUV radiation for the escape of gases from the Moon has been considered in some detail by Opik and Singer. These authors conclude that electric forces resulting from the ionizing effects of solar EUV are more important than gravitational forces (Opik and Singer (1960)). They also conclude that "there is not much likelihood that light or heavy gases evolving from the Moon will be retained by the Moon. The only gas in the vicinity of the Moon can come from interplanetary space itself." Unfortunately, Opik and Singer had to use very crude simplifying assumptions for their

quantitative calculations of the ionization rates of interesting gases such as hydrogen, krypton, or xenon. They considered solar 304 A radiation as the exclusive agent, taking a flux of 2.3×10^{11} ph cm^{-2} sec^{-1} that is probably far too high. On the other hand, they had no knowledge of the photon fluxes of wavelengths longer than 304 A determined recently (II; 1.2.). For these wavelengths the ionization cross sections are considerably higher than those at 304 A. Therefore the numerical calculations by Opik and Singer will have to be revised considerably. Inclusion of the most effective ionizing photon fluxes such as those of the hydrogen Lyman continuum (II; 1.2.) in these calculations revises the total ionization rates in the upward direction by a factor that is even greater than that by which Opik and Singer are believed to have overestimated the 304 A photon flux (i.e. at least 30). As a result their conclusion as to the importance of ionizing effects of solar EUV radiation for the lunar atmosphere must be maintained here with an increased emphasis. Improved measurements of the incident solar EUV photon fluxes (II; 1.3.) as well as attempts to measure any absorption of EUV radiation passing through the lunar atmosphere are therefore considered to be a valuable contribution to lunar physics. Another desirable experiment would be that of measuring EUV radiation from the Moon with sufficiently good resolution separating ordinary scattering and reflection of solar radiation from EUV emissions that may be caused by electron bombardment of the lunar surface.

The present discussion of the applications of EUV monochromator measurements to the study of planetary atmospheres must not be concluded without mentioning the interesting group of experiments designed to study EUV radiations that may originate from planetary atmospheres.

4. THE INTERPLANETARY MEDIUM

The existing semi-empirical knowledge of the solar EUV radiation fluxes incident upon the earth's atmosphere (II; 1.2.) leads to the conclusion that the interplanetary medium must be practically fully ionized not only near the earth but also at distances from the sun much greater than one astronomical unit. The consideration of any other sources of interplanetary ionization, e.g. solar corpuscular radiations, can of course only increase the estimated total percentages of ionization beyond those estimated to be due to solar EUV radiation alone. Preliminary estimates of the ionization probability of hydrogen and helium in the interplanetary space near the earth (Hinteregger (1960)) have been reproduced here as Table I. The last row refers to the estimated total effect of solar EUV radiation of all those wavelengths which have been covered by rocket monochromators. The photoionization time of hydrogen corresponding to the value of $\sum \sigma_j \Phi_0$ listed for H in Table I is only about 20 days near the earth. The corresponding fractional degree of ionization is less than 99.0,

TABLE I

Wavelength band, or wavelength $\lambda_1 - \lambda_2$, λ in A	Solar photon flux density Φ_0 Φ (210 km) in 10^9 $cm^{-2}sec^{-1}$		Intensities I I (210 km) in erg $cm^{-2}sec^{-1}$		Approx. Ionization Cross-Sections $\bar{\sigma}_j$ in 10^{-18} cm^2					Ionization Probabilities per Unit Time $\bar{\sigma}_j \Phi$(210 km) White Sands, near noon, Jan. 1960 in 10^{-9} sec^{-1}			$\bar{\sigma}_j \Phi_0$ "on top of atmosphere" in 10^{-9} sec^{-1}				
					H	O	N	N_2	He	O	N	N_2	H	O	N	N_2	He
1216	370	370	6.0	6.0													
1300-1040	50	40	0.85	0.68													
1040-1000	45	36	0.90	0.72													
1000-950	40	18	0.80	0.36													
950-912	20	6	0.40	0.13													
912-850	50	20	1.10	0.45	6	3.5				70			300	175			
850-650	30	3	0.80	0.08	4	7	11	(28)		21	33	84	120	210	330	840	
650-475	30	3	1.10	0.11	2	14	11	25		42	33	75	60	420	330	750	
475-300	10	1.5	0.50	0.08	0.7	14	7	12	4.5	21	10	18	7.0	140	70	120	45
304	6	3	0.40	0.20	0.3	10	1.7	3.4	1.6	30	5	10	1.8	60	10	20	10
300-250	7	4	0.50	0.30	0.2	6	1.0	2	1.3	24	4	8	1.4	42	7	14	9
250-170	8	6	0.76	0.57	0.1	2	0.3	0.6	5	12	1.8	3.6	0.8	16	2.4	4.8	40
170-110	3	0.5	0.45	0.08	0.05	0.6	5	10	1.7	0.3	2.5	5	0.2	2	15	30	2
110-60	2	1.5	0.46	0.35		2	1	2	0.5	3	1.5	3		4	2	4	1
1300-60	670	510	15	10						220	90	200	450	1000	750	1700	100

99.9, or 99.99 per cent for the idealized case assuming that there is only hydrogen, that the total particle number density is less than $500/cm^3$, and that the effective recombination coefficient is of the order of 10^{-11}, 10^{-12}, or 10^{-13} cm^3/sec respectively.

EUV measurements of the optical thickness of the interplanetary medium between the sun and any given planet are important not only for solar physics and the study of the interplanetary medium per se, but also for the study of planetary atmospheres (see II; 3.). Experimental studies of the solar emission spectrum prior to the advent of rocket spectrometry had been restricted to the same wavelength range within which astronomers had looked successfully into distances that are many orders of magnitude greater than the distance of the farthest planet from the sun. Thus there has been no doubt as to the optical transmission (in these same wavelengths) of the medium between the sun and the planets. Experiments outside the terrestrial atmosphere, however, open an entirely new view.

Although rocket measurements of the solar EUV and soft x-ray spectrum have just begun, the mere fact of their existence has established important empirical knowledge. It has demonstrated that the interplanetary medium between the sun and the earth's atmosphere must be significantly transparent also in the interesting range of wavelengths below about 915 A. This range is of particular interest because no stellar radiation of these wavelengths has been found to be detectable so far. The experimental techniques of detecting stellar EUV radiation, however, are still in their infancy. Therefore our present knowledge of the opacity of the interstellar medium (along interstellar distances) for these wavelengths, still appears to rest primarily on the accepted theoretical picture assuming that the average density of the interstellar medium is of the order of one particle per cubic centimeter and that these particles are mostly neutral hydrogen.

Although no specific theoretical model of the interplanetary medium appears to have been generally accepted, a few general model concepts and some order of magnitude considerations will be presented below. Such considerations are desirable not only for any preliminary selection of EUV monochromator experiments for studies of the interplanetary medium per se, but also for an appraisal of the significance of interplanetary absorption effects for monochromator experiments designed mainly to study the sun and planetary atmospheres.

Without restricting ourselves to any specific theoretical model, we shall merely assume that the total particle number density, n, is a function of distance from the sun, r, that decreases as $r^{-\delta}$, where δ lies between zero (constant density) and $\delta = 2$ (inverse-square law). The wide range of δ seems to accommodate a sufficiently large variety of different specific models.

Since the solar photon fluxes $\Phi(\lambda)$ must fall off at least as rapidly as r^{-2}, and since the ionization cross sections of the neutral interplanetary hydrogen can be taken as constants, the "characteristic density" defined by the expression $n_c \equiv (\sum \Phi\sigma)/\alpha$ (Hinteregger, loc. cit.) also decreases at least as rapidly as the inverse-square distance, as long

as the recombination coefficient, α, can be considered to be essentially constant (at least not to decrease significantly for increasing distances from the sun). Thus the characteristic density* can be described by the function $n_c \approx n_{c,r_0} (r/r_0)^{-(2+\gamma)}$ with $\gamma \geq 0$, which of course decreases more rapidly than the actual total particle number density. Beyond a certain as yet unknown distance from the sun, the relative abundance of neutral hydrogen is therefore expected to increase beyond that of the ions until a more or less stationary situation characteristic of the local interstellar medium may be reached.

To obtain some typical approximate figures, let us assume that the effective recombination coefficient is of the order of 10^{-12} cm^3/sec and adopt Hinteregger's (loc. cit.) estimated value of the photoionization probability of hydrogen. The corresponding characteristic density near the earth's orbit assumes the high value of about 5×10^5/cm^3. On the other hand, it seems certain that the characteristic density beyond a distance of 1000 astr. units from the sun becomes smaller than the average interstellar particle density, even if we assumed completely negligible absorption (i.e. $\gamma = 0$). At a distance up to at least 30 to 50 astr. units, however, the characteristic density is probably still well above the actual local density. Therefore the interplanetary medium out to the farthest major planets, Pluto and Neptune, is believed to be largely ionized (i.e. at the orbit of Pluto still certainly more than 50 and most likely more than 80 per cent).

Too little is known at present about interplanetary density and composition to present any quantitative estimates of interplanetary EUV absorption here. The foregoing crude considerations, however, suggest the following qualitative picture to be in reasonable agreement with the meager body of existing observations:

For most wavelengths in the EUV region the optical thickness of the medium between any two points within the interplanetary space is probably extremely low, because protons and electrons rather than neutral hydrogen are the main constituents.

Since the density of *neutral hydrogen* can hardly exceed a few particles/cm^3 anywhere within the interplanetary space, Lyman-α is probably the only significantly absorbed line of the solar hydrogen emission spectrum. For a section of the interplanetary medium between a point near the base of the solar corona and a point near the earth's orbit, however, the optical thickness still appears to be much smaller than unity even for the Lyman-α line. It is quite possible that even for much further planets the corresponding optical thickness is still a small fraction of unity.

The time of photo-ionization of neutral helium ($He \rightarrow He^+$) appears to be about 5 times larger than the time of photo-ionization of neutral atomic hydrogen. This difference is not large enough to account for

* n_c represents the total particle number density below which a given local radiation flux (and also given effective recombination coefficient) would lead to a fractional ionization greater than $\frac{1}{2}(\sqrt{5}-1)$, i.e., about 61 per cent (Hinteregger, loc. cit.).

any significant abundance of neutral helium, at least out to distances of a few astr. units from the sun. On the other hand, doubly ionized helium (formed either by direct double photoionization, $He \rightarrow He^{++}$, or ionization in steps, $He \rightarrow He^{+} \rightarrow He^{++}$) is hardly more abundant than singly ionized helium. This is probably of considerable importance as a cause of possibly quite significant interplanetary absorption of solar He^{+} Lyman emissions that are among the strongest photon fluxes within the solar EUV spectrum (see II; 1.2.). Not knowing the actual contribution of helium to the interplanetary density, we cannot offer any significant opinion whether or not the interplanetary medium between the earth and the source region of solar 304 A radiation may be truly optically thick in this wavelength.

The foregoing picture of interplanetary absorption of EUV radiation is very crude and could even be quite wrong as to certain implications. If it is at least qualitatively correct, however, experimental determinations of interplanetary absorption appear to be fruitful mainly for the Lyman-α lines of solar H and He^{+} radiation. The most important conclusion to be drawn at present, however, is to recognize the rudimentary character of the existing knowledge and the need to obtain additional information on the interplanetary medium from experiments other than optical measurements (e.g. charged particle analysis).

REFERENCES

Bates, D. R., and Seaton, M. J., 1949, M. N. **109**, 698.

Friedman, H., 1960, Tenth International Astrophysical Symposium (to be published).

Herring, J. R., and Licht, A. L., 1960, The First International Space Science Symposium (to be published).

Hinteregger, H. E., 1960, Astrophys. J. (in press).

Jacchia, L. G., 1960, Smithsonian Astrophysical Observatory, Report Nr. 39

Jeans, J. H., 1954, "The Dynamical Theory of Gases," p. 344, Dover Publications, New York.

Opik, E. J., and Singer, S. F., 1960, submitted for publication in J. Geophys. Research

Pecker, J. C., 1960, Tenth International Astrophysical Symposium (to be published).

Priester, W., Martin, H. A., and Kramp, K., 1960, Mitt. Univ. Sternwarte Bonn, Nr. 34.

Purcell, J. D., Packer, D. M., and Tousey, R., 1959, Nature, **184**, 8.

Spitzer, L., 1952, "The Atmosphere of the Earth and Planets," ed. G. P. Kuiper, p. 241, U. of Chicago Press.

Tousey, R., 1960, Tenth International Astrophysical Symposium (to be published).

Urey, H. C., 1952, "The Planets, Their Origin and Development," Yale Univ. Press.

Watanabe, K., 1960 (private communication).

Weissler, G. L., and Lee, P., 1952, J. Opt. Soc. Am. **42**, 200.

5. SOME PLANS FOR EXPERIMENTS IN SPACE

Bruno Rossi
Massachusetts Institute of Technology

I would like to say a few words about two experiments to be carried out in space, which are being prepared by members of the Cosmic Ray Group of the Massachusetts Institute of Technology.

The first experiment is aimed at a study of interplanetary plasma. The persons working on this experiment, in which I, too, have an active interest, are Herbert Bridge, Constance Dilworth, and Frank Scherb. Collaborating with us also is Ervin Lyon of the Lincoln Laboratory.

The purpose of the second experiment is an investigation of high-energy γ-rays from extra-terrestrial sources. This experiment was conceived and is being carried out by William Kraushaar and George Clark. The importance of γ-ray astronomy had been emphasized by P. Morrison (Nuovo Cimento, V, 858, 1958).

I. INTERPLANETARY PLASMA

To appreciate the significance of experiments in the near-by interplanetary space, we must realize that the earth lies within the solar atmosphere; i.e., within a mass of gas whose behavior is dominated by the presence of the sun.

Presumably, this gas consists for the most part of ionized hydrogen. Otherwise, we know remarkably little about it. Estimates of its density by various astronomers range all the way from one proton per cm^3 to several thousand protons per cm^3. It seems likely that occasionally at least there are winds with velocities of the order of 10^8 cm sec^{-1}. In our terrestrial neighborhood, the temperature of interplanetary gas might be as high as a million degrees, or might be considerably lower. Moreover, it is not clear that protons and electrons have the same temperature, and it is not even clear that one can meaningfully speak of a temperature for either component. In other words, the velocity distribution of electrons and protons in the frame of reference moving with the gas may not resemble a Maxwellian distribution.

From the likely values of the densities, temperatures, and magnetic fields, and from the characteristic linear dimensions that are involved, it appears certain that the interplanetary gas is a practically "perfect" plasma, in which collisions play a negligible role and whose dynamic behavior is controlled by the long-range electric and mag-

netic interactions. The interpretation of the behavior of the interplanetary gas is thus a problem of magneto-hydrodynamics. I would like to mention here one important prediction about which we can feel reasonably sure. Because of the extreme dilution of interplanetary matter and the consequent small frequency of collisions, one might think that occasionally two fully ionized plasma streams may meet and continue to move undisturbed, one through the other, in different directions. This is actually not possible. Perpendicularly to the magnetic lines of force, all charged particles drift with exactly the same velocity $\mathbf{v} = (\mathbf{E} \times \mathbf{B})/B^2$, where $\mathbf{E}$ and $\mathbf{B}$ are the electric and the magnetic fields respectively. There is thus no possibility for two different ionized components of the plasma to have a differential velocity perpendicular to $\mathbf{B}$. This argument does not apply to motions parallel to the lines of force. One finds, however, that a differential motion in this direction would soon develop a shock which would quickly equalize the bulk velocities of the two components. Thus at each point of space, we can describe the bulk motion of the plasma by a single velocity vector, $\mathbf{v}$.

Presumably, $\mathbf{v}$ varies from point to point and from time to time. Observations of the comet tails have lead astronomers to believe that for most of the time $\mathbf{v}$ points directly away from the sun (in the region where comets are observed); there seems to be a "solar wind" as if the sun were continuously evaporating into interstellar space. But we cannot be sure that this solar wind is there all the time, or that it exists everywhere in the solar system. It has been pointed out, for example, that the gravitational attraction of the sun ought to produce a "wind" in the opposite direction, an infall of particles of interstellar matter toward the sun. Possibly both phenomena occur and the "interplanetary weather" is determined by the interaction between the outgoing and the incoming streams.*

There is no doubt that this interplanetary weather influences or even controls many phenomena observed on the earth or in its immediate vicinity. The outer radiation belt is almost certainly due to particles of the solar stream captured by the earth's magnetic field (even though it is not yet clear whether these particles come from the sun with their full energy, or are further accelerated while travelling in the trapped orbits). Other effects certainly related to solar streams are the aurorae, the magnetic storms, and certain variations of cosmic-ray intensity.

However, only direct observations will teach us what the conditions of the interplanetary plasma actually are. These observations must be made outside the region of space directly influenced by the presence of our planet. The magnetic field is the most significant of the terrestrial disturbing effects, thus we must reach a place where the dipole field of the earth becomes lost under the general interplanetary

* Of course, non-ionized gas pulled toward the sun from interstellar space could move freely through the solar plasma if it did not become ionized (by photoelectric effect or otherwise).

magnetic field carried by the plasma. It is estimated that this happens at distances of the order of 10 or 15 earth radii.

The experiment that we are planning is an attempt to obtain some preliminary information on the density, the velocity, and the direction of motion of the interplanetary plasma. I wish to stress the exploratory character of our program. On one hand, we have to work under severe limitations of weight, power, and telemetering capabilities. On the other hand, we are completely ignorant of the situation that our equipment will encounter in interplanetary space. Thus our main concern is not to achieve any degree of accuracy in our measurements, but rather to insure that the probe will yield significant data under a wide variety of conditions. For example, we believe that usually the bulk velocity of the plasma relative to the vehicle will be large compared with the thermal velocity of the plasma protons. In this case the vehicle will see a practically unidirectional flux of mono-energetic protons, and our probe must be so constructed as to respond to this flux. But sometimes, perhaps, the opposite situation will prevail, so that the vehicle will see protons coming from all directions, with a wide energy distribution. The probe must be able to detect such omnidirectional flux and to distinguish clearly between this situation and that described before.

In designing our instrument, we started from the concept of a simple Faraday cup. Suppose that on the skin of the space vehicle there is an opening covered by a grid. Let us assume that the bulk velocity of the plasma is large compared with the thermal velocity of the plasma protons. When the opening faces the plasma "wind," electrons and protons will stream through it. Behind the window there is a collecting plate. If the plate is kept at a negative voltage with respect to the grid, the protons will flow to the plate and the electrons to the grid or to other parts of the satellite's body, and a measurable electric current will result. Let n be the ion density and v the bulk velocity of the plasma. Then the current density (in elementary charges per cm^2 per sec) is nv. The density, n, is probably between 10 and 1,000 cm^{-3}, and the velocity, v, between 10^6 and 10^8 cm sec^{-1}. The corresponding current density is then between 10^7 and 10^{11} elementary charges sec^{-1} cm^{-2}, or between 10^{-12} and 10^{-8} amperes cm^{-2}. Using a collector of several cm^2, the resulting current would be easily measurable if it were not for the disturbing interference of the photoelectric effect. For, when the probe faces the sun (and this may well be the most interesting direction to look at), ultra-violet light produces a photoelectric current of several times 10^{-9} amperes cm^{-2}. One can try to suppress the photoelectric current by placing in front of the collector a second grid held at a negative potential with respect to the collector. In this case, however, photoelectrons released from this grid will produce a "reverse" photoelectric current which, even though smaller, may still be bothersome.

We are trying to eliminate the background caused by the photo effect by modulating the plasma current without, at the same time, modulating the residual photoelectric current, and then using an a.c. amplifier.

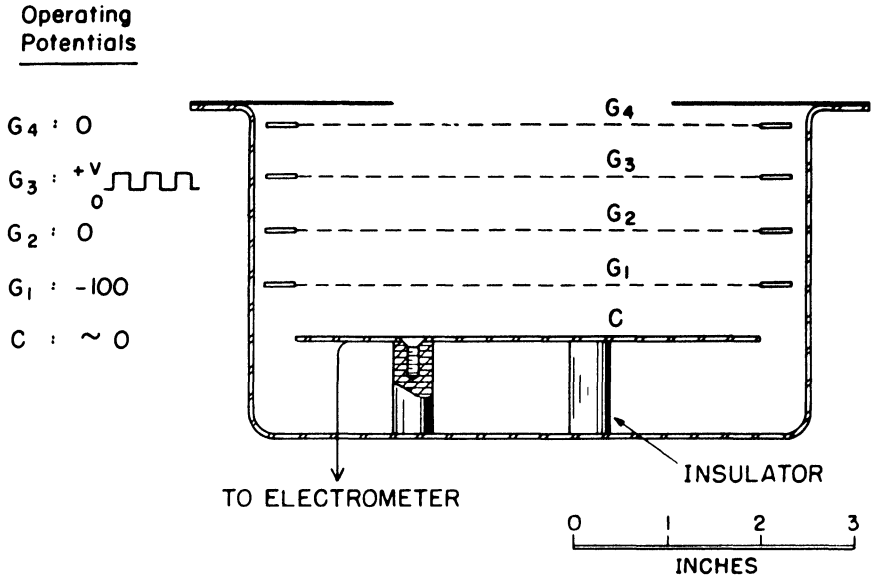


Fig. 1. Section of the plasma probe.

Figure 1 shows a diagram of the plasma probe. Grids G_4 and G_2 are kept at the voltage of the satellite, to be taken as zero. The collector is a circular plate of about 75 cm^2 area. Grid G_1 is kept at a constant voltage of about −100 volts. The modulating voltage is applied to the grid G_3. It is in the form of a square wave of about 1,500 cycles per second, oscillating from zero to some positive voltage. The spacing of the wires in grid G_2 is very small to provide good electrostatic shielding of the collector. The transparency of this grid is thus only 40%, while the other grids have transparencies of more than 90%. The collector current is amplified by a transistorized a. c. amplifier with quasi-logarithmic response; its input resistance is 16,000 ohms. The amplified a. c. current is then rectified to provide a d. c. voltage which is used to frequency-modulate the transmitter. The narrow-bandwidth noise level of the amplifier corresponds to an input current of about 2×10^{-12} amperes. Since the effective area of the collector is about 25 cm^2, the minimum detectable current density ought to be of the order of 10^{-13} amperes cm^{-2}.

Our first instrument is scheduled to be flown on a Thor-Delta deep space probe. The same vehicle will also carry three magnetometers, prepared by a NASA in-house group. The physical design of the vehicle is shown in Fig. 2. Initially, the vehicle will spin around its axis of symmetry with an angular velocity of about 2 rps, but it is expected that it will soon begin to tumble. The vehicle will be spin-stabilized, and a photoelectric sensor will give continuous attitude information.

We shall have available five seconds telemetering time every two minutes. We plan to use different modulating voltages; for example,

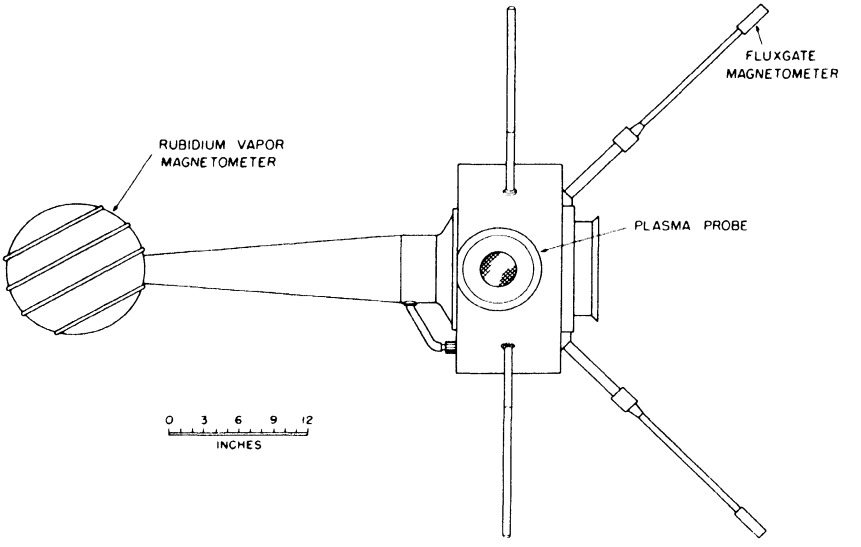


Fig. 2. Preliminary design of the vehicle that will carry the plasma probe and the magnetometers.

30, 100, 300, 1,000, and 3,000 volts, changing from one voltage to the next every time we make a measurement. In this manner we hope to obtain information on the kinetic energy of the incoming protons; if, for example, the kinetic energy is 200 e.v. (corresponding to a velocity of 2×10^7 cm sec^{-1}), no modulation will occur with modulating voltages of 30 or 100 volts, while 300, 1,000, and 3,000 volts will give complete modulation.

If, as we have assumed, the bulk velocity of the plasma relative to the vehicle is greater than the thermal velocity of the protons, the spin of the vehicle will produce a periodic change in the intensity of the proton current, the maximum occurring when the probe looks in the direction of the plasma wind (more exactly, when the angle between the wind velocity and the axis of the plasma probe goes through a minimum). If, on the contrary, the proton thermal velocity were large compared with the bulk velocity, then the current would be practically independent of the aspect. For a situation intermediate between these two extremes, the amount of modulation produced by the spin of the vehicle will give an indication of the relative values of the bulk velocity and the thermal velocity.

II. GAMMA-RAY ASTRONOMY

The "gamma-ray telescope," which is being constructed by William Kraushaar and George Clark, is designed to detect γ rays of energy greater than about 50 Mev. Presumably, γ rays of these energies are produced almost exclusively by the decay of π^0-mesons, and π^0-mesons arise either from nuclear interactions of high-energy particles (such as cosmic rays) or from the annihilation of nucleons with anti-nucleons. Since γ rays travel along straight lines, unaffected by interstellar or terrestrial magnetic fields, they may give us information about the occurrence of one or the other of these interesting processes in distant parts of our universe.

Gamma rays are not too readily absorbed by our atmosphere. Thus it would seem that one might be able to detect them with instruments carried aloft by balloons. Actually, only comparatively strong sources could be discovered in this manner, because of the large background of γ rays produced by nuclear collisions of cosmic-ray particles in the atmosphere. Suppose, for example, that the telescope is looking vertically upwards from an atmospheric depth of 5 g cm^{-2}. Since the collision mean free path of cosmic-ray particles in the atmosphere is about 70 g cm^{-2} and since 3 or 4 γ rays may result from each nuclear collision, the γ-ray background is 20% or 30% of the primary cosmic-ray intensity; i.e., of the order of 0.1 γ ray cm^{-2} sec^{-1} $sterad^{-1}$.

Balloon experiments for the detection of high-energy γ rays have been and are being carried out, but the results so far have been negative. The satellite experiment now under preparation ought to be able to detect γ-ray sources considerably weaker than those detected from balloons.

The essential requirements which have dictated the design of the γ-ray telescope are: 1) light weight, 2) reliability of operation, 3) strong discrimination against background radiation, and 4) directionality. The instrument is shown in Fig. 3. The telescope consists of a sandwich of NaI and CsI scintillating crystals (20 g cm^{-2} total thickness) viewed by a single photomultiplier, and of a Cerenkov detector viewed by two photomultipliers. It is completely surrounded by a shield of scintillating plastic viewed by five photomultipliers. The decay time of the light flash from the NaI crystal is about 0.25 μ sec., while the decay time of the light flash from the CsI crystal is about 1.25 μ sec. Thus the electric pulse of the photomultiplier that views the sandwich consists of a "fast" and of a "slow" component, which are separated electronically. A coincidence anti-coincidence circuit selects events in which the sandwich detector and the Cerenkov detector give simultaneous pulses that are not accompanied by pulses in the plastic shield. When this happens, the amplitudes of both the "slow" and of the "fast" pulse from the sandwich detector are telemetered. With this selection criterion, γ rays arriving upon the telescope from the appropriate directions are detected with high efficiency because most of them will traverse the anti-coincidence shield without interaction and will then undergo pair production in the NaI-CsI sandwich

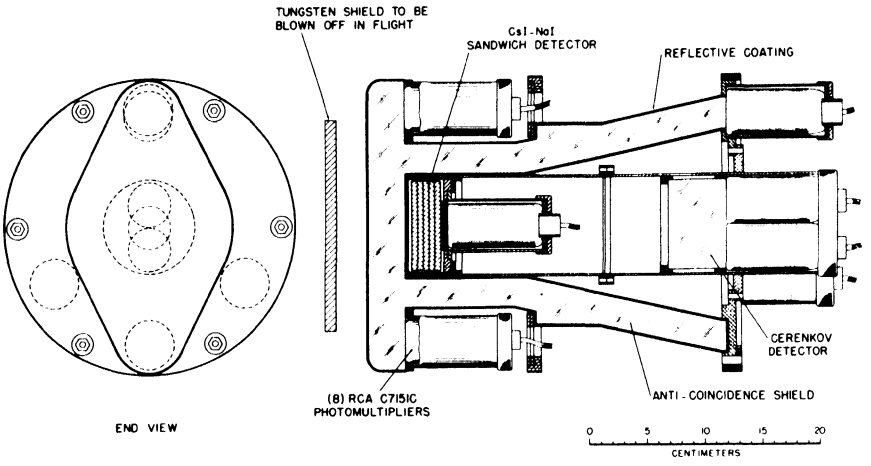


Fig. 3. Section and view of the γ-ray telescope.

with a high probability that one or both of the resulting relativistic electrons traverse the Cerenkov detector. In the majority of the cases the "slow" and the "fast" pulses from the sandwich detector will be of comparable sizes.

The area of both the sandwich and the Cerenkov detectors is 50 cm^2, and the distance between centers is 20 cm. Thus the total solid angle of acceptance of the telescope is 50/100 = 1/2 steradian, or 4% of the whole sphere. The solid angle subtended by the Cerenkov detector at any one point of the sandwich detector is 1/8 steradian, or 1% of the whole sphere.

Cosmic-ray particles will produce about one coincidence per second between the sandwich detector and the Cerenkov detector. The anti-coincidence shield, however, will discriminate against these particles with high efficiency. The Cerenkov detector is only activated by charged relativistic particles, and discriminates against particles going upward. This will practically eliminate all background due to cosmic-ray albedo from the atmosphere (the charged albedo particles are just protons and electrons because mesons do not have a sufficiently long mean life to reach the altitude of the satellite). Spurious counts may arise from neutron interactions in the sandwich detector. However, these interactions will usually produce heavily ionizing particles of short range, whose presence will be recognized by a large difference between the amplitudes of the "fast" and the "slow" pulse. It is hoped that this criterion, together with the other requirements, will greatly reduce this background. All in all, it appears that the total spurious counting rate may be less than 1/1000 of the cosmic-ray coincidence rate recorded without the anti-coincidence shield; i.e., less than 10^{-3} per second. Kraushaar and Clark plan to test this prediction by initially placing, in front of the telescope, a tungsten shield about 10 g cm^{-2} thick which ought to absorb most of the incident γ

rays, so that practically only the background will be recorded. After one or a few days, this shield will be blown off by a small explosive charge, upon radio command from a ground station.

The telescope with the associated electronic circuits will weigh about 25 lbs. It will be placed in a 600 km circular orbit by a Juno II rocket. It will remain attached to the last rocket stage, and the total weight of the satellite in orbit will be about 80 lbs. The final configuration has not yet been decided upon, but Fig. 4 gives an indication of what it may look like. The satellite will initially spin about its longitudinal axis at 400 rpm. The ratio of the moment of inertia about this axis and about an axis perpendicular to it will be approximately 1/40. The structure of the satellite is sufficiently different from that of a rigid body that in a short time dissipation of energy will cause the satellite to spin about a transverse axis at a rate of approximately 10 rpm. From previous experience with similar satellites, it is anticipated that the spin axis will slowly precess, and eventually the telescope will scan the whole sky.

The data will be telemetered directly, and also stored on magnetic tape to be played back on demand when the satellite is in sight of a receiving station. Power will be furnished by solar cells, and a total time of operation of about one year is planned.

One can estimate the minimum detectable intensity from possible γ-ray sources by considering the anticipated background and time of operation, and by assuming random scanning of the sky. In the case of a point source, the minimum detectable intensity turns out to be about 8×10^{-5} photons cm^{-2} sec^{-1}, which corresponds to a counting rate of about 4×10^{-3} sec^{-1} when the telescope is pointing directly at the source. For a diffuse source it is about 2×10^{-4} photons cm^{-2} sec^{-1} $ster^{-1}$, which corresponds to a counting rate of about 10^{-3} sec^{-1}. Of course, the minimum detectable intensity from a point source would be smaller if the instrument were to view a suspected region of the sky continuously.

Some estimates of the likely γ-ray intensities have been made. Most of these estimates are, of course, extremely uncertain and I am mentioning them here only as an indication of the sort of things one might be looking for.

(a) Collisions of Cosmic-ray Particles with Interstellar Matter in Our Galaxy

This is the only source whose existence appears virtually certain. Suppose that both the intensity of cosmic rays and the density of matter are constant throughout the galaxy. Then, if we look in a direction in which we see a thickness l of the galaxy, the ratio of the γ-ray intensity to the cosmic-ray intensity is simply given by $j_\gamma / j_{cr} = m\, l\, \rho / \lambda$, where m is the mean number of γ rays resulting from a nuclear collision, ρ is the density of interstellar matter, and λ is the mean free path of cosmic-ray particles. With $m = 4$, $\rho = 10^{-24}$ g cm^{-3}, $\lambda = 30$ g cm^{-2}, assuming a galactic disk 2,000 light years in thickness and 10^5

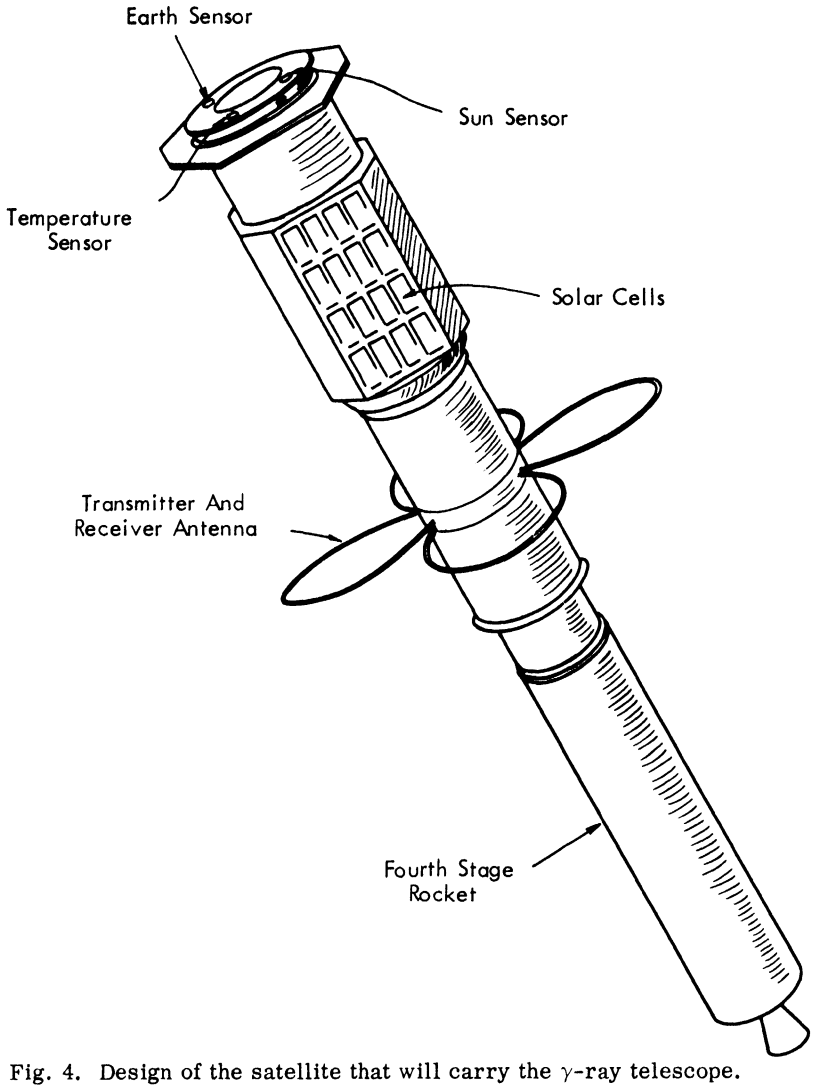


Fig. 4. Design of the satellite that will carry the γ-ray telescope.

light years in diameter, and taking into account the solid angle of our telescope, we find that the ratio of γ-ray counts to cosmic-ray traversals is about 10^{-4} when the telescope points perpendicularly to the plane of the galaxy and about 2×10^{-3} when the telescope points toward the center of the galaxy. Since there is about one cosmic-ray traversal per second, the above figures also represent the counting rates in sec^{-1}. However, it is quite possible that this estimate is too low because the density of matter near the center of the galaxy may be considerably higher than in our neighborhood, and because of the possible presence of a considerable amount of molecular hydrogen near the

galactic plane. (Some arguments for the existence of this molecular hydrogen have been given recently by M. Krook.) It is thus quite likely that the γ-ray source here considered might be detectable by the telescope.

(b) Large Magellanic Cloud

If this extra-galactic nebula were similar to our own galaxy as far as density of interstellar matter and density of cosmic rays are concerned, it would produce at the earth a γ-ray intensity of the order of 2×10^{-5} γ ray cm^{-2} sec^{-1}, giving a counting rate of about 10^{-3} sec^{-1} when the telescope points directly to the object. This intensity would escape detection by the present telescope. However, it seems that the Magellanic Cloud is a more active object than our own galaxy. Thus it probably contains a higher flux of cosmic-ray particles, in which case it might well be a detectable γ-ray source.

(c) The Crab Nebula

This object is the gaseous envelope of a supernova exploded about 1,000 years ago. It has a radius of about 3 light years and lies at a distance of about 4,400 light years from the solar system. From its radio emission and from the snychrotron radiation which accounts for much of its visible light, it is known that the Crab Nebula contains high-energy electrons. Ginzburg[1] estimates the total energy of these electrons to be of the order of 10^{59} to 10^{61} ev. High-energy protons are probably also present. In fact, if the electrons are accelerated by interactions with hydromagnetic disturbances through a Fermi-type process, one might argue that protons, too, should be accelerated by the same kind of process, and more efficiently than electrons. On the other hand, the injection energy for protons is higher than for electrons, which would tend to decrease the proton flux. Thus one can only make the wildest guess (ranging perhaps from 10^{49} to 10^{53}) as to the number of high-energy protons present in the Crab Nebula. If the mass of the Crab Nebula is of the order of the solar mass (about 2×10^{33} g), its density is of the order of 10^{-23} g cm^{-3}. From these data and considering the probable chemical composition of the Crab Nebula, it would seem that the maximum intensity of γ rays from this object should be somewhat less than 10^{-4} cm^{-2} sec^{-1}. Thus it is not likely that the Crab Nebula be detectable as a γ-ray source with the telescope now being built. Nevertheless, the uncertainties in the predictions are such that one will certainly want to look at it.

(d) The Sun

It is quite likely that protons are continuously accelerated to fairly high energies in the vicinity of the sun and that, for most of the time, are prevented from escaping by the solar magnetic field. If this is so, they will eventually lose their energy by nuclear collisions in

the solar corona, thus producing γ rays. Because of the proximity of the sun to the earth, the effective strength of such a γ-ray source may be fairly large. However, it does not seem possible to make any quantitative prediction at the present time.

(e) Other Point Sources

Among other potential point sources of γ rays are Cassiopeia A and Cygnus A.

Cassiopeia A, like the Crab Nebula, is the envelope of a supernova. It is three times closer than the Crab, but it seems to contain 300 times less energy in the form of high-energy electrons. Thus it is not a promising source of γ rays.

Cygnus A seems to consist of two colliding galaxies. Coming from the general direction of Cygnus A, there is a strong radio signal which, for a while, was thought to originate from two colliding galaxies. Some astronomers speculated that these two galaxies might consist one of ordinary matter and one of anti-matter, and that the energy released as radio waves might come from annihilation processes. According to these speculations, Cygnus A might have been also a strong source of γ rays. However, the identification of the radio source with Cygnus A is now in serious doubt and there is no longer any compelling reason to expect any γ rays from Cygnus A.

(f) Possibility of Matter, Anti-matter Annihilation in our Galaxy

If one accepts the point of view of the steady-state cosmology, one may speculate that perhaps the matter which is continuously created appears in the form of proton-antiproton pairs. Then from the value of Hubble's constant and from the average density of matter in the universe, one concludes that the rate of production of antiprotons is of the order of 10^{-22} cm^{-3} sec^{-1}. Kraushaar has pointed out that in our galaxy antiprotons will annihilate with protons and in these processes they will produce γ rays through the intermediary of π^0-mesons. In the equilibrium condition, the rate of annihilation equals the rate of production, and therefore amounts to 10^{-22} cm^{-3} sec^{-1}. On the other hand, the rate of collisions of cosmic-ray particles with interstellar matter (assumed to have a density of 10^{-24} g cm^{-3}) is of the order of 10^{-25} cm^{-3} sec^{-1}. Thus the intensity of γ rays coming from annihilation processes ought to be about 1,000 times greater than the estimated intensity of γ rays from cosmic-ray collisions. Such a strong γ-ray source, if actually present, would become apparent during the first few hours of observation.

REFERENCES

[1] V. L. Ginzburg, Progress in Cosmic Ray Physics, Vol. IV, J. G. Wilson and S. A. Wouthuysen, Eds. (North Holland Publishing Co., Amsterdam, 1958).

6. X-RAY AND ULTRAVIOLET RADIATION MEASUREMENTS FROM ROCKETS

Herbert Friedman
U. S. Naval Research Laboratory

INTRODUCTION

Astrophysical measurements from rockets have been performed both with spectrographic instrumentation, as described in the chapters by R. Tousey, W. A. Rense, and H. Hinteregger, and with photoelectric photometers responsive to relatively narrow spectral bands. Even in the far ultraviolet, solar radiation is intense enough to permit high resolution spectroscopy with exposure times limited to fractions of a minute. At x-ray wavelengths, however, the sun is much weaker and photography of the line spectrum has not yet been accomplished, although success may not be far off. With non-dispersive techniques based on (1) the unique transmission characteristics of various filters, (2) the ionization potentials of gases, and (3) the use of proportional and scintillation counters with pulse height discrimination, it has been possible to map the broad features of the solar x-ray spectrum and to observe certain ultraviolet emissions of the night sky. This chapter is devoted to an account of measurements made with such photometers.

DETECTORS

A variety of filter materials and gas absorbers are available for the construction of narrow band photon counters and ionization chambers.[1,2] In the x-ray region, short wavelength cutoffs are produced by the characteristic atomic absorption edges of thin foils and films. For example, 8 A marks the K edge of aluminum, 44 A the K edge of carbon, and 13 A the L_{III} edge of nickel. Plastic films of Mylar and Glyptal are composed primarily of carbon. To the short wavelength side of the absorption edge, transmission is very low. On the long wavelength side of the edge, transmission is high and falls off slowly, inversely as the wavelength cubed. The radiation that penetrates the window of an x-ray photon counter or ionization chamber is detected by photoelectric absorption in the gas. Virtually all the quantum energy is converted to electrons and ions at a rate of about 30 electron volts per ion pair. To minimize the spectral response at wavelengths much shorter than the K edge of the filter, a light gas such as helium may be

used which is transparent at the shorter wavelengths but comparatively opaque at longer wavelengths. The net result of window filtration and gas absorption is illustrated in Fig. 1.

Gaseous ionization detectors operating in the ultraviolet regions above 1000 A exhibit a spectral response compounded of: (1) a long wavelength surface photoelectric effect with a threshold above 2000 A for most metals; (2) an internal photoelectric effect confined to wavelengths below 1500 A; and (3) photoionization of the gas. The yield of the long wavelength surface photoelectric effect is small, of the order of 10^{-5} to 10^{-7} electron per quantum. For most metals a new threshold appears at a wavelength in the far ultraviolet, usually between 1000 and 1400 A, at which the yield may multiply abruptly by as much as 10^{3}. Finally, most gaseous molecules have thresholds for photoionization below 1500 A and exhibit such high cross-sections that yields of close to 100 per cent are possible. Table I lists a group of the most

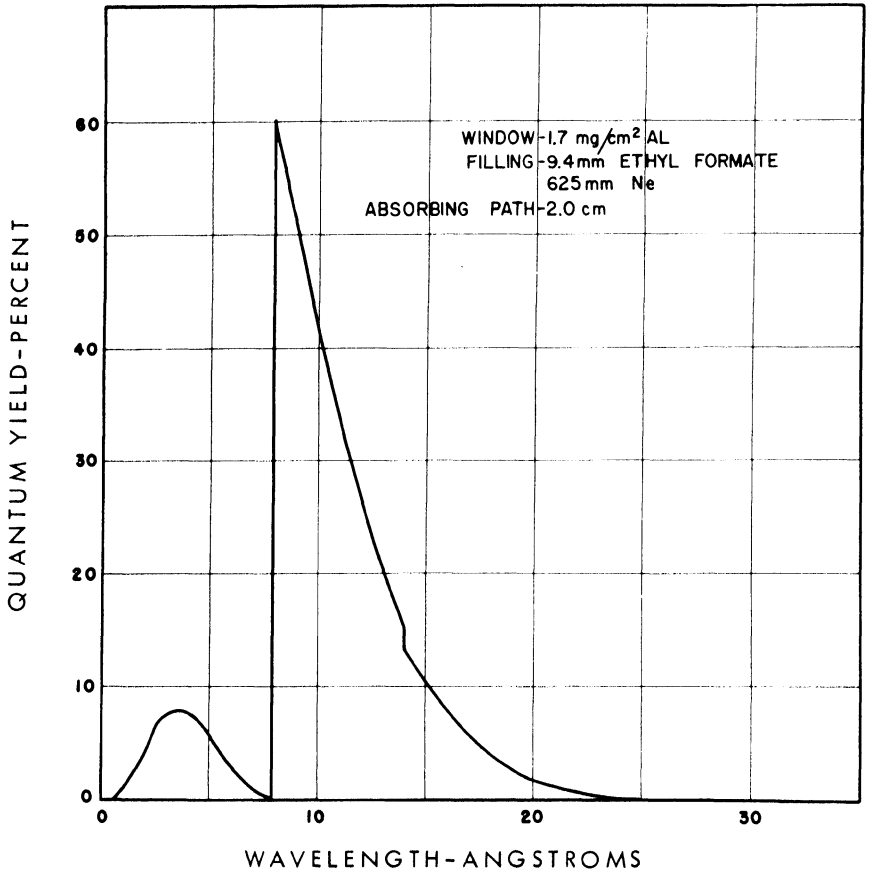


Fig. 1. X-ray quantum yields of photon counters with an aluminum window. The K absorption edge falls at 8A.

TABLE I
Narrow-Band Photon Counters and Ionization Chambers

Window	Thickness	Ionizable Gas	Response Band (Angstroms)
Beryllium	0.005 inch	neon	1-8
Aluminum	0.00025	neon	8-18
Mylar	0.00025	helium	44-60
Glyptal	0.00006	helium	44-100
Lithium fluoride	2 mm	nitric oxide	1100-1340
Calcium fluoride	2 mm	nitric oxide	1225-1340
Sapphire	1 mm	xylene	1425-1500

useful detectors employed in rocket astronomy for the past dozen years years.

Between 100 and about 1100 A, only the very thinnest films transmit appreciably and it is difficult to prepare windows that can meet the requirements of vacuum tightness and mechanical strength. A nitrocellulose film about 1000 A units thick transmits about 40 per cent at 46 A and about 17 per cent at 220 A. An evaporated film of pure aluminum, about 1500 A thick begins to transmit at 830 A on the long wavelength side and remains fairly transparent down to the L_{III} edge at 170 A. Purcell and Tousey[2] have suggested using an Al film over a layer of fluorescent material coated on the window of a photomultiplier tube to provide detection of wavelengths within the transmission range of the aluminum film.

It is also possible to dispense completely with the window material and to use photon counters or ionization chambers of the free-flow type. The solar spectrum is sufficiently intense that measurable responses can be obtained through a window as small as 0.005 inch in diameter. A small flask of gas may be used as a reservoir to maintain constant pressure within the photon counter as the gas flows out through the window. By selecting the fill gas from the rare gases, it is possible to control the long wavelength threshold in a number of steps. The ionization potentials of helium, neon, argon, krypton, and xenon are 507, 577, 791, 890, and 1027 A respectively. A helium free-flow ionization chamber makes an excellent monitor of the He II resonance line at 304 A.

Suppression of long wavelength response in vacuum photocells below 1100 A units also appears to be a possibility. T. A. Chubb at NRL has succeeded in preparing tubes with evaporated lithium fluoride surfaces that exhibit yields of 40 per cent at 585 A and less than 1 per cent at Lyman-α.

SOLAR X-RAYS

Attempts to compute the x-ray emission spectrum of the corona usually begin with the assumption of an ionization equilibrium in an isothermal atmosphere. X-ray emission arises from impact excitation,

electron-ion recombinations, and free-free transitions. The rates of the processes depend on both the electron density and the ion density. At constant temperature both densities are proportional to each other and so the emission per cubic centimeter varies as the square of the electron density. The appropriate temperature for the ionization equilibrium, however, is not easily determined. The temperature of the corona is indicated by a variety of characteristic features: (1) the gravitational equilibrium; (2) the absence of Fraunhofer lines in the white light corona; (3) the intensities of coronal emission lines arising from highly stripped ions of the heavy atoms; (4) the Doppler broadening of the coronal lines; (5) the absence of low temperature spectral lines typical of the chromosphere and prominences; and (6) the radio noise spectrum. All of these phenomena are indicative of coronal temperatures in the range from about 5×10^5 to 2×10^6 deg. K.

Elwert[3] computed both the x-ray continuum emission and the line emission for several temperatures between 7×10^5 deg. K. and 10^7 deg. K. Below the Lyman limit (912 A) part of the continuum is produced by the bound-free transitions of hydrogen. Recombinations with He II contribute to the continuum below 204 A, and at shorter wavelengths the emission is composed of a superposition of the continua of all the heavy ions. For the line emissions, Elwert found that the major process was electron impact excitation. At $T = 10^6$ deg., the theoretical continuum shows a maximum near 30 A and the line emission near 60 A. Figure 2 is an approximate representation of Elwert's x-ray spectrum, which contains about three times as much flux in the lines as in the continuum.

Since the only x-ray measurements that have succeeded thus far are those based on the use of photon counters of the types listed in Table I, it is clearly not possible to define the solar spectrum in any but the most approximate terms. In the work of the author and his colleagues at NRL[4] we have assumed a Planckian distribution and estimated the total flux on the basis of measurements made in the 44 to 60 A interval. If the coronal temperature was assumed to be 10^6 deg. K., the computed flux was about 0.13 erg $cm^{-2}s^{-1}$, at solar sunspot minimum in 1953; for an assumed $T = 2 \times 10^6$ deg. K., the computed flux was 0.35 erg $cm^{-2}s^{-1}$. To satisfy the requirement that the emission fall to a negligible flux at 20 A as is observed near solar sunspot minimum, the temperature must be closer to 0.5×10^6 deg. K. With the rise in coronal activity approaching solar maximum, more energy began to appear at wavelengths below 20 A. The shape of the measured distribution in the 8 to 20 A band, however, required a Planckian temperature of 2×10^6 deg. K. At that temperature, the Planckian x-ray flux needed to supply the observed counting rate of the 8 to 20 A photon counter would enhance the intensity from 20 to 100 A by less than one per cent. It appeared, therefore, that the sources of the higher temperature emission were restricted to an area of less than one per cent of the disk. This picture appeared to be consistent with radio interferometer measurements of the areas of coronal condensations.

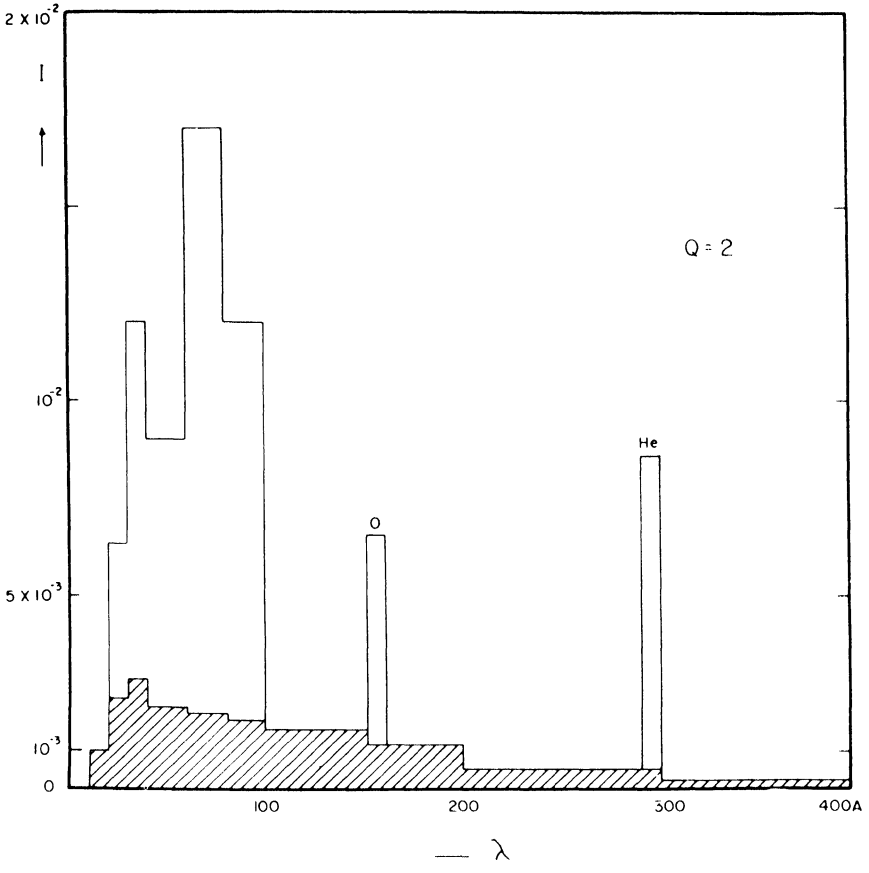


Fig. 2. Continuous x-ray emission (shaded) and line emission summed up from Elwert's computations for wavelength intervals of 10, 20, 50, or 100 A, according to the widths of the bars. From C. deJager, Ann. Geophys. 11, 30 (1955).

Over a solar cycle, rocket measurements of the total x-ray emission have varied from a minimum of 0.13 erg $cm^{-2}s^{-1}$ to a maximum of about 1 erg $cm^{-2}s^{-1}$, in the absence of solar flares. In the shortest wavelength emissions, the variations have been much wider.[5] Table II lists the observed counting rates in two bands, 2-8 A and 8-20 A, from 1949 to 1959. In the 8-20 A band there was a factor of 40 variation from 1953 to 1959 under quiet conditions. In the 2-8 A band, the emission almost disappeared near solar minimum.

During the past year some success has been achieved in extending the range of spectrographic measurements into the soft x-ray region. W. Rense[6] has reported the observation of emission lines to 83.9 A, but it appears that much improvement in spectrographic instrumentation is needed to provide well resolved x-ray spectra from 1-100 A.

TABLE II
X-Ray Counting Rates Observed Over a Solar Cycle

Time (UT)	Date	Counting Rate $\left(\frac{\text{Counts}}{\text{cm}^{-2}\,\text{s}^{-1}}\right)$ 2-8 A	8-20 A	Solar Activity
1730	9/29/49	1.0×10^4		$2^1/_2$ Hrs. after Class 1 flare
1459	6/1/52	495		Quiet
1344	5/5/52	< 125		Quiet
2240	11/15/53	< 40		Quiet
1546	11/25/53	332		Quiet
1529	12/1/53		4.5×10^4	Quiet
2250	10/18/55		1.4×10^5	Quiet
1915	7/20/56	1.2×10^5		Late in Class 1
1634	7/24/59	2.4×10^4	1.0×10^7	Quiet
1600	8/14/59	1.3×10^4	2.0×10^6	Quiet
2253	8/31/59	$> 7 \times 10^5$	$> 1 \times 10^7$	Class 2+

The instrumentation problems of high resolution x-ray spectroscopy are much more difficult than at longer wavelengths. X-rays cannot be focused with lenses or simple mirrors so that focused slit images cannot be obtained. Since very narrow beams are required, only a small length of ruled surface can be used and the resolving power is correspondingly small. To improve the resolving power, it is necesary to rule a great many more lines per unit length than for the optical region. For softer x-rays, concave gratings have been used quite successfully but the small glancing angle makes it necessary to use a large radius of curvature. If the ruled surface is too long, the spectrum will be filled with glancing incidence ghosts. The grating lines must be very fine and clean so that they do not block off too much of the radiation. In spite of these difficulties, considerable effort is being made by several laboratories to develop efficient ruled grating x-ray spectrographs for rockets and satellites.

A somewhat different approach is being attempted at NRL utilizing organic crystals rather than ruled gratings. Crystals of esters, fatty acids, ketones, hydrocarbons, and alcohols can be obtained with grating spacings of 20-75 A. With these spacings, the x-ray dispersion is very high. Reflectivities of a few tenths of a per cent have been measured at short wavelengths with a resolution of about 0.5 A. We plan to fly a simple Bragg-type rocking crystal spectrograph with photographic registration in an Aerobee rocket, if laboratory tests indicate that the available exposure time is adequate.

SOLAR X-RAY IMAGE

Figure 3 is a reproduction of the first photograph made of the sun in its x-ray emission, with a pinhole camera (R. L. Blake and A. Unzicker, NRL, April 19, 1960). The pinhole was 0.005 inch in diame-

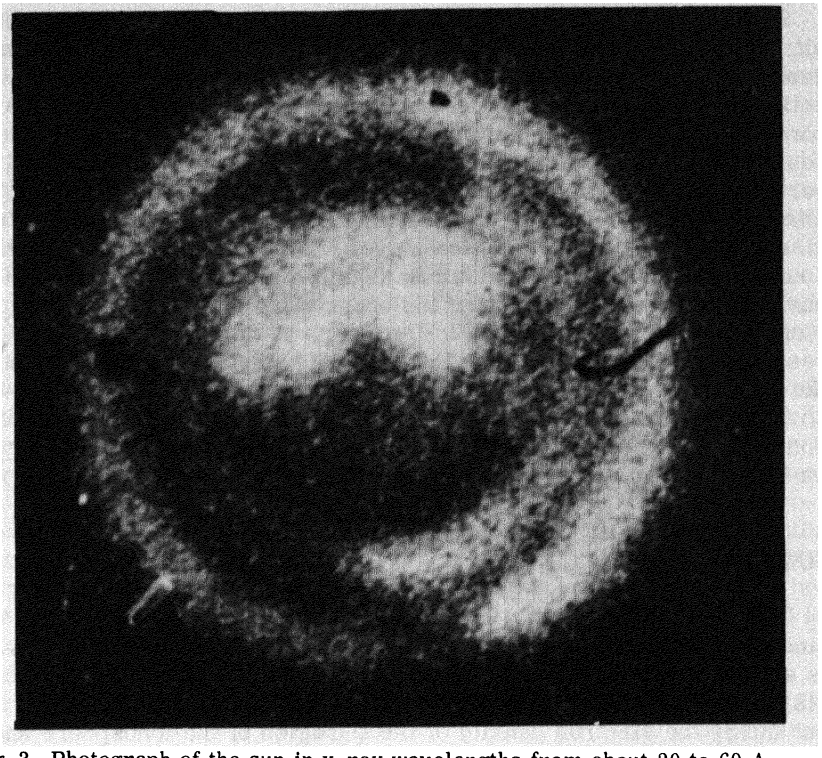


Fig. 3. Photograph of the sun in x-ray wavelengths from about 20 to 60 A, April 19, 1960. (R. L. Blake and A. Unzicker, NRL.)

ter and the length of the camera 6 inches. To obscure visible and ultraviolet light while passing x-rays, the pinhole was covered with a film of Parlodion, coated with a thin flashing of Al. Wavelengths between 20 and 60 A were effective in producing the image.

The camera was carried on a biaxial pointing control which counter-rotated to eliminate the roll of the rocket and swung in trunnions about an axis normal to the length of the rocket so as to aim at the sun. Still uncompensated for, however, was the rotation of the camera about the direction to the sun as a result of the precession of the rocket. Over the period of four minutes of x-ray exposure, the image rotated clockwise, in Fig. 3, for 15 degrees and then counter clockwise through 160 degrees. All of the x-ray emission can be identified with local sources superimposed on calcium plage formations and there is only minor evidence of limb brightening in the one small gap evident on the limb. Within the limited resolution of the image details, the bright x-ray regions are no more extended than the Ca plages. Elwert[7] has considered theoretically the distribution of x-ray intensity across the disk and concluded that there should be strong limb brightening, as much as a factor of 4 or greater. This feature is not indicated in the x-ray photograph.

At the eclipse of 1958 in the South Pacific, the residual x-ray and ultraviolet fluxes were measured at totality by means of rocket-borne detectors.[8] The Lyman-α flux was reduced to 0.05 per cent of the uneclipsed value, but 10 to 13 per cent of the x-ray flux remained. According to Elwert's computation of limb brightening, the predicted residual x-ray flux should have been in the neighborhood of 13 to 17 per cent. The agreement between experiment and theory may be fortuitous, however, since most of the limb emission may have come from discrete sources. This question arises in the interpretation of radio soundings of the E-region electron density during total eclipses. It has often been observed that of the order of 30 per cent of the normal electron density remains at totality, which could be explained by a residual flux of 10 per cent of the ionizing radiation. In many instances, the ionospheric variation showed abrupt changes in decline and recovery between second and third contacts and between third and fourth contacts, which were attributed to local sources of intense x-ray emission.

SOLAR FLARES

The emission of visible light accompanying a moderately large solar flare (Class 2 or 2+) is of the order of 10^{30} ergs and most of it is spread over an interval of about a half-hour. Accompanying the visible flash there must be a burst of ionizing radiation capable of enhancing the electron density of the D-region of the ionosphere and consequently producing radio fade-out and other SID phenomena. Prior to 1956, the favored hypothesis was an enhancement of Lyman-α, but direct measurements from rockets have since revealed no evidence for significant increases of this radiation during the course of a flare. Instead the observations showed marked enhancement of the x-ray emission, both an over-all increase of the entire x-ray spectrum and an extension to shorter wavelengths. The x-ray emission makes its appearance immediately with the onset of the visible flare and may amount to as much as 10^{31} ergs. It is, therefore, one of the major features of the flare outburst. In comparison, the energy dissipated in surge ejection of solar gas is of the order of 10^{29} ergs.

The first attempts to study solar flare x-ray emissions were made from balloon-launched rockets called "Rockoons." In 1956, the Naval Research Laboratory conducted a program of ten launchings from the deck of the USS Colonial in the Pacific Ocean, off the California coast.[9] Each morning a Rockoon was floated to 70,000 feet where it drifted through the day until word was radioed from Sacramento Peak or Climax that a flare was in progress. The rocket was then fired by radio command. Only one of the ten shoots caught a flare. Although the flare was no greater than Class 1, the measurements gave clear evidence of a short wavelength x-ray flash. With the beginning of the IGY, two-stage solid propellant rockets became available for launch from the ground. A series of experiments in 1957 confirmed the im-

portance of x-ray emission and gave the results listed in Table III. The shortest wave lengths observed were in the neighborhood of 1 to 2 A and penetrated well below the normal base of D-region. The fluxes were high enough to account for the observed SID events. It appeared that the enhancement of x-ray emission could be explained as a consequence of thermal excitation in regions of coronal condensations, with temperatures reaching 10^7 deg. K. Under such conditions, even atoms as heavy as iron in the coronal gas would be completely stripped of electrons and the x-ray emission would be expected to reach a short wavelength limit between 1 and 2 A.

The most recent series of measurements conducted by T. A. Chubb et al[10] in 1959 demonstrated clearly that x-ray quanta up to energies of at least 125 kev are emitted early in flares of magnitude 2+ or greater. Quanta in the energy range 30 to 125 kev were detected with a scintillation counter. The instrumentation included pulse height discrimination and therefore yielded spectral data. Table IV shows comparative results for a quiet sun and for an average Class 2+ flare, about three minutes after the first visible detection. The flares produced not only very short wavelength x-rays, but the entire spectrum was enhanced. Figure 4 shows (p. 117) pulse amplitude spectra obtained during the course of a Class 2+ flare about three minutes apart. The spectrum fell rapidly in intensity, about a factor of 2 for every 5-6 kev increase in energy, and softened noticeably during the three-minute interval between the sets of measurements. Although the quantum energies were high, the flux in the short wavelength tail, about 2×10^{-5} erg $cm^{-2}s^{-1}$, was a very small portion of the total x-ray flux produced by the flare. The x-ray emission above 30 kev could be attributed to Bremsstrahlung from electrons thermalized at temperatures in the neighborhood of 10^8 deg. K.

LYMAN-ALPHA IN THE NIGHT SKY

Rocket astronomy recorded the first far ultraviolet observations of the night sky in 1955. The experiment, which was conducted by NRL, was purely exploratory.[11] An Aerobee rocket was equipped with highly sensitive photon counters for three wavelength intervals: 1100 to 1350 A, which included Lyman-α (1216 A); 1225 to 1350 A to the long wavelength side of Lyman-α; and 1 to 5 A in the x-ray spectrum. Each counter saw an approximately 20 degree field of view, centered in a direction normal to the long axis of the rocket. The spin and precession of the rocket caused the counters to scan the sky. As the rocket rose above 90 km, all the detectors sensitive to Lyman-α were saturated. Those responding to the 1225 to 1350 A band remained on scale and showed discrete emission regions in the direction of the Milky Way. No signals above cosmic ray background were detected by the x-ray counters.

A second experiment was flown in the spring of 1957 using ionization chambers to measure the intense Lyman-α glow and photon counters

TABLE III
X-Ray Flares

Rocket	Launching Time (Z)	Class Flare	X-Ray Penetration km	X-Ray Wavelength (Angstroms)	X-Ray Flux erg $cm^{-2}s^{-1}$
Rockoon NN5.31	7/20/56 1217	1 No SWF	77	3-8	5×10^{-3}
Nike-Deacon NN7.42F	8/20/57 0949	1+ weak SWF	70	2.5-?	3×10^{-3}
Nike-Deacon NN7.45F	8/29/57 1412	2 1/2 hr SWF	77	3-8	2×10^{-2}
Nike-Asp NN7.49F	9/18/57 1054	Class 3 2 hr SWF	63.5	1.5-?	4×10^{-5} at 63.5 km 1.2×10^{-4} at 70 km

TABLE IV
X-Ray Flux (erg $cm^{-2}s^{-1}$)

Wavelength Interval	Background 8/14/59 1600 UT	2+ Flare 8/31/59 2253 UT
20-100 A	0.6	< 4.0
8-20 A	0.002	> 0.09
2-8 A	0.00055	> 0.03
0.6 A	—	0.000023

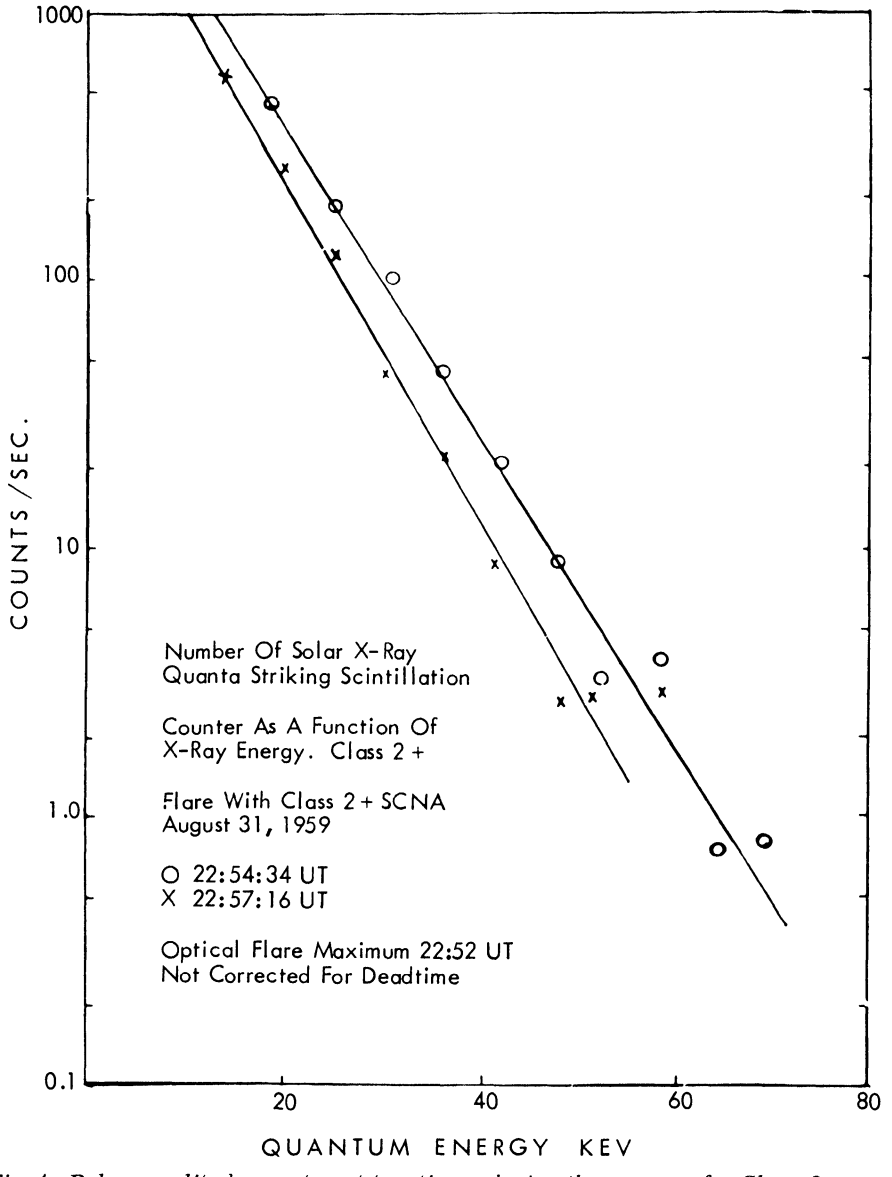


Fig. 4. Pulse amplitude spectra at two times during the course of a Class 2+ flare on Aug. 31, 1959.

again for the 1225 to 1350 A band. An x-ray counter, equipped with a one-quarter inch diameter window of Mylar film, 0.00025 inch thick, covered the 44 to 60 A band. The Lyman-α glow was found to be distributed diffusely across the entire hemisphere,[12] with a minimum in brightness approximately in the anti-solar direction (Fig. 5). The

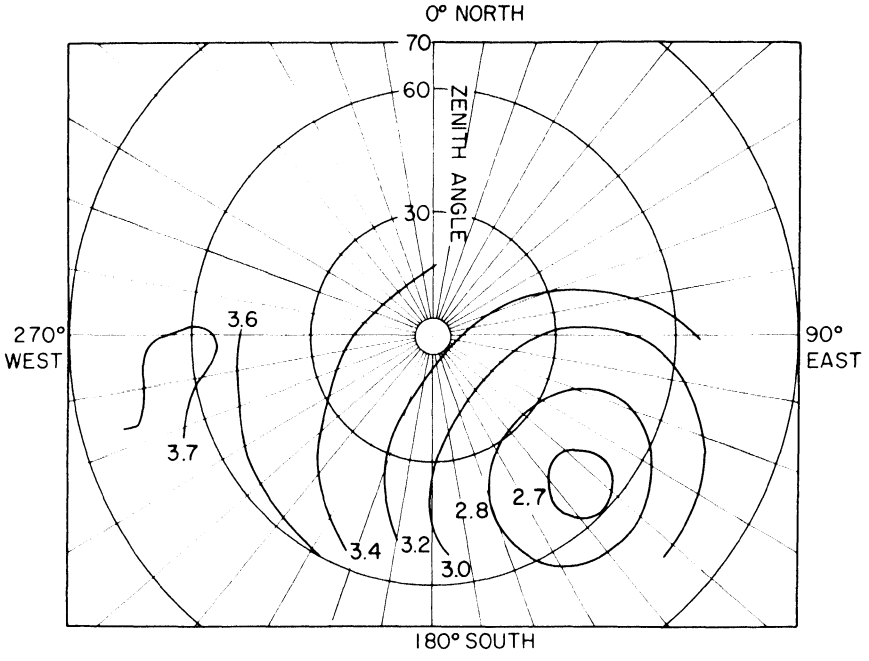


Fig. 5. Lyman-α directional intensity contours in the night sky. Data were obtained above 130 km from NRL Aerobee 31 on Mar. 28, 1957 at 2200 local time.

original interpretation of this phenomenon attributed the night sky glow to a Lyman-α resonance fluorescence of neutral hydrogen in interplanetary space. Later interpretations, in particular that of F. S. Johnson,[13] argued that the neutral hydrogen is contained in a geocorona extending out to perhaps ten earth radii. The interplanetary model requires about 0.2 atom per cc at one astronomical unit. Johnson's model puts about 7×10^{12} atoms per cm^2 column in the terrestrial atmosphere between 100 km and ten earth radii, with about 4×10^4 atoms per cc at the base of the exosphere and 10 per cc at about ten earth radii.

An important feature of the rocket measurements was the observation of an albedo of 42 per cent when the detectors looked down from heights greater than 120 km. The interpretation first offered by the experimenters was that the albedo was a scattering of the incoming flux by neutral hydrogen in the atmosphere below 120 km. This led to the conclusion that the temperature of the interplanetary gas was not greatly in excess of the atmospheric hydrogen between 85 and 120 km.

In a subsequent treatment, Brandt and Chamberlain[14] attempted to estimate the temperature of the assumed interplanetary gas from considerations of the absorption and scattering processes in an atmosphere containing both O_2 and H. They concluded that the interplanetary gas must have a temperature less than 7500 deg. K. if the night sky profile is Gaussian or an even lower temperature if the wings are

enhanced due to a central core. Using the Van Rhijn type of analysis, they showed that a distribution in the form of a shell of hydrogen at a distance of about 1.3 to 1.5 astronomical units from the sun would give the observed contours of Fig. 5.

To support his theory of a geocoronal distribution, F. S. Johnson pointed out that the motion of the earth through a stationary interplanetary gas would produce a Doppler shift large enough to prevent scattering by atmospheric hydrogen. The high albedo observed requires that all of the Lyman-α incident from the sky at considerable angles from the anti-solar direction must contribute to the albedo. This argues against the Doppler shift and supports the hypothesis that the cloud of hydrogen which scatters the night sky Lyman-α must be a part of the terrestrial atmosphere. It is difficult to dispute this interpretation unless, as suggested by Brandt and Chamberlain, an appreciable part of the so-called albedo is actually attributable to excitation of atmospheric hydrogen by particle bombardment.

ULTRAVIOLET STARS AND NEBULOSITIES

In the band 1225-1350A, just to the long wavelength side of Lyman-α, the emissions of celestial sources were again studied by means of photon counters. The field of view of the detectors was restricted to about 3 degrees in diameter at half maximum by placing bundles of nickel tubings, 0.03 inch in diameter and 0.6 inch long, in front of the detectors. With this improvement in geometrical definition, a fairly detailed mapping of most of the visible portion of the sky was accomplished. Whereas the 1955 experiment could only indicate that the radiations originated in the directions of the hot stars, Regulus, Gamma-Velorum, and Zeta Puppis, the higher resolution of the 1957 experiment showed that the sources are actually broad nebular emission regions surrounding the hot stars.[15] The stars themselves were not observable against the very bright nebular background. In addition to emission nebulosity identified with Orion and Puppis Vela in the galactic plane, isolated patches of nebulosity were observed at high galactic latitudes. The most interesting of these was a roughly circular region of about 20 to 25 degrees in diameter surrounding Spica.

Attempts to explain the observed nebulosity in terms of a continuum emission between 1225 and 1350 A have considered: (1) the ordinary optical processes of excitation by stellar radiation; (2) the two photon emission of continuum radiation from hydrogen excited to the 2S state; (3) atomic recombination processes involving sulphur, silicon and carbon; and (4) charge transfer processes within the nebular plasma leading to continuum radiation or emission in the Lyman bands of molecular hydrogen. None of these processes are adequate to explain the observed fluxes.

The total power radiated from Spica at wavelengths shorter than the Lyman limit should be 10^{37} ergs per second, if it is assumed that Spica radiates like a black-body at a temperature of 32,000 deg. K. The

power radiated in the observed ultraviolet nebulosity was also about 10^{37} ergs per second. Since most of the stellar energy radiated at wavelengths less than 912 A would be converted to Lyman-α in the nebula, the supply of Lyman-α from the nebula could be sufficient to account for the observed flux in the rocket experiments. However, some mechanism must operate to broaden the Lyman-α emission to such an extent that a major portion of it is detectable in the response region of the ultraviolet photon counter to the long wavelength side of the central frequency of Lyman-α. Shklovsky[16] has proposed that a major portion of the stellar power is radiated in the form of high spee protons. These may be neutralized in the nebular plasma and subsequently radiate strongly Doppler shifted Lyman-α.

Until the spectrum of the nebular emission is resolved, it will be difficult to explain its source. A recent experiment has shown that the nebulosity does not extend beyond 1350 A and, in the near future, experiments should determine within a few angstroms the true wavelength spread.

REFERENCES

[1]T. A. Chubb and H. Friedman, Rev. Sci. Instr. **26**, 493 (1955).
[2]H. Friedman, IRE Trans. Mil. Elec. **4**, 18 (1960).
[3]G. Elwert, Z. Naturf. **7a**, 432 (1952); Z. Astrophys. **38**, 143 (1955).
[4]E. T. Byram, T. A. Chubb and H. Friedman, J. Geophys. Res. **61**, 251 (1956).
[5]T. A. Chubb, H. Friedman and R. W. Kreplin, Proc. of the First COSPAR Symposium, Nice, France 1960.
[6]W. A. Rense and T. Violett, Astrophys. J. **130**, 954 (1959).
[7]G. Elwert, J. Atmos. and Terr. Phys. **12**, 187 (1958).
[8]H. Friedman, Proc. Inst. Radio Engrs. **47**, 272 (1959).
[9]T. A. Chubb, H. Friedman, R. W. Kreplin and J. E. Kupperian, Jr., J. Geophys. Res. **62**, 389 (1957).
[10]T. A. Chubb, H. Friedman and R. W. Kreplin, J. Geophys. Res. 1960 (In Press).
[11]E. T. Byram, T. A. Chubb, H. Friedman and J. E. Kupperian, Jr., "The Threshold of Space," The Pergamon Press, London, p. 203, 1957.
[12]J. E. Kupperian, Jr., E. T. Byram, T. A. Chubb and H. Friedman, Plan. and Space Sci. **1**, 3 (1959).
[13]F. S. Johnson and R. A. Fish, Astrophys. J. **131**, 502 (1960).
[14]J. C. Brandt and J. W. Chamberlain, Astrophys. J. **130**, 670 (1959).
[15]J. E. Kupperian, Jr., A. E. Boggess, III, and J. E. Milligan, Astrophys. J. **128**, 453 (1958).
[16]I. S. Shklovsky, A. J., USSR **36**, 579 (1959).

7. ULTRAVIOLET ASTRONOMICAL PHOTOMETRY FROM ROCKETS

Albert Boggess III
Goddard Space Flight Center

The observational program in ultraviolet astronomy has, to date, relied entirely upon rockets, primarily of the Aerobee type. The rockets have been unguided, preventing specification of the star, or even the area of sky, to be studied. In addition, there are so few detectors, filters, and calibration techniques available for the ultraviolet portion of the spectrum that only simple types of observations have been possible. Rapid progress is being made in removing each of these limitations; in the meantime it is necessary to rely upon broad band photometry in a few isolated spectral regions. Preliminary surveys of this type are of considerable value, nevertheless. They are not only the first observations available for comparison with predictions of ultraviolet intensities, but they also yield information which is essential for intelligent planning of later, more sophisticated experiments.

The data which have been acquired may be conveniently divided into two spectral regions, above and below 2000 A, each region requiring its own type of detector. In the middle ultraviolet, from 3000 to 2000 A, commercially available photomultipliers may be used for the detection of radiation. Various high silica glasses, chemical solutions, and doped crystals can be combined to give a number of different filters for spectral selectivity.[1] A typical rocket photometer designed for this portion of the spectrum contains a simple objective lens made of quartz or calcium fluoride, a filter, Fabry lens, and the photomultiplier. Figures 1 and 2 show two views of a pair of these photometers ready for insertion into a rocket. The objectives are mounted on a panel which becomes part of the rocket skin, while the filters, focal stops, and Fabry lenses are contained in the square cross-sections marked A and B in Fig. 2. These sections also hold solenoid operated shutters to provide optical zeros during flight. Each square section is fastened to a cylinder which can be slid in and out of the front panel casting for best focus. A tube containing the photomultiplier is screwed to the back end of each unit, and the amplifier is mounted on a bracket fastened to the photomultiplier tube. Photometers are constructed in pairs or triplets having parallel optical axes. Each photometer in the set is sensitive to a different spectral band so that simultaneous multicolor observations can be made. The panel containing the set of photometers is inserted into an aperture in the rocket skin such as is shown

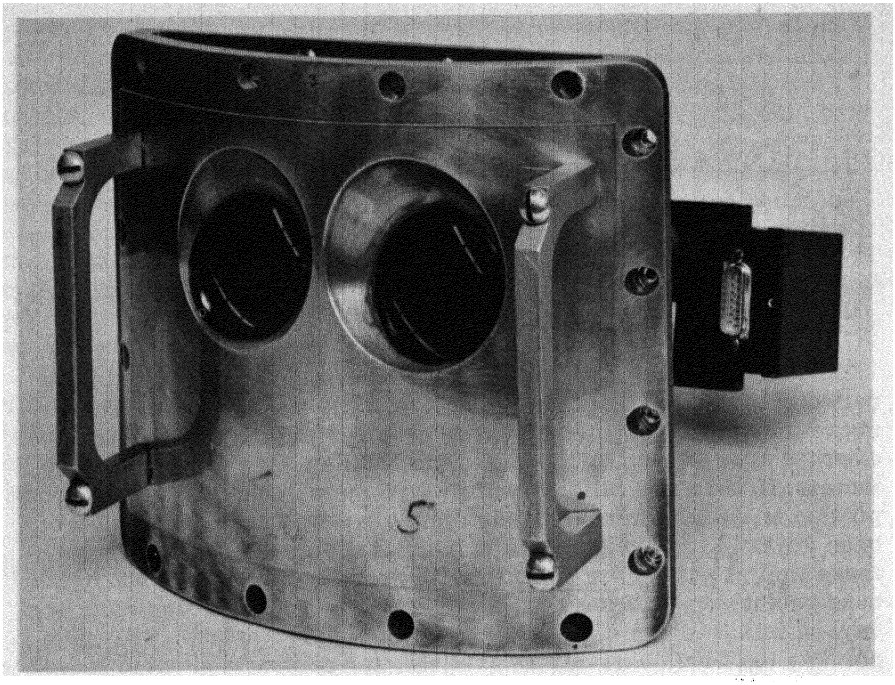


Fig. 1. Rocket photomultiplier photometers. Two inch quartz objective lenses are mounted in the panel, which bolts into the rocket skin. The amplifier box visible on the right is mounted on a photomultiplier tube projecting from the rear. The handles and protective plastic cover over the lenses are removed before flight.

in Fig. 3. Several photometer sets are flown in each rocket, mounted at different positions around the rocket skin and tilted at different angles with respect to the rocket axis, in order that as many stars as possible may be seen. The angular relationships between various photometer sets spaced around the rocket skin are measured after they are mounted in the rocket, and the photometers are calibrated. The λ 2537 line of mercury is a convenient photometric standard for this spectral region. Since all of the filters used so far have had at least slight transmission at this wavelength, absolute inverse-square law calibration can be obtained using a λ 2537 point source.

Until recently, detectors have been available for only two bands in the region below 2000 A: from 1350 to 1225 A and from 1350 to 1040 A. The latter of these bands includes the Lyman-α line at λ 1216 and so far has been useful only for studying Lyman-α radiation scattered locally within the solar system, leaving just the 1350 to 1225 A region for observation of stars and nebulae. Gas ionization techniques are used in this region, typically with nitric oxide as the fill gas and calcium fluoride as the window material. The ionization efficiency of nitric oxide at Lyman α is taken as the fundamental calibration standard for this portion of the spectrum.[2] The calibration is extended

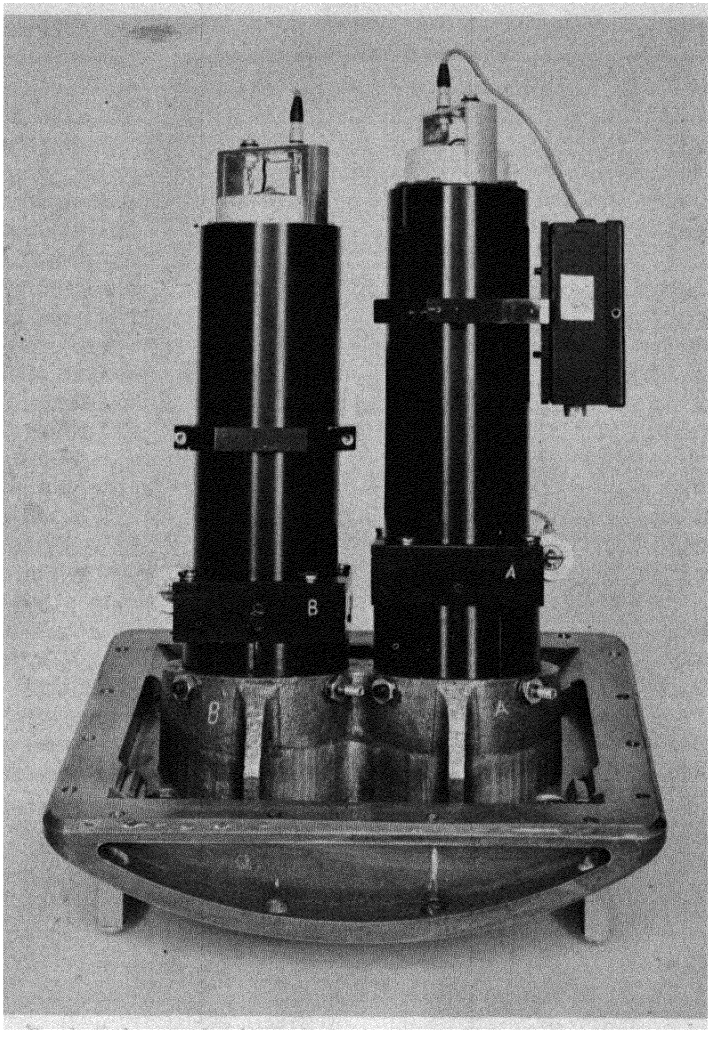


Fig. 2. Rocket photomultiplier photometers. The tubes containing filters, Fabry lenses, and photomultipliers slide in and out of the panel casting for focusing.

to other wavelengths by means of sodium salicylate phosphor which has an essentially uniform response throughout this spectral region.[3] The spectral response curve of a detector is measured by using a vacuum monochromator to alternately expose the sodium salicylate and the detector to the spectrum of molecular hydrogen. Photon counters were used as detectors because of their high sensitivity, but the development of the gas gain ion chamber has made it possible to eliminate the photon counter and its problems of stability and statistical uncertainty at low counting rates. The configuration of an ion chamber telescope is shown in the lower part of the rocket section

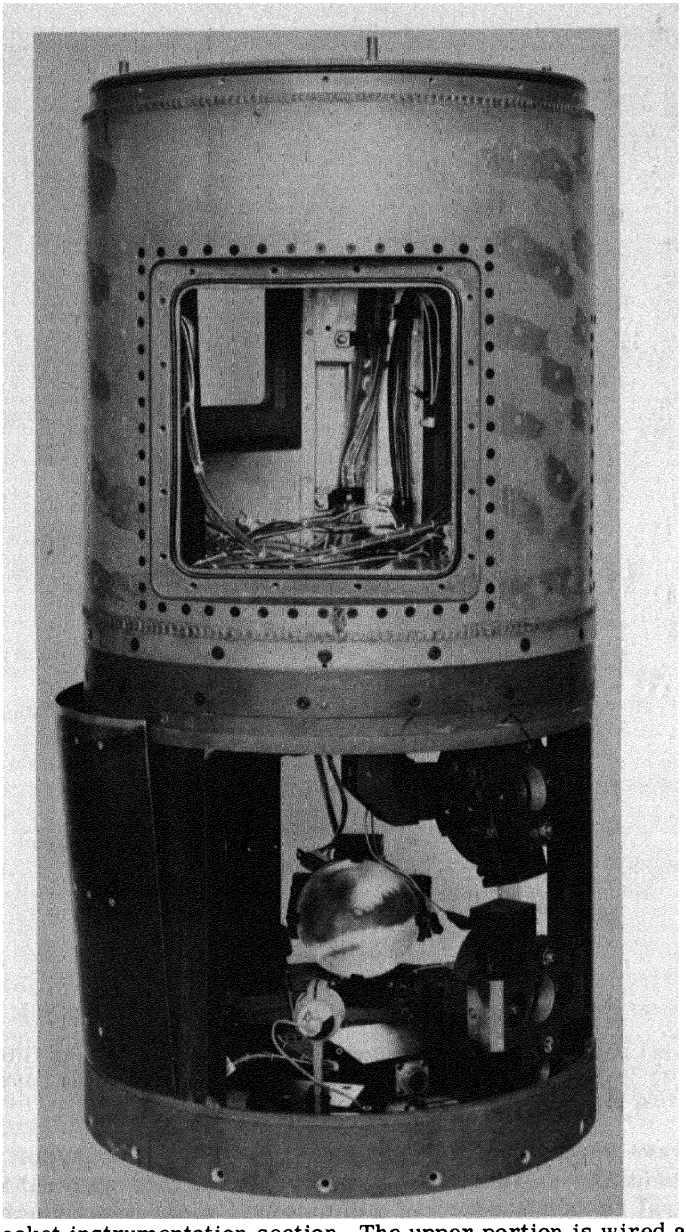


Fig. 3. Rocket instrumentation section. The upper portion is wired and ready for the photomultiplier photometers to be mounted. In the lower portion, an ion chamber in the foreground is at the focus of the mirror mounted to the rear. Two other mirror mounts are to the right, and one of the protective skin panels is shown partly ejected to the left. The nose cone, containing batteries, telemeter, etc., is bolted to the top of this section; the bottom mates to the rocket tankage.

illustrated in Fig. 3. An ion chamber is mounted on the near side of the rocket at the focus of a four inch mirror placed diametrically opposite. The backs of two other mirror mounts can be seen to the right. The chambers at the focii of these mirrors are hidden from view by the protective skin panel shown ready to leave the rocket on the left. Skin panels are fitted around the circumference of the rocket section during powered flight and are ejected shortly before observing altitude is attained, both to accelerate evacuation of air from the section and to give the telescopes access to the sky.

At observing altitudes the photometers scan the sky due to the combined rotational and precessional motion of the rocket. An ideal type of motion for a survey experiment would be one in which the rocket slowly turned end over end as it rotated, permitting a detector pointed out the side of the rocket to build up an area filling faster across the sky. Since this type of motion is rarely achieved in practice, several identical photometers are usually flown, mounted such that their scans of the sky will interlace to obtain a complete survey. A preliminary solution of the rocket motion can be obtained from magnetometer data and airglow signals. A few of the brightest stars can then be identified on the telemeter records and the final aspect solution proceeds rapidly.

In Fig. 4 a portion of the telemeter record from one photomultiplier photometer is reproduced. The optical axis of this photometer was inclined seventy-five degrees with respect to the rocket axis. During the upper-most trace the rocket was still rising out of the airglow layer, and stars may be seen superimposed on a slowly decreasing background due to the Hertzburg bands of molecular oxygen in the

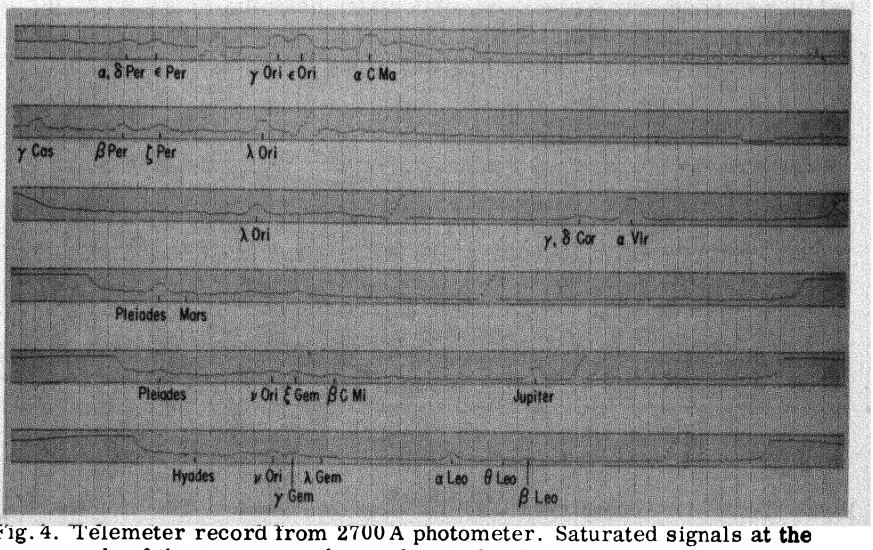


Fig. 4. Telemeter record from 2700 A photometer. Saturated signals at the ends of the traces are due to the airglow horizon. Vertical timing marks represent half-second intervals. Telemeter calibrations indicate one volt steps.

nightglow. As the rocket axis tilts from vertical, the photometer begins to spend part of the time pointed below the horizon. Saturation signals at the ends of each trace are due to airglow near the horizon. On each rotation less time is spent above the horizon due to the increasing tilt angle of the rocket. Many stars stand out clearly on the record; for those with good clean deflections the flux in absolute units can be measured to within about twenty-five per cent. This photometer was sensitive to a three hundred Angstrom band centered at $\lambda 2700$. Color effects are quite marked at these wavelengths. The limiting (visual) magnitude of this photometer varied from nearly five for early B stars down to zero for early F stars. The first stellar observations were made in this wavelength band,[4,5] since it was the only one for which a filter was available. Using it, some color anomalies were observed in A stars, perhaps due to the inclusion of the strong $\lambda 2800$ doublet of ionized magnesium within the band of the filter. More recently, data have been obtained with filters having effective wavelengths at $\lambda 2600$ and $\lambda 2200$, and a continuing program is now under way to measure stellar fluxes at these wavelengths.

More remarkable results have been obtained in the spectral band from 1225 to 1350 A. Data on this portion of the spectrum have been collected from five flights thus far. The most successful of these occurred on March 28, 1957, when four photon counters were flown.[6] A portion of the telemeter record from one of these counters is shown in Fig. 5. The counter swept across the sky from west to east, the earliest trace, marked a in the the figure, lying close to the southern horizon. Each successive trace lay a few degrees north of the preceding one. No point sources can be identified on this record. Instead, bright extended areas are seen, especially near the Milky Way. In trace a the detector first sees radiation in the southern part of Orion and is continuously active as it scans along the galactic plane through

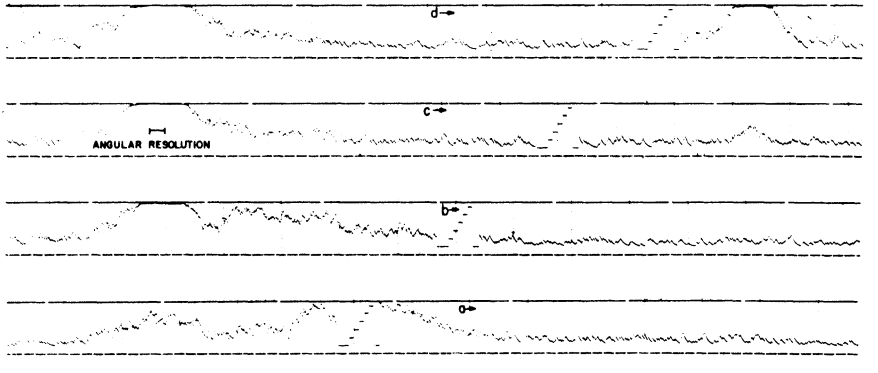


Fig. 5. Telemeter record from 1225-1350 A photon counter. The saturated regions on the left are in Orion. At the right ends of scans c and d are deflections due to the α Vir nebula. Individual counts are distinguishable at low intensities. Vertical timing marks represent half-second intervals.

Puppis and Vela. This trace occurred at low altitude and is significantly affected by atmospheric absorption. On succeeding traces the detector saturates as it sweeps more centrally through Orion, but the adjacent Milky Way is somewhat less bright. At the right hand edge of scan c a source well away from the galactic plane is observed, and on scan d the source saturates the detector. This source is in the direction of Alpha Virginis and will be discussed in more detail below.

That portion of the sky mapped out on this flight is shown in equatorial coordinates in Fig. 6. This map is a plot of the raw data and no correction has been applied for atmospheric absorption, which affected observations near the southern horizon. That portion of the sky, and particularly the region around Puppis and Vela, is much brighter than is indicated. The most striking area is in Orion, but other regions well away from the Milky Way were discovered. The brightest of these is in the direction of Alpha Virginis at 13^h4, $-10°$; others occur at 10^h, $+10°$ near Alpha and Rho Leonis and at 14^h, $+50°$ in the vicinity of Eta Ursa Majoris. Each of these regions were scanned several times during the flight and are well defined. The remaining areas in Fig. 6 were less well observed and are generally fainter, although a few of them are quite extensive. It may be significant that none of these latter areas are in the vicinity of bright early type stars.

Figures 7 and 8 show more detailed isophotes of the Orion and Alpha Virginis sources, which were the ones most thoroughly scanned on this flight. The greater detail shown in the Orion contours is possible since a pole of the rocket scanning motion was located in Orion, causing it to be criss-crossed with a tight network of scans. It must be remembered, of course, that contours derived from effectively random cross-sections are subject to considerable interpretational error. It is not in-

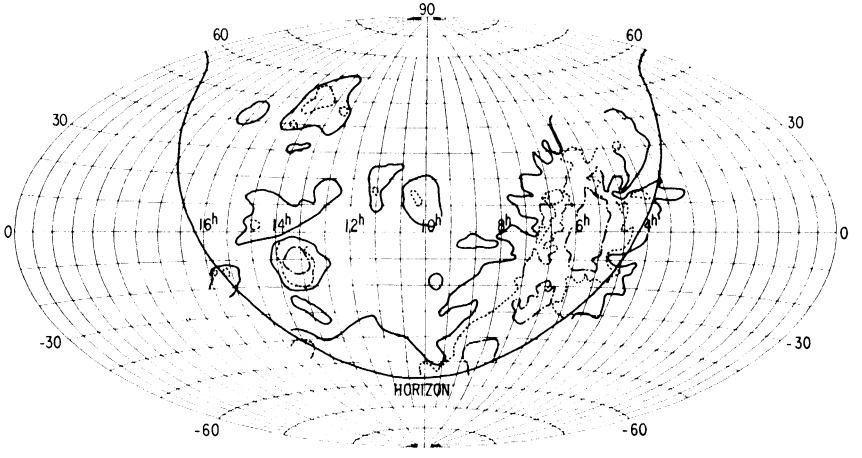


Fig. 6. Map of sky at 1225-1350 A. Contours are drawn at 1.2, 2.4, and 4.8×10^{-4} erg/cm^{2}sec per hemisphere. The heavy smooth curve indicates horizontal; the horizon is depressed about 15° at observing altitude.

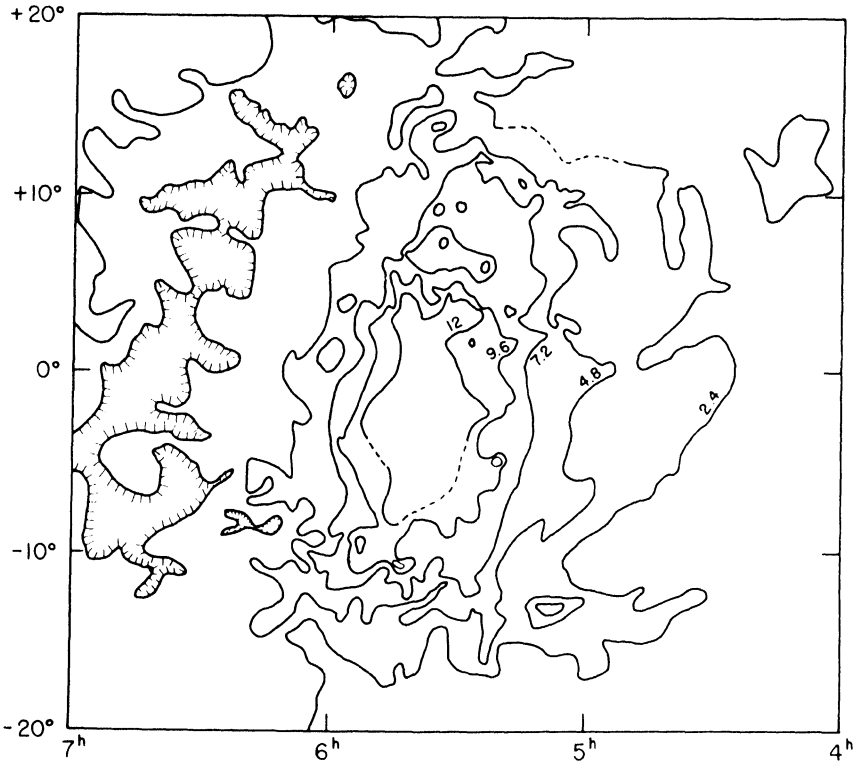


Fig. 7. Isophotes of Orion nebulosity at 1225-1350 A. Values of surface brightness are in units of 10^{-4} erg/cm^2 sec per hemisphere. Ciliated contours represent intensity minima; dashed contours are inferred from incomplete data.

tended that the details of the contours in Orion be taken literally; rather they are an indication of the structure which is present and comparable to the three degree resolution of the detectors. In each figure, the outermost contour shown is the faintest which is clearly separable from the background. The innermost contour is at the saturation level of the detectors scanning the region. Therefore the central intensity distributions are not known. From the nature of the signals in saturation it appears that in both areas the central intensities can be only a few factors greater than for the innermost contours shown. An interesting feature of the Orion region is the dark lane on the eastern edge of the nebulosity. This lane coincides approximately with the galactic plane and may indicate obscuration in the plane itself. This is the only portion of the Milky Way in which a reduction in intensity has been observed, but this is also the only portion of the Milky Way to be scanned in great detail, and a slight decrease in intensity might have passed undetected elsewhere.

The Alpha Virginis nebulosity shown in Fig. 8 is particulary intrigu-

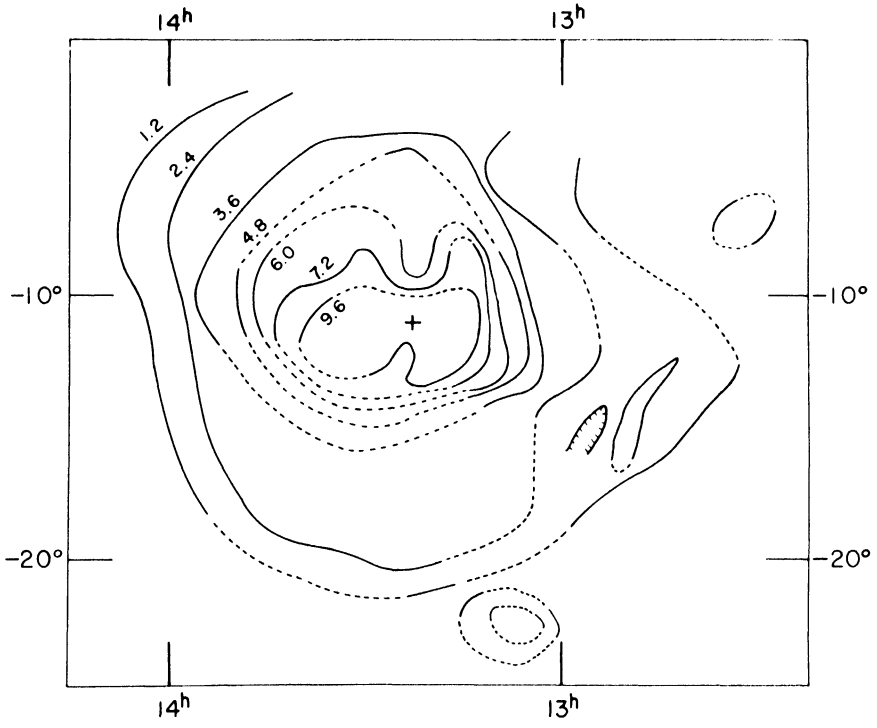


Fig. 8. Isophotes of α Virginis nebulosity at 1225-1350 A. Values of surface brightness are in units of 10^{-4} erg/cm^2 sec per hemisphere. The cross indicates the position of the star within the nebula. Dashed contours are inferred from incomplete data.

ing. It is well away from the galactic plane and is the brightest isolated object yet discovered. The cross indicates the position of Alpha Virginis within the nebula. The central location of the star and the symmetry of the nebula suggest that the two may be connected. The average diameter of the nebula is about twenty-two degrees. The intensity gradient increases abruptly about halfway in, forming a core eleven degrees in diameter which contributes sixty per cent of the radiation.

The data presented above is all dependent on a single flight, that of March 28, 1957. Nebular radiation at these wavelengths has been observed on three other flights, but they have been useful primarily as corroboration of the 1957 results. In particular, an earlier flight, in 1955, discovered the sources in Puppis-Vela, Leo, and Ursa Major.[7] In this first exploratory flight the detector was very broadly collimated and yielded no information on the nature of the sources, whether they were point or extended. Additional evidence on the size of the sources arose from a partially successful flight in May, 1960. This rocket spun at the rate of 2.2 revolutions per second, forcing the detectors to scan the sky at nearly eight hundred degrees per second.

The rocket was also unusually stable, so that the detectors swept over only a narrow belt which included the Milky Way in Scorpio and also Alpha Virginis. At such a high scan rate the resolution of the detector was not determined by its geometrical field, which was two degrees, but rather by the rise time of the detector amplifier. This rise time was approximately thirty milliseconds, corresponding to about twenty-five degrees. The slow rise time compared to the scan rate had the effect of severely reducing the sensitivity of the detector, so that only the brightest sources could be seen. Also no information about the size of the sources could be obtained from any one scan, especially in Scorpio where the many hot stars might appear as a single broad source. Alpha Virginis is isolated, however, and the slight precessional motion of the rocket permitted the detector to see this source for fifty-eight consecutive scans. Analysis of the rocket motion shows that near Alpha Virginis adjacent scans were separated by nine minutes of arc. During the fifty-eight scans the detector, therefore, saw the source over an angular extent of nine degrees. It appears that the detector was only sensitive enough to see the brighter core of the object illustrated in Fig. 8. The 1957 data was obtained with a photon counter using a geometrical collimator for spatial resolution. The 1960 flight employed an ion chamber at the focus of a four inch mirror as illustrated in Fig. 3. The significance of the latter data is due to its having been obtained with a different type of detector and a different observational technique. The extended appearance of the Alpha Virginis source is real and cannot be attributed to a peculiarity of the instrumentation.

The data on the Orion and Alpha Virginis nebulosities are summarized in the accompanying table. The calibration might be in error by as much as a factor of two depending on the spectral character of the radiation. But the brightnesses of the saturated central regions have been estimated conservatively. Also, the effects of interstellar absorption were completely neglected. As a result, the total luminosities and resulting volume emissions are probably lower limits. This is especially true in the case of Orion, where there is a great deal of obscuration in the field. Alpha Virginis, on the other hand, has no color excess, and the reduction of nebular intensities due to interstellar absorption in this direction should be small. Evidence as to

NEBULAR INTENSITIES AT 1225-1350 ANGSTROMS

	Orion	α Virginis	
Mean Surface Brightness	2×10^{-4}	1×10^{-4}	erg/cm^2 sec
Flux at Earth	5×10^{-5}	1×10^{-5}	erg/cm^2 sec
Luminosity*	2×10^{39}	1×10^{37}	ergs/sec
Mean Volume Emission	4×10^{-24}	2×10^{-23}	erg/cm^3 sec

*Based on distances of 520 pc for Orion and 87 pc for α Virginis.

the spectral character of this radiation is slight. It is extremely unlikely that the energy is due to Lyman-α radiation. The spectral sensitivity of these detectors has been carefully measured and is found to be down by a factor of 10^5 at λ 1216 due to absorption by the calcium fluoride window. In principle, some knowledge of the spectral distribution of the radiation can be obtained from the known wavelength dependence of the absorption coefficient of molecular oxygen,[8] the chief atmospheric absorber in this portion of the spectrum. The mean absorption coefficient for the observed radiation can be measured as the rocket rises through the atmosphere, and the wavelength which corresponds to this absorption coefficient is the spectral centroid of the radiation. In practice, any one source is rarely seen often enough during a flight to determine an absorption coefficient. Data for both the 1955 and 1957 flights indicate that the spectral centroid may lie between 1260 and 1280 A and that the radiation is confined to a rather narrow spectral band—or may even be monochromatic. However, these results are based on insufficient data and should be treated with caution.

The emission of such large amounts of energy in the 1225 to 1350 A band is difficult to explain. There is no indication of any nebulosity around Alpha Virginis at visual wavelengths. Furthermore, the density of interstellar material in this direction is thought to be low.[9] What is required is an abundant, efficient ultraviolet radiator which is undetectable in the visible. The material most likely to fulfill these requirements is molecular hydrogen. Certainly it cannot be detected by conventional observations and may well be abundant in interstellar space. Two ways have been suggested by which it might emit energy in the 1300 A region. The Lyman bands can be emitted by scattering and fluorescence of the stellar Lyman α and continuum. Krook has pointed out that Raman scattering of Lyman α by molecular hydrogen produces a line within the band. This suggestion has some support from the evidence that the radiation may be narrowly concentrated at wavelengths acceptably close to the Raman line. Unfortunately, none of the mechanisms which have been suggested offers a satisfactory quantitative explanation of the observed energy.

Another point of considerable interest in connection with the results of the 1957 flight is that no point sources were observed. In fact, every bright early type star which might have been detected was surrounded by nebulosity. The best example is Alpha Virginis, which was not seen even though two of the detectors swept directly across the star. One characteristic of the photon counters is that they will reverse under the influence of strongly saturating stimulii in a way analogous to the reversal of a photographic emulsion. The fact that a reversal did not occur when the already saturated detectors were pointed towards Alpha Virginis permits an upper limit to be placed on the stellar flux. The upper limit is 2×10^{-7} erg/cm^2 sec in the 1225 to 1350 A band. This upper limit is an order of magnitude less than is predicted by the model atmosphere for Alpha Virginis. It was tempting to consider that the deficiency of stellar energy was in some way connected with the

nebular radiation. This no longer appears to be the case. In June, 1960, a rocket containing an ion chamber telescope sensitive to this spectral region was flown. The attitude of the rocket was such that the only bright B star that could be seen by the detector was Epsilon Persei. In this case the star itself was observed and no surrounding nebulosity was detected. The measured flux was 10^{-7} erg/cm^2 sec, again approximately an order of magnitude less than indicated by the stellar models. This observation is the most recent information obtained in the 1225 to 1350 A band. It indicates that not all early B stars are associated with extended ultraviolet emission regions, but that early B stars as a class may be inherently less bright than model atmospheres predict.

REFERENCES

[1] Dunkelman, L., and Childs, C. B., in press.
[2] Watanabe, K., J. Chem. Phys., **22**, 1564, 1954.
[3] Johnson, F. S., Watanabe, K., and Tousey, R., J. Opt. Soc. America, **41**, 702, 1951.
[4] Boggess, A., and Dunkelman, L., A. J., **63**, 303, 1958.
[5] Boggess, A., and Dunkelman, L., Ap. J., **129**, 236, 1959.
[6] Kupperian, J. E., Boggess, A., and Milligan, J. E., Ap. J., **128**, 453, 1958.
[7] Kupperian, J. E., and Milligan, J. E., A. J., **62**, 22, 1957.
[8] Watanabe, K., Zelikoff, M., and Inn, E.C.Y., Absorption Coefficients of Several Atmospheric Gases ("Geophysical Research Papers," No. 21, 1953 [Air Force Cambridge Research Center]).
[9] Strömgren, B., Ap. J., **108**, 242, 1948.

Section II. The Theory

8. THE SOLAR CORONA AND THE INTERPLANETARY GAS

*Sydney Chapman**
Institute of Science and Technology, The University of Michigan

1. TEMPERATURES IN THE SUN

The temperature T in the sun decreases outwards from the center to the apparent "surface," the photosphere. The decrease is from a value of order 20 million degrees to a few thousand degrees. Thus the mean gradient, over the radial distance 700,000 km, is about 30°/km. The pressure, temperature and density distributions within the sun must be nearly spherically symmetrical. Above the photosphere, most surprisingly, the temperature gradient is reversed. In ascending through the chromosphere to the corona, in a distance h_0 of order 40,000 km, T rises again to a maximum value T_0 of a few million degrees. If the maximum average temperature at this height h_0 is two and a half million degrees, the average gradient of mounting temperature is about 60°/km.

2. CORONAL IRREGULARITIES

At and above the height h_0 the distributions of coronal temperature and density may be far from spherically symmetrical. Hot spots at temperatures up to 4 or 5 million degrees sometimes appear. The luminosity distribution in the corona often shows strongly marked structure. In high latitudes there are the polar plumes, and in middle and low latitudes there may be irregular rays. In their lower parts these rays often seem to be related to prominences.

During one eclipse a coronal ray was found—by two observers, at different stations—to extend outwards to 15 R, that is, fifteen solar radii (six million miles). So far as my knowledge goes, this is the most remarkable optical observation of great coronal extension hitherto made. Details of it are given in a brief Appendix.

* Also of the Geophysical Institute, University of Alaska; and of the High Altitude Observatory, Boulder, Colorado, (there engaged in a program of research sponsored by the National Bureau of Standards and the Air Force Geophysics Research Directorate).

The solar corona scatters radio waves that traverse it. At low coronal levels these waves are also refracted. Annually in the course of its orbit the earth "sees" one strong cosmic radio source, the Crab nebula, through the corona. The reception of the waves indicates the presence of irregularities in the corona. Their structure, according to Hewish (1958), appears to be of ray form. It has been suggested that the rays lie along lines of magnetic force. If so, these are nearly radial, very different—except near the solar poles—from those of a dipole field. Hewish has traced the coronal scattering and its irregularities out to about 30 solar radii.

3. THE QUIET CORONA; THE OUTFLOW OF HEAT

Sometimes, however, the corona subsides to regularity. Waldmeier (1955) has given the most notable evidence of this, by photographs taken during the eclipse of 30 June 1954. This occurred in an interval of at least two weeks in which the sun was exceptionally quiet. The corona was almost spherical, but had two small regular equatorial projections, one on each limb (E and W). At such a time the corona may be in quasi-static equilibrium, its lower part, at least, rotating steadily with the sun.

The corona loses heat by radiation, convection and conduction. How these losses are made up, so as to maintain the high temperature, is still uncertain. As the gas is fully ionized—consisting mainly of protons and electrons—the thermal conductivity K is high. Its value may be estimated (Chapman 1954) to be $5 \times 10^{-7} T^{5/2}$ erg/cm. deg. sec. Thus K varies strongly with the temperature. Woolley and Allen (1950) estimated that 1.1×10^{27} ergs/sec are *conducted* downwards from the corona, back to lower levels. They estimated the loss by *radiation* to be 2.7×10^{26} ergs/sec. This is only about a quarter of the downward conductive loss. Zirin (1957) estimated the radiative loss from a level in the corona somewhat above the height h_0, where T is greatest. He found that it is probably small compared with the conductive loss.

The *outward* conductive loss of heat from the corona depends, naturally, on the temperature gradient. It depends also on whether there is turbulence, because in a turbulent fluid heat can be conveyed by eddies. They add an eddy thermal conductivity K_e to the molecular thermal conductivity K_m. In the *earth's* atmosphere, up to 1 km height and more, K_e/K_m can be very large, of order 10^5 to 10^6. It varies with the weather conditions and the time of day. At the ground K_m is about 2400 erg/cm. sec. deg. In the lowest km of our atmosphere the ratio K_e/K_m increases upwards (Lettau 1957). How it varies at greater heights is not well known. It is thought that the importance of eddy conduction relative to molecular conduction ultimately decreases greatly with increasing height. However, while there will be some analogies between the atmospheres of the sun and the earth, it must be remembered that one is heated from within and the other from outside.

In the corona, at the level h_0 of maximum T (taken to be 2×10^6), K_m is far greater (3×10^9) than in our atmosphere. We can hardly guess what K_e may be in the corona, but the ratio K_e/K_m may well be much less than in the earth's atmosphere.

4. THERMAL CONDUCTIVE EQUILIBRIUM

In 1957 I considered what would be the temperature and density distribution in the corona in certain idealized conditions (Chapman (1957)). Perhaps these are never realized. The first main condition was that the corona is in static equilibrium, relative to axes rotating with the sun. The second condition was that T decreases outwards to a low value, in such a way that the molecularly conducted heat flux $-K_m dT/dr$ is steady. This implies that T varies as $1/r^{2/7}$. This relation would indicate a high value of T at the earth's distance, namely about 400,000°, if $T_0 = 2 \times 10^6$. Such a high temperature would ensure full ionization of the coronal gas up to this distance. Where the temperature falls to 30,000° or less, recombination will occur to an appreciable extent. The neutral hydrogen atoms thus formed can radiate energy to an important degree. There the outward fall of temperature may become much more rapid than according to the relation $T \propto r^{-2/7}$.

If this relationship were valid up to one astronomical unit, it would be possible to calculate the static density distribution in the corona along the sun's axis of rotation. But in other directions the calculation is not possible, beyond the distance where solar gravity is appreciably reduced by the centrifugal force corresponding to the solar angular velocity. At great distances the sun's coronal atmosphere must cease to follow the sun's rotation. At present we do not know how this occurs. Hence even if the coronal temperature were known up to the earth's distance, we could not calculate what would be the coronal density there. My attempt to do this, in 1957, ignoring the rotation of the interplanetary gas, could only be valid for points along the sun's axis.

5. ELECTRON DENSITY AND TEMPERATURE IN THE QUIET CORONA

Observations of the luminosity and polarization of the coronal light have been used by Blackwell (1955, 1956) to provide estimates of the electron number density n_e in the corona. The proton number density will have nearly the same value (but not quite the same, because of the presence of helium). Blackwell's estimates of n_e extend from 3 to 20 solar radii R. They were based on coronal observations made from an aircraft during the eclipse of 30 June 1954. Thus they correspond to coronal conditions shown by Waldmeier to be exceptionally quiet.

Assuming static equilibrium relative to the rotating sun, I have used Blackwell's values of n_e to infer the coronal temperature, be-

tween 3 R and 20 R (Chapman (1959)). The calculated lapse (or outward decrease) of T was found to be more rapid than would correspond to the constant conductive heat flux already mentioned. Extrapolated back to the coronal level h_0, the inferred value of T_0 somewhat exceeded 2×10^6. This agrees well with the value of T_0 adopted by Billings (1959) and other authorities. The inferred value of T at 20 R was 280,000°. This is materially less than the value I had previously (1957) estimated for that distance. Assuming that $T_0 = 10^6$ I had inferred that T at 20 R is 430,000°. For $T_0 = 2 \times 10^6$ this value must be doubled. Thus the inferred gradient up to 20 R is steeper than the gradient corresponding to conductive equilibrium.

Pottasch (1960) has calculated the coronal temperature distribution, assuming hydrostatic equilibrium, from electron density data based on eclipse observations. He used values of n_e from 1.0043 to 1.072 R given by Athay, Menzel, Pecker, and Thomas (1955), and values from 1.2 to 10 R given by Michard (1954). These were derived from the 1952 eclipse. He also used Blackwell's 1954 eclipse values, from 3 to 20 R. He took account of the presence of helium ions (1 for each 10 protons); my neglect of this refinement reduced my estimates of T by a few per cent.

The maximum coronal temperature T_0 inferred by Pottasch is 1.43 million degrees. According to his Table 1 (p. 70, loc. cit.) this is the temperature from 1.1 to 1.7 R; according to a section heading on his next page (71) it extends up to 3 R. Beyond 3 R his values of T agree fairly well with mine (Chapman (1959), p. 474) as here shown in Table I. The values attributed to him in this comparison are read from a graph based on his Table 1, for the range 1.7 to 22.6 R.

These rather similar temperature distributions may be differently interpreted. Pottasch suggests that the heat flux through the gas (over a sphere of radius r) is decreasing outwards: "this is a strong argument for the plausibility of some kind of radiative cooling occurring in the outer regions of the corona. To produce the source of the cooling is difficult, since there are many lines, not all known, to consider, and the collision cross-sections and f-values associated with most lines are poorly known. If we use the collision cross-section given by Woolley and Stibbs (1953), we find that one line, the resonance transition of O V at λ 630, can produce at least 1 per cent of the cooling required, if the usual abundance of oxygen is assumed concentrated in this stage of ionization."

To me an altogether different interpretation seems more likely.

TABLE I
Different Estimates of the Coronal Temperature from 3 to 20 R: the Unit is 10,000 Degrees

Distance in solar radii	3	4	5	8	10	15	20
Pottasch	107	89	76	54	45	33	26
Chapman	97	75	62	45	40	33	28

The heat flux F across a sphere of radius r is

$$4\pi r^2 K dT/dr,$$

where $K = K_e + K_m$. We know that K_m is proportional to $T^{5/2}$, but the variation of K_e with T, or with r, is not yet known. The flux F over this range of distance must be greater than I inferred in 1957, because of the inclusion of K_e in K, and because of the more-than-conductive temperature gradient—as inferred from the electron density distribution. It may be that in time it will become possible to estimate the amount of radiative cooling of the coronal gas at distances beyond 3 R. At present the arguments in favor of this rate being appreciable relative to F seem to me unconvincing.* It seems more likely that F is practically constant, and that from the "observed" (or rather inferred) temperature gradient it will be possible to deduce something about K_e, the eddy thermal conductivity.

6. CORONAL TURBULENCE

In the earth's troposphere, the lowest layer in our atmosphere, the average temperature gradient is normally controlled by small scale turbulence. It approximates to adiabatic equilibrium for moist air. In a layer of constant composition in adiabatic static equilibrium under gravity (g), the number density n varies as T^q, where $q = 1/(\gamma - 1)$, and γ denotes the ratio of the specific heats at constant pressure and constant volume. The adiabatic temperature gradient dT/dr or T'_{ad} is $-q'mg/k$, where $q' = (\gamma - 1)/\gamma$, m denotes the mean particle mass, and k Boltzmann's constant. For the solar corona $T'_{ad} = -6.0 \times 10^{-5} (r_0/r)^2$, taking $g = g_0(r_0/r)^2$, $g_0 = 2.44 \times 10^4$, $\gamma = 5/3$, and $q' = 0.4$. Here the suffix 0 refers to the coronal level $r = R + h_0$ or 1.06 R. At the coronal level h_0 this formula gives 6°/km. This gradient considerably exceeds the conductive gradient there, whose value, corresponding to $T \propto r^{-2/7}$ and $T_0 = 2 \times 10^6$, is only 0.78°/km.

Some turbulence above the hottest level of the corona may be expected, at least on a small scale--as in our troposphere. This accords with my inference from Blackwell's electron densities, that near the sun T falls decidedly more rapidly than would correspond to conductive thermal equilibrium. But—again as in our atmosphere —active turbulence producing a temperature gradient approaching the adiabatic value must be confined to a layer of moderate thickness, at least for the lower range of levels. If in our atmosphere the adiabatic tropospheric temperature gradient (6°/km) continued from the ground upwards over as much as 50 km, the temperature would

* As was pointed out by Zirin (1957), the concentration of the heavier elements in the coronal gas is likely to fall off sharply with height, thus reducing the cooling possibilities in the outer corona. Thermal diffusion also will tend to impel the multiply ionized elements, including helium, towards the regions of highest temperature (Chapman 1958). Turbulence will reduce, but seems unlikely to annul, these tendencies.

approach absolute zero: actually the greatest depth of the troposphere, in equatorial latitudes, is only about 20 km. Likewise in the sun, if T_0 is 2×10^6, the adiabatic gradient would cause the temperature to fall to absolute zero at a radius less than 3 R. (Of course when T approached 30,000° the conditions would be changed—recombination would begin.)

The adiabatic temperature gradient $-q'mg/k$ decreases as r^{-2} along the sun's axis. In the equatorial plane it decreases rather more rapidly, because of the centrifugal force in the rotating atmosphere. The conductive temperature gradient T'_c would vary with r as $r^{-9/7}$ or $r^{-1.29}$. If it were maintained over a large range of distance, the adiabatic gradient would at some distance become less than the conductive. But as T decreases faster than as $r^{-2/7}$, the conductive gradient T'_c also decreases faster than as $r^{-9/7}$.

A gas cannot be stable if it has a negative temperature gradient numerically greater than T'_{ad}. The gradient T'_{ad} corresponds to uniform potential temperature* T_p; any numerically greater (negative) gradient would correspond to an upward decrease of T_p.

Along the sun's axis of rotation the value of gravity g is known, hence it is possible to calculate T'_{ad} at any distance. The following table gives values of T'_{ad} (axial) and also of T and T' and T'_c. The values given for these last three quantities are based on my calculations from Blackwell's 1954 electron densities. (A slight smoothing has been made, so that the values of T differ from—at some distances are slightly less than—my values quoted in Table 1 above). The ratios T'/T'_{ad} are also given. The inferred values of T at 3 and 5 R are based on *equatorial* values of n_e.

Over the range from 3 to 20 R the temperature gradient T' inferred from the electron densities is about half the adiabatic. The conductive gradient is still smaller.

The ratio T'/T'_{ad} attains a minimum near 8 R, and then increases steadily to 20 R. In order to try to estimate the temperature distribution at greater distances, I have assumed that the ratio T'/T'_{ad} continues to increase outwards, up to its maximum value unity. By graphic extrapolation from the values given in Table II, values of T'/T'_{ad} were adopted for greater distances. The maximum value unity is thus inferred to be nearly attained at 50 R. Knowing T'_{ad} (axial) at all distances, the adopted ratios T'/T'_{ad} give values of T'. By numerical integration from 20 to 80 R, and beyond that by analytical integration, the further outward decrease of T beyond this distance has been calculated. The results are given for a few typical distances in Table III (values of T' and T were calculated also at some intermediate dis-

* The potential temperature T_p is that which a gas would acquire if brought adiabatically from its actual pressure p to some standard pressure p_0. According as p is less or greater than p_0 the change would increase or decrease the actual temperature. In the case of the coronal gas, the standard pressure might, for example, be taken to be that at distance 2R. So long as the coronal gas remains fully ionized, e.g., atomic hydrogen (or hydrogen and helium), the change of pressure will involve no change in the nature of its particles.

TABLE II
Coronal Temperatures and Temperature Gradients up to 20 R, Along the Sun's Axis of Rotation

Distance z (unit 1 solar radius)	3	5	8	10	15	20
T'_{ad} (axial) deg/km	0.732	0.263	0.103	0.0659	0.0292	0.0165
10^{-4} T (Chapman, 1959)	97	63	45	40	32	27
T′ deg/km	0.372	0.126	0.0417	0.0295	0.0166	0.0112
T'/T'_{ad} (axial)	0.52	0.47	0.415	0.45	0.565	0.68
T'_c	0.133	0.052	0.023	0.0115	0.0087	0.0055

TABLE III
Coronal Temperature Gradients and Temperatures from 20 to 300 R Along the Sun's Axis

z = r/R	35	50	80	150	215 (1 A.U.)	300
T'/T'_{ad}	0.88	0.95	0.98	1	1	1
T'_{ad} (axial)	0.00538	0.00263	0.00103	0.00029	0.00014	0.00007
T′ deg/km	0.0047	0.0025	0.00101	0.00029	0.00014	0.00007
10^{-3} T (axial)	193	157	123	96.3	87.0	80.9
T'_c deg/km	0.0023	0.0013	0.00063	0.00026	0.00017	0.00011

tances up to 80 R, so that the change of T in each interval of integration was suitably small).

This Table indicates that the inferred temperature at a distance of one astronomical unit along the solar axis is 87,000°K. The values of T_c' in the last line indicate that the conductive gradient continues to be less than T′ until somewhat beyond 150 R.

7. THE VARIATION OF THE THERMAL CONDUCTIVITY ALONG THE SUN'S AXIS

Suppose that the corona is in a steady state, and that the outward heat flow F from the corona is constant over the range of distance here considered. This implies that there is no appreciable loss of heat, e.g., by radiation, and also no gain of heat, *in situ*. Then

$$F = 4\pi r^2 K T' = \text{constant}$$

or, what is equivalent,

$$K \propto 1/T' z^2 \qquad (z = r/R)$$

Table IV shows how K_z/K_3° varies, where K_3 and K_z denote the values of K at 3 R and z R.

This table indicates a remarkably small range of variation of K. It appears to increase by 25 per cent from 3 to 8 R, and then declines, at a decreasing rate, to approach a limiting value of almost exactly 1/2 at around 1 A. U.

The range of the molecular thermal conductivity K_m is far greater; as T declines from 970,000° at 3 R to 81,000° at 300 R, the decrease of K_m, proportional to $T^{5/2}$, is in the ratio 500 to 1. The total conductivity K, equal to the sum of K_m and of the eddy conductivity K_e, shows no comparable variation. It may be that K_e much exceeds K_m at all distances. It is of interest to note that K is greatest where the temperature gradient T′ has its smallest ratio to $T'_{a.d.}$.

In my 1957 paper I estimated F to be 1.3×10^{26} erg/sec. This estimate assumed that the flow is purely conductive, and that the maximum coronal temperature is 1 million degrees. The conductive part of the flux at 3 R, according to Table II, will be 9.4×10^{26} erg/sec. The total flux may be of order 10^{27} or 10^{28} erg/sec or possibly even more.

8. THE ELECTRON DENSITY DISTRIBUTION ALONG THE SOLAR AXIS

The equation of hydrostatic equilibrium in the coronal gas may be expressed in the form

$$\log(n_1/n_2) = \log(T_2/T_1) - 0.4343\ (\bar{m}g_0/k) \int_{z_1}^{z_2} dz/(Tz^2)$$

$$= \log(T_2/T_1) - 4.96 \times 10^6 \int_{z_1}^{z_2} dz/(Tz^2)$$

TABLE IV
Relative Variation of the Total Thermal Conductivity

z	3	5	8	10	15	20	30	40	50	60	80	100	150	215	300
K_z/K_3	1	1.06	1.25	1.14	0.89	0.75	0.61	0.57	0.54	0.53	0.52	0.52	0.51	0.51	0.51

TABLE V
The Electron Density Distribution Along the Solar Axis

z	20	35	50	80	150	215
n_e/cm^3	2600	1260	885	619	429	366

In the region beyond 80 R, where we may take $T' = T'_{ad}$, this equation can be simplified to the form

$$\log(n_1/n_2) = 1.493 \log [(z_2/z_1)(z_1 + 70)/(z_2 + 70)]$$

Using these formulae, and the values of T given in Tables II and III. the values in Table V of the electron density n_e have been determined. The value of n_e for 20 R is that given by Blackwell (1956).

9. THE ROTATION OF THE CORONA

In considering the conditions in the extended corona in the sun's equatorial plane or the ecliptic, it is desirable to take account of the rotation of the gas. It may be assumed that near the sun the corona shares in the sun's rotation, with angular velocity $\omega_0 = 2.90 \times 10^{-6}$ radian/sec. With increasing distance, however, the angular velocity must decrease. Where the corona merges into the interstellar gas surrounding the solar system, ω must tend to zero, or to a negligibly small value.

Lüst and Schlüter (1955) have considered how the sun's magnetic field affects the rotation. They concluded that if the field has a dipole character, and a polar strength of order 1 gauss, ω will remain equal to ω_0 up to 50 to 100 solar radii. If this were so, centrifugal acceleration would overcome solar gravity at about 36 R.

It is now considered that the sun's field is not a dipole field, except possibly near the poles. I shall not here attempt to give a physical theory of the coronal rotation. Instead, for illustration only, I consider empirically a form of the function $\omega(r)$ or $\omega(z)$ that fulfills the following necessary or likely conditions:

1) At $z = 1$, $\omega = \omega_0$

2) $\omega(r)$ continually decreases as r increases,

3) At a great distance $\omega(r)$ increases towards the Keplerian angular velocity $\omega_K(r)$ given by

$$\omega_K(r) = \omega_{K_0}/z^{3/2}, \quad \omega^2_{K_0} = g_0/R$$

where g_0 denotes solar surface gravity 2.74×10^4. Thus $\omega_{K_0} = 6.275 \times 10^{-4}$ radian/sec.

4) Ultimately ω/ω_K must tend to zero as z tends to infinity.

The third of these conditions is suggested by the form of the zodiacal light (Sec. 10). This is sunlight scattered by dust and interplanetary electrons. The direction of the axis of the zodiacal light suggests that the rotation of this interplanetary scattering medium for large values of z tends to be about an axis perpendicular to the ecliptic rather than about the sun's axis. This may be due to the continual impulse given to the medium by the orbital motion of the earth and the inner planets. I have suggested that the earth's at-

mosphere may have a radius many times greater than that of the solid earth (perhaps 100 times as great). If so, this will greatly enlarge its power to make the interplanetary gas rotate with the Keplerian angular velocity, or nearly so. But where the extended solar atmosphere meets the interstellar medium, ω and ω/ω_K must tend to zero.

The following empirical formula for $\omega(r)$ or $\omega(z)$ meets the above conditions:

$$\omega(z) = \omega_0 z^a e^{-b(z^2-1)}$$

where

$$a = -0.421, \quad b = 1.02235 \times 10^{-5}$$

This makes $\omega(1) = \omega_0$, and clearly ω continually decreases as z increases.

The ratio f of ω to the Keplerian angular velocity is given by

$$f(z) = \omega(z)/\omega_K(z) = f_0 z^{1.5+a} e^{-b(z^2-1)}$$

where

$$f_0 = \omega_0/\omega_{K0} = 4.622 \times 10^{-3}$$

The ratio f has a maximum at the distance z_m given by

$$z_m^2 = (1.5 + a)/2b$$

With the numerical values of a and b here given, $z_m = 230$; and the maximum value of f there attained is 0.951. Thus ω is there only 5% less than the Keplerian angular velocity.

The centrifugal acceleration $\omega^2 r$ has a maximum value at 62 R; there it is 1.77 times the value at the sun's surface. $\omega_0^2 R$, which is 0.585 cm/sec^2. The ratio of the centrifugal force to gravity has a maximum at 229 R, where the ratio is 0.91. This maximum may be an unreal consequence of the form of expression adopted for ω, though the unreality is unimportant in considering conditions up to the earth's distance.

Table VI gives values of ω/ω_0, ω/ω_K and of the centrifugal acceleration, at various distances from the sun. The last two lines give the values of the effective gravity along the polar axis and in the plane normal to the axis of rotation of the atmosphere. Up to 20 R the difference made by centrifugal force is almost negligible. Beyond 20 R the difference becomes increasingly important, and T'_{ad} is reduced accordingly.

The values of T' in the plane of rotation are similarly reduced, if T'/T'_{ad} is assumed to have the values given in Table III. Hence, the values of T are increased. The values of the electron density, in equilibrium, are increased still more. Table VII gives values of T and n_e at various distances in the plane of rotation. The values of n_e were derived by correcting those of Table V for the difference in the temperature distribution and for the effect of the centrifugal force in changing the pressure gradient.

TABLE VI
Empirical Angular Velocity Distribution: Centrifugal and Gravitational Acceleration

z	1	3	5	10	20	40	60	80	100	150	215	300
ω/ω_0	1	0.630	0.508	0.378	0.282	0.208	0.172	0.147	0.130	0.097	0.065	0.037
ω/ω_K	0.0046	0.0151	0.0262	0.0554	0.1166	0.2434	0.3678	0.4905	0.5975	0.8034	0.9466	0.865
$\omega^2 r$	0.585	0.696	0.754	0.841	0.932	1.014	1.039	1.026	0.988	0.815	0.531	0.229
g_0/z^2 (axial)	27400	3045	1096	274	68.5	17.13	7.612	4.282	2.740	1.218	0.593	0.304
g′ (ecliptic)	27399	3044	1095	273	67.6	16.11	6.57	3.25	1.75	0.403	0.062	0.075

TABLE VII
Temperatures and Electron Densities in the Plane of Rotation

z = r/R	20	35	50	80	150	215
T′ deg/km	0.0112	0.0045	0.0023	0.00078	0.00014	0.000015
10^{-3} T	270	194	161	133	115	110
n_e/cm^3	2600	1287	919	666	569	503

TABLE VIII
Number Densities, Dust and Electrons (Behr and Siedentopf)

Distance from sun (AU)	0.5	0.6	0.7	0.8	0.9	1.0	1.1	1.2
Distance in solar radii, z	107	129	150	172	193	215	236	258
10^{15} n_d/cc	0.8	1.0	1.2	1.2	1.2	1.2	1.2	1.2
n_e/cc	1070	1030	980	900	780	600	390	200

10. THE ZODIACAL LIGHT

The zodiacal light is generally agreed to be sunlight scattered by electrons and by dust particles in interplanetary space. It is visible under suitable weather conditions, after sunset and before dawn, especially from lower latitudes. The light is partly polarized. Behr and Siedentopf (1953), assuming that the polarization was due entirely to electron-scattered light (and making also some subsidiary assumptions), inferred the tabulated number densities of dust particles (n_d) and electrons (n_e) at various distances from the sun (see Table VIII).

There is much uncertainty as to the assumption that dust particles do not polarize the light they scatter. This was recognized by Behr and Siedentopf. In a paper of exceptional interest, Öpik (1954) pointed out that if dust does polarize, the above values of n_e may be excessive: "It is even quite possible that there is no significant amount of interplanetary gas at all, except very close to the sun" (loc. cit., p. 44). Also Blackwell (1956b, 1957) has stressed this possibility.

Blackwell and Willstrop (1957), from a study of the continuous spectrum of comet Arend-Roland, have inferred that dust-scattered light *can* be polarized. Blackwell (1956a, p. 64) connects the (unlikely) rapid outward decrease of n_e beyond the earth, inferred by Behr and Siedentopf (Table VIII) with the doubtful assumption as to polarization by dust. He remarks: "It is disturbing that at distances beyond 30 R the density of the interplanetary gas seems to decrease so slowly with increasing distance from the sun." The explanation here offered for this slow decrease is the high temperature of the gas (combined, in the plane of the ecliptic, by the weakening of apparent gravity by centrifugal force).

11. THE ZODIACAL LIGHT AND THE CORONA

In 1958 D. E. Blackwell and M. F. Ingham went to Chacaltaya in the Andes, near La Paz, Bolivia. Their object was to study the luminosity and polarization of the zodiacal light from a high level (17,000 feet). Redman (1959) has reported some of their provisional conclusions, based on their (not then completed) study of their data. "The present evidence suggests an electron density near the earth's orbit not more than 150 electrons cm^{-3}, but I should emphasize that this is still a somewhat tentative figure; the true value could be well below this."

These zodiacal light observations were taken near sunspot maximum, and the conditions in interplanetary space doubtless differed considerably from those during the 1954 eclipse. Redman reported an important observation to this effect by Blackwell and Ingham. Their "photographs extended over several evenings immediately before and after the very large solar flare of 1958 July 7. Following the flare there was a magnetic storm, and during the magnetic disturbance there was an increase of zodiacal light brightness by a factor of about 2. Also the axis of the light, normally near the ecliptic, was displaced

to the north. The evidence is convincing that at least on special occasions such as this the zodiacal light intensity can vary considerably .....But....there was a puzzling change of colour of the zodiacal light, not yet understood. No photographs of the spectrum were obtained during this particular period; indeed until now exposures have been so long that temporary changes lasting a day or so could be greatly smoothed out," (loc. cit., p. 179). He added (p. 181): "But we now have definite evidence of variability of the zodiacal light, and need to discover more about the range and frequency of the variation, which is probably due to varying numbers of electrons rather than a changing amount of dust."

It is clearly highly desirable, as an adjunct to space research by cosmic rockets, to use the opportunities afforded by zodiacal light observations to improve our knowledge of the interplanetary gas. Improved equipment should be used, able to provide good spectra with exposures of no more than a few hours. As Redman (1959) remarked, progress in these studies of the corona and the interplanetary medium "is still possible by the careful application of the best optical techniques either from the ground or from conventional aircraft. These methods are less spectacular than artificial satellites but they are far, far cheaper." It seems very desirable that there should be at least one well chosen station where the luminosity, polarization and spectrum of the zodiacal light should be regularly recorded. Chacaltaya appears to be particularly suitable for such work. If such records could be taken also at one or more stations in other longitudes, that offer similar advantages of height and good sky, the changes in the light could be more continuously followed.

Even at high level ground stations, however, the sky background light produces difficulties that could be removed, or greatly reduced, if such an optical observing program could be executed from one or more low-latitude satellites, circulating at a moderate distance above the earth.

12. ALTERNATIVE HYPOTHESES

The preceding discussion contrasts two estimates of the interplanetary electron density at the earth's distance. Blackwell and Ingham provisionally put the value as of order 150/cc or less. I have tried to infer the value from a reasoned extrapolation of Blackwell's estimates of n_e up to 20 R; the result is about 360/cc, or rather more than twice his tentative upper limit. In this field of research a discrepancy by a factor of only about 2 is to be regarded as very moderate. It is too soon to say whether it comes from an error in the estimates of n_e up to 20 R, or an error in my method of extrapolation. Blackwell's observation of a twofold increase of the zodiacal light after a solar flare suggests that the true value of n_e may vary by a factor of at least 2.

My extrapolated inferences as to the steady state of the inter-

planetary gas are in qualitative agreement with the apparent observed ellipsoidal form of the zodiacal light, suggesting rotation parallel to the ecliptic plane. My inference as to the temperature of the gas at the earth's distance is here made more precise than in my 1959 discussion; the estimated value remains high, and, as I have urged, implies a great extension of the earth's atmosphere. This may enable the earth to keep the gas in nearly Keplerian motion, and lessen the resistance to its own orbital motion.

At times the interplanetary gas is traversed by clouds and streams of solar gas moving with high speeds, of order 1000 km/sec. Parker (1958a, b) following Biermann (1957) has proposed that such emission is continuous from the whole sun—though accentuated from particular areas from time to time. This conception has been criticized, most recently by Chamberlain (1960), who presents a hydrostatic model of the atmosphere, rather different from the one here considered. He attributes importance to the evaporative escape of protons (with electrons). The escaping protons are those that have outward speeds greater than the escape speed at their distance from the sun. He estimates the loss to be at the rate 2×10^{36} electrons/sec. His illustrative calculations lead to a value of about $370/cm^3$ for n_e, and 110,000 for T at the earth's distance. These values are in remarkable accord with those here derived, but it may be unwise to regard the agreement as confirming either set of calculations. Their basic conceptions differ in important respects.

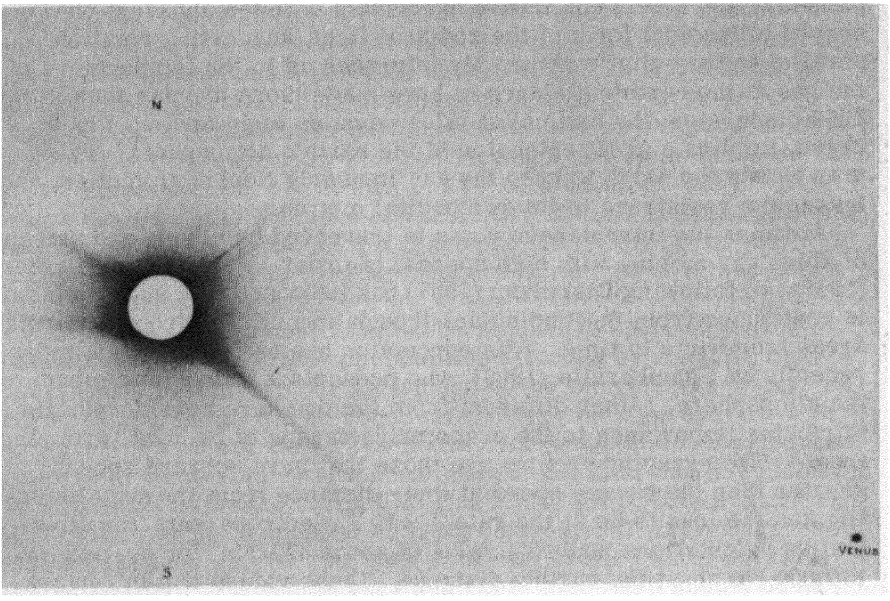
Thus there is need for more and better observations, of the corona and the zodiacal light, from the ground and from aircraft, and *in situ* from cosmic rockets. There is also need for further theoretical debate.

APPENDIX

THE EXCEPTIONALLY LONG CORONAL RAY OF 1898 JANUARY 22

For the eclipse of this date many expeditions went to India. The day was cloudless, the weather exceptionally good. The duration was about 105 seconds. The date was 4.0 years after the moderate sunspot maximum of 1894.1 (when the mean sunspot number $\bar{R}$ was 88), and 3.6 years before the sunspot minimum of 1901.7 ($\bar{R} = 3$). For January 1898 the monthly mean $\bar{R}$ was 30; on January 22 the daily number was 48). The period was magnetically quiet (January 23 was one of the five quiet days of the month).

At the British Astronomical Association station at Talni (lat. 20°8′N) (Maunder, 1898, p. 307) Mr. and Mrs. E. W. Maunder (1922) obtained "a coronal photograph on a small scale, showing a very long extension of one of the streamers" (M.N. 59, p. 287). A Dallmeyer astigmatic lens was used, of one and a half inches aperture and 9 inches focus. This photograph is reproduced on page 148.



The Astronomer Royal (Christie) at Sahdol (23°17'N, 81°22'E) photographed the corona, and Dyson (1927) published a composite drawing (by Wesley) from Christie's photographs. It shows much detail, with large streamers in each of the four quadrants. The most conspicuous, in the S.W., was observed visually by Christie (1898, p. [9]) during the eclipse. He estimated "the extreme extension of the S. W. streamer to be about two-thirds the distance of Venus from the Sun's centre, or about 3 1/2° from the limb." On the Maunder photograph the beam "was traced out for at least six million miles" (Maunder (1922), p. 542). These two estimates agree in giving the extreme distance from the sun's center to be 15 R, where R denotes the solar radius. (Many prominences were visible, fairly evenly distributed around the disc: for other details see Dyson (1927)). The lower part of each main coronal streamer had a synclinal structure, from which a straight tapering ray extended far outwards.

REFERENCES

[1] Athay, R. G., D. H. Menzel, J. C. Pecker and R. N. Thomas, Astrophysical J., Suppl., **1**, 12.
[2] Behr, A. and H. Siedentopf, 1953, Z. Astrophys. **32**, 19.
[3] Biermann, L., 1957, Observatory, **77**, 109.
[4] Billings, D. E., 1959, Astrophys. J., **130**, 961.
[5] Blackwell, D. E., 1955, Monthly Not. Roy. Astron. Soc., **115**, 629.
[6] Blackwell, D. E., 1956a, Monthly Not. Roy. Astron. Soc., **116**, 56.
[7] Blackwell, D. E., 1956b, Monthly Not. Roy. Astron. Soc., **116**, 365.
[8] Blackwell, D. E. and R. V. Willstrop, 1957a, Monthly Not. Roy. Astron. Soc., **117**, 590-599.

[9] Blackwell, D. E., 1957b, The Observatory, **77**, 187.
[10] Chamberlain, J. W., 1960, Astrophys. J., **131**, 47.
[11] Chapman, S., 1954, Astrophys. J., **120**, 151.
[12] Chapman, S., 1957, Smithsonian Contrib. Astrophys., **2**, 1.
[13] Chapman, S., 1959, Proc. Roy. Soc., A, **253**, 450.
[14] Christie, W. H. M., 1898, Monthly Not. Roy Astron. Soc., **58**, [9]
[15] Dyson, F. W., 1927, Phil. Trans. Roy. Soc., A, **226**, 366.
[16] Hewish, A., 1958, Monthly Not. Roy. Astron. Soc., **118**, 534.
[17] Lettau, H., 1957, Exploring the atmosphere's first mile, Pergamon Press, 306.
[18] Maunder, E. W., 1898, Monthly Not. Roy. Astron. Soc., **58**, 301; see also **59**, 287.
[19] Maunder, E. W., and A. S. D. Maunder, 1922, Monthly Not. Roy. Astron. Soc., **82**, 542.
[20] Michard, R., 1954, Ann. d'Astrophys., **17**, 429.
[21] Öpik, E. J., 1954, Z. Astrophys., **35**, 43.
[22] Parker, E. N., 1958a., Astrophys. J., **128**, 664.
[23] Parker, E. N., 1958b., Astrophys. J., **128**, 677.
[24] Pottasch, S. R., 1960, Astrophys. J., **131**, 68.
[25] Redman, R. O., 1959, Observatory, **79**, 172.
[26] Waldmeier, M., 1955, Z. Astrophys., **36**, 275.
[27] Woolley, R. v.d. R. and C. W. Allen, 1948, Monthly Not. Roy. Astron. Soc., **108**, 242.
[28] Woolley, R. v.d. R., and C. W. Allen, 1950, Monthly Not. Roy. Astron. Soc., **110**, 358.
[29] Zirin, H., 1957, Smithsonian Contrib. Astrophys., **2**, 13.

Note added in proof (December 14, 1960): Since the above paper and appendix were written, Dr. Blackwell has kindly sent me preprints of three papers by himself and Dr. Ingham dealing with their study of the zodiacal light at Chacaltaya, mentioned in Sec. 11. These papers are to be published in the Monthly Notices of the Royal Astronomical Society. They conclude that the zodiacal light is more polarized than had been supposed, and that normally the light is mainly dust-scattered. Hence the polarization of the coronal light at 20 R, which had been ascribed wholly to electrons (Blackwell 1956), must at least in part be due to dust scattering. On this account Blackwell's values of n_e from 5 R to 20 R must be reduced. This will entail a corresponding reduction of all my values of n_e beyond 20 R, viz. in Tables V and VII. The reduction factor at 20 R, Dr. Blackwell informs me, is about 4. If this same factor is applied to my values for greater distances, as seems reasonably legitimate, they are brought into better, indeed fair, accordance with the conclusions of Blackwell and Ingham.

9. THE SOLAR WIND AND THE INTERPLANETARY MEDIA

L. Biermann
Max Planck Institute

The solar corpuscular radiation has been known for a long time mainly from geomagnetic observations. In addition to the well-known phenomena of geomagnetic storms, observations at polar stations have shown that there is practically always some magnetic activity. This indicates that there is a certain level of continuous intensity of the solar corpuscular radiation, for which E. Parker has proposed the name of solar wind in contrast to the storm-like phenomena mentioned before. We shall see that certain observations of the comets provide another line of evidence on the intensities of these particle radiations of the sun.

The term interplanetary medium is used mainly to denote the medium responsible for producing the zodiacal light. The main constituent of this medium is a cloud of dust particles, with particle sizes ranging from several thousand Angstroms to a fraction of a mm, which is rather concentrated towards the ecliptic plane and extends at least to approximately one astronomical unit. Photoelectric measurements of the polarization of the zodiacal light have been taken by Behr and Siedentopf as evidence that free electrons of a number density of some 10^2 per cc contribute to the zodiacal light. Later discussion has shown that the interpretation of the zodiacal light observations is somewhat more complicated than was realized initially.

Direct and indirect evidence on the radiation fields and the magnetic fields in interplanetary space has come in recent years from rocket and satellite observations on one hand and from cosmic ray observations on the other. The former have yielded fairly reliable figures about the solar radiation in the ultraviolet and the x-ray region and their dependence on solar activity. The latter observations have given evidence of the presence of magnetic fields in interplanetary space.

The central problem in this area which has received attention in recent years is that of the interrelations between these various media and radiations and the relation of the interplanetary gas and the sun's corona. We shall see, largely on the basis of the observation of comets, that the interplanetary plasma should be identical with the solar corpuscular radiation, that it does not co-rotate with the sun, and that the magnetic fields seem to be related to the solar corpuscular radiation.

We shall now discuss in turn the evidence which may be derived from geomagnetic data, from cosmic radiation and from comets. There seems to be little relation between the zodiacal dust cloud and the solar corpuscular radiation, with the exception only of the fact that the latter limits the lifetime of the dust particles. It should be mentioned in passing that the zodiacal dust cloud is continuously replenished from comets dissolving under the influence of the sun's heat radiation.

The geomagnetic observations indicate that there are several levels of intensity of the solar particle radiation. In addition to the individual events which cause geomagnetic storms there are often long-lived centers of activity on the sun which cause geomagnetic disturbances at regular intervals of 27 days, the synodic period of rotation of the sun as seen from the earth. These centers are not connected with any visible feature on the sun's surface; they seem rather to be related to certain properties of the local magnetic fields on the sun in a way which we are at best only just beginning to understand. The evidence for the more or less continuous component of solar activity rests mainly on the magnetic observations referred to already and on those of comets which will be dealt with below. The magnetic observations indicate in a general way that the overall level of corpuscular activity depends also on the eleven year cycle of solar activity, with the important difference, however, against the sunspots, that whereas the sunspot numbers around the solar minima may be close to zero for fairly long periods of time (maximum figures of the order of 100), the magnetic character figures never drop to a level really small compared with the maximum level. This indicates in a general way that the solar corpuscular radiation varies to a relatively smaller extent than the sunspot figures would indicate.

We discuss now the evidence provided by cosmic ray observations. The observations of interest in this connection come mainly from events on the sun during which large quantities of high energy particles are locally produced in connection with solar flares.

Occasionally, on the average once in four or five years, a big solar flare seems to produce an increase of the cosmic ray intensity observable at sea level stations in middle latitudes. These increases are produced by ions of an energy of several up to about ten or 15 Gev (10^9 ev). The absence of particles of higher energies can be concluded from the fact that usually no increase is observed near the geomagnetic equator. These increases have also been observed near the geomagnetic poles but with a time delay of the order of half an hour or so. The detailed discussion of these events has shown that the solar ions of some Gev observed at polar stations cannot have come directly from the sun but must have travelled somewhat longer paths in interplanetary space before having been guided towards the earth. It seems obvious that only interplanetary magnetic fields could produce this effect. More recently evidence has come from various lines indicating that events on the sun, in the course of which charged particles are accelerated to energies of around 30, 100, or several 100 Mev, are very much more frequent. These observations come partly from radio astronomy, partly from

ionospheric observations at polar stations and partly from balloon observations of high energy particles at high geomagnetic latitudes. Certain types of radio bursts following solar flares seem to be explicable only on the basis of the assumption that relativistic electrons, in the energy range of some 10 Mev, spiral in the local solar magnetic fields. The so-called Type IV radio bursts seem to be due to synchrotron radiation of such electrons, but also the gamma bremstrahlung radiation of these electrons has occasionally been observed from balloons. The ionospheric observations refer to the so-called polar blackouts—heavy disturbances of the D-layer caused by fast protons coming from the sun. The correlation between big solar flares on the visible disc of the sun, between Type IV radio bursts and polar blackouts is such that a big solar flare is quite often followed by a Type IV radio burst which may occur say once per month during high level of solar activity, but that a polar blackout usually follows only if the flare has occurred on the western half of the visible disc.[1] On the other hand, no events have been observed so far which were *not* related to a flare on the visible disc of the sun. The conclusion seems to be indicated, therefore, that ions in the energy range 30 – 300 Mev (usually), but up to 1 Gev, are guided by interplanetary magnetic fields in such a way that they do not travel on straight paths between sun and earth; they seem to be guided rather by interplanetary magnetic fields along paths which appear to resemble the spiral pattern of continuous particle emission from long-lived centers on the sun familiar from geomagnetic theory. Such a structure of the magnetic fields in interplanetary space was first postulated on theoretical grounds by Parker. Since the theoretical problem of the relation between the magnetic fields in interplanetary space and the solar corpuscular radiation is very complex, it is gratifying that the observations last mentioned seem to yield unambiguous evidence.

The time dependence of the cosmic ray intensity after events of the kind just described yields another very interesting piece of information. After the big events, in particular the very spectacular one on February 23, 1956, it was observed that over a period of quite a number of hours the intensity of the additional cosmic radiation declined in a way suggesting isotropy of this radiation and a sort of confinement in some part of the interplanetary system bounded or filled by magnetic fields which allowed the solar particles only gradually to escape outwards by diffusion.[2] The intensity of these magnetic fields would have to be of the order of some 10^{-5} gauss. A similar decline extending over a number of days was observed recently after one of the events during which the solar ions reached energies of some 100 Mev. The longer time scale in the latter case can probably be understood on the basis of the smaller radii of curvature and the smaller velocity of the ions in the latter case.

Additional evidence on the influence of magnetic conditions in interplanetary space on the intensity of the general (normally constant) cosmic radiation is provided in particular by the variation of the low energy component (below 1 Gev) with the general eleven years cycle.

It is fairly certain that this has to be understood as a consequence of the variation of the general level of the solar corpuscular activity of the sun with the eleven years cycle of solar activity, known from the indices of magnetic activity, and of the connection between interplanetary magnetic fields and solar corpuscular radiation, but I cannot go into a detailed discussion of the theoretical schemes which have been proposed in this field.

We discuss now the evidence from comet observations, to the extent to which these are of interest in the present connection. The solid nucleus of a comet, of diameter probably of the order of one or some kilometers and a total mass of the order of $10^{15} - 10^{17}$ gm is made up of dust and meteoric particles and by compounds of C, N, O, and H, frozen together. When a comet approaches the sun, the compounds of the surface layer evaporate under the influence of the sun's heat, releasing thereby also a corresponding amount of dust particles. The main constituent of the coma and of the several kinds of tails of a comet are hence dust particles and molecules like CN, C_2, CO, N_2, and some others. The last two mentioned are only visible as ions and are among the main constituents of the long, essentially straight tails which some comets develop when they approach the sun. (It is quite possible that additional molecular ions are present, which have no resonance bands in the observable parts of the spectrum.) These tails of Type I in the classification of Bredechin are the only ones which are revelant to the present discussion.

There are mainly three properties which demand attention. First, the accelerations directed away from the sun and their connection with solar activity. Second, the mechanism and the rate of the ionisation of these molecules. Third, some details of the geometrical properties of these tails, in particular the fact that they usually lag behind (by a small angle, of the order of a few degrees), the radius vector joining the sun and the comet (in the sense of the orbital motion of the comet's nucleus round the sun).

The most certain evidence on the accelerations acting on the Type I tails comes from observations of individual clouds, visible on successive photographs. When expressed in units of solar gravity (0.6 cm/sec^2 at one a.u.) these accelerations are of the order of some 10^2, the individual values ranging from around 20 up to more than 2,000. It is easily seen that these accelerations are not explicable by the pressure of solar light. Also, the degree of variability and activity of these tails is a strong indication against any influence on the sun's photographic or visual light; the intensity of the ultraviolet light, which depends strongly on solar activity, is far too low to contribute significantly to the acceleration. The fact that these tails consist of molecular ions and necessarily also of electrons, that is to say of a plasma, means that we should expect a strong interaction with the solar plasma emitted as corpuscular radiation. The interaction to be expected in the absence of magnetic fields was discussed in 1951; it was found that with a number density in the solar stream of the order 10^3 (cm^{-3}), accelerations of the order of 10^2 could be expected under certain plausi-

ble circumstances. It is obvious and has been pointed out repeatedly that magnetic fields could only enhance the coupling and the transfer of momentum between the solar stream and the cometary ions. It was to be expected that correlations exist between geomagnetic phenomena and the activity of Type I tails. An excellent example was provided by comet 1942g, which was for a fairly long period of time in approximate opposition to the sun, and the detailed discussion revealed indeed the existence both of a recurrence period of activity in the comet's tail and its correlation with geomagnetic phenomena. Similar correlations were established for comet Halley during its apparition of 1910. It seems clear therefore that the high accelerations observed in Type I tails and their activity have to be understood as a consequence of the strong interaction between the tail plasma and the solar corpuscular radiation.

This fact allows us to regard comets with Type I tails as test objects for the solar corpuscular radiation, and it is therefore useful to recall some general properties of comets with Type I tails. First of all it is to be noted that comets with such tails have appeared in the past at every level of solar activity, as indicated by the annual mean of sunspot numbers. It may be that they are somewhat more prominent at high levels of solar activity, but there are a number of instances in which they have been observed during low minima of the sunspot number. In particular it seems that if a comet has got a Type I tail once, then it seems to show it without interruption as long as it is sufficiently near to the sun. On the other hand the appearance seems to change usually from night to night in such a way that the parts of the tail nearest to the coma are apparently made up by new material each night. In those comets which have been under continuous photographic observation it was possible to follow these changes in more detail; it has often been possible to follow certain structures in their motion away from the sun for several nights. In more active comets, for instance comet Moorehouse of 1908, certain structures which had the appearance of envelopes became visible during periods of time of the order of a fraction of an hour or about one hour, as described for instance in Eddington's classical paper of 1910. This fact is of particular significance. For some time these observations were regarded as evidence for a very high level of the intensity of solar light below 900 A. Since the cross section of photoionisation is at most of the order of 10^{-17} cm^2 this would have demanded a flux of solar quanta, in the energy range around 14 ev or more, of some 10^{13} or around 10^{14} per cm^2 per second. More recently rocket observations have indicated that the flux of quanta of this energy is very much lower — by several powers of 10. It has been suggested in 1952 that exchange of charge between the solar protons and non-ionised molecules of CO and N_2 is the mechanism responsible for the ionisation of the CO and N_2 molecules. The cross sections in question are of the order of 10^{-15} per cm^2, the most recent measurements indicating a value around 3×10^{-15} cm^2 for protons of 1 – 10 Kev. This means that a time scale of ionisation of 3,000 seconds would indicate a proton flux of 10^{11} particles per cm^2

per second, and a time scale of ionisation corresponding to the time interval between successive nights a proton flux around 3×10^9 particles per cm^2 per second. The corresponding number densities would be around 10^3 or around 30 to 50 per cc respectively, depending on the velocity of the solar protons, which is around 1,000 or 1,500 km/sec at a high level of solar activity, but apparently between 400 and 1,000 km/sec at low activity level. It is possible that the high values are statistically somewhat rare; in any case for judging long-term effects like the mass loss of the sun, or the lifetime of the dust particles which make up the zodiacal light unpolarized component, one should probably use only the values of the order of 10^9 particles per cm^2 per second. Some unpublished results by Stumpf indicate a somewhat higher particle intensity in the regions nearer to the plane of the ecliptic than towards the poles, as would be inferred also from the shape of the solar corona.

Lastly we turn to the discussion of some geometrical features. According to work done by Hoffmeister in 1943, the Type I tails statistically lag behind the radius vector by some degrees, as if the tail were decelerated in its motion around the sun by a resisting medium. The individual observations reveal somewhat larger angles (up to 10° or more) in some cases; in others values near to zero or even occassionally negative ones, such as to make the tail appear to precede rather than lag behind the radius vector. It is seen without difficulty that the average behavior is precisely what would be expected in the case of a purely mechanical interaction by particles coming directly from the sun along a straight path. In that case the angle in question would be equivalent to the ratio of the component of the orbital velocity of the comet perpendicular to the radius vector (of the order of 30 km/sec) to the velocity of the solar particles. If magnetic fields enhance the coupling between the solar plasma and the tail plasma, the situation is somewhat more complicated. What may be concluded from the observations is first that the solar plasma moves essentially radially away from the sun, second that there is no indication of a deviation in one sign, as would be present in the case of a co-rotation of the solar particles of an order of 30 km/sec (complete co-rotation would correspond to a velocity perpendicular to the radius vector of more than 400 km/sec). Furthermore the fluctuation of the angle indicates either fluctuations of the precise direction of the solar plasma or of the direction of the magnetic fields connected with it.

There are some more observations which indicate the presence of magnetic fields in Type I tails, e.g. long, fine streamers or, occasionally, screw-type, large-scale structures, but it is not possible to discuss these here in any detail.

The origin and early development of CO^+ structures near the head of a future comet could probably be best observed by photographs through an interference filter (half width say around 15 A) isolating the 4251 transitions; it should be possible to use a focal ratio of at least f:4, a diameter of the filter of around 1 inch and not too small a focal length (a field of say 30′ would probably be sufficient, corre-

sponding to 10^6 km at 2/3 a.u.). For comparison a similar filter for a strong CN or C_2 band would be useful.

Furthermore, sequences of photographs through ordinary filters using different types of filters and wider fields, in order to isolate the CO^+ transitions as well as possible from the CN and C_2, and from the continuum radiation would be desirable. For those parts of the Type I tail which are well separated from the coma and from the other tails (if there are any), no filter would be necessary or even desirable. The exposure times should be only a fraction of an hour, and a small focal ratio, though not a small focal length, would be useful.

Finally, spectra of Type I tails would be most desirable, though they are difficult to obtain.

We return finally to one question touched upon already in the opening section, the relation between the interplanetary plasma and solar corpuscular radiation. From the comet observations it seems clear that there can be no interplanetary plasma different from the solar corpuscular radiation. With respect to solar particles which would produce big geomagnetic storms on earth, it is of course possible to say that they penetrate an interplanetary gaseous plasma medium made up by the particles constituting the slower components of solar corpuscular radiation; this terminology might be useful in connection with certain aspects of geomagnetic storms. Furthermore it seems clear that the particles constituting the solar corpuscular radiation are, both with respect to their energy and to their rotational momentum, separated from the sun. They seem to merge ultimately with the interstellar gas.

REFERENCES

[1] A. R. Thompson and A. Maxwell, Nature, 185, 89 (1960).
[2] Simpson, Meyer, and Parker. Phys. Rev.

10. THE SOLAR WIND*

E. N. Parker
Enrico Fermi Institute for Nuclear Studies
and Department of Physics
The University of Chicago

I. EXPANSION OF THE SOLAR CORONA

For many years we have heard that such terrestrial phenomena as the aurora, and the geomagnetic fluctuations and storms, etc. are produced by solar corpuscular radiation: The aurora occurs every night in the auroral zone at latitudes of 70° and may be seen at much lower latitudes following intense solar activity; polar magnetic observatories record perpetual geomagnetic agitation, whereas planet-wide agitation occurs following intense solar activity.

In recent years Biermann (1951, 1952, 1957) has detected the solar corpuscular radiation in interplanetary space through his analysis of the acceleration and excitation of Type I comet tails. All Type I comets show evidence of solar corpuscular radiation regardless of their orbital inclination.

From these facts we conclude that 1) corpuscular radiation is probably a perpetual solar emission in all directions from the sun, and 2) the rate of corpuscular emission is exceedingly intense immediately following an outburst of activity on the sun. There is no evidence that the ejection of corpuscular material from the sun ever ceases, even during the quietest years at sunspot minimum.

Presumably the solar corpuscular radiation consists of typical solar material, viz. ionized hydrogen with smaller amounts of ionized helium and traces of the metals, etc. It shall be our purpose here to pursue the question of why the quiet sun should continually eject ionized gas in all directions. In round numbers the quiet day velocity of ejection is 500 km/sec. The density of the outward flowing gas at a radial distance of one astronomical unit (1.5×10^{13} cm) is perhaps $10^2/\text{cm}^3$, and represents a solar mass loss of some 10^{14} gm/sec. The velocity and density may fall to somewhat lower values at sunspot minimum. It may rise to higher velocities, perhaps 1500 km/sec, and very much higher densities, 10^3 - $10^5/\text{cm}^3$, for brief periods immediately following a large solar flare (Unsöld and Chapman (1949)). We

*This research is supported by the Geophysical Research Directorate, Air Force Cambridge Research Center, Air Research and Development Command, Contract AF 19 (604) - 4554.

shall restrict our discussion here to the mean quiet day solar corpuscular radiation.

Now the corona of the Sun has a temperature of about 2×10^6 °K (Billings (1959)), which shows no signs of diminishing outward for several solar radii. The thermal velocity of a hydrogen ion at this temperature is 220 km/sec. The gravitational field of the sun confines the corona in a potential well with a depth corresponding to some four or five hundred km/sec. Thus, only those few coronal ions far out on the tail of the Maxwellian thermal velocity distribution are free to escape from the corona directly out into space. This escape of the Maxwellian tail is called evaporation and was first discussed by Jeans, Stoney, etc. More recently the evaporation of ions from the solar corona has been discussed by Chamberlain (1960). Evaporation from the solar corona yields corpuscular velocities and densities far below the observed values; the evaporative mass loss to the Sun is of the order of only 10^{11} gm/sec.

Suppose, then, that we consider the bulk motion of the solar corona. Traditionally the corona is taken to be in hydrostatic equilibrium. Its temperature of 2×10^6 °K is believed to be maintained by the dissipation of shock waves and hydromagnetic waves generated in the convection zone beneath the photosphere, and by the granules and spicules in the photosphere and chromosphere. Chapman (1957; 1959) was the first to attempt to construct a quantitative model of the static corona. Since radiative losses (largely bremsstrahlung) from the outer corona are very small compared to the outward thermal conduction of some 2×10^{27} °K (Zirin, 1957), Chapman supposed that the corona was in hydrostatic and conductive equilibrium. From the fact that the coefficient of thermal conductivity $\kappa(T)$ in an ionized gas is proportional to $T^{5/2}$, it follows from the stationary heat flow equation

$$\nabla \cdot [\kappa(T) \nabla T] = 0$$

that the temperature falls off like $r^{-2/7}$ outward from the sun. It is then a simple matter to deduce the manner in which the density N(r) decreases outward from the sun using the equation for hydrostatic equilibrium

$$dp/dr = -GM_{\odot}M/r^2 \tag{1}$$

where p is the hydrostatic pressure (2NkT for ionized hydrogen) and M is the mass of a hydrogen atom. If we let the pressure be p_0 and the density be N_0 at a base level r = a, then elsewhere

$$p(r) = p_0 \exp\left\{\frac{7GM_{\odot}M}{10kT_0a}\left[\left(\frac{a}{r}\right)^{5/7} - 1\right]\right\} \tag{2}$$

and

$$N(r) = N_0\left(\frac{r}{a}\right)^{2/7} \exp\left\{\frac{7GM_{\odot}M}{10kT_0a}\left[\left(\frac{a}{r}\right)^{5/7} - 1\right]\right\} . \tag{3}$$

The density function can be compared with the actual coronal densities, observed out to some 20 solar radii. Chapman points out that the

observed coronal densities drop off a little faster than (3) at large distances from the sun, implying that the temperature begins to decrease a little more rapidly than $r^{-2/7}$. Pottash (1960) comes to a similar conclusion and postulates that the increased fall off of temperature is the result of hypothetical metallic ion emission in the ultraviolet.

We would point out a more general objection to this static model, however. We note that in the limit as $r \to \infty$, the hydrostatic pressure given by (2) does not go to zero but approaches the finite limit

$$p(\infty) = p_0 \exp(-7\, GM\odot M/10kT_0a)$$

If we choose an altitude of 3×10^5 km in the corona as our base level, then $a = 10^{11}$ cm and $N_0 = 3 \times 10^7/cm^3$. If $T_0 = 2 \times 10^6$ °K, then $p_0 = 1.7 \times 10^{-2}$ dynes/cm^2. It follows immediately that $p(\infty) = 0.7 \times 10^{-4}$ dynes/cm^2. But this is an enormous pressure, and we believe that far out from the sun in interstellar space we have a high vacuum; an interstellar density of one atom/cm^3 at 100°K yields only 1.4×10^{-14} dynes/cm^2. So there is nothing to contain this coronal pressure at infinity. Hence the corona cannot be in hydrostatic equilibrium if its temperature is in conductive equilibrium, $r^{-2/7}$.

Consider the hypothesis of Pottasch that the coronal temperature decreases outward more rapidly than $r^{-2/7}$ because of emission from metallic ions. It would then theoretically be possible to have a temperature falling off as rapidly as the adiabatic gradient if we postulate enough emission. The temperature could hardly fall faster than the adiabatic gradient because, if it did, convective instability would immediately yield vigorous overturning with convective transport of heat to restore the adiabatic gradient. Thus beyond the limit of coronal heating, say $r = b$, it is conceivable that the temperature decreases as fast as the adiabatic gradient. But as we will soon see, even with this extreme assumption we still cannot escape the problem of nonvanishing hydrostatic pressure at infinity. It is easily shown from the equation for hydrostatic equilibrium (1) and the adiabatic relation

$$N = N_0(p/p_0)^{3/5}$$

that

$$p(r) = p_0\left[\left(1 - \frac{GM\odot M}{5kT_0b}\right) + \frac{GM\odot M}{5kT_0b}\,\frac{b}{r}\right]^{5/2}.$$

The hydrostatic pressure can go to zero at infinity only if $GM\odot M/5bkT_0 > 1$ where the adiabatic atmosphere begins at $r = b$. If $GM\odot M/5bkT_0$ is not less than one, then we have

$$p(\infty) = p_0[1 - GM\odot M/5kT_0b]^{5/2}$$

and $p(\infty)$ is again a significant fraction of the pressure $p(b)$ at the reference level, just as in the conductive equilibrium atmosphere.

Observations of the solar coronal density at sunspot minimum extend out as far as 20 $R\odot$ and show no sign of an adiabatic gradient. The temperature decreases outward only very slowly if at all. If an adiabatic

gradient exists, it can be only beyond 20 $R_\odot$. From the analyses of Chapman and Pottasch we have $GM_\odot M/5kT_0b$ decreasing to 1.0 at the limit of observation, 20 $R_\odot$. Thus we see that we must postulate a full adiabatic gradient beginning immediately at the present limit of observation if we wish the static coronal pressure to fall to zero at infinity. Any gradient less steep than the extreme adiabatic limit will not suffice. Nor is it sufficient to have an adiabatic gradient beginning somewhere beyond the limit of observation, say at 25 $R_\odot$. Therefore, unless we are willing to make these extreme assumptions we find that the solar corona is so hot at sunspot minimum that it cannot be in static equilibrium unless it were confined by an artificial pressure $p(\infty)$ in interstellar space. And of course, during the years of solar activity the corona is even hotter, so that the tendency toward large pressures is even greater. The necessary confining pressures are only a few factors of ten less than at the base of the corona (10^{-2} dynes/cm^2), and so are enormous.

So let us abandon this traditional view that the solar corona is static, with at most an evaporative mass loss into interplanetary space. After all, in our opening paragraphs we pointed out that we observe, by several independent methods, that ionized gas is perpetually flowing outward from the sun in all directions. The densities of 3×10^7/cm^3 observed in the corona and the densities of 10^2/cm^3 observed in interplanetary space show that the collision length for the average thermal ion is everywhere small compared to the scale height and to the radial distance from the sun. Therefore any mass motions must be hydrodynamic in character. Interpenetration of gaseous masses is not possible, so that if we observe an outward flow of gas in interplanetary space, it follows that there is an outward hydrodynamic flow of gas at all levels in the corona. Instead of the hydrostatic equilibrium equation (1) we must use the hydrodynamic equation

$$\partial \mathbf{v}/\partial t + (\mathbf{v} \cdot \nabla)\mathbf{v} = -(1/\rho)\nabla p - \mathbf{g}$$

where $\mathbf{g}$ is the gravitational acceleration. With the usual simplifying assumption that the mean corona may be approximated by spherical symmetry* we have

$$dp/dr = -GM_\odot MN/r^2 - NMv\,dv/dr \qquad (4)$$

in place of (1), where v is the velocity of radial expansion.

Conservation of matter requires that

$$N(r)\,v(r)r^2 = N_0 v_0 a^2 \qquad (5)$$

where v_0 is the velocity at the reference level.

In order to solve (4), let us consider the simplest possible model. Let us suppose that coronal heating, by hydromagnetic waves etc., maintains an approximately uniform coronal temperature T_0 out to the

*Actually the corona is a little hotter over the solar equator than over the poles. The corona appears to be compressed slightly toward the equatorial plane by the general solar magnetic field (Babcock and Babcock, 1955; Babcock, 1960) particularly when it is relatively tenuous at sunspot minimum.

limit of heating $r = b$. Then in the isothermal region, $r < b$, it is readily shown that simultaneous solution of (4) and (5) yields

$$\psi - \ln\psi = \psi_0 - \ln\psi_0 + 4 \ln r/a - \lambda(1 - a/r) \tag{6}$$

where ψ is the kinetic energy of the individual ion measured in units of the thermal energy kT_0

$$\psi \equiv Mv^2/2kT_0 \tag{7}$$

ψ_0 is the value of ψ at the base level $r = a$, and λ is the gravitational potential of an ion at the base level measured in units of the thermal energy kT_0,

$$\lambda \equiv GM_\odot M/akT_0 \tag{8}$$

Numerically we have $\lambda = 8.0$ for $T_0 = 2 \times 10^6\,^\circ K$.

Beyond the heating limit $r = b$ let us assume that there is no heating whatsoever, so that the temperature varies adiabatically

$$T = T_0(N/N_0)^{2/3} \tag{9}$$

Then simultaneous solution of (4) and (5) yields

$$\psi = \Psi_1 - 5(\psi_1 b^4/\psi r^4)^{1/3} + \lambda a/r \tag{10}$$

where ψ_1 is the value of ψ at $r = b$, and

$$\Psi_1 \equiv \psi_1 + 5 - \lambda a/b. \tag{11}$$

The question is now, of course, whether there are any solutions (6) and (10) which go to small velocities as they approach the essentially static sun at small r, and at the same time approach zero pressure at infinity. That is, we wonder if there are any solutions for which $\psi_0 \ll 1$ and for which p, and therefore N, go to zero at infinity. We will now show that not only do such solutions exist, but that they are the only solutions which can exist when the sun is surrounded by a vacuum at infinity.

In Fig. 1 we show the form of the solutions (6) for various values of ψ_0. We note their singular nature. The critical value of ψ_0 is $(\psi_0)_c$ given by

$$(\psi_0)_c - \ln(\psi_0)_c = \lambda - 3 - 4 \ln \lambda/4 \tag{12}$$

If we begin at $r = a$ with a velocity ψ_0 larger than $(\psi_0)_c$, then ψ soon turns back toward $r = a$ and never extends to large r. $d\psi/dr$ becomes infinite when ψ reaches a value of one at a radial distance less than $\lambda/4$. Such solutions have no physical meaning because the gas obviously cannot turn around to return toward $r = a$ without its velocity first going through zero. If we begin with ψ_0 less than $(\psi_0)_c$, then ψ reaches a maximum value at $r/a = \lambda/4$, and this maximum value is less than one. The solutions return to the r-axis for large r, according to

$$\psi \sim \psi_0 (a/r)^4 \exp(\lambda - \psi_0)$$

On the other hand if ψ_0 is *precisely* equal to $(\psi_0)_c$ we have the singular solution

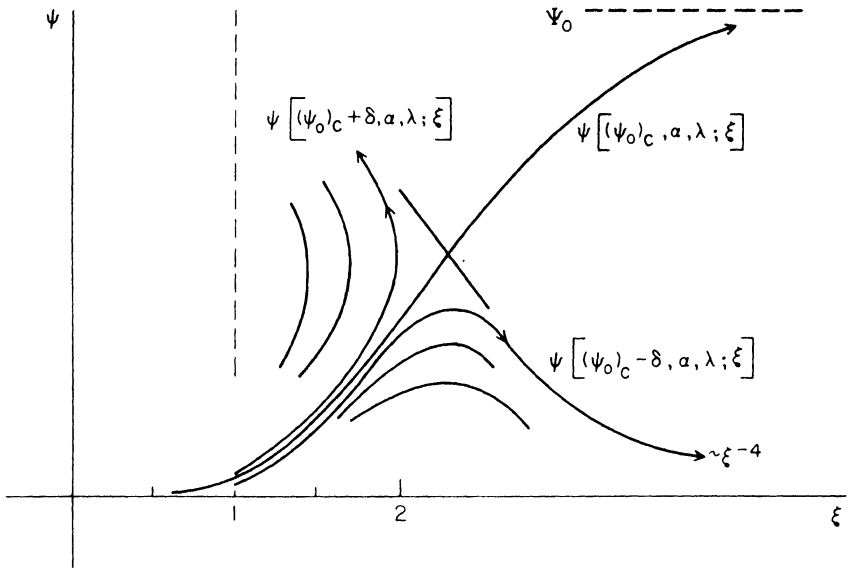


Fig. 1. The general form of the radial velocity function $\psi(\psi_0, \alpha, \lambda; \xi)$ for ψ_0 equal to the critical value $(\psi_0)_c$, and also slightly less and greater. We suppose that $\alpha < 3/2$ and $| \ll \lambda \ll 2\alpha/(\alpha - 1)$.

$$\psi - \ln\psi = -3 - 4 \ln \lambda/4 + 4 \ln r/a + \lambda a/r \tag{13}$$

This solution turns neither to the right nor to the left but passes straight across the critical point $(\lambda/4, 1)$ and increases monotonically as

$$\psi \sim 4 \ln r/2 + 0(\ln \psi) \tag{14}$$

for large r.

Now consider the adiabatic solution (10), which takes over from the isothermal solution (6), at r = b. At large r there are two branches of ψ,

$$\psi \sim \Psi_1 \tag{15}$$

and

$$\psi \sim \frac{125\,\psi_1}{(\psi_1 + 5 - \lambda a/b)^3} \left(\frac{b}{r}\right)^4 \tag{16}$$

We see immediately that (16) is not the desired solution since it yields $v \propto r^{-2}$, which in turn yields, from (5), N ~ constant > 0 at infinity. Thus N and p do not fall to zero at large distances from the sun, contrary to what is required by the lack of hydrostatic pressure in interstellar space. The branch given by (15), on the other hand, yields a constant velocity, and hence a density and pressure decreasing to zero like r^{-2} and $r^{-10/3}$, respectively.

Now how do we arrive on the upper branch, (15)? Let us write (4) in the form

$$\frac{d\psi}{dr}\left[1 - \frac{5}{3}\frac{\psi_1^{1/3} b^{4/3}}{\psi^{4/3} r^{4/3}}\right] = -\frac{\lambda a}{r^2} + \frac{20}{3}\frac{\psi_1^{1/3} b^{4/3}}{\psi^{1/3} r^{7/3}}.$$

It can be shown that if $d\psi/dr$ is positive at $r = b$, then ψ will increase monotonically with r and approach the upper limit given by (15). If $d\psi/dr$ is negative, then ψ decreases to (16). At $r = b$, where $\psi = \psi_1$, we have

$$\frac{d\psi}{d(r/b)} = \frac{20/3 - \lambda a/b}{(1 - 5/3\,\psi_1)}$$

We have already pointed out that observations of the coronal density yield a maximum value for $GM_\odot M/bkT$ at the beginning of the adiabatic gradient of 5. Thus $\lambda a/b < 5$. It follows that if $d\psi/dr$ is to be positive, so that we pass to the upper branch (15), we must have $\psi_1 > 5/3$. We must then require that $\psi_0 = (\psi_0)_c$ so that ψ_1 can be greater than one.* The expansion will be given by (13) from the base of the corona $r = a$ out to the limit of heating $r = b$ where $\psi_1 \equiv \psi(b) > 5/3$. Beyond $r = b$ the expansion velocity is given by (10), approaching the upper bound (15) at large r. The final velocity of expansion is, therefore,

$$v(\infty) = [\,(2kT_0/M)(\psi_1 + 5 - \lambda a/b)\,]^{1/2}$$

Since $\lambda a/b < 5$ and $\psi_1 > 5/3$ we have, as a lower limit on $v(\infty)$

$$v(\infty) > [\,(10/9)(3kT_0/M)\,]^{1/2}$$

Thus, beginning at the base of the corona ($r = a$) with a small velocity ($(\psi_0)_c \ll 1$) in a strong gravitational field ($\lambda \gg 1$) the solar corona expands with a velocity increasing outward and reaching supersonic values at large distances from the sun. As a specific example suppose that the temperature is $2 \times 10^6\,^\circ K$ out to $r = 4a$, and adiabatic beyond. Then $\lambda = 8$, $\lambda a/b = 2$, so that $(\psi_0)_c = 0.13$, $\psi_1 = 2.80$, and $\psi(\infty) = 5.8$. The velocity at $r = a$ is 66 km/sec; the velocity at infinity is 440 km/sec. With $N_0 = 3 \times 10^7/cm^3$ at $r = a$ we have a density of $200/cm^3$ at the orbit of Earth. And this we recognize as just the observed "solar corpuscular radiation" of some 500 km/sec and $10^2/cm^3$ which we discussed in our opening paragraphs.

Therefore, to summarize our results, we suggest that: 1) the solar corona cannot be static; 2) the solar corona expands hydrodynamically outward into space reaching supersonic velocity at distances of many solar radii; 3) the continually expanding hydrodynamic solar corona is in fact the solar corpuscular radiation observed in interplanetary space and in the terrestrial aurora, etc. We refer to the expanding solar corona in interplanetary space as the *solar wind.*

*If $\psi_0 < (\psi_0)_c$, then $\psi_0 < 1$ and $d\psi/dr < 0$ at $r = b$. We will be on the lower branch (16) and p will be large at infinity. Lacking any back pressure to contain this $p(\infty)$, the expansion will go faster, until $\psi_0 \to (\psi_0)_c$. There are no physical solutions for $\psi_0 > (\psi_0)_c$, so that we will soon have $\psi_0 = (\psi_0)_c$.

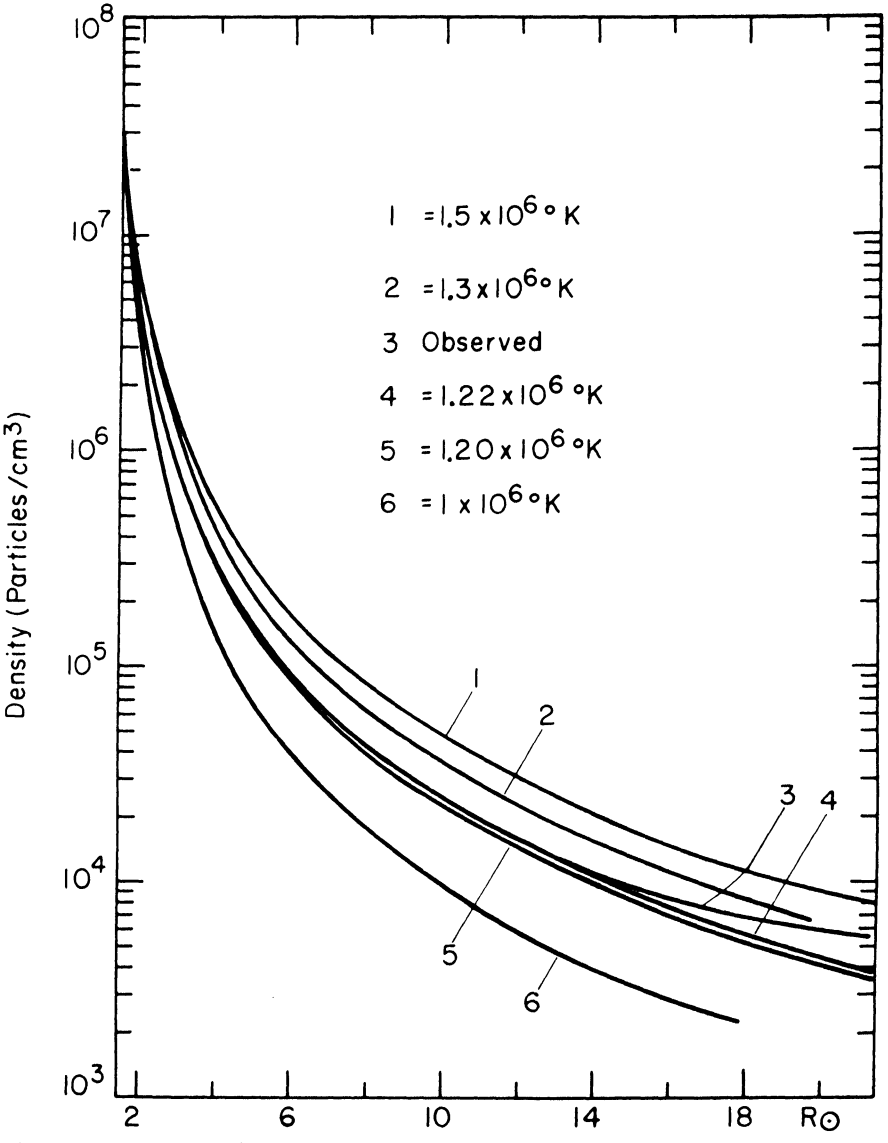


Fig. 2. Comparison of the observed coronal density at sunspot minimum with the theoretical densities for various temperatures in the simple spherically symmetric, isothermal coronal model with $T_0 = 1.22 \times 10^6$ °K out to 14R⊙. The decrease of the theoretical density below the observed density beyond 14R⊙ is to be attributed to the observed concentration of the corona toward the equator.

We may re-analyze the density distribution of the corona at sunspot minimum to deduce the temperature out to 20 R⊙. Instead of the static barometric relation (1) we must use the hydrodynamic equation (4). As

a first approximation we plot the theoretical density curve for a strictly isothermal corona in Fig. 2 for the temperatures $T_0 = 1.2$, 1.22, and 1.25×10^6 °K in order to compare them with the observed density. The agreement between the observed density and the theoretical density with $T_0 = 1.22 \times 10^6$ °K is precise out to 14 R⊙. Beyond 14 R⊙ our simple spherically symmetric isothermal model falls below the observed values. The discrepancy is most simply accounted for by the observed concentration of the corona toward the solar equatorial plane by the general solar magnetic field. It is remarkable, and probably fortuitous, that such a simple model as we have used should fit so well for as far as 14 R⊙. We conclude that the temperature of the solar corona, at the time the density observations were made during the minimum solar activity of 1954-1955, was approximately 1.22×10^6 °K for a distance of the order of 14 R⊙ out from the sun. This temperature replaces the outward decreasing temperature function deduced by Pottasch using the erroneous assumption of static equilibrium.

A more thorough discussion of the theoretical hydrodynamic properties of the corona and solar wind may be found elsewhere (Parker (1958a; 1960a; 1960b)).

We suggest that the solar wind, typical of the sun, may be a not uncommon property of other stars: Certainly if the corona of the sun expands supersonically to form the solar wind, then we would expect any other class G main sequence star to do likewise. It is readily shown that the gravitational parameter λ, which determines the expansion velocity, varies only a factor of two over the main sequence whether we take the coronal temperature to be independent of the spectral class or whether we take it to be proportional to the photospheric temperature. Thus we suggest that supersonic coronal expansion may be a property of most main sequence stars, and presumably of more active stars such as the T Tauri and Wolf-Rayet objects. This general phenomenon of *stellar winds* carries away enough mass, particularly during the early active period* of a star, as to be of importance in the theory of evolution of stellar interiors.

II. TERRESTRIAL EFFECTS

We have established that the solar corona expands continuously to form the supersonic solar wind in interplanetary space, with velocities and densities in agreement with those observed. Consider now what other observable effects we might expect from the solar wind.

The solar wind blows against the geomagnetic field, compressing it slightly on the sunward side. The horizontal component of the geomagnetic field at the surface of Earth is increased by a few gammas (one gamma = 10^{-5} gauss) everywhere around the equator by this solar wind pressure. The quiet day solar wind of 440 km/sec and $2 \times 10^2/\text{cm}^3$

*We are indebted to Professor W. A. Fowler for pointing out this important fact.

yields an increase of ~7 gammas. The solar wind can press in the geomagnetic field to the point where the wind pressure $NMv^2(\infty)$ is just balanced by the geomagnetic field pressure $B^2/8\pi$. If we assume a simple plane interface at a radial distance $R = R_1$ between the wind and the field, then we have, at the interface,

$$B \cong 2B_0(R_E/R_1)^3$$

in the equatorial plane, where R_E is the radius of Earth (6.4×10^8 cm) and B_0 is the mean horizontal intensity (0.35 gauss) of the geomagnetic field at the equator. It follows immediately that

$$R_1 \cong R_E[B_0^2/2\pi NMv^2(\infty)]^{1/6}$$

The quiet day solar wind yields $R_1 \cong 5.4\ R_E$. We would expect the outer Van Allen radiation belt to fall off rapidly at this radial distance, in agreement with observation. If we make the simple assumption that the quiet day aurora should appear at the foot of the lines of force which would normally cross the equatorial plane at R_1, then we predict that the auroral zones should occur at latitude ϑ where

$$\cos \vartheta \cong (2\pi NMv^2(\infty)/B_0^2)^{1/12}$$

We find $\vartheta \cong 65°$, in agreement with observation.

Those lines of force which enter the surface of Earth at higher latitudes than ϑ pass out into the solar wind where their instability (Parker (1958b)) causes them to be continually disturbed. Thus we would expect to find perpetual geomagnetic agitation toward the poles from the auroral zones, in agreement with observation.

When the sun exhibits a large outburst of activity, involving one or more large flares, the local coronal temperature may jump to 4×10^6 °K or more, resulting in a blast wave whose theoretical velocity is of the order of 10^3 km/sec, in agreement with the 2-day delay between the flares and the arrival of the blast wave at Earth. It is no longer possible to use the stationary spherically symmetric hydrodynamic equation, of course, but the effects at Earth may be briefly noted. An extreme solar wind of 1500 km/sec and 10^4/cm^3 may be expected to yield aurorae at latitudes as low as $\vartheta = 35°$.

There is, of course, no quantitative theory for the aurora, but it is interesting to note that the observed primary auroral proton spectrum (Chamberlain (1957)) and the observed electron energies (Van Allen (1955); Winckler, Peterson, Arnoldy, and Hoffman (1958); Winckler, Peterson, Hoffman, and Arnoldy (1958)) can be accounted for as a direct consequence of the solar wind blowing against and into the geomagnetic field (Parker (1958b, 1958c)).

The pressure of the wind against the geomagnetic field may result in transient increases of the horizontal field component at the surface of Earth of the order of

$$\Delta B/B_0 \cong R_E^3/8R_1^3$$

if we make the simple assumption of a plane interface between the wind and the field. For an extreme solar wind this may amount to one per

cent, which increase is to be identified with the observed sudden commencement and initial phase of the geomagnetic storm (Parker (1958b)). The main phase appears to follow when the wind has begun to ease up a little and the gas injected from the solar wind into the geomagnetic field has a chance to inflate the field and decrease the horizontal component at the surface of Earth (Dessler and Parker (1959)).

III. INTERPLANETARY MAGNETIC FIELDS

The sun has a general magnetic field of the order of one gauss (Babcock and Babcock (1955)) which appears to have opposite signs at each pole (Babcock (1959)). This general field will be drawn radially outward by the solar wind so that it decreases as r^{-2}, yielding approximately 2×10^{-5} gauss at the orbit of Earth. It is the presence of this approximately radial field which accounts for the observed free passage of high energy particles from solar flares on the visible surface of the sun to the Earth (Meyer, Parker, and Simpson (1956)), but which accounts for the observed lack of arrival at Earth of particles from flares on the back side of the sun.*

A spiral develops in the field at large radial distances from the sun as a consequence of the approximately 27-day rotation of the sun, so that beyond the orbit of Earth the field becomes more azimuthal than radial, and decreases outward as r^{-1}. The lines of force in the equatorial plane of the sun are shown in Figure 3 for a 500 km/sec wind. The angle between the lines of force and the radial direction is 39° at the orbit of Earth. The higher the solar wind velocity, the more nearly radial are the lines of force, of course. The lines of force are given by

$$r \cong [v(\infty)/\Omega]\phi$$

where Ω is the mean angular velocity (2.7×10^{-6} radians/sec) of the sun and ϕ is the azimuthal angle measured from the direction of emergence of the line from the surface of the sun.

Beyond the orbit of Earth there are at least two instabilities expected to occur which will disorder the interplanetary field. As the solar wind density falls below $10^2/cm^3$ the ion collision rate may become so low that anisotropy of the thermal motions will result from the preferential expansion of the outward streaming gas in the two directions perpendicular to the radial direction: Since the gas is moving radially with essentially constant velocity, it experiences no expansion in the radial direction; the divergence of the flow in the two directions perpendicular to the radius causes the thermal motions in those two directions to decrease adiabatically. Thus an anisotropic thermal velocity distribution results, in which the thermal motions

*The uniqueness of the radial field, necessary to exclude back side flare particles, to the solar wind model was emphasized to us by Professor L. Davis.

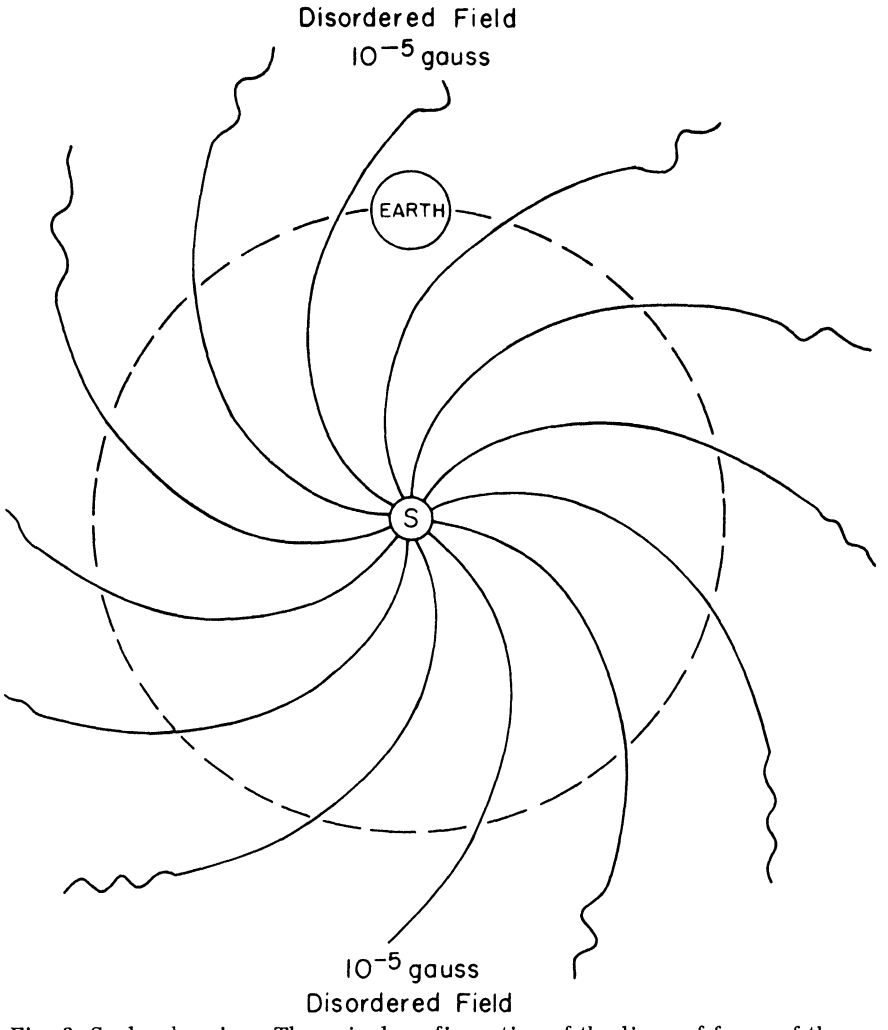


Fig. 3. Scale drawing. The spiral configuration of the lines of force of the general solar magnetic field in the equatorial plane drawn out by a 500 km/sec solar wind. The sun and Earth are not drawn to scale.

in the radial direction are greater. It is well known that anisotropic thermal velocities lead to instability of a weak magnetic field in the gas: The hose instability is the result if the field lies along the direction of greater thermal velocity; the centrifugal force of the ions moving along the lines of force around a perturbation in the field draw out further the perturbation. The pancake instability is the result if the field lies in the direction of lesser thermal velocity; the thermal motion is principally in circles around the lines of force so that the ions are trapped in, and inflate, any regions of weaker field.

The occurrence of instabilities in the interplanetary field beyond the orbit of Earth yields disordered fields of the order of 10^{-5} gauss (the field at the orbit of Earth is 2×10^{-5} gauss). If it is the hose or the pancake instability responsible for the instability, the scale of the disordering is expected to be of the order of 10^6 km. Thus we expect that the inner solar system is enclosed by a thick shell of disordered field of 10^{-5} gauss with a small scale structure of perhaps 10^6 km (Parker (1958d)). The existence of this disordered shell was predicted earlier from observations (Meyer, Parker, and Simpson (1956)) from a detailed analysis of the trapping of solar cosmic ray particles in the inner solar system for many hours following their production in a large solar flare.

We have shown elsewhere (Parker (1958e)) that the outward convection of galactic cosmic ray particles by the disordered field moving outward with the solar wind will produce a depression of the cosmic ray intensity at Earth whose amplitude increases with the level of solar activity and the coronal temperature. The size of the depression and its dependence upon the cosmic ray particle energy bears a quantitative similarity to the observed 11-year variation of the cosmic ray spectrum. Thus we appear to have ready made an explanation for the observed depression of the cosmic ray intensity during the years of solar activity (Meyer and Simpson (1957; 1958)).

IV. EXPERIMENTAL TESTS OF THEORETICAL MODELS

Except for Biermann's analysis of the acceleration and ionization of comet tails, there are no direct *quantitative* observations of the solar wind. The perpetual polar geomagnetic agitation and the nightly occurrence of the high latitude aurora are only direct *qualitative* observations of the solar wind; they yield quantitative results only when their latitude is interpreted on the basis of the theoretical assumptions which are simplest.

Therefore it is highly desirable to obtain direct observational confirmation of the velocity, density, and fluctuations in the solar wind, along with the associated magnetic fields and cosmic ray intensity variations. We need, first of all, better observations of the solar corona. If the electron density of the corona were to be observed out to 30 $R_\odot$ at all solar latitudes during sunspot minimum, or to 15 $R_\odot$ at all solar latitudes during the years of solar maximum, we would be able, in principle, to fit a quantitative hydrodynamic model to the solar corona so that the flow everywhere throughout the inner solar system would follow deductively without ambiguity.

Second, we need direct observation of the solar wind velocity, density, and temperature from space vehicles. A number of laboratories are currently planning such observations, so that in another year or so the question of the existence of the continuous solar wind should be settled. We would like to emphasize, however, the importance of making a number of distinct kinds of observation simultaneously from the

same space vehicle, in coordination with observations from Earth. The solar wind is not a perpetually steady phenomenon. It possesses a 27-day variation, and even more important, it sometimes increases abruptly to large velocities ($\sim 10^3$ km/sec) and enormous densities (up to $10^5/cm^3$) as the result of sudden solar activity. A large number of ideas have been put forth as to the nature of the sudden enhancement of the solar wind and the magnetic fields which it places in interplanetary space. It has been suggested that sunspot fields may be drawn out past the orbit of Earth by an explosive outburst of gas. It has been suggested that clouds of tangled magnetic field are blown out into interplanetary space. Therefore, it is essential that simultaneously with the solar wind velocity and density one should measure at least the magnitude of the interplanetary magnetic field and one should measure the cosmic ray intensity (energies $>$ 100 Mev) and the low energy particle intensity (energies $<$ 100 Mev). All of these observations should be carefully correlated in time with cosmic ray and geomagnetic observations at Earth. Only with a comprehensive battery of simultaneous observations will it be possible to conclusively narrow the field of arguable theoretical models and thereby achieve a step forward in our understanding of the solar corona and interplanetary space.

REFERENCES

Babcock, H. D., 1959, Ap. J. **130**, 364.

Babcock, H. W., and Babcock, H. D., 1955, Ap. J. **121**, 349.

Biermann, L., 1951, Z. Astrophys. **29**, 274; 1952, Z. Naturforsch, **7a**, 127; 1957, Observatory, 107, 109.

Billings, D. E., 1959, Ap. J. **130**, 215.

Chamberlain, J. W., 1960, Ap. J. **131**, 47.

Chapman, S. 1957, Smithsonian Contr. Astrophys. **2**, 1; 1959, Proc. Roy. Soc. **253**, 462.

Dessler, A. J. and Parker, E. N., 1959, J. Geophys. Res. **64**, 2239.

Meyer, Parker, and Simpson, 1956, Phys. Rev. **104**, 768.

Meyer, P. and Simpson, J. A., 1957, Phys. Rev. **106**, 568; 1958, Suppl. Nuovo Cim. **8**, 233.

Parker, E. N., 1958a, Ap. J. **128**, 664; 1958b, Phys. Fluids **1**, 171; 1958c, Phys. Rev. **112**, 1429; 1958d, Phys. Rev. **109**, 1874; 1958e, Phys. Rev. **110**, 1445; 1960a, Ap. J. **132**, 175; 1960b, Ap. J. **132** (Nov.)

Pottasch, S. R., 1960, Ap. J. **131**, 68.

Winckler, Peterson, Arnoldy, and Hoffmann, 1958, Phys. Rev. **110**, 1221.

Winckler, Peterson, Hoffmann, and Arnoldy, 1958, J. Geophys. Res. **64**, 597.

Unsöld, A., and Chapman, S., 1949, Observatory **69**, 219.

Van Allen, J. A., 1955, Phys. Rev. **99**, 609.

Zirin, H., 1957, Smithsonian Contr. Astrophys. **2**, 13.

11. THE MOON

T. Gold
Cornell University

We all believe that great progress in the exploration of the moon will be made within the next few years. Instrumented landings, roving vehicles under remote control from the earth, instrumented vehicles surrounding the moon, all these will be a reality before very long, and we can look forward to the new knowledge that this will give us.

Of what kind will this new knowledge be? This form of research work is very expensive, and to make it worthwhile the information gained must be more than merely a description of another little piece of our solar system. I think that in fact it will be a great deal more. I think we can confidently expect that the exploration of the moon will result in an understanding of the history of the solar system. The moon's surface has preserved a record of past events over much greater periods of time than the surface of the earth. All the great activity on the surface of the earth which geologists and geophysicists have investigated, namely the processes of mountain building and perhaps of continental growth, of erosion by wind and water, of ocean sedimentation, have been absent on the moon. What processes there are in the vacuum conditions of the lunar surface certainly act very much more slowly. Where the investigations of the earth's surface merely relate to events of local significance, surface investigations on the moon will relate to events that occurred in the construction of the moon itself and perhaps with that of the earth and the terrestrial planets. The moon is the object which is most likely to have preserved a record of the origin of at least the inner part of the solar system and it is very fortunate that this interesting body is our closest neighbor.

It may be thought that with the exploration of the moon not very far off, there is no point in discussions and speculations concerning the moon's surface which will be superseded before long by definite knowledge. But this is really not a tenable point of view. On the contrary, just now in preparing for the great exploration we must discuss all the possibilities, we must think carefully of all the questions to ask of our remotely controlled apparatus, we must provide for all the possibilities in the design of the instrumentation and in the stage by stage planning of the exploration.

What is the kind of information we now have about the lunar surface? There is information derived from the optical appearance, the detailed study with telescopes with the maximum possible resolution, of the

shapes and colors of the lunar landscape. Secondly, there is the information obtained from the thermal radiation emitted from the lunar surface at varying depths depending upon the wavelength measured. This thermal radiation has been measured in the near infrared where it relates to depths only insignificantly below the surface and at radio wavelengths in the centimeter band, where the probable effective depths of emission are of the general order of a few tens of centimeters. The third major source of information is from the radar measurements that define the scattering and absorbing properties of the moon's surface at wavelengths between a few centimeters and a few meters.

What kind of a picture of the surface structure has emerged from all this? What can one say so far about the history of the moon? What kind of equipment should first be landed there, what kind of experiments should first be done, and how must this equipment be designed to operate under lunar surface conditions?

It is certain that the major part of the surface area is not composed of solid rock. The thermal measurements indicate a very much lower heat conduction than any solid rock would have, and the radar measurements indicate a degree of small scale smoothness which it would be difficult to suppose a rocky landscape to possess. The surface material must be finely divided or exceedingly porous, just in order to match the thermal properties, and it must have been distributed so as to leave a surface configuration that has few irregularities on the scale of the radar wavelengths used, that is a few inches and up to a few feet.

The large scale features which can be seen and resolved with telescopes are dominated by the circular crater markings. These range in scale from diameters as small as can be resolved—about 1 km.—to the large circular surroundings of the so-called maria. There is no clear break in this entire sequence of sizes although there is of course a gradual change in some of the characteristics. It would therefore seem improbable that more than one mechanism should be invoked for the generation of the great majority of craters spanning this large interval of size. The explanation in terms of impact seems entirely satisfactory, and it is not intended here to review or discuss this interpretation which is widely believed.

The configurations of the craters allow conclusions to be drawn concerning the gradual changes that must be taking place on the lunar surface. If the impacts that formed the craters occurred distributed over a period of time during which other general changes occurred on the surface, then a difference in the appearance of old and young craters would be expected. If this general process was in the nature of an erosion, degrading the shapes and flattening the features, then old craters of a given diameter would be expected to be less high than new ones, and their features would be expected to be less steep. In cases of multiple overlapping craters there exists of course an independent criterion for judging the relative age. The younger crater is the one that has destroyed part of the wall of the older one. There are hundreds of examples of overlapping craters where in the region of overlap the wall of one is complete and where the sequence of the formation

is thus known with certainty. It is found in all those cases that if there is a difference in the appearance of the pair, then it is indeed the older one that looks the more degraded. For a given diameter it is the older one that has the smaller height and the less steep and sharp features. Groups of overlapping craters can be found where the order of occurrence of as many as five can be clearly recognized. In all those cases it is quite clear that the same rule applies, while the reverse is never found.

This observation therefore makes a strong case for the suggestion that some form of erosion has been active all over the lunar surface during the interval of time during which the process of crater formation has taken place. The degradation of some craters where the height of the rim, even in the not obviously damaged places, is 3 km. less than it would be in new craters of the same diameter. The erosion process must therefore have been capable in some cases of a removal of such amounts. Most of this removal cannot have been on very steep slopes; the erosion process must continue to function when the slopes have been degraded to a few degrees inclination.

The rate of erosion that would be required to account for this appearance would however not be very great. If we assumed a time scale of the order of 4 billion years for the lunar surface (corresponding to the terrestrial ages of surface rocks), a removal of 4 km. would after all only correspond to one micron per year. One is therefore interested in processes that could take place in the lunar surface conditions that can move material at this slow rate.

Transportation of finely divided material by the mechanism of repeated contraction and expansion in the large heating and cooling cycle is sometimes discussed. Quantitative estimates of such a process show it however to be quite inadequate even on the long lunar time scale.

Transportation by the repeated stirring of small scale explosive impacts of micrometeorites is a possibility. As the scale of the meteorite is decreased, so the transparency of the region affected to its own radiation becomes greater. A larger fraction of the incident energy is then emitted as radiation, and less is given in kinetic energy to the neighboring material. This makes it seem unlikely that for micrometeorites much material can be accelerated so as to leave the moon altogether (although it must be admitted that there is no good experimental or theoretical treatment to prove this point). In a period of time in which the horizontal movement of material by this process is significant, the addition of new material is even more significant. On this basis one could understand a degradation of shapes, but only if it were coupled with a general blanketing. From the coloration effects it is however quite clear that the moon is not covered by a general blanket of dust. A transportation mechanism must be at work which does not add more material than is transported, and which in any case works faster than the accumulation of meteoritic dust.

The coloration effects are very significant to the discussion of the nature of the erosion that must be taking place on the moon. As a

general rule, most of the high ground is rough and densely covered with craters, while most of the low ground is smooth with a much smaller number density of craters upon it. The low ground has a surface which is mostly level, or possesses very slight gradients only; it is mostly of darker color than the rough high ground. This is true not only for the large areas of low ground—the so-called maria—but it is also true for the smaller regions of low flat ground that appear within many craters in the highlands. The main departures from this rule concerning the coloration are the patterns of so-called rays that radiate out very prominently from a small number of craters situated both in the highlands and in the maria. Those particular craters are invariably classified as young, both on the criterion that no other craters overlap them, and on the criterion that they possess the steepest slopes and the sharpest features. The ray patterns are interpreted as material ejected in the explosion that formed the crater, just as occurs in bomb explosions on the earth. The ray deposits so caused are probably very thin only and in no case is there any elevation sufficient to cause a shadow associated with a ray. One does not wish to assume that a very small number of the more recent craters are intrinsically different from all the others, and it would therefore appear that ray patterns caused by each crater-forming impact disappear in an interval of time shorter than that in which any other discernible changes occur.

If the surface material had never been moved, then all would be covered over with a layer of meteoric dust. The rate at which meteoric dust deposits on the earth at the present time would assure that an optically opaque layer is formed in a time very short compared with the presumed age of the main lunar features. A time as short as one million years would probably suffice to make an opaque layer. It is true that such a covering would account for the disappearance of the rays; but then it would remove any reason for having a different color on the different types of terrain. The clear correlation between color and terrain would have no explanation.

It may well be that gases and vapors escape from the moon's interior, as they undoubtedly do from the earth. The moon can clearly not be substantially outgassed and internal seepage of bottled up gases must take place. Such seepage through dusty surface layers may well be responsible for changes in the surface chemistry and therefore in the color. While such an interpretation seems permissible for some patches of different color, it would seem too far fetched to suppose that such seepage is everywhere accurately related to the underlying terrain and has so accurately and consistently produced the observed difference in color between highlands and lowlands.

The situation is quite different if we are allowed to suppose that a surface migration of material has taken place. This may then not only have been responsible for reducing the heights of the older craters, but it would very naturally assure a consistent coloration difference between the ground which is getting denuded and the ground which is getting filled up. The average length of time for which the surface has been exposed is very brief on the ground which is being denuded.

There it is just the length of time that it takes to remove an optically opaque layer, a time which may be less than a year. The average length of time for which a surface particle has been exposed in the areas in which the sediment is being deposited is however very much longer, namely the average length of time that it takes for a particle to be transported from the high ground to the low. This may well be hundreds of thousands of years. Any coloration change which is induced in the material as a consequence of the surface irradiation would therefore show up in the deposit. It is indeed generally the case that silicates become darkened by being exposed to ionizing radiations and it would therefore be immediately clear that the deposited material would be expected to be the dark one.

The ray material would presumably also get darkened by irradiation. The time it takes for a ray to disappear may however depend also upon the much lower speed of the denudation process, even though the thickness of the ray material to be removed is less than that which would cast a visible shadow.

Material whose color has been darkened by absorbing ionizing radiation will generally return to the lighter color through being heated. It is therefore no surprise to find that fine powder flung out in an explosion and deposited to make the rays is of light color even if the original material was dark for fine dust would certainly have been subjected to intense heating in the impact explosion.

The conclusion that the meteoric deposition should have resulted in uniform material over the entire surface of the moon is thus avoided through the action of a transportation of surface material and the irradiation on the surface by ionizing photon and particle fluxes. This irradiation is likely to be a very major phenomenon on the surface of the moon in any case, for it is certainly very intense and would induce many chemical and crystallographic effects. It is a good approximation to say that the entire ionizing flux which keeps the ionosphere of the earth in its state of ionization is absorbed on the moon in a few microns depth. The physical and chemical nature of the material on the surface is certainly very dependent upon the radiation and high vacuum laboratory investigations with ionizing fluxes which will be required to demonstrate the processes that may be taking place.

Let us now continue the discussion of the mechanism that might be responsible for transporting material. If the material to be transported were in the form of large solid pieces then it would be hard to think of anything other than explosions to move it over slopes over which it would not tumble by itself. If however it were in the form of a fine powder, then a number of other agencies might be at work. Of the possibilities for moving a fine powder, electrostatic forces seem the most promising. On the small scale of powder particles, or indeed on any scale small compared with the Debye length, the space behaves like an insulator. Small particles are therefore very much subject to electrostatic forces. Any irradiation which is capable of knocking electrons out of dust particles may therefore leave them in a state of charge. If uneven charge distributions can be set up, then forces may

result that will move the particles on the surface. If two neighboring particles receive at one instant a sufficient charge of similar sign they may jump apart. The detailed uneveness in the surfaces of dust grains and the statistical fluctuations of an ionizing flux would indeed assure that an erratic pattern of charge distribution is set up all the time. Calculations show that the actual ionizing flux can produce electric fields capable of stirring up the surface layer of dust; but it is perhaps better to tackle a problem of this kind by experiment. A preliminary experiment set up by a graduate student at M.I.T., Mr. Harwit, has already succeeded in demonstrating that dust can be moved on the surface by bombardment with kilovolt electrons. Further experimentation is planned with bombarding conditions that correspond more accurately to those on the lunar surface. The present information makes clear already that transportation rates can be expected from this mechanism in lunar conditions which are ample for the requirement of denuding the high ground on the moon by one micron per year.

If the low ground is the deposit of dust removed from the higher ground, then it is necessary to suppose that the transportation mechanism will keep operating until the surface is very nearly accurately flat. The statistics of jumping particles must approximate the fluidization of the surface. If this is the case then there is no further need for supposing any other fluid to have been responsible for the flat surfaces. The idea which has often been discussed that gigantic lava flows have taken place on the moon and have filled up the low lying regions with flat lava beds is then unnecessary. We need to account for the whereabouts of the eroded material missing from the high ground and the only place where we might find it is the cover on the low ground. If it can be distributed flat over the low ground then there is no need for supposing that the low ground was flat in the first place.

The idea of gigantic lava flows on the moon of far greater magnitude than any that ever occurred on the earth is in any case a very disturbing one. The large deformations of the surface which in the case of the earth have always been associated with volcanic and intrusive activity are evidently entirely absent on the moon. The oldest discernible markings are much worn down but they are not at all distorted. Circles have evidently remained circles over the entire period during which the present surface has been shaped. On the earth with a scale of volcanic activity very much smaller than that which would be required for this explanation there are few areas in which a circle would not have been very greatly distorted in geological times. If large amounts of lava have come out from the interior of the moon, then the moon must have been very hot and a lot of internal adjustments would have taken place. A thin solid crust with a liquid layer below would have suffered from many instabilities whose consequences are not seen on the moon. The radar evidence showing that most of the surface is smooth even on a scale of 10 cm. speaks against the buckled and contorted surface that freezing lava usually produces. The thermal measurements indicate that the surface material cannot be solid lava but must be much more finely divided and the coloration of the low ground

could in any case not be attributed to lava because of the necessary blanketing with meteoric material. There seem therefore to be strong arguments for leaving out the lava hypothesis altogether if the dust flow can account for the configurations.

It is interesting perhaps to discuss what the nature of such deposited material would be and how this would affect the work of scientific investigation and exploration. Will the surface be very soft and treacherous like quicksand so that landing space vehicles will sink in? What will be the chemical properties of such irradiated material? Are there any substances that might be useful for the explorers when they get to the moon? How deep is the dust?

We don't know the answers yet, but it will not be very many years before these answers will be known to every school child in the United States. Dust in a vacuum has usually a strong tendency for the grains to stick to each other in the absence of a layer of adsorbed gas molecules. The material is probably not like quicksand therefore, which flows readily, but is more likely to be a light crunchy material which has a finite bearing strength that can be compressed to a small fraction to its previous volume, somewhat like snow perhaps. At a slight depth under the surface the grains would probably have got sufficiently well attached to each other so that a trench could have a vertical wall without collapsing.

Liquid water might exist in the ground at a not very great depth. It seems for example that the rate of diffusion through the dust would be so low that water at a depth of 100 meters would not have resulted in any noticeable water vapor concentrations above the lunar surface.

Let me speculate a little on the way in which this kind of material of the moon's surface might be useful in the explorations. For unmanned soft landings and instrumented roving vehicles, it will presumably be necessary to see to it that the landing does not dig the vehicle in too deeply and that the bearing pressures are kept sufficiently low. For manned explorations there are however many interesting possibilities. People flying around in space ships will all the time be very conscious of the radiation hazards that occur during intense solar flares. In all probability they will not be able to carry around with them a sufficient thickness of material to shield them against the most energetic of these events; but on the other hand these events are sufficiently rare for it to be reasonable to take a risk. The moment that the explorers land on the moon they would therefore be very anxious to find some way of digging in, of using lunar material to provide the shielding. The lunar dust would be extremely convenient from this point of view. It will be sufficiently compressible so that digging in does not involve excavating the material. Indeed if it is a really homogeneous crushable powder structure, then one could easily devise a vehicle that can bore its way through it: a lunar submarine so to speak. In this way the explorers could gain protection not only from the penetrating radiation but also from the unfavorable temperature conditions which they would have to face on the surface. If traces of water vapor or other gases can be found on the surface, then those substances may be found in a

much higher concentration in a well of not very great depth. Indeed water in liquid form is a possibility.

These are perhaps wild speculations now, but some of them may move into the realm of down to moon engineering only a few years from now.

12. THE ELECTRIC UNIVERSE

H. Bondi
King's College, London

The theory recently proposed by R. A. Lyttleton and myself[1] is based on three main considerations. The first one of these is purely local. All the so-called laws of nature are abstractions from physical observations, and all these experiments and observations have only a finite accuracy. Therefore their results are not established absolutely but only within certain limits of error. It is also known from many cases that an investigation of the possible small changes in a law of physics that are compatible with known observations may yield fruitful results. One such law is that the charges of the electron and proton are equal and opposite. Experiments show that the charges are very nearly equal and opposite, and it is a convenient assumption to suppose that they are exactly equal and opposite. It is, however, a fact that a small difference in the absolute value of these two charges would be entirely compatible, not only with direct experimental knowledge, but also with the whole structure of quantum theory. This would imply that the charge of the anti-proton, being necessarily equal and opposite to that of the proton, would be different from the charge of the electron, and similarly the neutron would have a small residual charge. Provided only that the difference between the charge of the electron and the opposite of the charge of the proton is reasonably small, no conflict with observation will arise. It is therefore a task for theoreticians to investigate what observable consequences, if any, would flow from the assumption that the charges of the electron and proton are not exactly equal and opposite. It is clear that the residual charge implied by this hypothesis has the same sign for every atom. Accordingly, a small but additive force arises and it is likely that its most significant results will lie in the sphere of observations of very large-scale phenomena.

The second consideration arises on this large scale and concerns a well-known puzzle. In problems of astronomy extending in size from the solar system through the galaxy to clusters of galaxies, gravitation appears to be the dominating force, leading to central motion and inward accelerations. However, in the entire universe of galaxies, instead of an inward motion an outward motion is observed with no evidence of inward acceleration. Moreover, if it were supposed that gravitation was still the dominating force and that the inward acceleration had simply escaped observation owing to its smallness, it would be necessary to postulate a singular and violent explosion in the not too

distant past to account for the rapid outward motion now seen. If on the other hand, it is considered more probable that the outward motion results from a permanent outward force, then the problem arises, that up to the scale of clusters of galaxies inward force (gravitation) predominates whereas over the very large distances it is an outward force that dominates.

Our third consideration is wholly cosmological. It is well known that a number of theories are current concerning the overall structure of the universe. The simplest of these seems to be, at least to the writer of this article, the steady state theory. According to this theory the universe is in a steady state in spite of the outward motion of the galaxies because its density is maintained by a universal continual creation of matter. This also serves to keep the average age down by constantly injecting new material into the system of galaxies which individually evolve and grow old. The only geometrical model of such a stationary universe is that given by de Sitter in 1917. The de Sitter universe is in any case one of the best known and simplest of all the possible model universes that arise from the assumption of uniformity which is accepted, on strong observational evidence, by all cosmological theories. Given any geometrical model of the universe, the field equations of the general theory of relativity may be applied to this geometrical structure in order to ascertain its material content. Owing to the uniformity of any such model, the resulting density is bound to be uniform in space and the resulting pressure isotropic and uniform in space. If the field equations of general relativity in their usual form are applied to the de Sitter model of the universe, a positive density of reasonable magnitude results together with a pressure equal to the density in magnitude, but of negative sign, i.e. a universal tension. Owing to the stationary character of the model, both the density and the tension are constant in time. This situation is not difficult to understand mathematically. The field equations of relativity imply a law of conservation of matter and energy. The expansion implicit in the de Sitter model leads to a constant outward motion of matter. However, the stationary character requires a constant density and thus a continual creation is required. By virtue of the conservation laws this can only occur if the requisite amount of work is done by the universe in its expansion. This will be the case, provided there is a universal tension in space of the correct magnitude, and this is therefore what the equations give. When de Sitter first proposed this model, the idea of a negative density was wholly unpalatable. Instead of applying the equations of general relativity in their ordinary form, he applied the equations including the so-called cosmological term added by Einstein as an afterthought and not much later vigorously rejected by him though still retained by many cosmologists. When this term, which contains the arbitrary so-called cosmological constant, is added then an amount given by the cosmological constant is subtracted from the density and added to the pressure. If then the condition is made that neither the pressure nor the density should be negative, the cosmological constant must be chosen such as to reduce both density and pres-

sure to zero, making the de Sitter model an entirely empty one. This emptiness caused a certain amount of difficulty for it cannot easily be understood in what sense an empty universe can be said to be expanding. For a long time it was supposed that the de Sitter universe was an idealization of our actual universe which was supposed to be nearly, though not quite, empty, and tending towards complete emptiness as the expansion progressed. Indeed, the most favored of the relativistic models, that due to Lemaitre, tends asymptotically to the de Sitter model.

Although the steady state theory immediately gave geometrical significance to the de Sitter model, its relativistic implications were not understood until McCrea[2] proposed in 1951 that the field equations of general relativity should be used without the cosmological term, and that the tension so inferred should be understood as a zero-point property of the vacuum, like all the other properties of the vacuum that occur naturally in quantum theory. While this alteration of the interpretation of the terms involved reconciled general relativity with the steady state theory, it had very much the nature of an *ad-hoc* change, since no other consequences of the assumption of the fixed tension of the vacuum could be found.

With these considerations in mind, we began to investigate the consequences of a general excess of charge, that is of a difference between minus the charge of the electron and the charge of the proton. With such a difference there would be a residual charge both in a neutron and in the hydrogen atom, and indeed there would be a residual charge in every body of matter containing only unionized atoms. Any such body of matter would therefore be charged. Since this charge would have the same sign for all such bodies, there would be a repulsion between bodies. Moreover, the charge being proportional to the number of protons and neutrons, this charge would be proportional to the mass of the bodies, and therefore a repulsive force would arise of precisely the same character as gravitation but of the opposite sign. It turns out that owing to the weakness of gravitation, a minute difference between the charges of the electron and the proton (barely one part in 10^{18}) would be sufficient for this electrostatic repulsion to counterbalance gravitation completely. Thus the question arises why gravitation is observed when there appears to be a force counteracting it. It is immediately seen that in any large body composed of residually charged atoms there will be a strong electrostatic outward force trying to remove the excess charge. If therefore, the body is conducting then the excess charge will be removed and will go to the surface. If then a number of such bodies are embedded in a conducting medium, then the bodies will lose their charge since in a conducting medium there can be no electric field. Thus within such a conducting region the ordinary force of gravitation will apply fully. Between any two such conducting regions separated by a non-conducting region there would however be a repulsion provided only that the charge difference between electron and proton exceeded the very low limit given before. Very roughly speaking, this situation appears to represent our uni-

verse correctly if the size of the conducting regions is supposed to be that of clusters of galaxies. If these regions (units as we shall call them) are separated by a non-conducting intergalactic space then our problem of reconciling the local predominance of gravitation with its apparent inversion on the cosmic scale would appear to be resolved naturally.

This type of interpretation is rather too local in character to account in every detail for the cosmological situation. As has been pointed out before, the most crucial property of our universe is its uniformity and isotropy. It is clear that an actual electric force pulling along a galaxy could be observed locally and would thus lead to a deviation from the isotropy which forms part of the most important and fertile postulate of cosmology. Moreover, if we accept the steady state theory, the continual creation of matter demanded by this theory would imply a continual creation of charge. This is clearly incompatible with Maxwell's equations which demand the absolute conservation of charge. In other words, the theory of charge inequality cannot be reconciled with the steady state theory unless Maxwell's equations are modified. The only plausible way of carrying out such a modification is that due to Proca, in which multiples of the four-potential are added to the usual form of the equations. We thus have

$$F_{\mu\nu} = K_{\mu,\nu} - K_{\nu,\mu}$$

$$F^{\nu}_{\mu;\nu} = 4\pi J_{\mu} - \lambda K_{\mu}$$

where a comma denotes ordinary differentiation and a semicolon covariant differentiation, K_{μ} is the 4-potential, $F_{\mu\nu}$ the electromagnetic field, J_{μ} the charge current vector, and λ a universal constant. In this set of equations, there is no automatic law of conservation of charge as can be seen by taking the divergence

$$F^{\mu\nu}{}_{;\mu\nu} = 0 = 4\pi J^{\mu}{}_{;\mu} - \lambda K^{\mu}{}_{;\mu}$$

Thus a continual creation condition

$$4\pi J^{\mu}{}_{;\mu} = \lambda K^{\mu}{}_{;\mu} = 9 = \text{constant}$$

would be the natural generalization of the Lorentz condition. An energy stress tensor may be constructed in the usual way from these modified Maxwell equations allowing for the fact of electromagnetic energy creation due to creation of charge at the potential at which the charge is placed. Otherwise the stress tensor must account through its divergence in the usual way for the work done by the electromagnetic field. It is readily seen that the only possible energy-stress tensor is

$$4\pi E_{\mu\nu} = -F_{\mu\alpha} F^{\alpha}_{\nu} + \tfrac{1}{4} g_{\mu\nu} F_{\alpha\beta} F^{\alpha\beta} + \lambda [K_{\mu} K_{\nu} - \tfrac{1}{2} g_{\mu\nu} K^{\alpha} K_{\alpha}]$$

Consider now the significance of these equations in a smooth de Sitter universe, given in the usual notation by its metric

$$ds^2 = dt^2 - \exp(2t/\tau)\,(dx^2 + dy^2 + dz^2)$$

where units have been chosen such that the velocity of light equals unity. In these coordinates the system is completely uniform in space and time and isotropic. Accordingly, only the time component of the four-potential can be different from zero. In these circumstances the electric field vanishes and the energy-stress tensor is as follows[3]

$$-E_0^0 = E_1^1 = E_2^2 = E_3^3 = -\frac{\lambda}{8\pi} K_0^2$$

while

$$4\pi J_0 = \lambda K_0$$

with all other components vanishing. With a negative value of λ a universal tension therefore results together with a negative universal density of energy. This universal tension is, as has been said, precisely of the type required to keep the de Sitter model uniform. It is owing to this tension that the universe is producing enough energy by its expansion to create matter at the rate required to keep its density.

Our universe contains matter in addition to electromagnetic fields. The total energy momentum tensor $T^{\mu\nu}$ therefore consists of a material part $M^{\mu\nu}$ and an electromagnetic part $E^{\mu\nu}$ which we found above, so that

$$T^{\mu\nu} = M^{\mu\nu} + E^{\mu\nu}$$

Only the total energy momentum tensor $T^{\mu\nu}$ is strictly conserved. Substituting the de Sitter metric given above into the field equations of general relativity one finds that $T^{\mu\nu}$ is diagonal and that

$$T_0^0 = T_1^1 = T_2^2 = T_3^3 = \frac{3}{8\pi G\tau^2}$$

where G is the constant of gravitation. The tension implied by the space components is now equated with that due to the electromagnetic part of the tensor. It then follows satisfactorily that the material part of the tensor has only a time component and so is due entirely to a uniform distribution of matter at rest in our coordinates. The density of the matter is of an order of magnitude in agreement with astronomical observations. Thus an investigation of the exactness of the charge equality has led directly to an account not only of the limiting size of features in which gravitation predominates, but also to a clear description of the main features of the de Sitter model of cosmology and with it of the steady state theory.

The constant multiplying the new terms in Maxwell's equations is of dimension $(\text{length})^{-2}$ and it is therefore clear that if this length is of cosmic dimension, then on any significantly smaller scale the usual consequences of Maxwell's equations will apply. In particular it will be clear that within the unit of conducting material surrounded by non-conducting material all the ordinary conditions of electrodynamics will apply, making the interior of the unit effectively free of any electromagnetic fields. The potential of any such unit as a whole turns out to be strongly dependent on the radius of the unit and of order 10^{21} v.

Since the units differ appreciably from each other in size, one would expect substantial potential differences between different units. Therefore charged particles escaping from one unit sufficiently fast to have negligible cross section in intergalactic space might be expected to enter another unit with an energy of the order of 10^{20} ev. It may not be entirely fanciful to suggest that the most energetic component of cosmic rays is of this origin.

REFERENCES

[1] R. A. Lyttleton and H. Bondi. Proc. Roy. Soc. A **252**, 313 (1959)
[2] W. H. McCrea. Proc. Roy. Soc. A. **206**, 562 (1951)
[3] An error of sign in this formula in reference 1 has recently been pointed out by F. Hoyle.

Section III. The Instrumentation

13. ASTROSTATS FOR ASTROPHYSICAL RESEARCH IN SPACE

Russell A. Nidey
*Kitt Peak National Observatory**

INTRODUCTION

To widen the observable spectral range of the electromagnetic radiation from the celestial targets, and to obviate the washing out of the seeing, it is expedient to loft the instruments of astrophysical research into space above the absorbing and turbulent atmosphere of the earth. Since the researcher cannot survive the rigors of the space environment to manually aim his instrument at the celestial target, he must delegate this responsibility to an automatic device. This device is the *astrostat.*

The word *astrostat* has been compounded from the Greek-derived combining forms, *astro* meaning of or pertaining to the stars, and *stat* meaning a device to maintain something stationary. It is intended as a generic word; hence, any device that stabilizes an instrument relative to a celestial target can be logically termed an astrostat. More specifically, however, astrostat should connote an automatic device that senses the celestial target and invokes a motive element to modify the orientation of the instrument to correct the alignment error.

Several astrostats have been utilized to date, ranging from the early V-2-borne Sun-Follower[1] to the more recent Russian Automatic Interplanetary Station.[2] The chief of the rocket-borne astrostats has, however, been the University of Colorado's Solar Pointing Control.[3] To more clearly define astrostat, the latter device will first be described in some detail. The design criteria of the astrostat in space will then be generalized. After discussing the general ramifications pertaining to the target sensors, gimbals and motive elements, other astrostats, including the Russian AIS, the Satellite-borne Solar Pointing Control, and the Kitt Peak National Observatory's proposed astroguider will be used to illustrate specific points and refinements.

Of the several astrostats only the Aerobee-borne Solar Pointing Control, as shown in Figs. 1 and 2, has been used in sufficient quantity to establish reliability and performance standards.

---

*Operated by the Association of Universities for Research in Astronomy, Inc., under contract with the National Science Foundation.

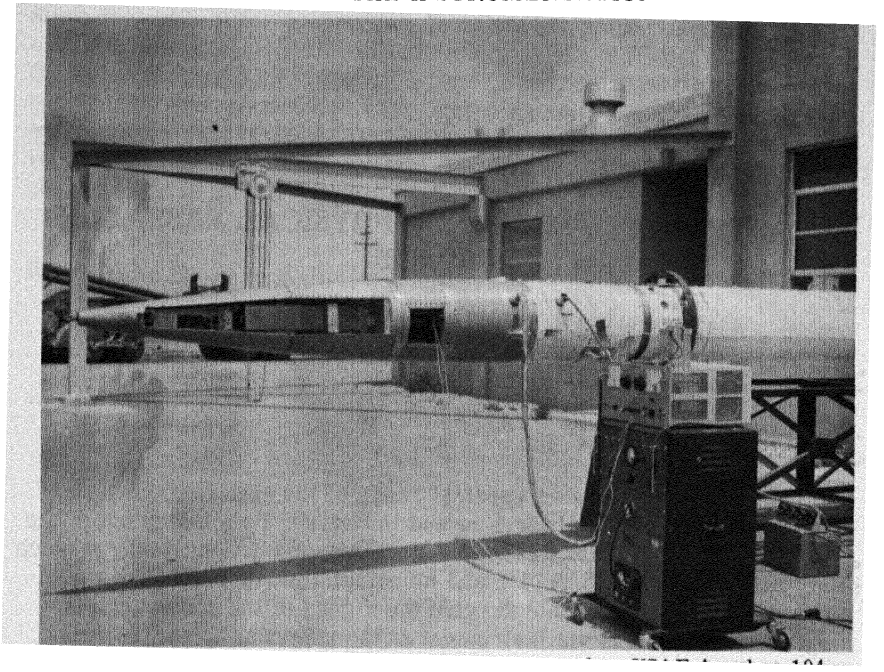


Fig. 1. Solar pointing control (BPC XXIV) mounted on USAF Aerobee 104 during preflight checkout. [Official USAF Photo]

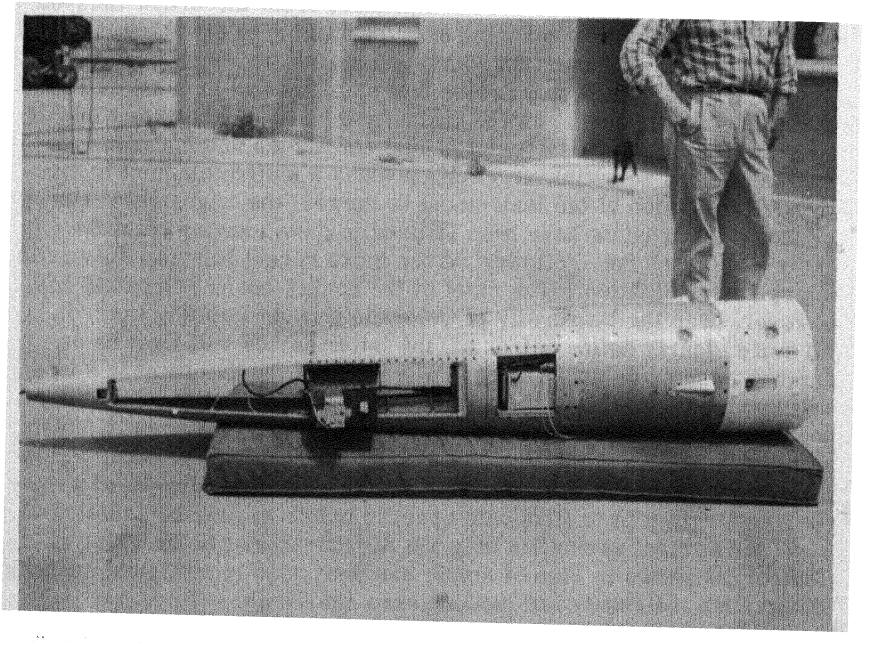


Fig. 2. BPC XXIV with AFCRC's (Jursa) spectrograph. Note eyeblock on forward end of instrument. [Official USAF Photo]

THE SOLAR POINTING CONTROL

As of mid-February 1960, 34 missions of the Aerobee-borne Biaxial Pointing Control had been logged. Of these, 23 witnessed successful operation of the Pointing Control; 5, failure; 5, compromise by vehicle malfunction; and 1, unknown. The utilization of these Pointing Controls to date by agency and investigator served is given in Table I.

TABLE I
Utilization of Solar Pointing Controls

Pointing Control	Mission Date	Agency	Investigator
BPC I	4-12-51	University of Colorado	Pietenpol
IV	12-12-52	" " "	Rense
VI	10-7-53	" " "	Rense
VIII	6-2-54	" " "	Rense
XII	9-30-55	" " "	Rense
XIII	12-3-55	" " "	Rense
XIV	5-8-56	" " "	Rense
XVIII	8-6-57	" " "	Rense
XXI	6-4-58	" " "	Rense
XXIII	3-13-59	" " "	Rense
XXV	6-2-59	" " "	Stuart
II*	6-28-51	" " " and University of Rhode Island	Pietenpol / Quirk
III	5-1-52	" " " "	Quirk
V	7-14-53	" " " "	Quirk
IX	9-17-54	" " " "	Quirk
VII	2-2-54	Naval Research Laboratory	Tousey
X	2-21-55	" " "	Tousey
XV	6-4-56	" " "	Tousey
XVII	5-3-57	" " "	Tousey
XX	5-5-58	" " "	Tousey
XXII	3-13-59	" " "	Tousey
XXVI	7-21-59	" " "	Tousey
XI	3-29-55	A. F. Cambridge Research Center	Jursa
XVI	8-3-56	" " " " "	Jursa
XIX	3-18-58	" " " " "	Jursa
SPC 101†	3-21-58	" " " " "	Hinteregger
102	8-15-58	" " " " "	Hinteregger
103	2-27-59	" " " " "	Hinteregger
104	3-12-59	" " " " "	Hinteregger
BPC XXIV	5-5-59	" " " " "	Jursa
SPC 201‡	9-15-59	" " " " "	Miczaika
105	1-19-60	" " " " "	Hinteregger
106	1-29-60	" " " " "	Hinteregger
BPC XXVII	2-12-60	" " " " "	Jursa

* V-2 vehicle; all others Aerobee vehicle.
† SPC's constructed by the Ball Brothers Research Corporation; all others by the University of Colorado.
‡ Bent-ogive version.

Many of the instruments accommodated by the Pointing Control have been spectrometers recording the vacuum ultraviolet solar spectrum; though solar insolometers and spectroheliographs have also been flown. Perhaps the more noteworthy of the flights were BPC IV, BPC X, BPC XXII, and BPC XXVI, during which the solar Lyman-α line was first photographed,[4] the solar Lyman-β line was first recorded,[5] an excellent Lyman-α spectroheliograph was obtained,[6] and a high-resolution Lyman-α line profile was recorded,[7] respectively.

The accuracy of pointing has been refined markedly from the original one-quarter degree in each of the two degrees of freedom to the order of one minute of arc. At the same time reliability has been tremendously enhanced such that since BPC IX only one unit, namely BPC XX, has failed to function satisfactorily.

Of more immediate concern during each mission is whether the vehicle performance will be compatible with the operation of the two-axis astrostat. Because of the gimbal restraints implied in a two-axis gimbal system the gyrations executed by the airframe are of basic significance to the achievement of the experimental objective.

The Aerobee sounding rocket is a fixed fin vehicle which is relatively long and thin.[8] Inasmuch as the longitudinal principal moment of inertia is quite small in comparison with the transverse principal moment of inertia, moderate cross-spin (rotation about a transverse axis, or tumble) results in a gross precession of the axis of symmetry during the free-fall trajectory. The angular motion over apogee may be characterized as 30° half amplitude precession with a 200-second period in conjunction with spin about the longitudinal axis of the order of 1/2 revolution per second. Hence, both servoloops of the Pointing Control must be reasonably fast to counter the vehicle motion.

Since the spin is the more rapid of the two motions, the axis of the outer of the two gimbals is parallel to the longitudinal axis of the rocket; whereas, the axis of the inner gimbal is normal to the outer, hence, transverse to the airframe axis.

In addition to discriminating against the vehicle spin, this configuration also achieves the more expeditious coverage of the sky. However, as is true of all two axis gimbal systems, the Pointing Control is subject to gimbal lock if the solar target approaches the tip or tailward direction. Hence, each round must be scheduled in early morning or late afternoon to ameliorate the probability of gimbal lock during flight.

The solar target is initially sensed by two pairs of coarse "eyes" which are photoelectric detectors with extremely wide, nearly cosine, fields of view.[9] These serve as aspect eyes to acquire the target after exit of the vehicle from the atmosphere and deployment of the protective airfoil. After the coarse eyes have served to reduce the pointing error to the order of a few degrees, the sun is then within the field of view of the fine eyes.[10] The fine eyes are miniature photoelectric telescopes incorporating a reticle and objective lens to produce a high gain solar position transducer. The coarse and fine eyes are shown in Fig. 3, whereas, the internal construction and angular characteristics are shown in Figs. 4 and 5, respectively.

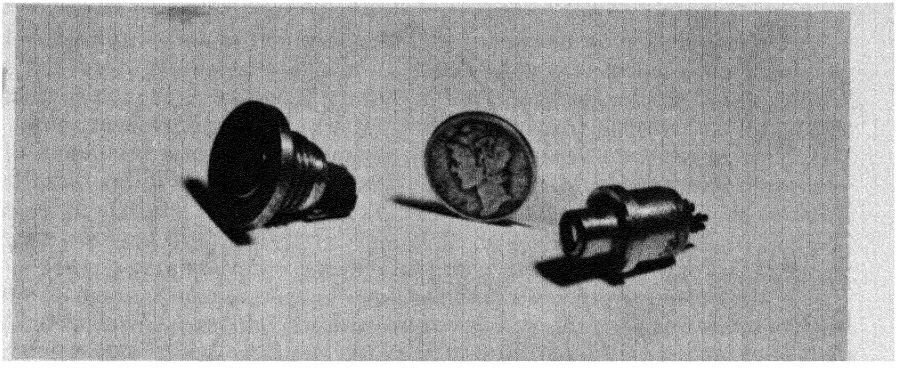


Fig. 3. Coarse (left) and fine eyes used to photoelectrically sense the position of the sun. Two of each required for each of the two control axes.

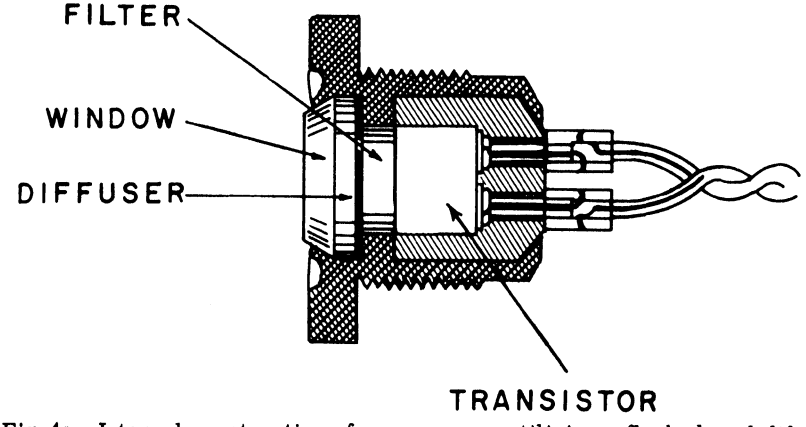


Fig. 4a. Internal construction of a coarse eye utilizing a flashed opal diffuser.

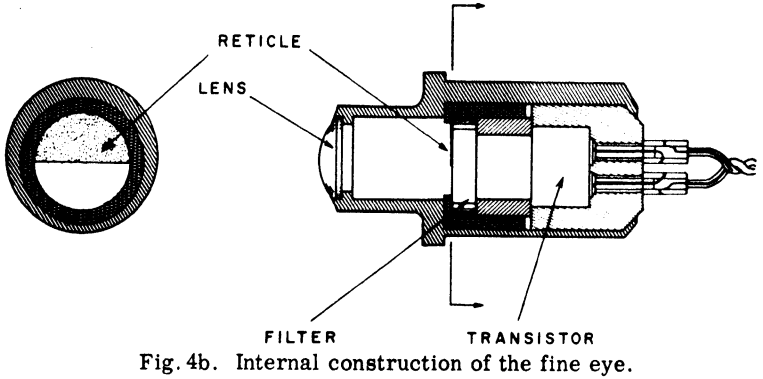


Fig. 4b. Internal construction of the fine eye.

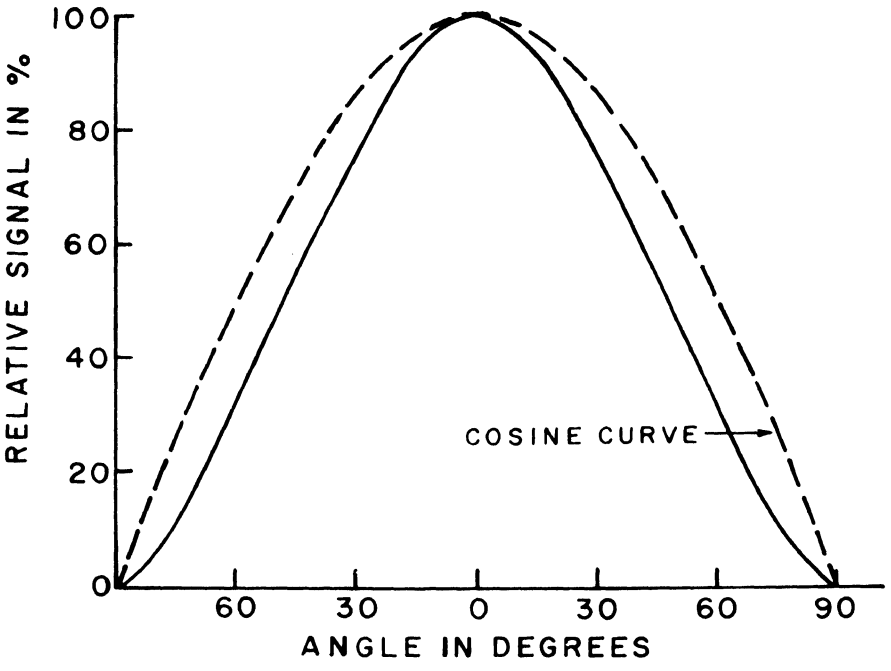


Fig. 5a. Angular characteristic of the coarse eye.

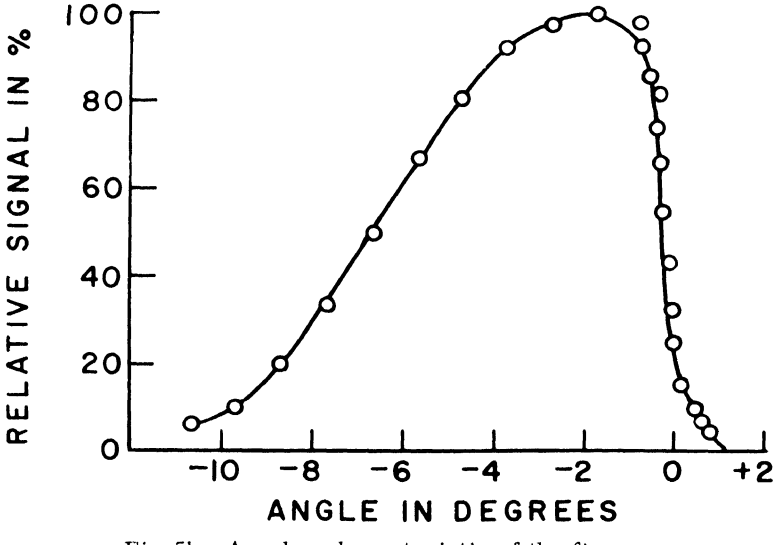


Fig. 5b. Angular characteristic of the fine eye.

The fine eyes, an opposed pair for each of the two control axes, are mounted parallel to the optical axis of the instrument on the inner, transverse gimbal, as are the transverse coarse eyes. The longitudinal coarse eyes are mounted on the periphery of the outer gimbal.

Because of differential drift in the individual photocells, the absolute position accuracy is limited to the order of a minute of arc. The short term accuracy is similarly limited by the mechanical system, even though the photoelectric transducers inherently have extremely high position resolution.

To accommodate the continual spin of the vehicle, the longitudinal drive system uses a pair of contradriven electromagnetic fluid clutches; whereas, the transverse drive has heretofore represented a more conventional position servo with a spring-biased high ratio spur gear train with a field control servo-motor. More recently clutches have been incorporated in the transverse drive by the University group, and a torque motor, by the Ball group.

Since the target is inertial, more nearly optimum pointing is achieved by using a form of error rate compensation to stabilize the servo-loops. Passive RC networks approximate derivative as well as integral control.

An all DC system is used to effect the epitome of simplicity to enhance the overall reliability. Ruggedized vacuum tubes are as yet used in the amplifiers, though solid state devices are beginning to be incorporated.

Several variations of the Pointing Control are now being developed such as the unconventional bent-ogive version shown in Fig. 6. By bending the forward portion of the nose cone orthogonal to the vehicle axis after atmospheric exit, the transverse degree of freedom can be achieved by a simple turntable. This configuration provides much increased instrument space among other significant advantages. The advantages are not, however, without compromise. In particular, the optical axis must be normal to the transverse axis, hence, along the short dimension of the nose cone. Secondly, the asymmetrical mass distribution of the gimbal system introduces rather severe gimbal forcing functions if the precessional motion of the airframe is inordinate. Contrary to one's first reaction, no increased sky coverage or reduction of gimbal lock is afforded.

The Stratoscope I astrostat, shown in Fig. 7 (this device was used by Princeton University astronomers to obtain the high resolution photographs of the solar granulation from an altitude of 80,000 feet[11]), was a direct reinterpretation by the author and associates at the University of Colorado of the Aerobee-borne Pointing Control to the balloon environment.

Electromagnetic clutch drives were used in both the azimuth and elevation gimbals to achieve decoupling of the gondola motion from the telescope. The batteries were deployed in a reaction wheel intermediate between the azimuth (outer) gimbal and the multipoint suspension to the balloon. The multipoint suspension permitted rejection of undue angular momentum from the wheel to the balloon. Windup of the sus-

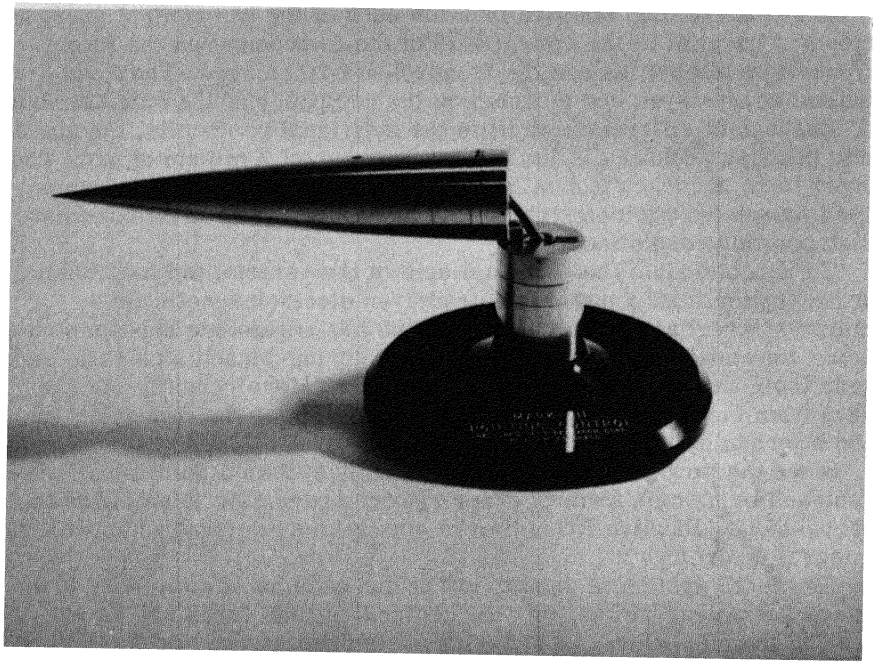


Fig. 6. Model of the bent-ogive version of the solar pointing control. Nose cone is bent to orthogonal position after exit from the atmosphere.

pension was prevented by a special non-viscous torque limiter set comfortably below the windup limit of the soft multipoint suspension. A soft suspension was militated by appropriate separation of the torsional pendulum frequency from the critical azimuth servo response band.

Though the DC accuracy was limited by the use of the rocket form of fine eyes to the order of a minute of arc, the short term accuracy achieved during the test round in August of 1957 was of the order of 6 seconds of arc in each of the two degrees of freedom.

The three-axis balloon-borne system now under development by the Perkin-Elmer Corporation for Princeton's 1961, 36-inch, Stratoscope II program should achieve one second of arc accuracy by eliminating the deleterious cross-spin forcing of the azimuth gimbal.

ASTROSTAT DESIGN CONSIDERATIONS

Whether explicit or implicit gimbals are to be used depends on the mission to be executed. Explicit gimbals are militated in the balloon environment, but may be foregone in the free fall state of the vertical probe or satellite mission.

If the mass of the instrument to be pointed is small as compared to the vehicle mass, explicit gimbals are advantageous since electrically



Fig. 7. Stratoscope I Astrostat under preparation for maiden flight on a Skyhook Balloon early 8-23-57. [Official U.S. Navy Photo]

generated torque can be utilized in the motive element; whereas, elimination of the friction noise in the gimbal bearings by the use of implicit gimbals potentially offers enhanced accuracy of pointing.

However, until the specific impulse and adaptability to proportional control of the gas jets are tremendously improved, jets will not be appropriate as the motive element in conjunction with the implicit gimbal for either the long duration or the precise mission. Ion jets now under development offer promise on both key factors but will not

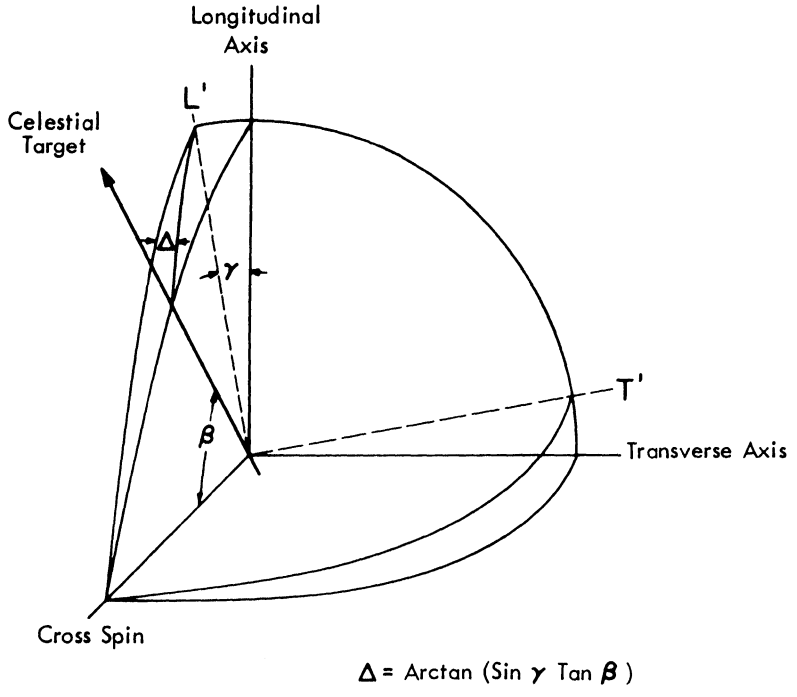


Fig. 8. Forcing of the longitudinal control loop induced by cross-spin motion of a two-gimbal astrostat.

be adequately refined for some time. Hence, reaction wheels will undoubtedly be used as the motive element on the earlier high precision satellite-borne astrostats.

The noise in the reaction wheel bearings will in this instance remain as the major residual high-frequency perturbation on the pointing accuracy. Specific provision must, however, be made to externally dump the accumulated angular momentum in the wheels and to circumvent the cross-coupling due to precessional effects.

Whether two or three gimbals are to be used in the astrostat is also militated by the mission. Only two axes are required to point an instrument at a target. The third axis may, however, be expedient to obviate cross-spin forcing, to accommodate offset guiding, or to ameliorate gimbal lock.

Cross-spin forcing is illustrated in Fig. 8. If the target is not normal to the outer or longitudinal axis of the two-axis gimbal, motion of the vehicle about the cross-spin axis necessitates corrective motion about the longitudinal axis. This corrective motion not only consumes power (which may or may not be a major disadvantage in the specific mission), but also requires an appropriate error signal to produce the driving torque.

In many instances it is advantageous to use offset guiding during

which the radiant used to produce the guiding signals may not be coincident with the target to be observed by the primary telescope. This is particularly true when observing nebulosities or extended sources. In this event the third axis control must be invoked to obviate the offset guiding error. The signal for the third axis must be derived from a second radiant or from an inertial element. Not only should the control axes be maintained nearly orthogonal to optimize the offset guidance performance, but likewise the error detectors. Hence, offset guiding poses special boundary conditions on the number as well as order and configuration of the gimbals and error transducers.

It is much less difficult to ameliorate gimbal lock. A simple redundant gimbal in general suffices. The error signal may in this event be readily derived from transducers attached to the two basic pointing gimbals.

In addition to the cross-spin forcing, explicit gimbals introduce three other deleterious perturbations. The gimbal bearing noise has already been mentioned. Inertial and viscous coupling within the motive element and gear train assembly constitute the remaining conspirants.

Disadvantageous inertial coupling between the gimbals is produced if the rotor of the motive element is geared to the gimbal shaft. Motion of the vehicle then requires acceleration of the rotor even though the instrument remains inertial. Since the reflected rotor inertia is proportional to the square of the gear ratio, this ratio should be minimized to achieve optimum decoupling. This criterion is in direct contradiction to that usually applied; that is, for maximum power transfer. However, significant motive power may be required to acquire the target or to counter the gimbal forcing function; hence a compromise must in general be made.

Back emf in the rotor or friction in the motor and the gear train produces viscous coupling between the vehicle and the instrument. This, too, can be ameliorated by minimizing the gear ratio and, in addition, by judicious choice of motor characteristics or by appropriate tachometer feedback.

Thus, it is apparent that the usual motive element ramifications must be reinterpreted in the astrostat application. The ease of excitation of the AC servo-motor and excellent frequency response may perforce be foregone, as a case in point, in the light of backlash problems compounded by the inertial and viscous coupling difficulties.

In this respect the DC torque motor is quite attractive since the rotor can be coupled directly to the gimbal axis. Multiwatt transistor amplifiers are now practical to produce the high current rotor excitation required. The brush friction noise and the related life limitation are the chief disadvantages.

The dual over-running contra-rotating clutches combine power gain, relative freedom from backlash, viscous and inertial coupling, but are wasteful of power and in general deliver an inferior frequency response.

The signal to drive the motive element, be it the motors of the ex-

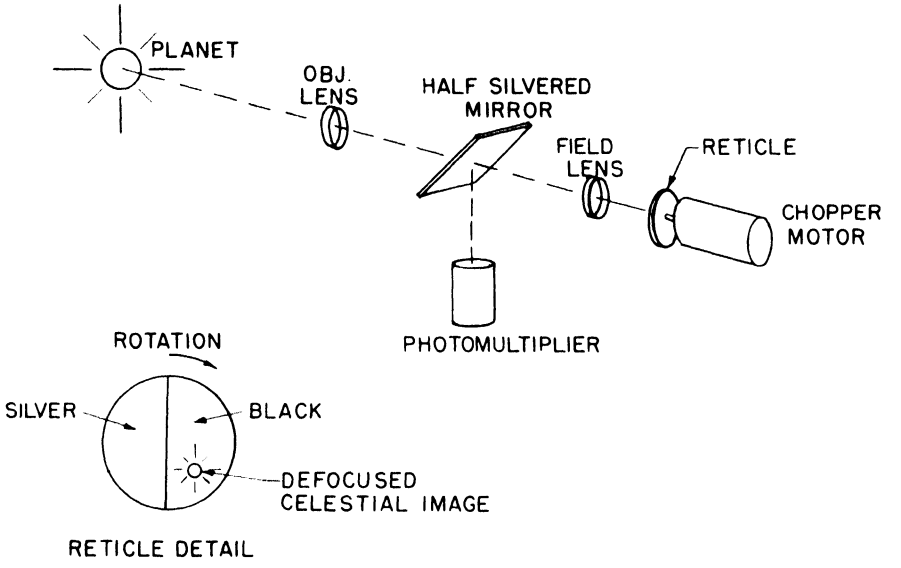


Fig. 9. A photoelectric guide telescope utilizing a rotating image position analyzer.

plicit gimbal system or the jets or reaction wheels of the implicit gimbal system are derived by the photoelectric guide telescope.

Many forms of guide telescopes have been devised. All incorporate four basic elements: The objective element, image position analyzer, field element and photodetector, singly or in combination.

The objective element collects the incident radiation and forms an image of the target on the analyzer. The analyzer determines the magnitude and sense of the image position error by appropriate channeling of the radiation through the field element to the photodetector; whereas, the field element defines the field of view of the telescope and ideally images the objective aperture entirely within the sensitive area of the photodetector.

Figure 9 depicts a guide telescope incorporating all the basic elements. If the target image encompasses a segment of the rotating knife-edge, synchronous demodulation of the photoelectric signal derives two quadrature proportional sinusoidal error signals. This form of automatic guide telescope was first used by Babcock[12] at Mount Wilson and has since been used in various forms in many different devices.

Alternatively, the analyzer could be a four-sided prism splitting the convergent beam from the objective element into four bundles of light incident on four photocells to derive DC signals;[13] or four objective elements could be combined with four knife-edges and four photocells in an array as in the Solar Pointing Controls.

The chief disadvantages of the rotating analyzer are the power re-

quired to drive the knife-edge, the mechanical noise associated with the bearings, and the equivalent target motion induced by bearing run-out. The advantage is freedom from accumulative time dependent errors due to differential phototube drifts and dark currents.

The reliability of the active analyzer must be weighed against the additional three phototubes required in either of the passive DC versions.

More complex analyzers or elaborate photodetectors such as spoked reticles and mosaics can be used to enhance subordinate characteristics [14,15,16]

Because of the limited field of view of the guide telescope, an auxiliary aspect signal must be derived to facilitate initial target acquisition. Solar aspect eyes such as used on the Solar Pointing Controls can be used to determine two of the three degrees of freedom to find the celestial targets other than the sun. Scanning about the third axis or determination of local vertical by photoelectric horizon scanners can then be invoked. Storage of angular information in an inertial element is also possible for vertical probes, but less so for the satellite mission. In addition, ground command can be incorporated to facilitate initial acquisition.

The easiest of these to automate is, of course, solar acquisition since the sun is the strongest source of radiation in the celestial sphere. This technique was used on the October 1959 Automatic Interplanetary Station.

THE AUTOMATIC INTERPLANETARY STATION

Little has been published concerning the astrostat used by the Russian scientists to photograph the far side of the moon. Blagonravov[17] cites the use of compressed air jets, eight in number, to point the cameras opposite the sun as dictated by solar eyes. A lunar detector then assumed control to reduce the initial 13° misalignment.

As depicted in Fig. 10, the solar eyes were apparently similar to those used on the Solar Pointing Control, though shadow-casting ridges on the forward set ostensibly served to introduce a region of high gain near zero solar error to obviate error due to differential drift and stray light.

Two pairs of longitudinal jets were used to control motion about the longitudinal axis apparently commanded by a rate gyro, whereas, the solar and lunar signals in turn commanded the two pairs of orthogonal transverse jets.

The accuracy attained was probably the order of a fraction of a degree. Thus, this astrostat is notable, not so much for the excellence of performance, but rather because it was the first astrostat, not only to go far beyond the terrestrial environment, but to successfully seek and acquire a target other than the sun.

Other astrostats will make use of implicit gimbals and cold gas jets. The Satellite-borne Solar Pointing Control, in particular, invokes jet control to obviate gimbal lock.

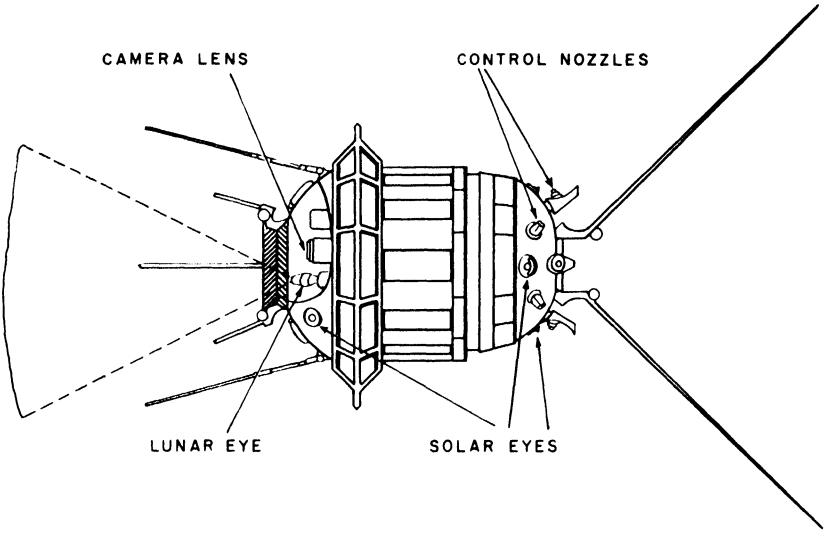


Fig. 10. The automatic interplanetary station, Russian Lunik III. [After Blagonravov]

THE SATELLITE-BORNE SOLAR POINTING CONTROL

This astrostat is best envisioned as two-axis explicit gimbal device with a third redundant implicit gimbal. As shown in Fig. 11, the explicit gimbals are similar to those of the conventional Aerobee-borne device. Torque motors are, however, to be used to drive both the longitudinal and transverse gimbals relative to the spinning base. A pair of jets is to be fixed to the longitudinal gimbal parallel to the transverse axis. Thus, a torque normal to both the longitudinal and transverse axes is produced, resulting in controlled precession of the satellite axis about an axis parallel to the transverse axis as shown in Fig. 12.

The satellite is to be injected into a 300-mile,35° orbit with the longitudinal axis normal to the solar vector. Subsequent automatic operation of the cold gas jet control will thereafter maintain orthogonality for an expected lifetime of six months.

Accuracy of pointing during sunlit passage is to be of the order of a minute of arc in each of the two degrees of freedom. The instrument to be accommodated will probably be somewhat larger than that by the conventional Aerobee-borne device. The coarse and fine eyes of the latter device will be but slightly modified for the satellite environment.

The Satellite-borne Solar Pointing Control is being developed by the Ball Brothers Research Corporation and should be flown in late 1960 or early 1961.

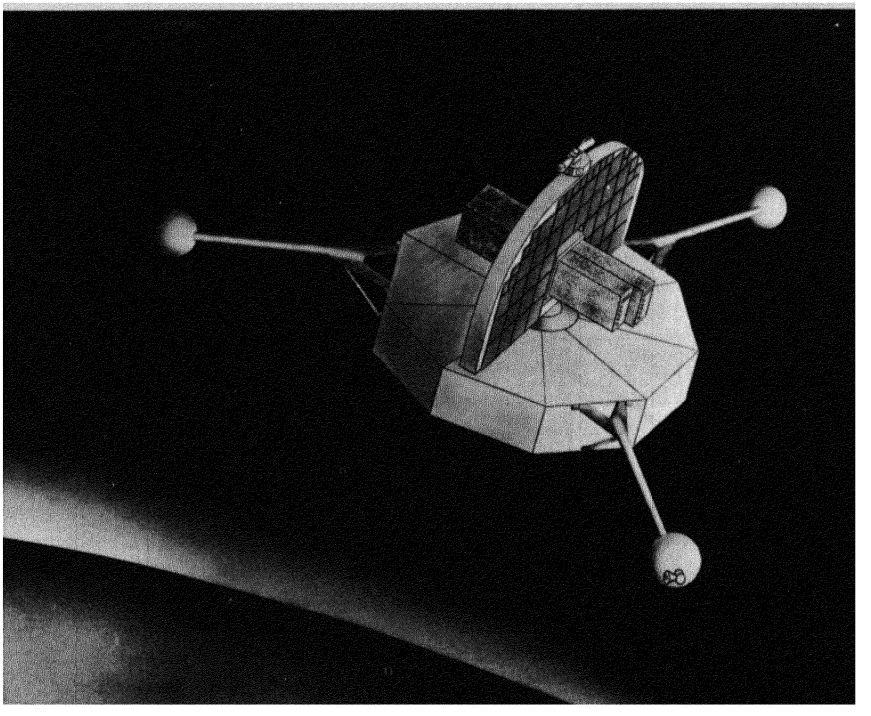


Fig. 11. The satellite-borne solar pointing control. [Courtesy Ball Brothers Research Corp.]

To extend the observation to stellar targets with enhanced accuracy of performance, the National Aeronautics and Space Administration is planning a series of Orbiting Astronomical Observatories. These are to provide an accuracy approaching one second of arc with telescopes up to 36 inches in aperture. Telemetry and ground command are to be invoked perhaps to identify the stellar field by television as well as to operate the experiment.

Looking beyond these astrostats, and independently sponsored by the National Science Foundation, the Kitt Peak National Observatory is studying a 50-inch orbiting telescope system. The astroguider for this telescope embodies many of the refinements previously discussed.

THE KITT PEAK NATIONAL OBSERVATORY'S ASTROGUIDER

A 50-inch diffraction limited optical system must be stabilized to at least 0.1 second of arc to achieve the full capability of the system. Furthermore, to extend the observations from first magnitude objects to nebulosities with no degradation of performance, a fully offset bi-stellar guidance system is expedient.

A guidance system making use of a pair of orthogonal navigational

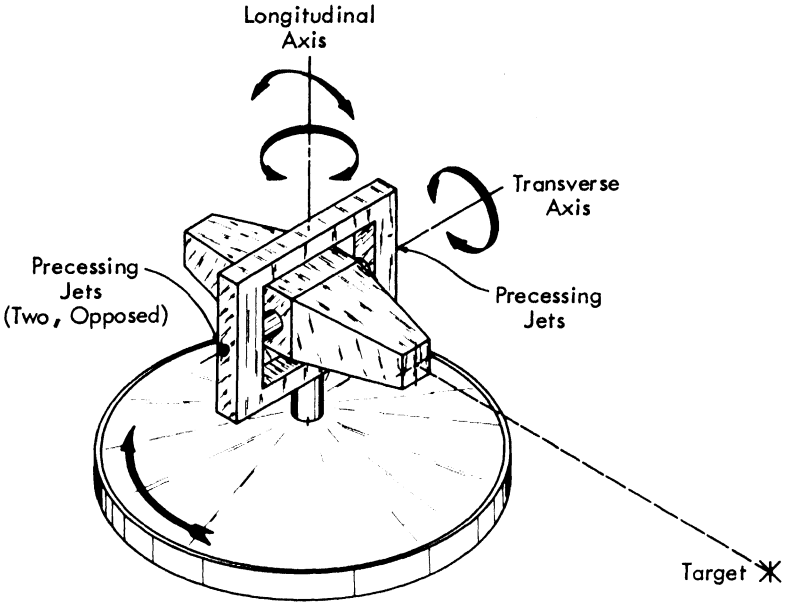


Fig. 12. The control axes of the satellite-borne solar pointing control showing the redundant cold-gas control concept.

stars is, however, appropriate only if the orbit radius is large enough that the earth does not ever occult either of the guide stars. Otherwise, additional guide stars with appropriate switching devices would be required, an artifice not only detrimental to reliability, but also not conducive to continual 0.1 second of arc accuracy.

At 22,200 miles above the equator, corresponding to a 24-hour geocentric stationary orbit, the earth subtends less than 18°, hence, a pair of first magnitude nearly orthogonal guide stars can readily be selected which would be in view of the satellite continuously.

Equally important, the 24-hour orbit greatly facilitates continual telemetry and command transmission, obviating the elaborate data storage capability and necessity of rapid read-out and command execution usually associated with the near earth orbits.

The earth derived perturbations are also much attenuated in magnitude, while at the same time correspondingly reduced in frequency, both of which ameliorate the appertinent stabilization difficulties.

These then are the ground rules of the KPNO study. A diffraction limited 50-inch reflective optical system is to be lofted into approximately a 24-hour circular orbit, inclined perhaps as much as 35° to the equatorial plane. One or three ground stations will be required, depending upon the accuracy of the injection. A sophisticated telemetry-command system providing continual real time communication will be incorporated, not only to slew to the selected target, but to

monitor and refine the accuracy of pointing in each of the three degrees of freedom of an offset bi-stellar guidance system.

The bi-stellar guidance system, the astroguider, will incorporate three orthogonal reaction wheels in a triaxial gimbal system. The reaction wheels with integral motors and the two photoelectric guide telescopes will be mounted on the inner gimbal so that the reaction wheels will remain fixed in the inertial frame of reference provided by the bi-stellar reference system.

The three gimbal drive motors serve to slew the primary (50-inch) telescope relative to the inertial reference system established by the inner gimbal. These can be set by ground command to an accuracy of the order of a minute of arc making use of conventional angular transducers between the three gimbals. Signals from the primary beam can then be invoked by telemetry and ground command to adjust vernier controls to set on a specific celestial target to an accuracy of 0.1 second of arc.

The vernier controls will probably be biaxially gimballed plane parallel plates in the convergent beams preceding the analyzers of the guide telescopes.

By using hermetically sealed motors with special windings and rotors, commanded directly by the guide telescope signals, it is anticipated that the astroguider will be able to maintain 0.1 second of arc stabilization in spite of the on-board perturbations due to motion of gratings for spectral scanning, filters for multicolor photometry, etc.

Saturation of the motors must be avoided by articulation of trim devices to continually dump the accumulated angular momentum. Two major external perturbations produce secular accumulation of angular momentum: Solar radiation and divergence of the gravitational field of the earth.[18] Though both torques are exceedingly small, the accumulative effects are significant when integrated over a period of days.

Specifically, if the center of pressure of the solar radiation is within one-half inch of the center of mass of the satellite, and if the principal moments of inertia of the satellite are equal to one part in a hundred, the two influences will be comparable. Either would result in saturation of the inertial wheel system anticipated in about seven days. Since both specifications will be difficult to achieve in preflight procedures, in-flight trimming of the area projected to the sun and the figure of the satellite will be used not only to reduce the accumulation of angular momentum, but also to dump that already accumulated.

Figure 13 depicts a schematic model of the 50-inch orbiting telescope. Two complete astroguiders are to be incorporated, the second to provide a reserve unit in the event of catastrophic failure of the first. This redundancy also facilitates change of guide star pairs to obviate incomplete sky coverage occasioned by obstruction of the astroguider view by the satellite or by gimbal limit stops.

Perhaps three different star pairs will be required to cover the entire celestial sphere. Though the entire sphere can be covered during a year in orbit, the necessity of keeping the primary telescope

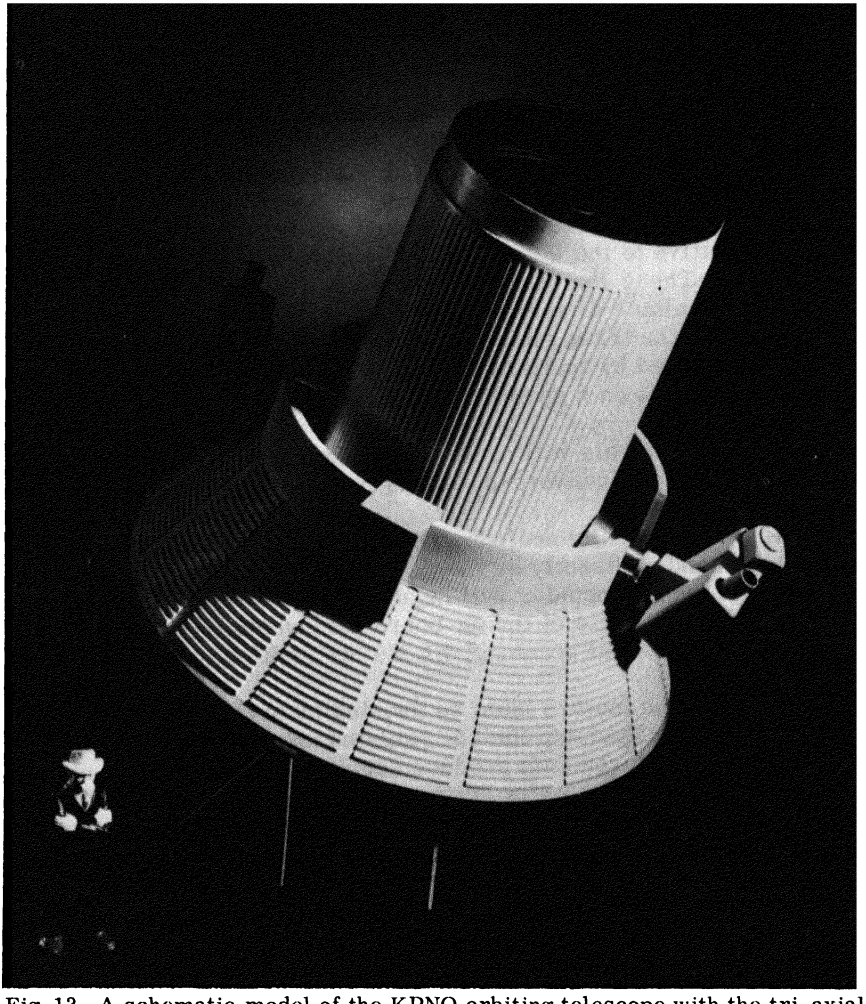


Fig. 13. A schematic model of the KPNO orbiting telescope with the tri-axial bi-stellar offset guidance system.

directed away from the sun to avoid scattered sunlight in the primary beam may limit the immediate coverage to the hemisphere opposite the sun.

Solar cells covering the aft surface will be used to supply the primary power for the satellite. Approximately one kilowatt of maximum power assimilation will be obtained. Hence, the average power budget will be the order of 500 watts.

To balance the power budget, time-sharing will probably be invoked. An observing program requiring more power than assimilated will be judiciously interrupted to direct the solar cell array fully to the sun to recharge the chemical batteries. Slewing of the satellite to

recharge the batteries will, of course, be done with the astroguider to avoid the necessity of reacquisition of the celestial frame of reference.

Initial acquisition will involve trimming of the angular momentum of the satellite probably by cold gas jets controlled by rate gyros. Then body fixed reaction wheels controlled by solar coarse and fine eyes will be used to direct the primary telescope in the antisolar direction to an accuracy of the order of a minute of arc. The satellite will then be slowly programed about the solar vector until the guide star pair desired appears in the fields of view of the guide telescopes of one of the astroguiders. Primary control will then be given entirely to that astroguider with the body fixed wheels held in reserve as backup in the event of failure of one of the two astroguiders.

After switching to the astroguider, the primary telescope may be slewed as desired to execute the observing program.

The instruments projected for the 50-inch orbiting telescope include an ultraviolet spectrometer, infrared spectrometer, multicolor photometer, absolute bolometer, and a narrow field image orthicon. The optics of the primary telescope are to be executed such that in addition to the central image position to service the image tube, four radially separated, off-axis, highly corrected image points will also be provided to serve the remaining four instruments. Hence, selection of the instrument for the particular observation is to be effected by appropriate vernier pointing of the primary telescope by the astroguider.

Since only two of the three degrees of freedom are required for pointing, the primary telescope can be rotated about its axis to avoid having two different targets under simultaneous observation by two of the five instruments.

Of the five instruments, the image tube requires the greatest power for operation, the more precise pointing, and is probably the least reliable. Thus, this instrument will probably be given maximum use during the immediate post-injection period. As subsequent component failures degrade performance, less stringent instruments will be used. By this artifice a usable lifetime of the order of five years is anticipated.

Since the total instrument payload will be the order of two to three tons, a boost vehicle of the Saturn capabilities will be required. Hence, several years will be available to perfect the astroguider, refine the optical techniques, develop detectors, and optimize the structural design to ameliorate the severe thermal environment.

CONCLUSIONS

Many interrelated decisions and compromises must be made to execute an astrostat for a specific mission. The choice of number, order and configuration of the gimbals must reflect the vehicle dynamics.

Though the explicit gimbals have been adequate for the Aerobee

vehicle and the earlier balloon flights, three are required to avoid gimbal restraint of the instrument.

Implicit gimbals such as used on the Russian Interplanetary Station and in part on the Satellite-borne Solar Pointing Control obviate gimbal bearing noise and perturbations, both inertial and viscous, of the conventional motive elements. However, inadequacies of the jet devices militate in favor of pseudo-implicit gimbals making use of reaction wheels.

By mounting the reaction wheels on the inner gimbal of a bistellar astroguider, offset guiding of a 50-inch earth-period orbiting telescope is projected. Continual ground command of the triaxial gimbal system of the astroguider is to provide general target selection.

REFERENCES

[1] H. L. Clark, Electronics **23**, 71 (1950).
[2] A. A. Blagonravov, ARS Journal **30**, 22 (1960).
[3] Stacey, Stith, Nidey, and Pietenpol, Electronics **27**, 149 (1954).
[4] Pietenpol, Rense, Walz, Stacey, and Jackson, Phys. Rev. **90**, 156 (1953).
[5] Johnson, Malitson, Purcell, and Tousey, Ap. J. **127**, 80 (1958).
[6] H. Friedman, J. Geophys. Research **64**, 1751 (1959).
[7] J. D. Purcell and R. Tousey, J. Geophys. Research **65**, 370 (1960).
[8] J. W. Townsend, Jr., and R. M. Slavin, Jet Propulsion **27**, 263 (1957).
[9] R. A. Nidey and D. S. Stacey, Rev. of Sci. Inst. **27**, 216 (1956).
[10] Ibid.
[11] M. Schwarzschild, Ap. J. **130**, 345 (1959).
[12] H. W. Babcock, Ap. J. **107**, 73 (1948).
[13] R. H. Weitbrecht, Rev. of Sci. Inst. **28**, 122 (1957).
[14] R. B. Horsfall, ARS Journal **29**, 981 (1959).
[15] J. T. Wallmark, IRE Proc. **45**, 474 (1957).
[16] R. A. Nidey, Rev. of Sci. Inst. **28**, 658 (1957).
[17] Loc. Cit.
[18] R. A. Nidey, ARS Journal **30**, 203 (1960).

14. ATTITUDE CONTROL OF ARTIFICIAL SATELLITES

R. B. Kershner and R. R. Newton
Johns Hopkins University

1. THE NEED FOR ATTITUDE CONTROL

The earliest artificial satellites of earth were carefully designed to avoid any special requirements for the control of their attitude. For example, turnstile or other reasonably isotropic antenna systems were used so that communication to and from the satellite could be carried out with any satellite orientation, and the experiments carried out were non-directional. However, as the mission to be performed by an artificial satellite increases in scope and complexity, requirements soon arise that can only be met by imposing some form of control on the attitude of the satellite. First of all, the experiments to be performed may require instruments (such as cameras or telescopes) which are inherently directional in character. Again, if the communication requirements are quite severe, it may not be feasible to supply the power necessary for the use of isotropic antennas, so that directional antennas must be adopted and, of course, pointed. Finally, if solar power is used, it is always advantageous, and may be mandatory, to point the power system at the sun.

A special situation arises when it is not necessary to control the attitude itself but it is necessary to control the rate of change of attitude. An example to this effect is provided by the TRANSIT navigation satellites. These satellites transmit a group of very stable frequencies and a primary objective is to record, on the ground, the Doppler signal generated by the relative motion of the satellite and the receiving station. The satellite antenna pattern is nominally isotropic but, of course, exhibits some variation of gain with angle. If the TRANSIT satellites were permitted to spin at a large angular rate, then the variation of antenna gain as a function of attitude would result in a frequency modulation of the received signal which would degrade the accuracy of the Doppler measurement. To avoid this, the TRANSIT satellites include devices for limiting their spin rate to a low value.

A requirement for attitude control can also stem from a desire to perform any maneuver (requiring thrust) after the satellite is in orbit. This may be necessary for orbit adjustment if there are special requirements on the orbit that cannot be readily achieved during the initial launch phase. For example, the establishment of satellites in stable 24-hour orbits, desired for communication purposes, will prob-

ably require such adjustment. Placing a satellite in orbit around the moon is another such example. A particularly important case that requires the application of directed thrust after a satellite is in orbit is that of a satellite which it is desired to bring back from orbit. The DISCOVERER series and Project MERCURY are well known examples.

2. TYPES OF ATTITUDE CONTROL

Often it is possible to meet the attitude control requirements for a particular satellite by orienting properly a particular distinguished axis of the satellite with no requirement concerning the roll of the satellite about this axis. In other cases a full three axis control is required. An intermediate case occurs when one axis control is adequate but the roll rate about this axis must be controlled to some degree. In the case of single axis control the axis whose orientation is controlled may be referred to as the spin axis, since the satellite may always be assumed to be spinning about this axis. Indeed a lack of spin could only result from some form of control (intentional or unintentional) of the other axes. For this reason the case of single axis control will be referred to as control of the spin axis. In a similar way the intermediate case will be referred to as control of the spin axis and spin rate. Finally, the three axis control case will be referred to as full attitude control.

It is also useful to distinguish attitude control systems in terms of the reference coordinate system, or reference body with respect to which stabilization is maintained. The most commonly considered are stabilization in inertial space (with respect to the fixed stars), stabilization toward the sun, and stabilization toward the earth. Other systems may occur, of course, as for example stabilization toward the moon, toward Mars or other planets, etc. However, the consideration of the first three cases will suffice for the present discussion.

Stabilization in inertial space meets the requirements of a satellite taking observations on the fixed stars (the orbiting observatory). It is also important because it is often rather easily attained. For example, if a satellite has a reasonably high rate of spin about a given axis, then this spin axis will automatically maintain its orientation in inertial space by the gyroscopic effect of the spin. Inertial space stabilization of the spin axis has been used in some satellites where something else would more ideally meet the requirements, just because of the great simplicity of this particular form of attitude control. A good example is furnished by the TIROS weather satellite. In this satellite the primary objective is to take photographs of the cloud formations over the surface of the earth. Obviously stabilization toward the earth would best meet the needs. However, in the interest of simplicity and reliability the satellite was designed using gyroscopic stabilization of the spin axis in inertial space. Photographs were then taken only at those times when the orientation of the cameras happened to be proper for obtaining the desired pictures.

Stabilization toward the sun is most commonly considered in connection with the use of solar power as the source of satellite energy. Solar power supply systems of various types, including solar cells and solar furnaces, are the leading contenders for the role of long-lived satellite power supply. However, unless a satellite axis is directed toward the sun, the use of these power supply systems requires the provision of a tremendous redundancy of elements so that enough power can be gathered from the amount of energy gathering surface that happens to be oriented properly. As satellites become more complex and require more power, the desire to avoid this redundancy and the attendant weight penalty becomes very large, so that stabilization toward the sun will be increasingly important in the future. Stabilization toward the sun also may be required for a satellite whose mission is to study radiations or emanations of any sort originating in the sun.

Stabilization toward the earth may be required, as indicated above, by the need to use a directional antenna for communicating with the earth. It may also be required by the fact that the mission of the satellite concerns the observation of phenomena attached to the earth. Weather observation satellites and reconnaissance satellites are obvious examples, but there are many others. Actually the first satellites which were stabilized with respect to the earth were those in the DISCOVERER series. Here a principal requirement was to align a retro-rocket with the velocity vector of the satellite (relative to earth), so that when fired it would slow the satellite down and initiate re-entry.

3. SOURCES OF TORQUE

Control of the attitude of a satellite requires, of course, some means for generating a torque on the satellite. In the special case of stabilization in inertial space, it might be thought that no torque need be applied. In a sense, this is correct. However, as will be seen, some accidental or unintended torque is always present. The only way to achieve the desired zero torque needed for maintaining a fixed attitude in inertial space is to have a means for generating a torque equal in magnitude and opposite in sense to the accidental torque present.

For a body which at first thought appears to be isolated in space and hence, by the conservation of angular momentum, not subject to torque at all, sources of torque, either accidental or purposeful, are surprisingly numerous. In this section we shall describe qualitatively most of the significant sources of torque, and then in subsequent sections, we shall discuss the most important sources quantitatively.

a. Reaction Torque

Perhaps the most obvious way to apply a torque to a satellite is by ejecting some mass from the satellite in a direction which does not pass through the center of mass. This means circumvents the pres-

ervation of angular momentum in an isolated system by breaking the system into two subsystems. Then, as long as the over-all angular momentum is preserved, the total angular momentum can be distributed in any way between the two subsystems. Thus any desired change in the angular momentum of the main portion of the satellite that is not ejected is, in principle, achievable.

A specific and commonly used method for providing torque is to discharge or eject mass in the form of jets of gas (hot or cold). In fact the first fully attitude controlled satellites, the DISCOVERERS, used gas jets for their stabilization. However, there is, of course, no requirement that the material ejected be gaseous and, for example, solid weights may be thrown out. A special case of the use of solid weights is the device known as yo-yo which was invented at the Jet Propulsion Laboratory and independently, somewhat later, at the Applied Physics Laboratory. This device, used to remove the spin about a given axis, is described in a later section. It has been successfully used in a number of satellites including TIROS and TRANSIT.

The provision of torque by ejecting material is straightforward but has the obvious disadvantage of requiring the use of material which had to be carried into orbit. Thus it is most applicable for one-shot corrections (like the removal of an initial high spin rate by the use of yo-yo) or for relatively short duration stabilization (a few days in the case of DISCOVERER). The duration over which this technique is applicable may be extended by using very small masses of material ejected at extremely high velocity. Ion propulsion is an extreme in this direction and may well prove useful for fairly extended stabilization periods in some cases. However, for satellites with a requirement for attitude stabilization over a period of years, it is apparent that a method for providing torque without requiring the ejection of any mass at all would be advantageous. Fortunately there are a number of such methods.

One very simple way to alter the attitude of a satellite is to include within the satellite a disk or wheel which can be rotated (by a motor) with respect to the satellite. Then, by conservation of angular momentum, any angular momentum imparted to this wheel is balanced by an equal momentum of opposite sense for the remainder of the satellite. Hence, by a trivial integration, if the wheel, starting from rest, is turned through an angle θ and stopped, the remainder of the satellite (if the external torques are balanced) will turn through an angle $k \cdot \theta$, where k is the ratio of the appropriate moments of inertia. If three-axis stabilization is required then, of course, three reaction wheels with mutually perpendicular axes would be used.

It is apparent that the use of reaction wheels would provide an extremely simple and practical means for controlling the attitude of a satellite with precision, if there really were no external torques acting on the satellite. However, the existence of any external torque poses very serious difficulties. A reaction wheel can counter an external torque only by accelerating its angular motion. Hence, sooner or later, if the external torque persists, the reaction wheel will over-

speed. This problem has so far prevented the use of reaction wheel attitude control in satellites and, in fact, means that reaction wheels cannot be used without adding some means for countering external torques. However, such means exist and the use of reaction wheels together with means (which can be rather crude) for applying (countering) external torques is expected to become very important in the more sophisticated satellites of the future.

b. Gravitational Torque (Libration)

If the mass distribution of the satellite is rigorously spherical (i.e., if the inertia-tensor is proportional to the unit matrix) then the gravitational force acting on the satellite may be rigorously assumed to act through the center of gravity of the satellite and no torque arises due to the gravitational attraction of the earth. However, due to the existence of a gravitational gradient across the satellite, there may be a torque caused by the gravitational field in the case of a non-spherical satellite. To visualize the source of this torque, it is convenient to consider a satellite consisting of two spheres joined by a rigid rod. If this dumbbell shaped satellite is oriented with one sphere closer to the center of the earth than the other, there is a difference in the gravitational force on the two spheres, due to their different distances from the center of the earth. This difference in gravitational attraction on the two spheres results in a torque tending to align the rod joining the spheres (the principal axis of the dumbbell) in a direction pointing toward the center of the earth. It is this type of torque which causes the Moon and Mercury to keep one face pointing at the earth and sun respectively.

The gravitational torque provides a possibility of establishing a purely passive stabilization toward the earth. However, the gravitational torque can also be used in active systems by providing, for example, sliding weights within a satellite to control the moments and products of inertia in any desired fashion. This possibility is discussed further in the sequel.

The gravitational torque is important as a source of accidental or undesired torques for any stabilized satellite, since it is impossible to make a satellite with a rigorously spherical mass distribution. However, for any satellite in which precision attitude control is desired, care should be used to approach a spherical mass distribution as closely as possible, in order to minimize the difficulties caused by gravitational torques.

c. Radiation Pressure

It is known that light exerts a pressure on any body on which it shines. This pressure is extremely small, and correspondingly very difficult to demonstrate experimentally, but it has been exhibited by properly designed experiments. And, in an artificial satellite in which all types of external torque have been reduced to an extremely small

value, it is easily possible to have a situation in which electromagnetic radiation pressure is a significant or even a dominant source of external torque.

Qualitatively it is convenient to think of radiation pressure as arising from a momentum transfer from the individual photons striking the surface. From this it is seen that for a completely reflective (white) surface, from which the photons bounce in billiard ball fashion, the radiation pressure will be exerted normal to the surface, while for a completely absorbing (black) surface, which absorbs the photons, the radiation pressure is exerted along a continuation of the line of arrival of the radiation. In particular, if a satellite has a spherical shell, then no torque will arise, due to radiation pressure, from any element of surface which is completely reflective. On the other hand, any black area of surface tends to be pushed away from the sun. From this, it is seen that if a spherical satellite is painted white on one hemisphere and black on the other, then radiation pressure will tend to align it with the white side pointing at the sun. These considerations indicate the possibility of a satellite which is solar oriented by completely passive means. Of course, for a practical system, some type of damping is needed.

Active systems, using light pressure as the activating torque, are also possible. For such a system, we would have to provide suitably oriented areas which could be changed from reflecting to absorbing, or whose projected areas could be changed. Expanses of "Venetian blind" material, with a means of rotating the "slats," naturally suggest themselves.

In addition to the torque arising from incident (received) radiation, one must also consider the reaction (recoil) from radiation emitted by the satellite. If large differences in the amount of radiated energy from various parts of the satellite occur, due to differences in temperature or color in various portions of the satellite skin, it is possible for an appreciable torque to be generated from this source.

d. Aerodynamic Torque

For the sake of completeness, it should be mentioned that an appreciable aerodynamic torque can occur for a satellite of earth at a sufficiently low altitude that it enters the appreciable atmosphere. In addition to the obvious torques that arise due to the shape of the satellite, there may be a somewhat less obvious torque, even for a spherical body, due to the existence of a density gradient across the satellite. Due to this gradient there is somewhat less drag on the top of the satellite than on the bottom. This, of course, produces a torque. Fortunately, for reasonable dimensions, this torque is negligible even in comparison with other very small torques we have been considering.

e. Micrometeorite Impacts

Torques may arise for a satellite from the momentum transfer

that results when a high velocity particle of space debris physically strikes the satellite off center. This source of torque is extremely hard to evaluate quantitatively. In the absence of accurate information about the density of micrometeorites, and their momentum distribution, there is little point in discussing this source of torque further.

f. Magnetic Torques

For a satellite in the near vicinity of the earth, or of any other body possessing a magnetic field, the existence of a magnetic field in the space occupied by the satellite provides another means of applying torque to the satellite; namely, the torque tending to align a magnet along the magnetic field. For satellites near the earth, these torques can readily be made large compared with any of the other torques we have been discussing. These torques are also quite convenient to produce and control, for example, by using electromagnets which can be activated, reversed, or extinguished by simple current switching.

However, there are certain difficulties inherent in the use of magnetic torquing. The first difficulty is that full three-axis control is not available at any given instant. Specifically, it is impossible to obtain a torque causing a rotation about an axis which is aligned with the magnetic field. The second difficulty is that the direction of the magnetic field in inertial space changes drastically as the satellite moves in its orbit. Actually, this second difficulty is not too serious, since it is always possible either to compute or to sense this changing direction. In fact, the changing direction of the field can be used to alleviate the first difficulty. If rotation about a particular axis cannot be obtained at a given instant because that axis is aligned with the field, then shortly the field direction will change and rotation about the desired axis will become possible. Thus three-axis attitude control appears to be achievable with magnetic torques and, for any particular application, magnetic control should be seriously considered as a competitor to the use of reaction wheels or jets.

It is noteworthy that the simple inclusion of a permanent magnet in a satellite provides a crude form of passive stabilization. If the magnet is strong enough it will maintain a specific axis of the satellite in alignment with the local magnetic field. For a high-inclination orbit, this will cause this satellite axis to rotate at twice the orbital rate. Another possibility is to use a weak magnet and, taking advantage of the fact that the time average field parallel to the earth's axis is not zero except for an inclination of 33° (for a circular orbit); thus maintain a rough stabilization with one axis parallel to the earth's axis.

Perhaps the most important feature of the use of magnetic torques is the relative ease with which damping of angular velocity can be obtained. In fact, there are two distinct mechanisms which can be used to provide damping—one which is effective for high angular velocities and one which is effective for low angular velocities. The phenomena associated with these two mechanisms are induced electric current and magnetic hysteresis respectively.

To provide damping of angular velocity by induced electric current, all that is required is a coil of wire with the ends joined (a shorted coil). The effectiveness can be very greatly increased by winding the coil on a core made of a material with high magnetic permeability so that more lines of magnetic force are carried through the coil. When the coil rotates in the earth's magnetic field a current is generated in the coil and the coil is heated. The energy is taken from the rotational kinetic energy and the rotation will be slowed. From the elementary laws the amount of energy for each complete rotation of the coil is proportional to the speed of rotation, so that the overall rate of energy dissipation in the coil is proportional to the square of the angular velocity. Thus, if ω is the angular velocity and I the moment of inertia of the satellite, then

$$\frac{d}{dt}\left(\frac{1}{2} I \omega^2\right) = -\text{const.} \times \omega^2,$$

whence

$$I\dot{\omega} = -\text{const.} \times \omega.$$

Since $I\dot{\omega}$ is the retarding torque, it is seen that a shorted coil produces a retarding torque which reduces to zero at zero angular velocity but is increasingly effective at higher velocities.

It should be mentioned that the provision of a carefully designed shorted coil is not necessary to produce damping in the earth's magnetic field. In fact, in almost any conducting material, including metal package covers and the satellite skin (if it is made of conducting material), there will be induced eddy currents which will dissipate the rotational energy of the satellite. This fact causes difficulties for satellites like TIROS, in which it was desired to maintain a steady angular velocity for long periods. In fact, TIROS used spin-up jets which were actuated to restore the desired spin rate after eddy current damping had reduced the spin rate below an acceptable lower limit. However, when effective damping is desired it can be greatly enhanced by the use of a properly designed shorted coil.

A quite different damping mechanism can be based on the phenomenon of magnetic hysteresis. If a rod of high magnetic permeability is placed in the earth's magnetic field, magnetism will be induced in the rod and a torque will be produced by the tendency of this induced magnet to align itself with the field. The value of this torque depends on the orientation of the device relative to the field and the magnetic properties of the material. For those materials, which are said to exhibit magnetic hysteresis, this torque (and the degree of induced magnetization) also depends on the previous history of magnetization of the material. For such materials, if the rod is slowly rotated through a complete revolution, the torque will not average zero but instead will have a specific non-zero value and a direction which depends on the direction of rotation of the rod. The basic law governing the behavior of a rod of high permeability material with hysteresis, rotating in a magnetic field, is that for every complete revolution of

the rod a fixed amount of energy is dissipated in the rod. This amount of energy is the area of the standard hysteresis loop. Thus the rate of energy loss is proportional to the angular velocity or

$$\frac{d}{dt}\left(\frac{1}{2} I \omega^2\right) = \text{const.} \times \omega$$

whence

$$I \dot{\omega} = \text{const.}$$

It is seen that the incorporation of such a rod in a satellite produces a constant retarding torque opposing any rotation. The fact that this opposing torque remains constant in value even for very slow rotation makes the use of hysteresis damping very effective at low angular velocities.

It is, of course, very easy to combine the two types of magnetic damping described above in a single device simply by using a material with large hysteresis loss as the core for a shorted coil. Such a device will produce damping which is primarily due to the induced current in the coil at high angular velocity but is primarily due to hysteresis loss at low angular velocity. Such a device has been used in the TRANSIT satellites and the results will be discussed quantitatively in the next section.

The use of magnetic damping torques appears to provide a simple and effective means for damping even when some other means are used to provide the primary stabilization torques. For example, a complete three axis stabilization system can be based on the use of reaction wheels, with magnetic damping to solve the overspeed problem mentioned in the earlier discussion of reaction torques. An effective specific system is obtained by placing a shorted coil (induced current) damping device on each of the reaction wheels. Then this device will produce a retarding torque opposing the wheel speed, and this torque becomes increasingly large as the wheel speed increases. It is true that this mechanism may be ineffective on one of the three wheels at a given moment, if the axis of that wheel is aligned with the magnetic field, but this situation, for any particular wheel, can only obtain for a small fraction of any one satellite orbit. During such periods the stabilization requirements are met by reaction wheel accelerations. As soon as the orientation changes enough for the induced current damping to become effective the wheel will automatically decelerate. Such a system has been thoroughly analyzed at the Applied Physics Laboratory and appears to meet readily the most stringent requirements for attitude stabilization that have been considered to date—the requirements for the NASA orbiting astronomical observatory.

g. Gyroscopic Torques

Since a satellite is totally unconstrained in attitude, it is particularly necessary to consider carefully all of the various couplings be-

tween axes that can occur. An interesting illustration of the need for care in this connection was provided by some of the earliest satellites launched by the United States. These satellites were roughly cylindrical, with a length greater than their diameter, and were given an initial spin about the long axis. It was observed that rather shortly they had ceased spinning about the long axis and instead were tumbling, i.e., spinning about a transverse axis. The mechanism for this is qualitatively reasonably simple, although very complex in detail. Since the moment of inertia about a transverse axis is greater than the moment of inertia about the long axis, it is clear that the satellite can maintain its initial angular momentum with a lower angular velocity and hence a lower kinetic energy by spinning about a transverse axis. If there is any mechanism for dissipating energy (for example, by structural flexing, sloshing of fluid in batteries or the like) the satellite will seek the lowest energy state compatible with the required conservation of angular momentum. The solution for this problem is simple. If it is desired to maintain a satellite spinning for an extended period of time about a particular axis it is convenient to design the satellite so that this desired spin axis is also the axis about which the moment of inertia is maximum. This observation explains the disk-like shape of such satellites as TIROS. And while TRANSIT is externally spherical it is packaged to have the mass distribution of a disk.

4. QUANTITATIVE DISCUSSION OF TORQUES

In this section some of the more important sources of torque will be discussed from a more quantitative viewpoint.

a. The Yo-Yo

Consider a disk-shaped satellite spinning about the axis of the disk. Assume that a wire has one end fastened to the circumference of the disk and is then wrapped about the circumference in a direction opposite to the direction of rotation. A weight is attached to the outer end of the wire and held against the circumference. At a given instant the weight is released. It swings out under centrifugal force and, through the wire, exerts a retarding moment on the satellite. Actually, two diametrically opposite weights and wires are released simultaneously, so as to avoid transverse forces on the axis of the disk. However, for simplicity, we will consider the case of a single weight and assume the disk axis is fixed.

The geometry of the situation after release of the wire is shown in Fig. 1, where φ is the angle turned by the satellite after release of the weight, R is the radius of the satellite, s is the amount of wire paid out, and r, φ, and θ are the polar coordinates of the weight. Clearly, from the geometry,

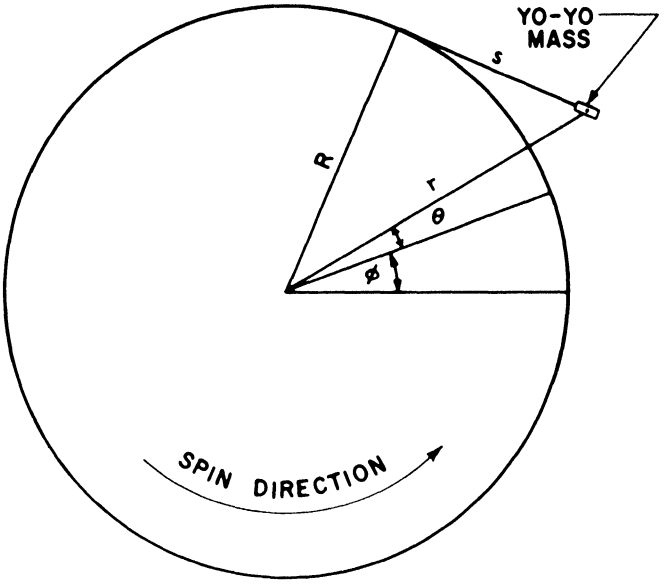


Fig. 1. Geometry for spin energy removal by means of the Yo-Yo.

$$\theta = \frac{s}{R} - \tan^{-1}\frac{s}{R} \tag{4.1}$$

$$r = \sqrt{s^2 + R^2}$$

Let I be the moment of inertia of the satellite (without the yo-yo weight) and m the mass of the weight, so that $I_0 = I + mR^2$ is the initial moment of inertia of the satellite before release of the weight. Let ω_0 be the initial angular velocity.

The equations expressing the conservation of angular momentum and kinetic energy are

$$\begin{aligned} I\dot{\varphi} + mr^2(\dot{\varphi} + \dot{\theta}) &= I_0\omega_0 \\ I\dot{\varphi}^2 + mr^2(\dot{\varphi} + \dot{\theta})^2 + m\dot{r}^2 &= I_0\omega_0^2 \end{aligned} \tag{4.2}$$

Now if r, θ, $\dot{r}$, $\dot{\theta}$ are expressed in terms of s, $\dot{s}$ by means of (4.1), then (4.2) become

$$(I_0 + ms^2)\dot{\varphi} + \frac{ms^2}{R}\dot{s} = I_0\omega_0 \tag{4.3}$$

$$(I_0 + ms^2)\dot{\varphi}^2 + \frac{2ms^2}{R}\dot{s}\dot{\varphi} + \frac{m}{R^2}s(\dot{s})^2 = I_0\omega_0^2 \tag{4.4}$$

If (4.3) is multiplied by $(\dot{\varphi} + \dot{s}/R)$ and subtracted from (4.4) the result is

$$\dot{s} = R\omega_0, \tag{4.5}$$

and this, substituted in (4.3), immediately yields

$$\dot{\varphi} = \omega_0 \frac{I_0 - ms^2}{I_0 + ms^2} . \tag{4.6}$$

Eqs. (4.5) and (4.6) can be immediately integrated with the obvious boundary conditions to give

$$\begin{aligned} s &= R\omega_0 t, \\ \varphi &= 2\sqrt{\frac{I_0}{mR^2}} \tan^{-1}\left(\omega_0 \sqrt{\frac{mR^2}{I_0}}\, t\right) - \omega_0 t. \end{aligned} \tag{4.7}$$

However, most of the important features of the yo-yo operation are more easily obtained directly from (4.5) and (4.6) without integration. For example, from (4.6), it is clear that $\dot{\varphi} = 0$ when

$$s = \sqrt{I_0/m} \tag{4.8}$$

Thus, when the amount of wire given by (4.8) has been paid out, the satellite will have been brought to rest, and, if any further wire is paid out, the satellite will begin to turn in the opposite direction. The limiting value, for infinite s, is also obvious from (4.6); namely, $-\omega_0$ (the same angular speed as the initial speed but the opposite sense of rotation). If the wire is arranged to detach from the satellite after a length s, given by Eq. (4.8), has paid out, then the satellite will be left without angular velocity and the weight will depart carrying the entire angular momentum of the system with it.

It is particularly important that Eq. (4.8) does not contain the initial angular velocity ω_0. Thus, if the yo-yo is properly designed, with a mass m and length of wire s satisfying (4.8), its operation will remove whatever angular velocity exists. However, while it is not necessary to know what the angular velocity will be to design a yo-yo to remove it, it is necessary to know the direction of the angular velocity.

While practical manufacturing tolerances make it impossible to realize a yo-yo design that really removes all the angular velocity, it is perfectly possible to design one that reduces the angular velocity to, say, one percent of its initial value and then deploy a second yo-yo to remove all but one percent of the residual remaining after the first was deployed. Thus, by cascading, the angular velocity can be reduced to as low a value as desired.

Various simple modifications of the yo-yo scheme have been devised. For example, in one variant the wire is not released when it is tangent to the circumference. Instead, the weight is allowed to swing until the wire has become radial and is then released. If the geometry is properly chosen, this arrangement again stops the rotation. Since the wire is radial, at the ideal instant of release, the torque exerted is small near the ideal instant. Thus, the tolerances are less stringent then for release with the wire tangential, when the torque exerted is a maximum.

In summary, the yo-yo provides an extremely simple and practical means for removing almost all of any initial angular velocity from a satellite. It has been used, quite successfully in several satellites, including TIROS and TRANSIT 1-B. In the case of TRANSIT 1-B, the weights were arranged to be released when the wires were nearly tangential, so that the formulae developed above approximately held. The initial moment of inertia was 9.62 slug ft^2 and the two weights weighed 2.36 lbs. each. Hence, the theoretical length of wire, according to Eq. (4.8) was

$$s = \sqrt{\frac{9.62 \times 32.2}{4.72}} = 8.1 \text{ ft.} = 97.2 \text{ in.}$$

Actually, due to the specific details of the release mechanism, release was effected somewhat late and accordingly the optimum length, which was determined experimentally by ground testing was $94\frac{5}{8}$". The effect on the spin velocity of TRANSIT 1-B when the yo-yo was actuated is shown in Fig. 2.

b. Libration

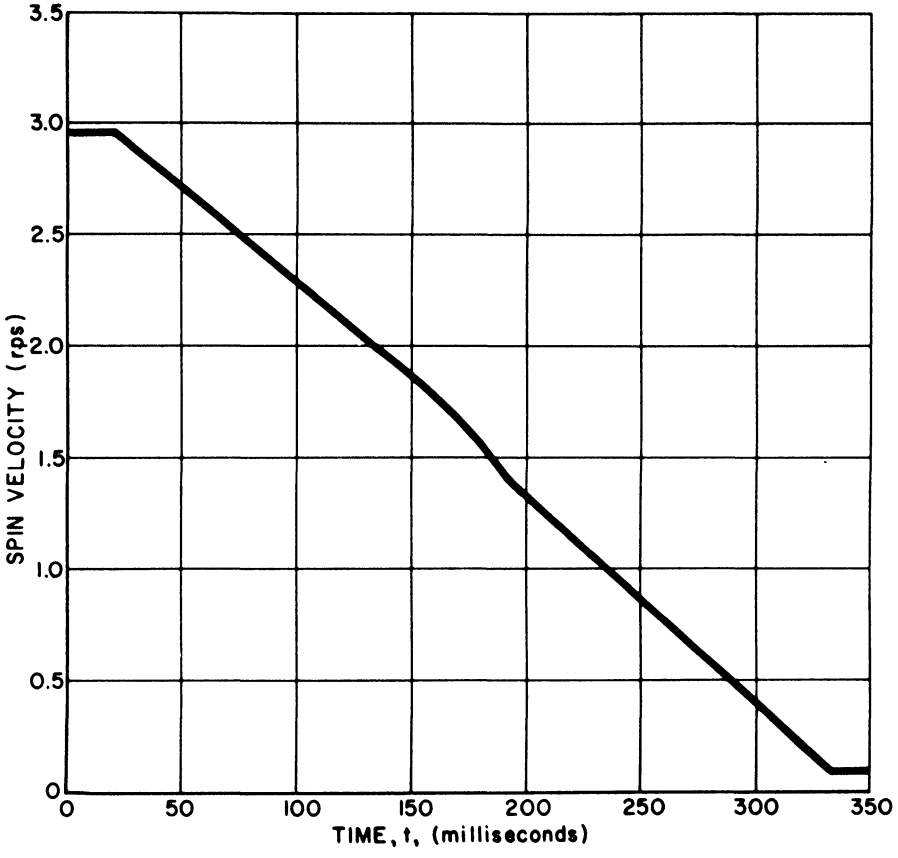
The value of the torque due to the gravitational gradient across a non-spherical satellite has been discussed by many writers. The treatment by Roberson and Tatistcheff[1] is perhaps the most thorough. For understanding the basic phenomenon, perhaps the most useful form, given by one of us,[2] is that the libration torque is given by

$$T = 3(g_0/R_0)(-I\, I_{YZ} + J\, I_{XZ})$$

where Z is the vertical axis through the center of mass of the satellite, X is horizontal and is chosen so that the total angular momentum vector lies in the XZ plane, and Y is chosen to complete a right-handed set. I and J are unit vectors along X and Y, and I_{YZ}, I_{XZ} are products of inertia about the indicated axes, being functions of the principal moments of inertia and the attitude of the satellite. R_0 is the distance of the center of mass from the center of the earth, and g_0 is the gravitational acceleration at that distance.

If a spherical satellite is built with movable masses arranged so they may be slid along rods in three mutually perpendicular directions then movements of these weights can be used to generate libration torque around any desired axis.

At some instant, let us suppose that the satellite has an angular momentum, in a known direction, which we wish to remove. We cannot do anything about the component of angular momentum that is vertical at the moment except wait; that component will be horizontal in one quarter of a period. The product of inertia I_{XY} is not involved in the torque, so it does not matter what value it has. We want to make I_{XZ} zero, since we do not want a torque normal to the angular momentum. Specifying the magnitude of the torque desired in the X direction, together with the condition $I_{XZ} = 0$, then determines the positioning of the movable masses. We can either use a "bang-bang"



NOTE: TIME t=0 IS AT THE INSTANT OF ACTIVATION OF THE ELECTRICAL SWITCH WHICH INITIATES THE DEPLOYMENT OF THE YO-YO.

Fig. 2. Spin velocity of the TRANSIT 1B satellite after actuation of the Yo-Yo.

mode of operation, making I_{YZ} as large as we can within the limits of the geometry, or we can use proportional or any other type of control program, depending upon the total system considerations.

If we require that we be able to remove, within one orbital period, an angular velocity of 1° per period, the mass requirements are modest; the movable mass need have only about 1/2 percent of the total vehicle mass.

c. Radiation Pressure

The pressure of solar radiation near the earth, but outside its atmosphere is given, for example, by Roberson[3] as

$$P = 0.43 \times 10^{-5} \text{ newton/sq meter.}$$

While small, this is enough pressure to give torques competitive with

others in the environment of a satellite. For example, consider the case, described earlier, of a spherical satellite with one hemisphere white and one hemisphere black which stabilizes with the reflecting half facing the sun. With an angle θ between the symmetry axis and the direction to the sun, the torque is

$$T = (2/3)\, P\, a^3 \sin^2 \theta$$

where a is the radius of the sphere. For a satellite weighing 100 kg, a radius of 0.5 m and an inertia unbalance of one part in a thousand this radiation torque will balance the libration torque at an angle of about 22°. The actual radiation torque at this angle is about 5×10^{-8} newton meters.

There are many geometries which provide a torque tending to stabilize one axis toward the sun. For example, Sohn[4] has suggested a flat sail arranged so that the center of mass lies in the plane of the sail. This arrangement tends to stabilize with the sail away from the sun, like the tail of a comet. Sohn does not specify the reflection characteristics of the sail but we obtain results that do not agree with those of Sohn for any reflection characteristics. In fact, Sohn indicates that the torque (for small ψ) is approximately

$$T = PA\ell\, \psi$$

where T is the torque, P the radiation pressure, A the area of the sail, ℓ the distance from the center of mass to the center of pressure of the sail and ψ the yaw angle of the sail. In contrast we find

$$T = \alpha\, PA\ell \sin^2 \psi$$

where $\alpha = 1$ for an absorbing sail and $\alpha = 2$ for a reflecting sail.

d. Magnetic Torques

To appreciate the magnitude of the magnetic torques available, consider, again, a satellite with a diameter of one meter. Suppose a coil of wire with N turns is wrapped around a great circle. Let R be the resistance of one turn and P the power used to create an electromagnet. Then the torque is

$$T = 1.8 \times 10^{-5} \sqrt{NP/R} \text{ newton meters.}$$

For example, if N = 1000, R = 1 ohm then a power of one milliwatt will generate a torque of 1.8×10^{-5} newton meters. This is about 300 times the torques due to radiation pressure (at 22°) or libration in the preceding section. Incidentally, in copper, the wire would be 0.01" in diameter and weigh about 2 lbs.

e. Magnetic Damping

Two different mechanisms for obtaining damping (induced current or eddy current loss and magnetic hysteresis) have been discussed qualitatively above. A thorough quantitative treatment has been given

by Fischell.[5] Most of the complexity in the analysis comes from adequately describing the earth's magnetic field encountered by the satellite as a function of time. The instantaneous rates of damping corresponding to a given value of magnetic are rather easily stated.

The voltage induced around a closed loop of a conducting material rotating in a magnetic field is

$$V = -A\, B_m\, \omega \cos \omega t \times 10^{-8},$$

where A is the area of the loop, B_m the maximum flux density in gauss, and ω is the angular velocity. If the loop does not enclose ferro-magnetic material, B_m is equal to H_m, the strength of the earth's field. Clearly, the effect of induced currents is enhanced greatly by the presence of ferro-magnetic material. If the resistance of the loop is R, the rate of decrease of rotational energy is

$$dE/dt = -V^2/R.$$

The actual value of dE/dt oscillates within one rotation of the satellite, but we need only the average rate. Since the average value of $\cos^2 \omega t$ is 1/2, the average value of dE/dt is

$$(dE/dt)_{ave} = -A^2 B_m^2 \omega^2 \times 10^{-16}/2R.$$

Among other conclusions to be drawn is that the effectiveness of this type of damping is proportional to the square of the permeability of the material within a conducting loop.

As indicated in the earlier qualitative discussion, this law for loss of energy leads to the law for spin deceleration

$$\dot{\omega} \propto -\omega.$$

Hence, by integration, ω decreases exponentially with time.

To get the overall time average of spin damping, the magnetic field must be properly averaged over the orbit of the satellite, and we shall not try to carry out this process here. The main conclusion, that the spin decreases exponentially on the average, is unaltered.

This type of magnetic damping is illustrated by the Vanguard I satellite (1958 β 2). This satellite contained almost no ferro-magnetic material, and the principal damping came from induced currents in the aluminum structure. The spin history of this satellite is shown in Fig. 3, taken from Fischell's reference. The fact that the plot is a straight line on semi-log paper shows that the spin decreases exponentially with time.

In hysteresis damping, the loss of energy per rotation of the satellite is

$$(V/4\pi) \oint H dB,$$

where V is the volume of the permeable material, and $\oint H dB$ is the area of the hysteresis loop of the material. Hence

$$dE/dt = -\omega(V/4\pi) \oint H dB.$$

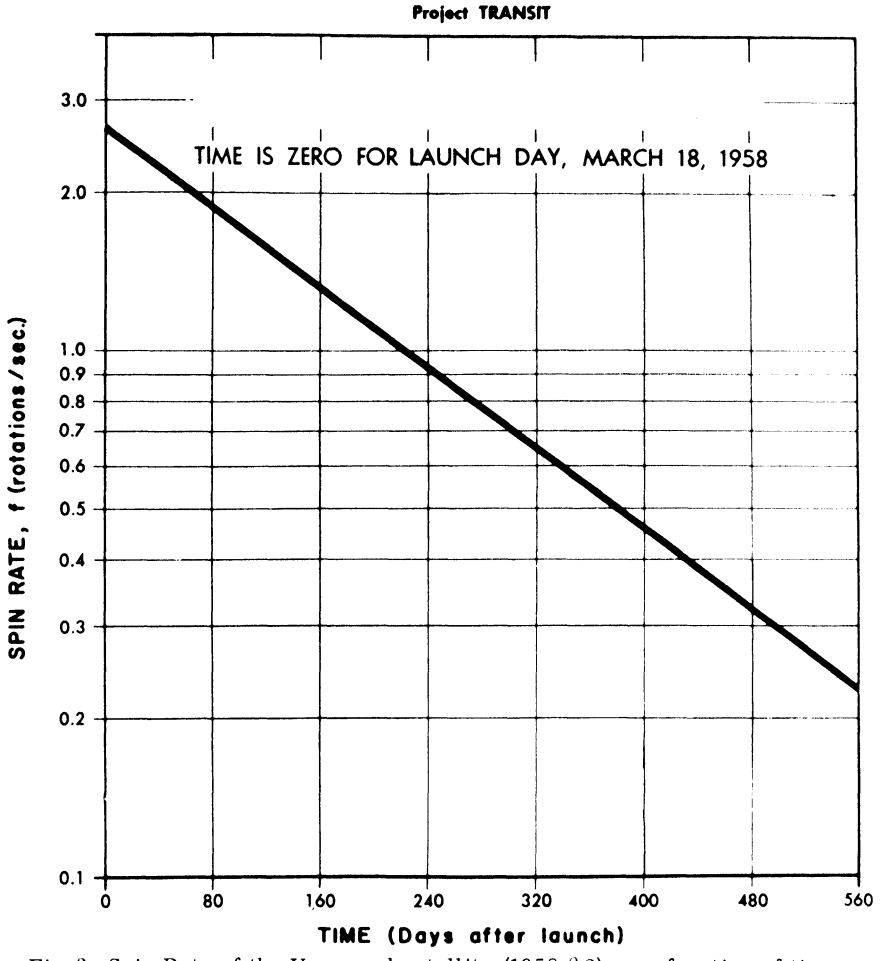


Fig. 3. Spin Rate of the Vanguard satellite (1958 β 2) as a function of time.

As stated earlier, this law for energy loss leads to a linear decrease of spin with time. Since the area of the hysteresis loop depends upon the field strength, it is again necessary to average the rate of decrease over all values of the magnetic field encountered by the satellite.

The TRANSIT satellites 1-B and 2-A have made use of hysteresis damping in addition to a yo-yo. The specifications of the magnetic systems in the two satellites are given in Table I (p. 225). Arrangement of magnetic material is shown in Fig. 4. The 2-A satellite actually contained some shorted coils surrounding magnetic material to give some induced current loss. However, there were not enough coils to make the induced current loss significant. Fischell[5] has estimated that the torque produced by the shorted coils was only about 10 per-

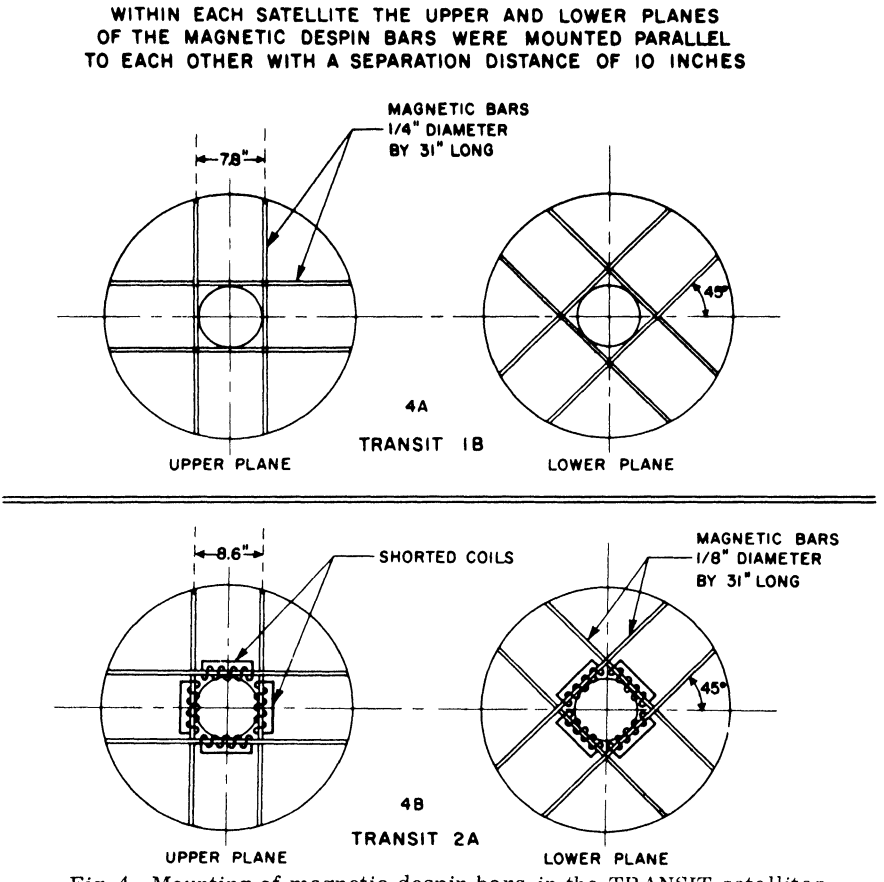


Fig. 4. Mounting of magnetic despin bars in the TRANSIT satellites.

cent of that due to hysteresis, even at the highest spin rate of the satellite, so that induced current loss can be neglected to first approximation.

The spin history of TRANSIT 1-B is shown in Fig. 5. The spin decreased linearly from launch for seven days, because of hysteresis. At this time, the yo-yo was released, decreasing the spin by about 97 percent. Following this time, the spin again decreased linearly until it was slightly more than 0.02 rps. The final spin rate expected was two revolutions per orbit, or about 0.0003 rps., caused by the permanent dipole moment of the satellite following the earth's field. Between these two rates, the spin rate was affected by both the hysteresis loss and the effect of the permanent moment, and the spin rate history became more complicated.

The spin history of TRANSIT 2-A is shown in Fig. 6. Again, we have a linear decrease for seven days, when the timer for the yo-yo

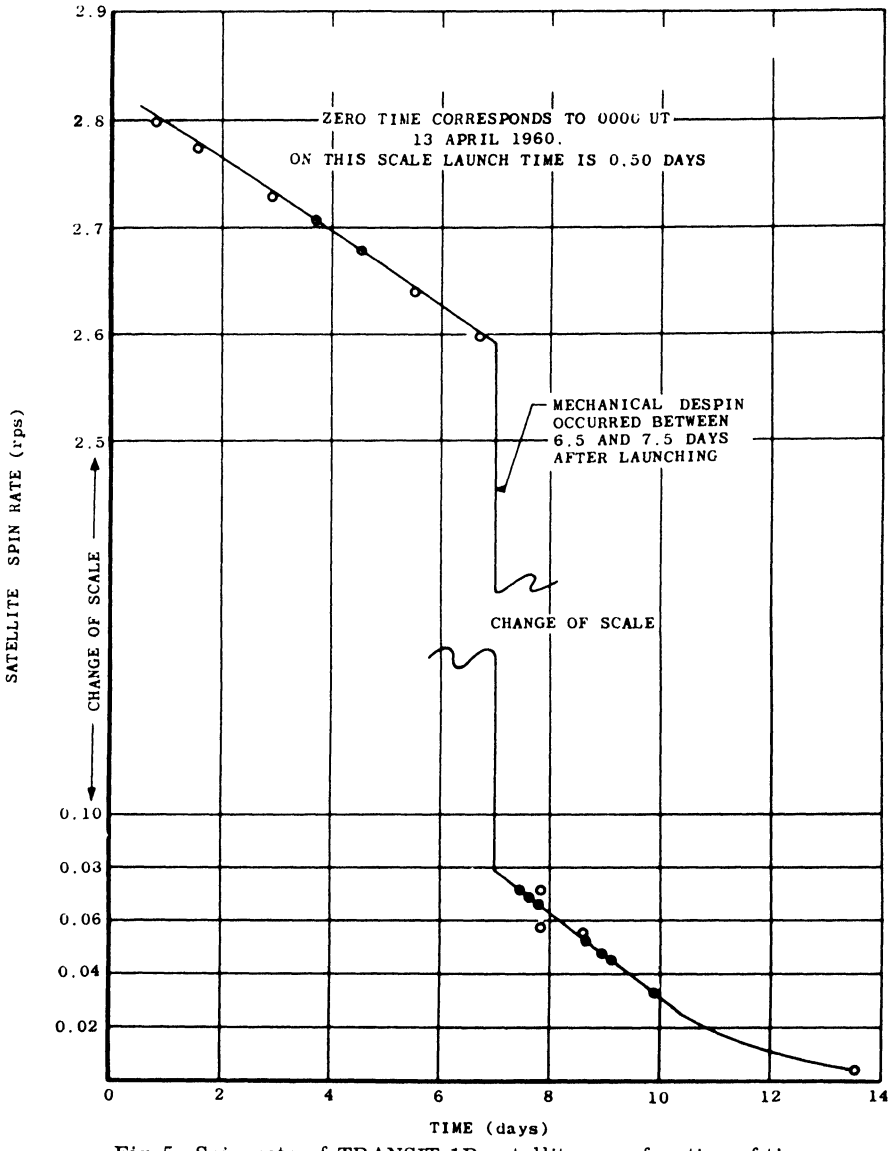


Fig. 5. Spin rate of TRANSIT 1B satellite as a function of time.

fired. This time, however, the initial spin rate of the satellite was only about 0.8 rps, which was on the low side of the nominal expected spin rate of 1.0 rps. Because of partial failure in the guidance system of the launching vehicle, the attitude and the perigee of the orbit were distinctly different from the desired objectives. As a result the effectiveness of the magnetic damping was increased so that at seven days

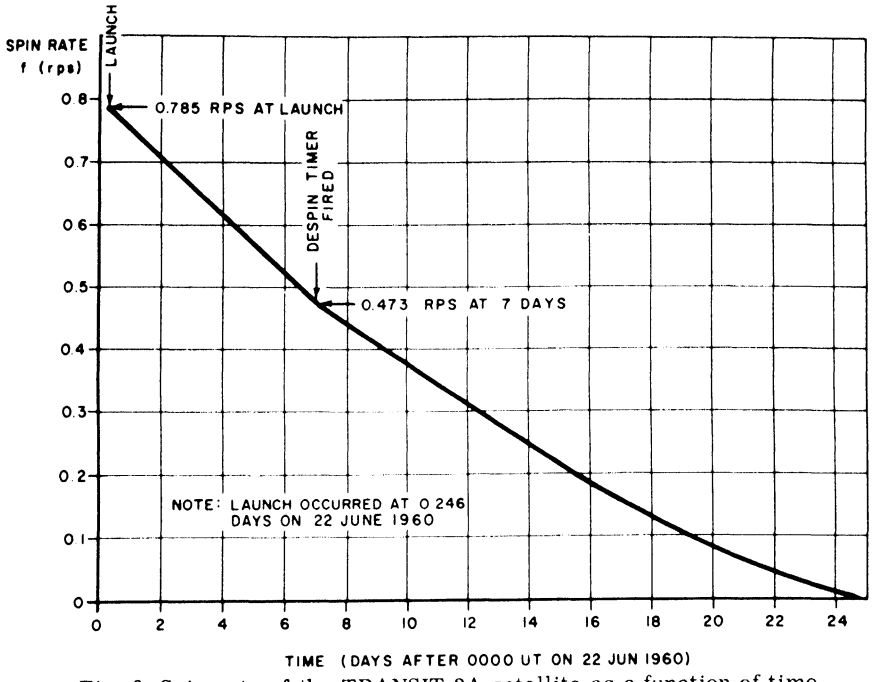


Fig. 6. Spin rate of the TRANSIT 2A satellite as a function of time.

after launching when the despin weights were to be deployed, the spin rate was lower than expected. As a result, the centrifugal force on the yo-yo masses was inadequate to allow them to break some small wires which were holding them in place. When the yo-yo actuator was fired it resulted merely in an angular impulse which caused some change in the attitude of the satellite. This change of attitude caused the magnetic despin devices to be slightly less effective thereby resulting in a lower slope evident seven days after launching, as shown in Fig. 6. Spin continued to decrease as a result of hysteresis until the satellite began to approach its final state of rotating with the earth's field. The failure of the yo-yo was not serious; the final result was merely delayed by about two weeks.

CONCLUSION

It is seen from the discussion in this chapter that there are a remarkable number of sources of appreciable torque on a nearby satellite of earth. Most of these torques are present to some degree for any satellite. The problem of stabilization or control of a satellite attitude then consists essentially of including provisions to enhance and control certain of these sources of torque sufficiently to overcome the disturbing effect of the remaining uncontrolled torques.

TABLE I
Specification and Experimental Results for Magnetic Despin Systems of the TRANSIT 1-B and 2-A Satellites

I. Specification	TRANSIT 1-B	TRANSIT 2-A
Number of bars	8	8π
Bar diameter	0.25 inches	0.125 inches
Bar length	31 inches	31 inches
*Length-to-diameter ratio	124	248
Weight per bar	0.48 lb.	0.12 lb.
†Bar material	AEM-4750	AEM-4750
Magnetic Properties (for H_m = 0.35 oersted)		
Permeability	2710	7670
Maximum flux density	950 gauss	2680 gauss
Coercive Force	0.035 oersted	0.074 oersted
Remanence	120 gauss	725 gauss
‡Hysteresis loop area	120 g-o	576 g-o
Bar resistivity	51.2 μ-ohm cm	51.2 μ-ohm cm
Number of shorted turns	0	173
Wire size	--	No. 18 AWG
Resistance of shorted coil	--	0.055 ohm
Satellite spin moment of inertia	9.62 slug ft^2	8.53 slug ft^2
Placement of bars in satellite	See Fig. 4-A	See Fig. 4-B

II. Experimental Results

A. The despin curve for TRANSIT 1-B is shown in Fig. 5.
B. The despin curve for TRANSIT 2-A is shown in Fig. 6

*See Fig. 7 (p. 226) for hysteresis loop of the bars for the L/D ratios of 124 and 248 used in TRANSIT 1-B and 2-A respectively.

† AEM-4750 is a trade name of the Allegheny-Ludlum Steel Corp. This material is an alloy of 47.5% nickel, 52.5% iron sometimes referred to as 47.5% permalloy. The nickel and iron are extremely high purity, melted in a vacuum and annealed in an atmosphere of dry hydrogen.

‡See Fig. 8 (p. 227) for the measured values of the hysteresis loop area as a function of peak magnetizing field.

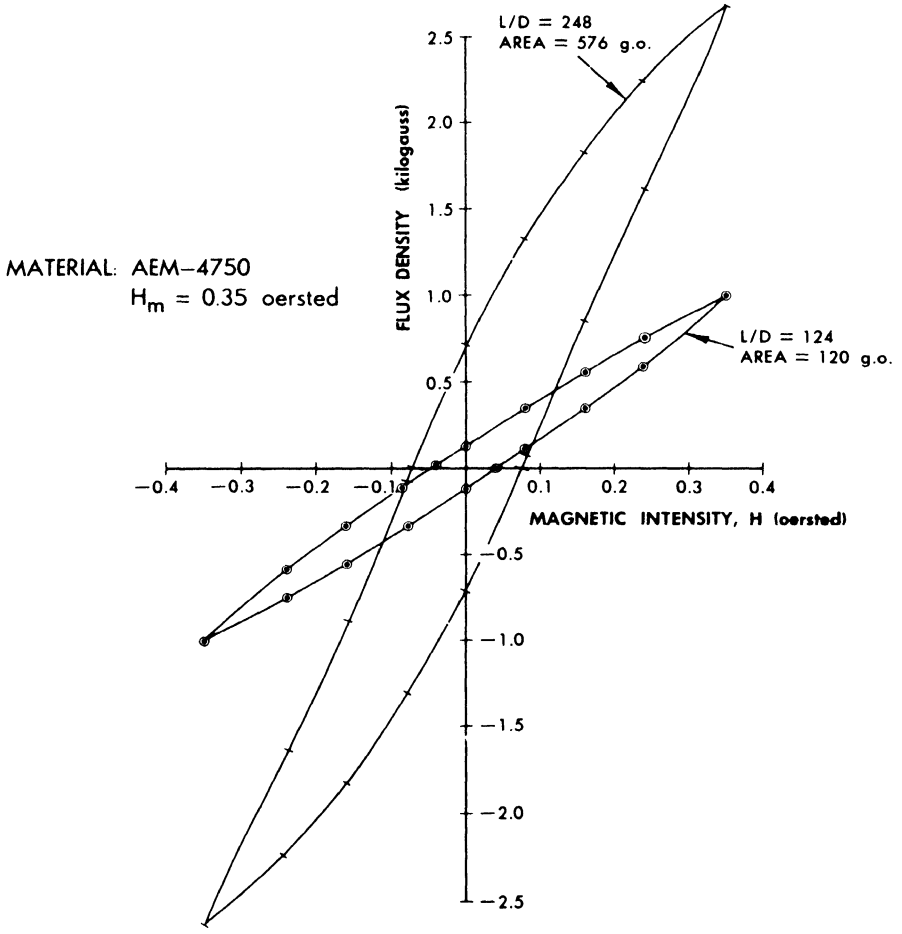


Fig. 7. Hysteresis loss as a function of L/D ratio.

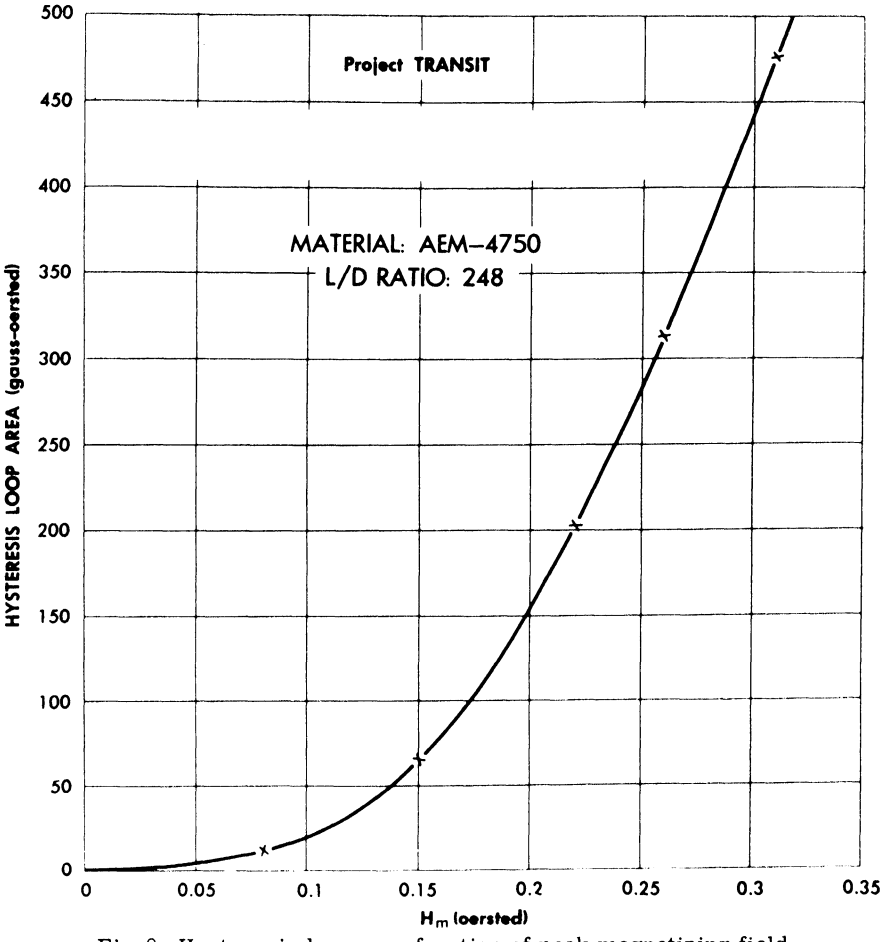


Fig. 8. Hysteresis loss as a function of peak magnetizing field.

REFERENCES

[1] Roberson, R. E., and Tatistcheff, D., "The Potential Energy of a Small Rigid Body in the Gravitational Field of an Oblate Spheroid," J. Franklin Inst., vol. 262, 1956, p. 209.

[2] Newton, R. R., "Method of Stabilizing an Astronomical Satellite," ARS Journal, vol. 29, 1959, p. 665.

[3] Roberson, R. E., "Attitude Control of a Satellite Vehicle—An Outline of the Problem," Proc. 8th Astronautical Congress, Springer-Verlag, Vienna, 1959, p. 317.

[4] Sohn, Robert L., "Attitude Stabilization by Means of Solar Radiation Pressure," ARS Journal, vol. 29, No. 5, May 1959, p. 371-373.

[5] Fischell, R. E., "Control of Earth Satellite Motions by Magnetic Devices," Applied Physics Laboratory Report TG 60-30, 1960.

15. CHOICE OF GRATING MOUNTINGS SUITABLE FOR A MONOCHROMATOR IN A SPACE TELESCOPE

Takeshi Namioka
Kitt Peak National Observatory,
Association of Universities for Research in Astronomy, Inc.

I. INTRODUCTION

Recent effort for the establishment of space telescopes above the earth's atmosphere will open the entire electromagnetic spectrum to observation. A space telescope will initially be concerned with the vacuum ultraviolet region which is of greatest astrophysical interest at the present time. Therefore, the design of the entire optical system is largely dependent upon the shortest wavelength to be used. Furthermore, a space telescope must work in a vacuum for its entire lifetime without the benefit of service. Reliability, therefore, is the prime requisite to the instrument system, and the best way to achieve reliability is to keep the system as simple as possible.

Although in this article we restrict our discussion to monochromators auxiliary to the space telescope, the prime requisite to monochromators is still reliability, i. e., simplicity. To design a monochromator suitable for a space telescope, it is most desirable to fulfill the following conditions: (1) The monochromator must provide a maximum resolution of at least 1 A; (2) it is desirable to have an f-number as low as that of a space telescope; (3) the wavelength coverage must be met with the requirement of a particular space telescope; (4) the direction of the line connecting centers of the entrance slit and of the grating must remain constant regardless of wavelength; (5) the position of the entrance slit must remain fixed; (6) the monochromator action should be achieved by a mechanism as simple as possible; and (7) the number of moving and adjustable parts should be minimized.

As the first step to determining the most suitable monochromator, we should examine very carefully all the grating mountings ever reported up to the present time, bearing in mind the conditions cited above. First of all, there is the question as to what kind of grating should be chosen as the main optical component. To our present knowledge on the reflecting power of coating materials in the vacuum ultraviolet region, we should think of spherical concave gratings first and then plane gratings. Despite technological difficulties, ellipsoidal concave gratings should also be considered with hope in the near future. For spherical (or ellipsoidal) concave gratings the following

mountings are known at present: (1) the Rowland mounting,[1-3] (2) the Abney mounting,[4] (3) the Wadsworth mounting,[5-8] (4) the Paschen-Runge mounting[9-12] (ordinary normal incidence-type mounting[13,14] is considered here as a special case of the Paschen-Runge mounting), (5) the in-plane Eagle mounting,[15-17] (6) the off-plane Eagle mounting,[18-21] (7) the grazing incidence mounting,[22-25] (8) the radius mounting (or Beutler mounting),[26-28] (9) the Seya-Namioka mounting,[29-31] and the Johnson-Onaka mounting.[32,33] For the use of plane gratings, only one mounting, the Ebert-Fastie mounting,[34-38] is worthwhile to be considered at present.

Since the over-all efficiency of the telescope plus the observing instruments must be maximized, the choice of the monochromator must be considered in close relationship to the telescope and other auxiliary instruments. In this article, however, we will not discuss any specific coupling scheme between the telescope and the monochromator except assuming simply that the telescope provides more than two simultaneous focal positions allowing efficient coupling of three or more instruments.

In the following sections, we review briefly the theory of the concave grating and then discuss the grating mountings cited above.

II. THEORY OF THE CONCAVE GRATING*

Before examining grating mountings, it is worthwhile to review the theory of the concave grating (both spherical[1,18,20,21,39-57] and ellipsoidal[58-60]) which provides necessary information on performance of a specific grating mounting. We treat the spherical concave grating first, then the ellipsoidal concave grating.

(1) Spherical Concave Grating

One approach to the theory of the aberrations of a concave grating geometrically is through the use of Fermat's principle. Let the origin O of the Cartesian coordinate system be the center of the grating rulings; let the z axis be parallel to the ruling, and let the x axis be the grating normal (see Fig. 1). A (x, y, z), B (x′, y′, z′), and P (u, w, l) are, respectively, an illuminated point on the entrance slit, a focal point, and any point on the grating rulings. w takes only discrete values, i.e., the ratio w/σ is an integer, where σ is the grating constant. For the sake of simplicity, we assume simple lines of zero width as the rulings; namely, we ignore the groove shape which would be important in the calculation of the intensity distribution in the spectrum.

For the ray APB the light path function F should be represented by

$$F = \overline{AP} + \overline{PB} + \frac{wm\lambda}{\sigma}, \tag{1}$$

where λ is the wavelength and m the spectral order. According to

*For details of the calculations in this section, refer to references 57 and 59.

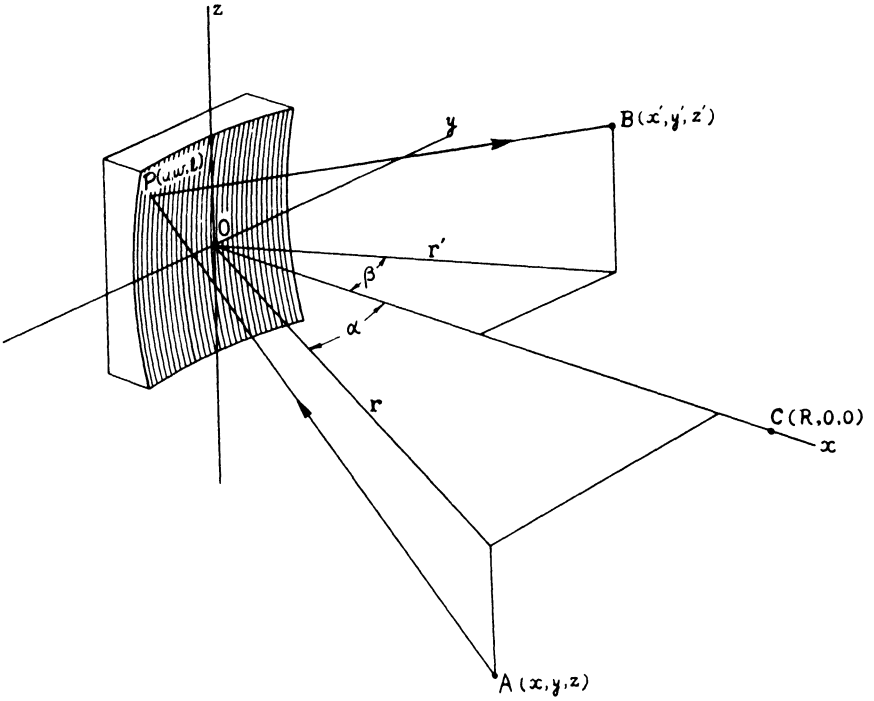


Fig. 1. Schematic diagram of the optical system. A (x, y, z) is an illuminated point on the entrance slit; B (x′, y′, z′) is an image point; and P (u, w, l) is a point on the grating rulings. The origin, O, of the cartesian coordinate system is the center of the grating rulings and C (R, 0, 0) is the center of curvature of the grating. α and β are the angles of incidence and diffraction, respectively, both measured in the xy plane. The signs of α and β are opposite if A and B lie on different sides of the xz plane. r and r′ are the distances between the center of the grating rulings and the projected points of A and B on the xy plane, respectively. R is the radius of curvature of the grating.

Fermat's principle, the focal point B is located so that F will be an extreme for any point P on the grating rulings, namely,

$$\frac{\partial F}{\partial w} = 0 \tag{2}$$

and

$$\frac{\partial F}{\partial l} = 0 \tag{3}$$

If (2) and (3) could be satisfied simultaneously by any pair of w and l for the fixed point B, then B would be the point of perfect focus. Since $\partial F/\partial w$ and $\partial F/\partial l$ are still functions of w and l, these functions may not be made zero for the fixed point B unless the constant term and all coefficients of w and l involved in $\partial F/\partial w$ and $\partial F/\partial l$ are identically zero. A ray diffracted from P goes into the direction

specified by β and z'/r' which are determined by (3) and (4), where $r' = (x'^2 + y'^2)^{1/2}$. Since β and z'/r' are functions of w and l, this direction of the diffracted ray changes slightly with the position of P. Therefore, when the point P wanders over the ruled area of the grating, diffracted rays fall on slightly different points on the focal plane. In order to produce an image with least aberration, the dependence of β and z'/r' on w and l must be minimized. This can be done by taking

$$r = R \cos \alpha \quad \text{and} \quad r' = R \cos \beta, \tag{4}$$

or

$$r = \infty \quad \text{and} \quad r' = \frac{R \cos^2 \beta}{\cos \alpha + \cos \beta}, \tag{5}$$

where $r = (x^2 + y^2)^{1/2}$. Equation (4) represents a cylindrical surface of diameter R, i.e., the Rowland cylinder whose intersection with the xy plane is the Rowland circle. Equation (5) expresses the focal condition for the Wadsworth mounting. Therefore, we can obtain the minimum aberration in the Wadsworth mounting or in mountings using the Rowland cylinder.

Since the aberrations produced by finiteness of the ruled area become smaller and smaller as w and l tend to zero, we may set the constant terms in (2) and (3) to zero for the central ray AOB:

$$\sigma (\sin \alpha + \sin \beta_0) \left(1 + \frac{z^2}{r^2}\right)^{-1/2} = m \lambda \tag{6}$$

and

$$\frac{z}{r} = - \frac{z_0'}{r'}, \tag{7}$$

where (r', β_0, z_0') are the cylindrical coordinates of the image point for the central ray. Equations (6) and (7) give the grating equation and the geometrical relation between the point light source and the image point for the central ray.

Substituting (4), (6), and (7) into (2) and (3), we obtain for a finite illuminated length of the entrance slit

$$\left(\frac{\partial F}{\partial w}\right)_0 - \cos \beta_0 \cdot \Delta\beta = 0 \tag{2'}$$

and

$$\left(\frac{\partial F}{\partial l}\right)_0 - \frac{1}{R}\left(\frac{\Delta z}{\cos \alpha} + \frac{\Delta z'}{\cos \beta_0}\right) = 0, \tag{3'}$$

where $z = z_0 + \Delta z$, $z' = z_0' + \Delta z'$ and z_0 and z_0' are the z coordinates of the center of the entrance slit and of corresponding image point for the central ray. Solving (2') and (3'), the amount of deviations of the image point from the focal point of the central ray in the direction

of run of the spectrum and in the direction perpendicular to run of the spectrum are, respectively, expressed by

$$\Delta\lambda = \frac{\sigma}{m}\left(\frac{\partial F}{\partial w}\right)_0 \tag{8}$$

in units of wavelength, and

$$\Delta z' = R\cos\beta_0\left(\frac{\partial F}{\partial l}\right)_0 \tag{9}$$

in units of actual length, to a very good approximation. By solving (8) and (9) simultaneously the equation of the image may be obtained. It should be noted that if $z_0 \neq 0$, then (8) can be minimized by rotating the entrance slit from the position where the slit is parallel to the grating rulings by the amount given by

$$\varphi = \frac{z_0}{R}\tan\alpha_0 \sec\alpha_0, \tag{10}$$

where α_0 is the angle of incidence measured at the center of the slit.

Assuming the actual grating width is always not wider than the optimum width, which will be discussed later, we obtain from (9) the length of the astigmatic image per unit length of the rulings for a point light source as

$$\frac{[z']_{ast}}{L} = \sin^2\alpha\,\frac{\cos\beta_0}{\cos\alpha} + \sin^2\beta_0, \tag{11}$$

where L is the total length of the grating rulings.

In order to obtain good definition and reasonably strong intensity, we must examine the limitation imposed on the grating width. A good measure of the optimum grating width may be obtained from the width of the first Huyghens zone on the grating at $l = 0$ for $\Delta z = \Delta z' = 0$. Under these conditions, the optimum grating width is given by

$$W_{opt} = 2.12\left[\left\{\frac{4z_0^4}{\cos^4\alpha} + \frac{2R^3\sigma}{m}\tan\left(\frac{\alpha+\beta_0}{2}\right)\frac{\cos\alpha\cos\beta_0}{1-\cos\alpha\cos\beta_0}\left(1+\frac{z_0^2}{R^2\cos^2\alpha}\right)^{-1/2}\right\}^{1/2} - \frac{2z_0^2}{\cos^2\alpha}\right]^{1/2} \tag{12}$$

If the optical components do not lie on the Rowland cylinder, the optimum grating width is limited to a much smaller value than that given by (12) and only a measure of it may be given without going through complicated calculations based on physical optics. Contrary to concave gratings, plane gratings have no such theoretical limitation on their widths.

The theoretical optimum resolving power is given by

$$\mathcal{R}_{opt} = 0.92\,\frac{m}{\sigma}\,W_{opt} \tag{13}$$

for the in-plane mountings in which the centers of the optical components lie on the Rowland circle, and

$$\mathcal{R}_{opt} = 0.95 \frac{m}{\sigma} W_{opt} \tag{14}$$

for the off-plane mountings in which the center of the optical components lie on the Rowland cylinder but not on the Rowland circle. It is, in general, very cumbersome to compute the optimum resolving power for the case where optical components do not lie on the Rowland cylinder. For plane grating, theoretical resolving power is always given by

$$\mathcal{R} = \frac{m}{\sigma} W \tag{15}$$

for a given width W.

(2) Ellipsoidal Concave Grating

For the case of the ellipsoidal concave grating we add the following assumptions to those for the spherical concave grating: (1) The axes of the ellipsoid coincide with the Cartesian coordinate axes, and (2) the centers of all the optical components lie on the Rowland plane, i.e., the xy plane. Following the same procedure as that for the spherical concave grating, we obtain the results: The focal condition is given by

$$r = \frac{b^2}{a} \cos \alpha \quad \text{and} \quad r' = \frac{b^2}{a} \cos \beta \tag{16}$$

or

$$r = \infty \quad \text{and} \quad r' = \frac{b^2 \cos^2 \beta}{a(\cos \alpha + \cos \beta)}, \tag{17}$$

and the grating equation is

$$\sigma(\sin \alpha + \sin \beta_0) = m \lambda, \tag{18}$$

where a and b are lengths of the semi-axes of the ellipsoid in the directions of the x- and y- axis, respectively. Under the focal condition (16) we obtain the following equations: Amount of astigmatism is expressed by

$$\frac{[z']_{ast}}{L} = (1 + \sec \alpha \cos \beta_0) \left| 1 - \frac{b^2}{c^2} \cos \alpha \cos \beta_0 \right|, \tag{19}$$

and the optimum grating width is

$$W_{opt} = 2.12 \left[\frac{2R^3 \sigma}{m} \tan \left(\frac{\alpha + \beta_0}{2} \right) \frac{\cos \alpha \cos \beta_0}{1 - \frac{b^2}{a^2} \cos \alpha \cos \beta_0} \right]^{1/4}, \tag{20}$$

where c is length of the semi-axis of the ellipsoid in the direction of

the z-axis. As can be seen from (19), the ellipsoidal concave grating shows stigmatic images at the point for which

$$\frac{b^2}{c^2} = \sec\alpha \sec\beta_0 \tag{21}$$

is satisfied. In the region where

$$\cos\beta_0 \leq \frac{2c^2}{b^2 + c^2} \sec\alpha \tag{22}$$

is valid, the ellipsoidal concave grating gives less astigmatism (for $a = c \neq b$ or $a = b \neq c$) and wider grating width (for $a = c \neq b$) than the spherical concave grating does.

For $b = c$, nothing is gained by the use of the ellipsoidal concave grating, but for $a = b \neq c$ it provides less astigmatism and for $a = c \neq b$ less astigmatism and wider optimum grating width are obtained. The ellipsoidal concave grating shows much better optical performance over the spherical one, especially in the grazing incidence and in the case that the sum of the angles of incidence and diffraction is constant, but not much advantage is obtained for the small angles of incidence.

III. GRATING MOUNTINGS

Since all of the mountings of the concave grating, except those of Wadsworth, Seya-Namioka, and of Johnson-Onaka, are adaptations of the principle, that all the optical components lie on the Rowland circle, originally stated by Rowland in 1883, optical characteristics of such mountings can be calculated by the equations derived in the previous section.

Since the advantages of using the ellipsoidal concave grating are appreciable only in the grazing incidence mounting and in the Seya-Namioka mounting, the numerical data presented in this section are mostly for the spherical concave grating unless mentioned otherwise.

(1) The Rowland Mounting

The characteristics of this mounting can be seen from Fig. 2 without any detailed explanation. The mounting shows the constant linear dispersion of σ/mR A/mm, e.g., 8.3 A/mm for $R = 1$ m, $\sigma = 1/1200$ mm, $m = 1$. Despite this advantage, the mounting is somewhat cumbersome, and the fact that the grating and exit slit both move quite a distance is a disadvantage. To cover the spectral range 500-4500 A the grating and the exit slit must move along their rails about 15.6 cm and 48 cm, respectively, for $R = 1$ m and $\sigma = 1/1200$ mm. These distances determine the size of the monochromator.

Since $\beta_0 = 0$ and $z_0 = 0$ in this mounting, (6), (11), and (12) are reduced to

$$\sigma \sin \alpha = m\lambda,$$

$$[z']_{ast}/L = \sin \alpha \tan \alpha,$$

and

$$W_{opt} = 2.12\left[\frac{2R^3\sigma}{m}\cot \alpha\right]^{1/4}$$

Figures 3 and 4 show all the important optical properties of this mounting, i.e., the values of λ, $[z']_{ast}/L$, and W_{opt} as functions of α.

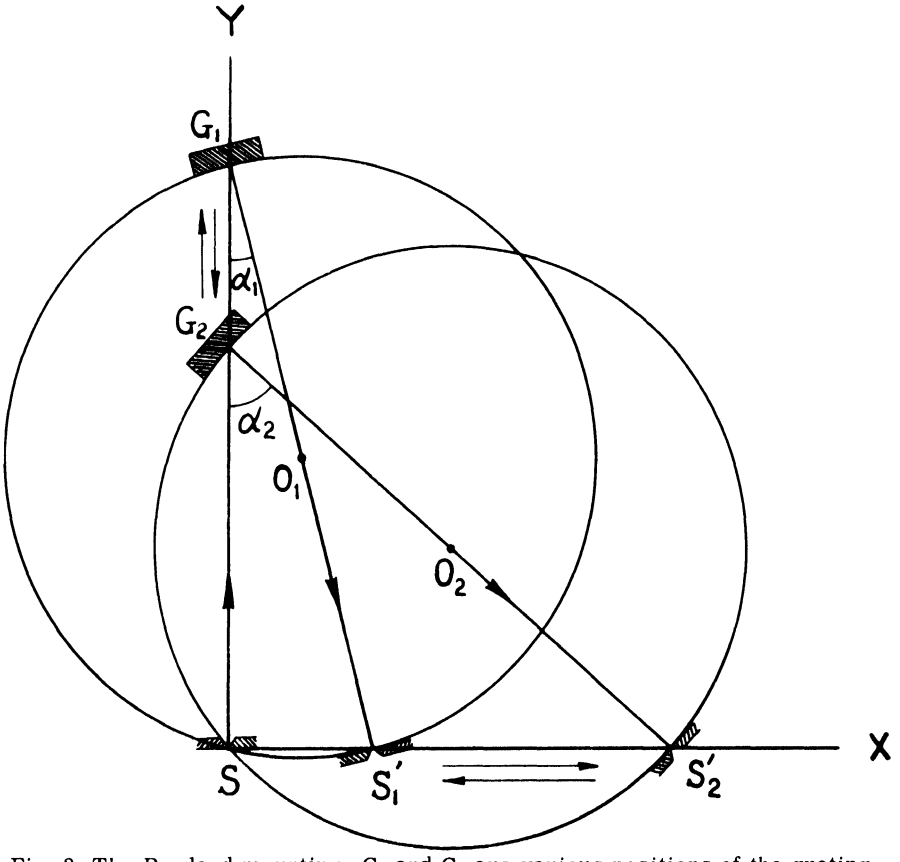


Fig. 2. The Rowland mounting. G_1 and G_2 are various positions of the grating center along the rail YS; S_1' and S_2' are various positions of the exit slit along the rail SX; and G_1S_1' and G_2S_2' are various positions of the bar on which both the grating and the exit slit are rigidly mounted. The length of the bar is equal to the radius of the grating. Both ends of the bar are held on carriages that run on rails, SX and SY, placed at right angles to one another. S is the fixed entrance slit; O_1 and O_2 are various positions of the center of the Rowland circle; and α_1 and α_2 are various angles of incidence. The angle of diffraction is always zero.

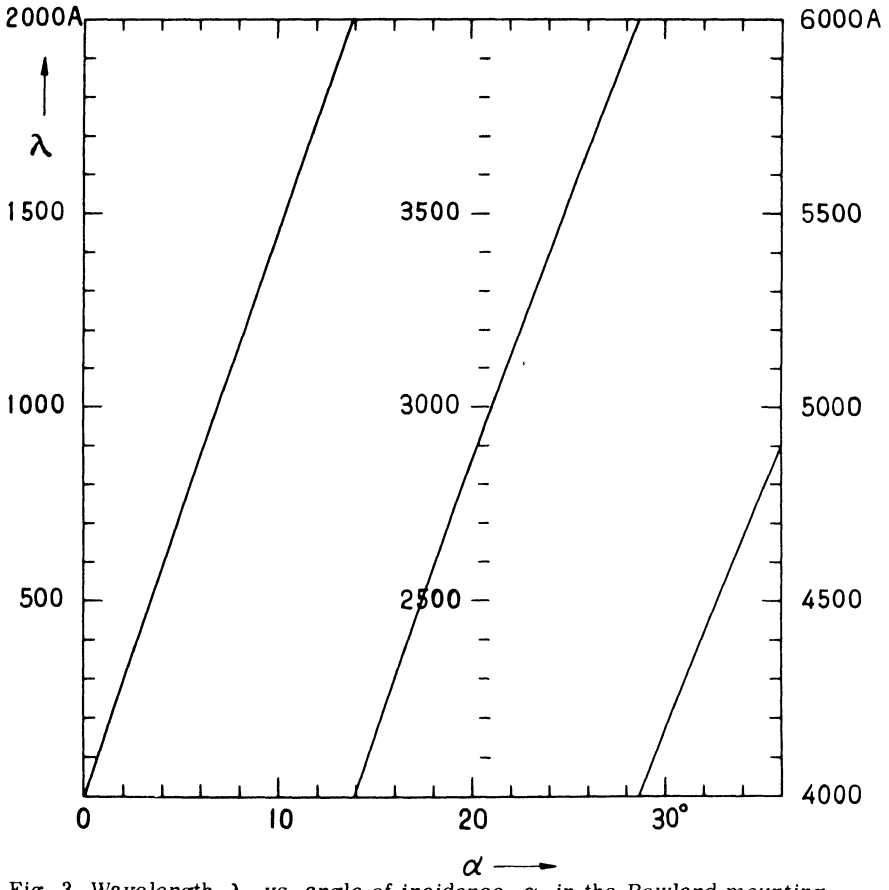


Fig. 3. Wavelength, λ, vs. angle of incidence, α, in the Rowland mounting. A 1200 grooves/mm grating and the first order are assumed here.

(2) The Abney Mounting

This mounting, shown in Fig. 5, is a variant of the Rowland mounting and the optical properties are, therefore, identical with those of the Rowland mounting (see Figs. 3 and 4).

Whenever a change of wavelength is required, the light source and the entrance slit must move. This cannot be met within our requirements (the conditions 4 and 5 in INTRODUCTION). In conclusion, the Abney mounting is definitely not suited to our purpose.

(3) The Wadsworth Mounting

This mounting, in which the Rowland circle is not utilized, is shown in Fig. 6. Since $\beta_0 = z_0 = 0$, the grating equation is identical with that of the Rowland mounting, namely,

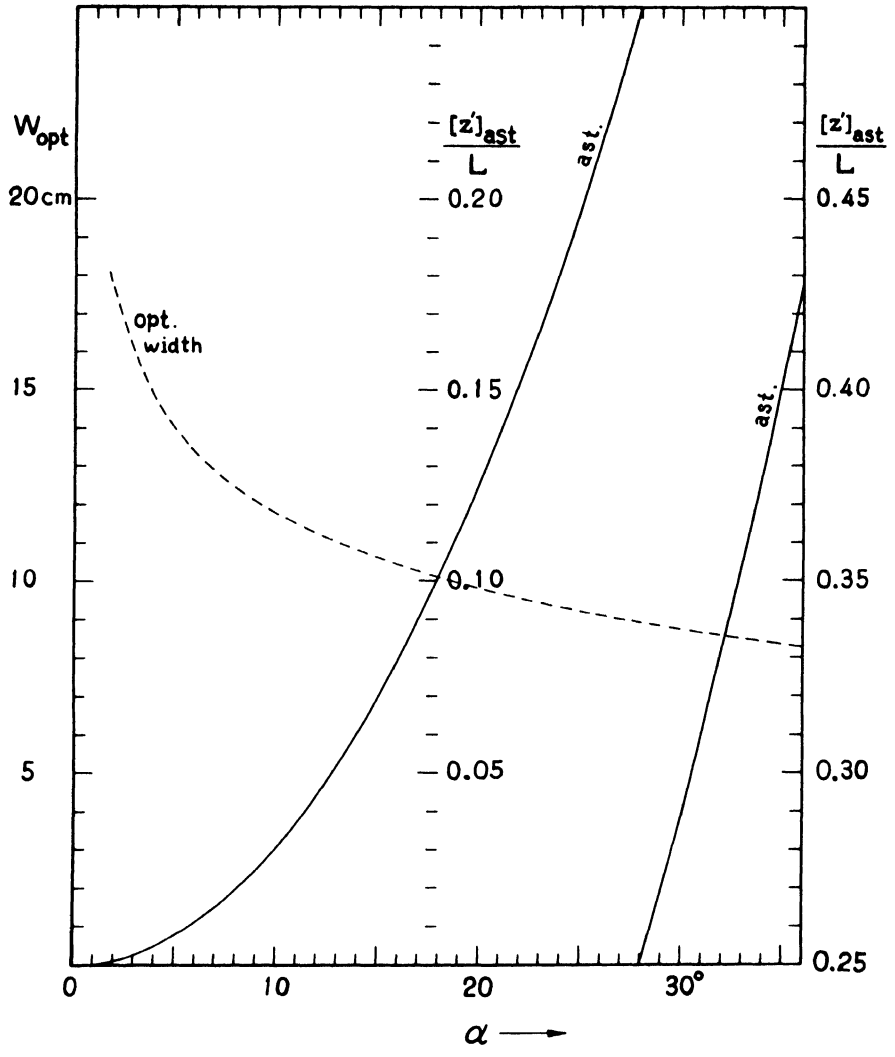


Fig. 4. The optimum grating width, W_{opt}, and the length of astigmatic image for a point light source per unit length of the grating rulings, $[z']_{ast}/L$, in the Rowland mounting. A 1 m grating with 1200 grooves/mm and the first order are assumed. α is the angle of incidence.

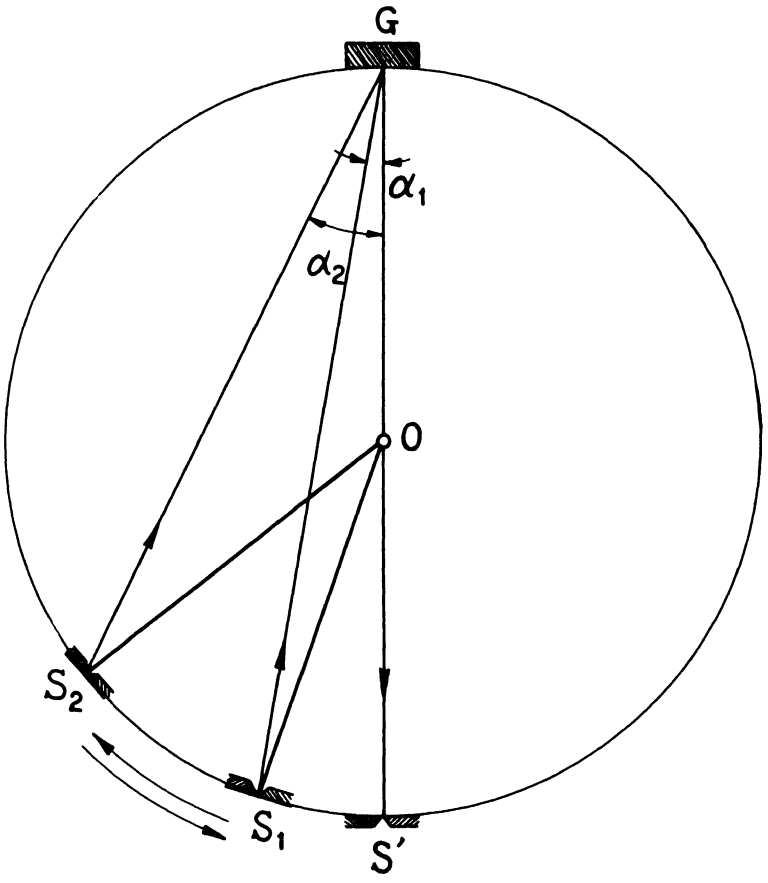


Fig. 5. The Abney mounting. G is the fixed grating; S′, the fixed exit slit; O, the center of the Rowland circle and the pivot point of the radius bar OS; S_1 and S_2, various positions of the entrance slit mounted on the radius bar; OS_1 and OS_2, various positions of the radius bar whose length is equal to the radius of the Rowland circle; and α_1 and α_2, various angles of incidence. The diffraction angle is always zero.

$$\sigma \sin \alpha = m \lambda ,$$

thus, the relation between λ and α is easily seen from Fig. 3. The major advantage of this so-called stigmatic mounting is that astigmatism vanishes on the grating normal. Also, since the grating is used at about half the image distance, the spectrum is made correspondingly brighter than the spectrum of the same grating in the Rowland circle mounting. However, the focal distance of the grating varies with wavelength as

$$r' = \frac{R}{1 + \cos \alpha} \qquad (5')$$

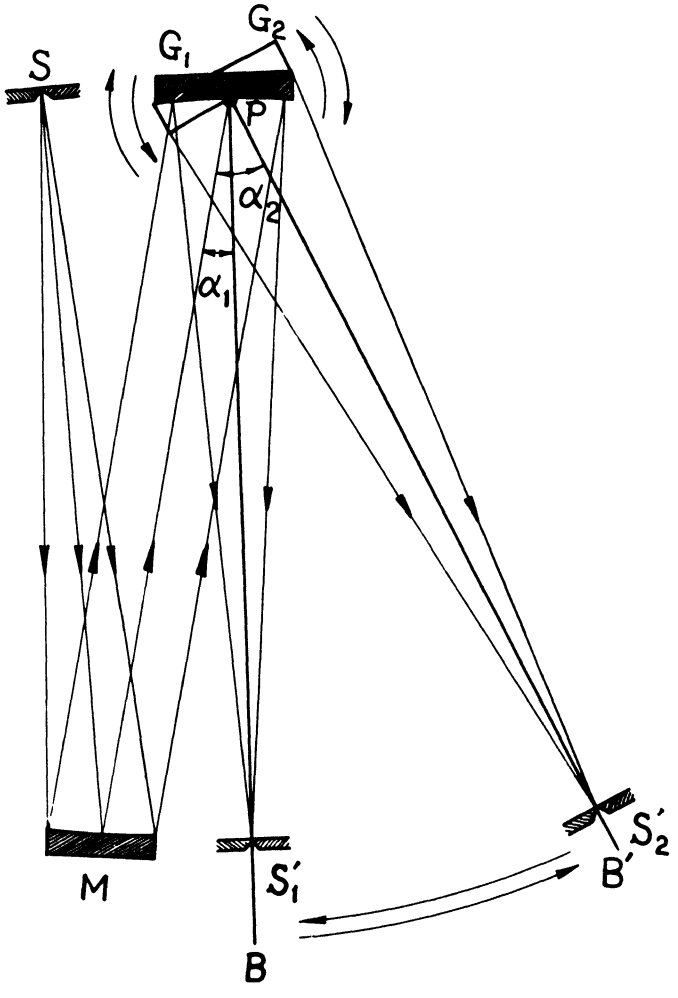


Fig 6. The Wadsworth mounting. S is the fixed entrance slit; M, the fixed collimating mirror; G_1 and G_2, various positions of the grating; P, the center of the grating and the axis of rotation of the grating; PB and PB′, various positions of the bar along which the exit slit slides; S_1' and S_2', various positions of the exit slit; and α_1 and α_2, various angles of incidence. The angle of diffraction is always zero.

at the grating normal, and this fact makes the mechanism, which performs monochromator action, more complicated. Table I shows variation of r' with the angle of incidence α.

In addition to this fact, utilization of this mounting depends entirely on the optical characteristics of the collimating system. The position of the mirror must be considered very carefully in the design of a

TABLE I.

Focal distances on the grating normal in the Wadsworth mounting for various angles of incidence. α, r', and R are the angles of incidence, focal distance, and radius of curvature of the grating, respectively.

$\alpha°$	r'/R	$\alpha°$	r'/R	$\alpha°$	r'/R	$\alpha°$	r'/R
1	0.50004	11	0.5046	21	0.5172	31	0.5385
2	0.50015	12	0.5055	22	0.5189	32	0.5411
3	0.50034	13	0.5065	23	0.5207	33	0.5439
4	0.5006	14	0.5075	24	0.52259	34	0.5467
5	0.5010	15	0.5087	25	0.5246	35	0.5497
6	0.5014	16	0.5099	26	0.5267	36	0.5528
7	0.5019	17	0.5112	27	0.5288	37	0.5560
8	0.5024	18	0.5125	28	0.5311		
9	0.5031	19	0.5140	29	0.5334		
10	0.5038	20	0.5156	30	0.5359		

monochromator in such a way that it does not cut any part of diffracted rays of desired wavelengths. This requirement sets the shortest wavelength limit available in the mounting. Furthermore, the allowed width of the collimating spherical mirror is determined by

$$W_m = \left(\frac{\rho^2 \lambda}{\sin\theta}\right)^{1/3}, \tag{23}$$

where θ and ρ are the angle of incidence and the radius of curvature of the mirror, respectively. Since in practice we choose the mirror setting such that $\rho = R$, and $\sin\theta \simeq W_m/R$, (23) is reduced to

$$W_m \simeq (R^3 \lambda)^{1/4}. \tag{24}$$

The values of W_m are listed in Table II as a function of R and λ. As is easily seen from Table II, we cannot hope to construct a monochromator suitable for our purpose using a concave mirror as a collimating system.

The optimum grating width is given by

$$W_{opt} = 2\left[\frac{2R^3\sigma}{m} \tan\frac{\alpha}{2} \sec^2\alpha\right]^{1/4}, \tag{25}$$

TABLE II.

Allowed width of collimating spherical concave mirror. R and λ are the radius of curvature of the grating and wavelength, respectively.

R \ λ	500A	1000A	2000A	3000A	6000A
2 m	2.51 cm	2.99 cm	3.56 cm	3.94 cm	4.68 cm
3 m	3.41 cm	4.05 cm	4.82 cm	5.33 cm	6.34 cm

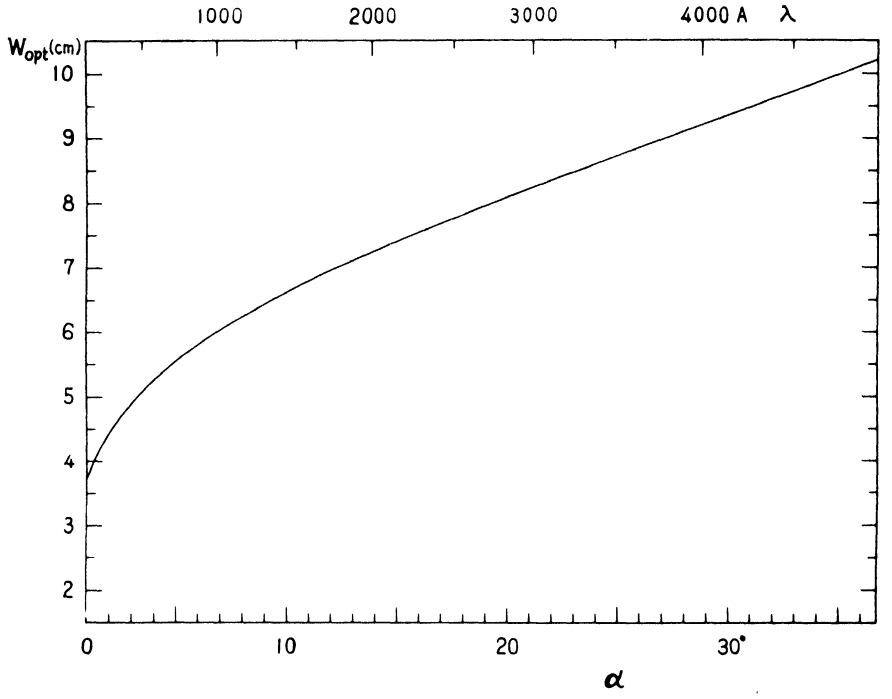


Fig. 7. Optimum grating width, W_{opt}, in the Wadsworth mounting. R = 2m, σ = 1/12000 cm, and m = 1 are assumed here, where R is the radius of curvature of the grating, σ is the grating constant, and m the spectral order. α is the angle of incidence, and λ the wavelength.

because β_0 is always kept zero. Equation (25) is shown graphically in Fig. 7 for R = 2 m, σ = 1/1200 mm, and m = 1. Since $W_{opt} > W_m$, the f-number of this system is dependent upon the proper choice of an aspherical collimating mirror.

(4) The Paschen-Runge Mounting

To utilize this mounting as a monochromator, the exit slit must move along the Rowland circle as is seen in Fig. 8. For our present purpose, there are two possibilities in choosing the angle of incidence: Normal incidence and grazing incidence. The former gives high resolution and the latter provides the highest reflectivity and high dispersion in the vacuum ultraviolet. In this section we treat only the normal incidence type and will discuss the grazing incidence type in a separate section.

In Fig. 9, wavelengths are plotted as a function of the angle of diffraction for various angles of incidence. In each case the optimum

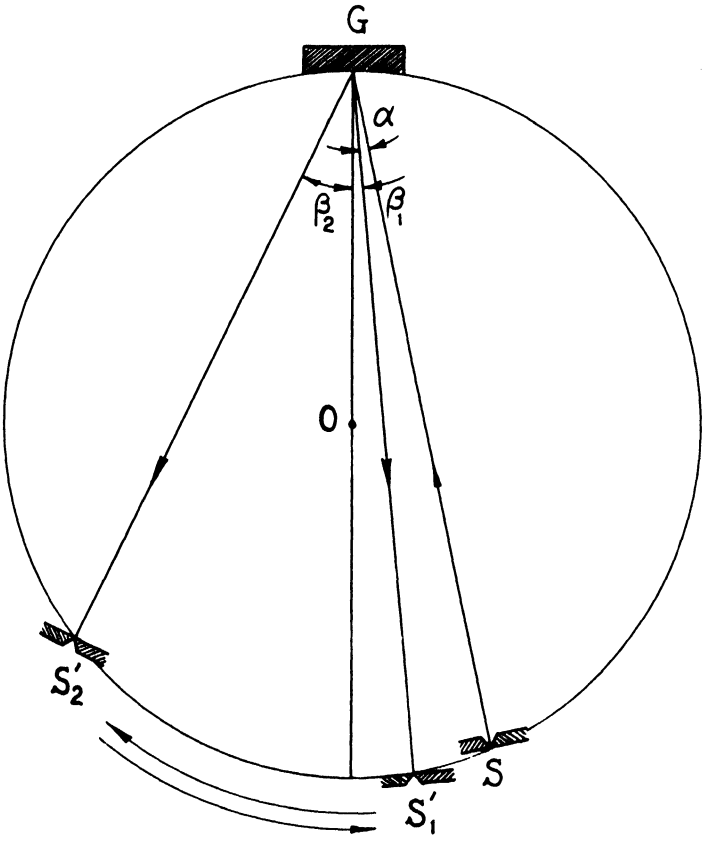


Fig. 8. The Paschen-Runge mounting. To perform a monochromator action, the exit slit moves along the Rowland circle. G is the fixed grating; O, the center of the Rowland circle; S, the fixed entrance slit; S_1' and S_2', various positions of the exit slit; α, the angle of incidence, constant; and β_1 and β_2, various angles of diffraction.

grating width and the length of the astigmatic image are shown graphically in Figs. 10 and 11, respectively.

As is easily seen from Figs. 10 and 11, at the positive spectrum side we have less astigmatism and wider optimum grating widths than those at the negative spectrum side. Choice of the proper angle of incidence depends largely upon the coupling scheme of the telescope system to the monochromator and other instruments. Therefore, without specific knowledge on the coupling scheme, it cannot be said which angle is the best.

(5) The In-Plane Eagle Mounting

In this mounting $\alpha \simeq \beta_0$ and this provides the least astigmatism and widest optimum grating width up to the wavelength limited by the grating constant.

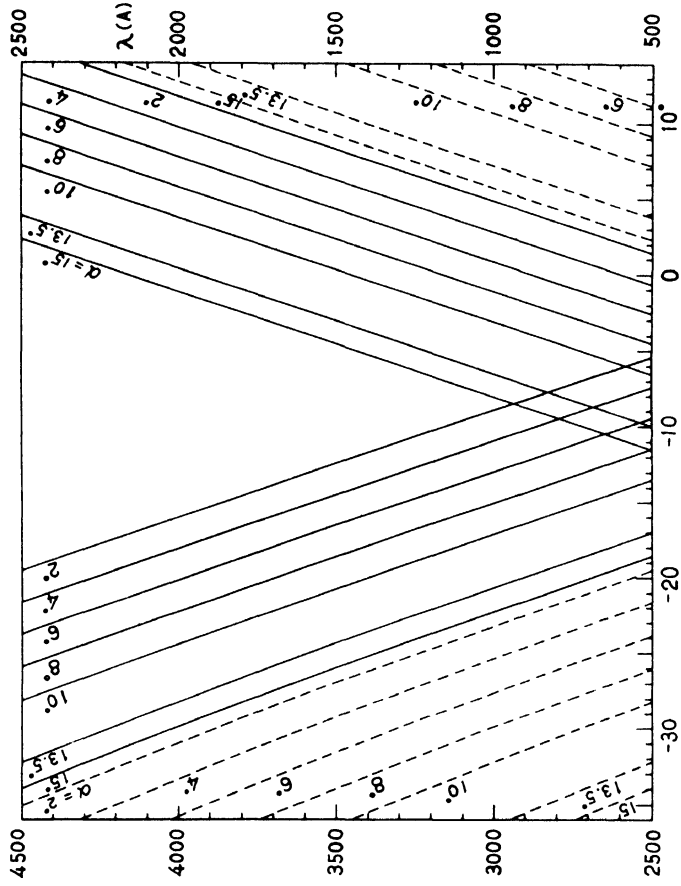


Fig. 9. Wavelength, λ, vs. angle of diffraction, β_0, in the normal incidence mounting. A 1200 grooves/mm grating and the first order are assumed. Use the right ordinate for the solid curves and the left ordinate for the dotted curves. α is the angle of incidence.

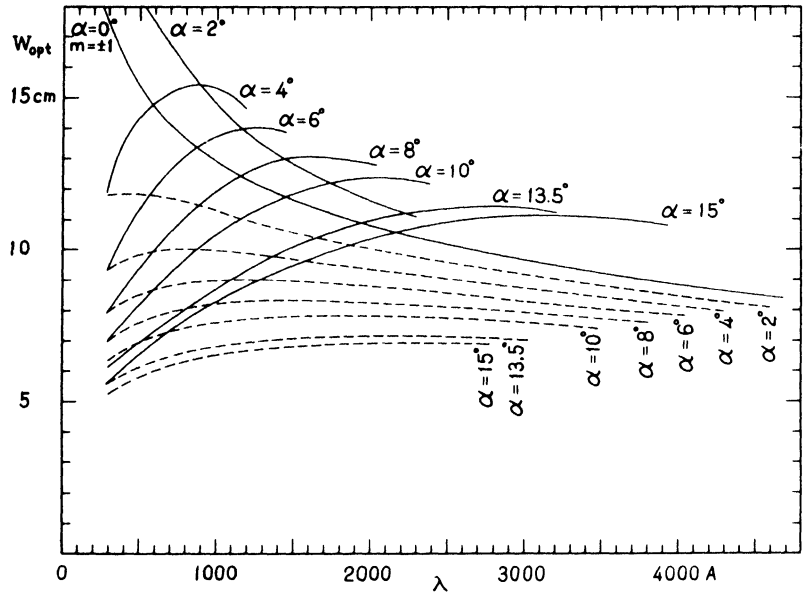


Fig. 10. Optimum grating width, W_{opt}, vs. wavelength, λ, in the normal incidence mounting. Angle of incidence, α, is taken as a parameter. Graphs are shown both for m = + 1 (solid curves) and m = − 1 (dotted curves), where m is the spectral order.

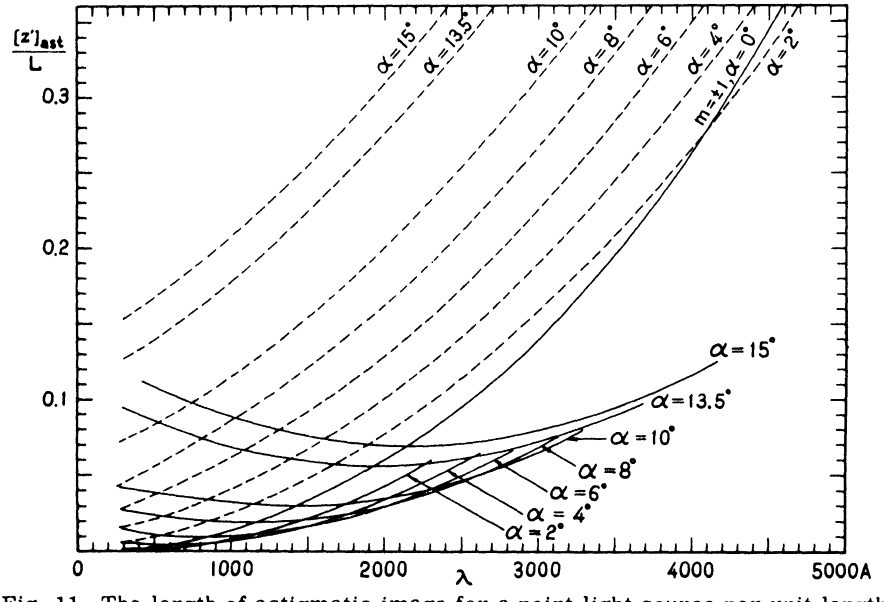


Fig. 11. The length of astigmatic image for a point light source per unit length of the grating rulings, $[z']_{ast}/L$, in the normal incidence mounting. Graphs are shown for several angles of incidence, α, and also for m = + 1 (solid curves) and m = − 1 (dotted curves), where m is the spectral order.

Assuming $\beta_0 = \pm 3°$ for $\alpha = 0°$, e.g., $\overline{SS_1'} = 5.23$ cm for R = 1 m, which provides enough space to place a detector behind the exit slit, we can calculate the wavelengths, optimum grating widths, and astigmatism for various angles of incidence. These values are shown graphically in Figs. 13 and 14.

If the coupling of the monochromator to the telescope system leaves enough space behind the exit slit to place detectors, this mounting gives the most desirable optical performance (Fig. 14). The scanning mechanism looks complicated (Fig. 12), but can be operated by a fairly simple link motion. We can also set two exit slits with different widths at both sides of the entrance slit, and both exit slits can be brought into exact focus simultaneously by one link motion. This adds another attractive feature to this mounting.

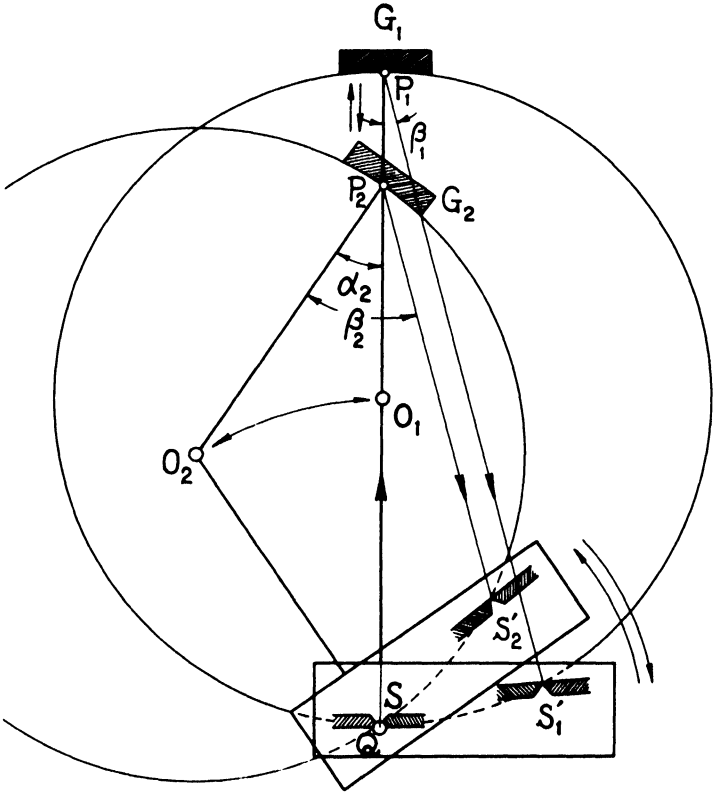


Fig. 12. The In-plane Eagle mounting. G_1 and G_2 are various positions of the grating whose motion is constrained along the rail G_1S; P_1 and P_2, various positions of the pivot point for grating rotations; O_1 and O_2, various positions of the center of the Rowland circle; S_1' and S_2', various positions of the exit slit; S, the fixed entrance slit; Q, the pivot point for exit slit rotation; $\alpha_1 = 0$ and α_2, various angles of incidence; β_1 and β_2, various angles of diffraction; and P_1O_1, O_1S, P_2O_2, and O_2S, various positions of link arms.

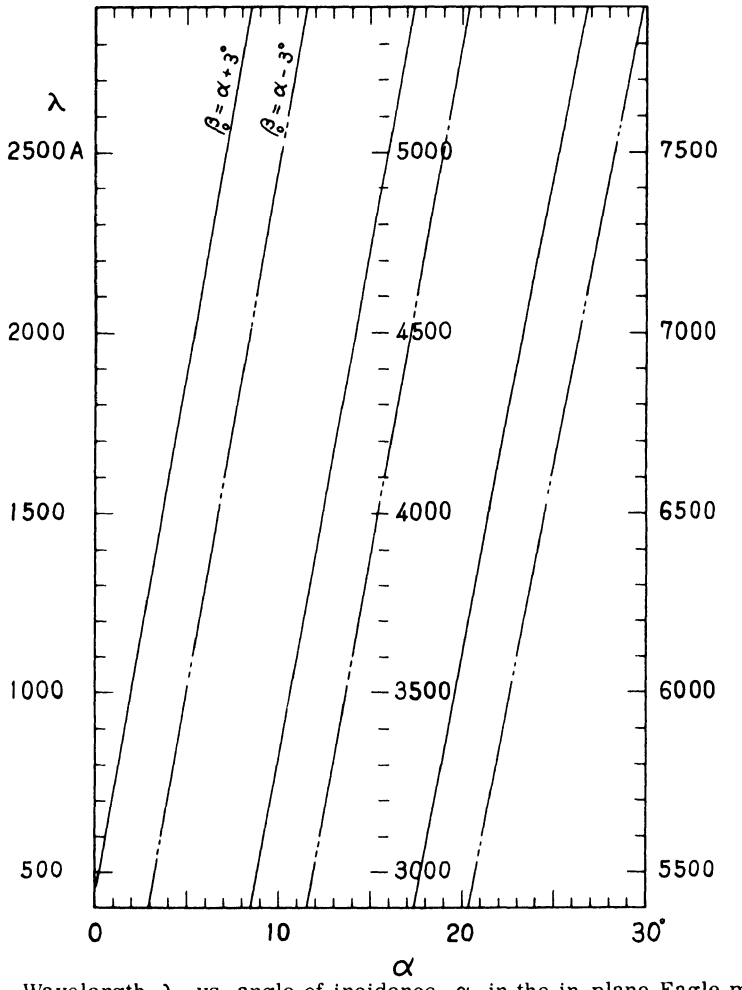


Fig. 13. Wavelength, λ, vs. angle of incidence, α, in the in-plane Eagle mounting. λ is calculated by assuming a 1m grating with 1200 grooves/mm, the first order and the diffraction angle $\beta_0 = \alpha \pm 3°$.

(6) The Off-Plane Eagle Mounting

To provide the relation $\alpha = \beta_0$ exactly, both the entrance and exit slits can be displaced symmetrically from the Rowland plane above and below. In this case displacement of the slits must be limited to a certain amount in order to get the best definition. Besides this, the entrance slit must be rotated by a small amount of angle from the position where the slit is parallel to the grating rulings (refer to Eq. (10)).

Numerical calculations on the resolving power[21] show that this mounting is very useful for gratings larger than 3 m but not for small gratings like 1 m. Therefore, we shall not discuss the subject any further.

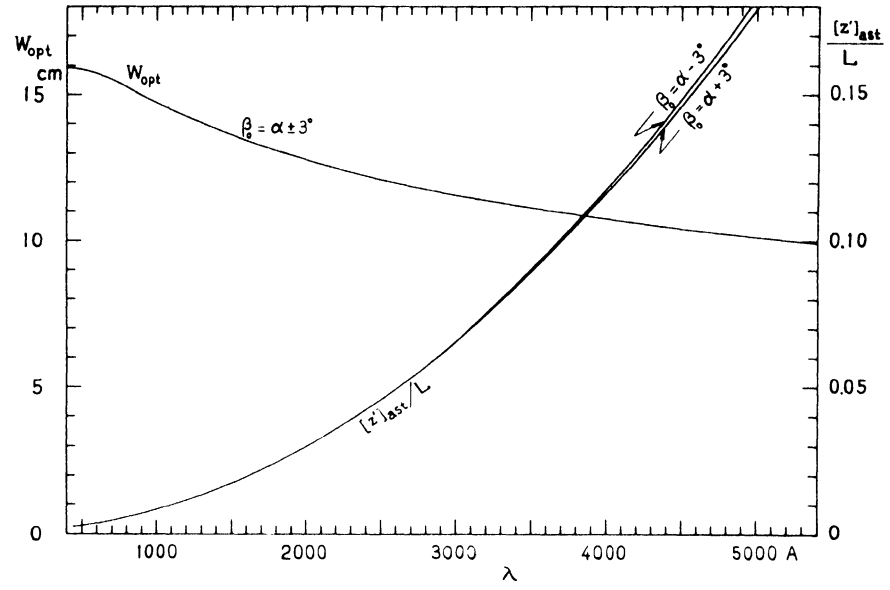


Fig. 14. Optimum grating width, W_{opt}, and length of astigmatic image for a point light source per unit length of the grating rullings, $[z']_{ast}/L$, in the in-plane Eagle mounting. $\beta_0 = \alpha \pm 3°$, a 1 m grating with 1200 grooves/mm, and the first order are assumed in the calculation where α and β_0 are the angles of incidence and diffraction, respectively.

(7) The Grazing Incidence Mounting

It is essential to use the grazing incidence mounting (Fig. 15) for detecting spectra with wavelengths shorter than about 500 A. The

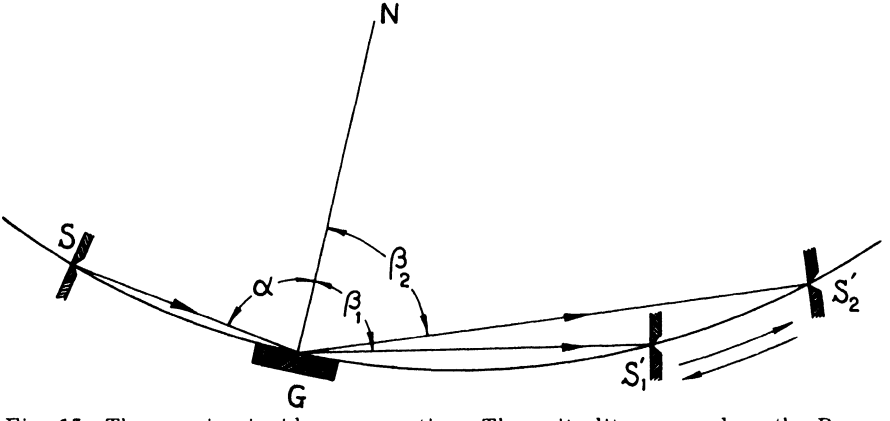


Fig. 15. The grazing incidence mounting. The exit slit moves along the Rowland circle to perform a monochromator action. S is the fixed entrance slit; G, the fixed grating; S_1' and S_2', various positions of the exit slit; α, the angle of incidence; β_1 and β_2, various angles of diffraction; and GN, the grating normal.

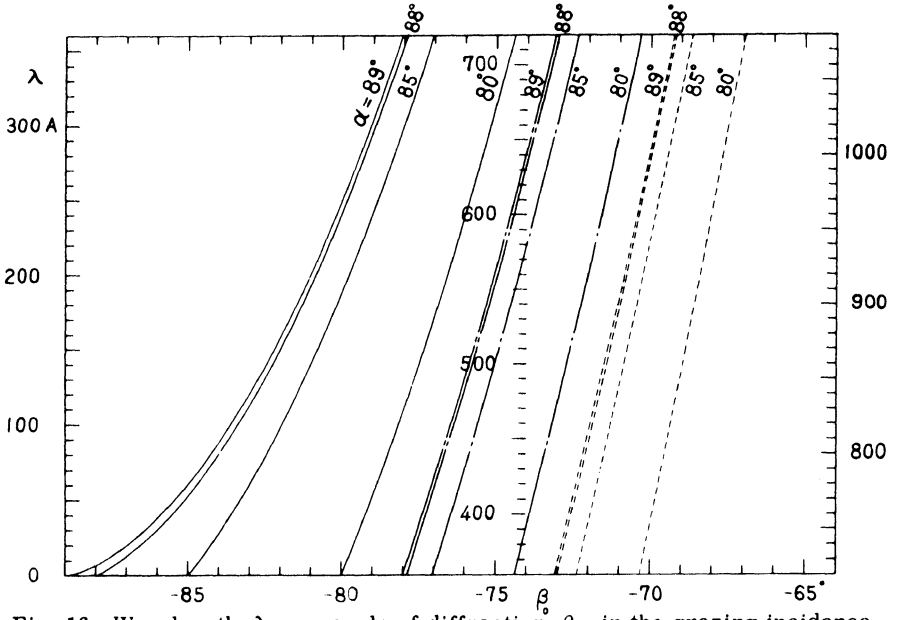


Fig. 16. Wavelength, λ, vs. angle of diffraction, β_0, in the grazing incidence mounting. Use the left-, middle-, and right-ordinates for the solid curves, dash-dot curves, and dotted curves, respectively. α is the angle of incidence. A 600 grooves/mm grating and the first order are assumed for the wavelength calculation.

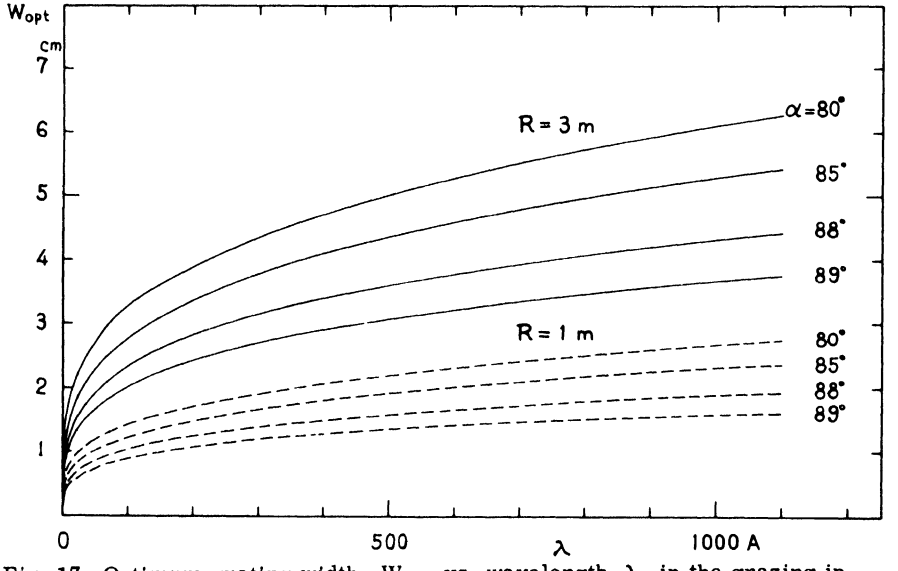


Fig. 17. Optimum grating width, W_{opt}, vs. wavelength, λ, in the grazing incidence mounting. α is the angle of incidence and R is the radius of curvature of the grating. For the calculation, 600 grooves/mm and the first order are assumed.

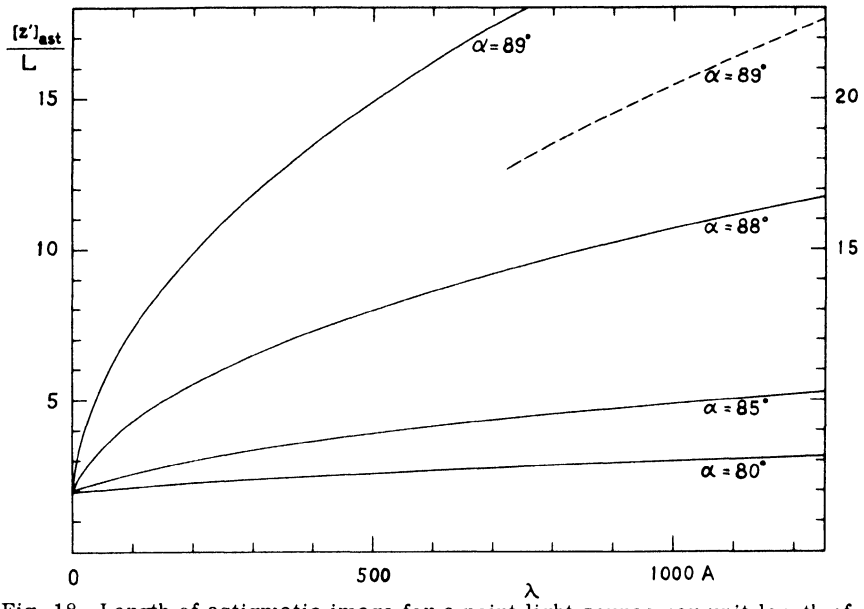


Fig. 18. Length of astigmatic image for a point light source per unit length of the grating rulings, $[z']_{ast}/L$, in the grazing incidence mounting. α and λ are the angle of incidence and the wavelength, respectively. Use the right ordinate for the dashed curve. The grating constant of 1/600 mm is assumed for the wavelength calculation.

shortest detectable wavelength depends largely on the angle of incidence and the higher the angle of incidence the shorter the threshold wavelength, e. g., 75, 53, and 12 A for 80°, 85.6° and 89° incidence, respectively.

With increase in the angle of incidence, the astigmatism increases rapidly, while the optimum grating width decreases. These characteristics are readily seen in Figs. 17 and 18. In Fig. 16 wavelengths are plotted as a function of the angle of diffraction for several angles of incidence. In these calculations 600 grooves/mm is assumed for the gratings.

To overcome large astigmatism and narrow optimum width, an ellipsoidal concave grating might be used. In a limited wavelength region, and ellipsoidal concave grating with $a = c \neq b$ provides not only less astigmatism, but also wider optimum width than a spherical concave grating. The optimum value of c/b is expressed by [59]

$$\frac{c}{b} = \left\{ \left[(\beta_2 - \beta_1)(3 + 4\cos^2\alpha) + 12(\sin\beta_2 - \sin\beta_1)\cos\alpha + 2(\sin 2\beta_2 - \sin 2\beta_1)(1 + \cos^2\alpha) + \frac{4}{3}(\sin 3\beta_2 - \sin 3\beta_1)\cos\alpha + 1/4(\sin 4\beta_2 - \sin 4\beta_1) \right] \Big/ \left[8(\beta_2 - \beta_1) + 2(\sin\beta_2 - \sin\beta_1)(4\cos\alpha + 3\sec\alpha) + 4(\sin 2\beta_2 - \sin 2\beta_1) + \frac{2}{3}(\sin 3\beta_2 - \sin 3\beta_1)\sec\alpha \right] \right\}^{1/2} \quad (26)$$

for a given value of α and a given range of β_0, $\beta_1 \leq \beta_0 \leq \beta_2$. As an example, the numerical values of the optimum ratio c/b are listed in Table III, where wavelengths are calculated by assuming $\sigma = 1/600$ mm Figs. 19 and 20 show the astigmatism calculated by (19) for the values of c/b listed in Table III. Figs. 21 and 22 show the optimum width of the ellipsoidal concave grating for $b^2/c = 1$ and 3 meters, respectively, and the first order (Eq. (20)). For the wavelength calculation $\sigma = 1/600$ mm is assumed.

If only reduction of the astigmatism is required, as was introduced by Rense and Violett,[54] a combination of a toroidal mirror and a spherical concave grating gives better results over a wide wavelength range than the ellipsoidal concave grating. In this case, the toroidal mirror must provide the horizontal focus at the entrance slit and the vertical focus at the vertical focus of the grating. Under such conditions, the astigmatism of the system is expressed by

$$\frac{[z']_{ast}}{L} = \left| \sin^2\beta_0 - \cos\beta_0 \sin\beta_0^* \tan\beta_0^* \right|, \tag{27}$$

where β_0^* is the angle of diffraction for which the stigmatic spectral image is formed. The optimum value of β_0^* for a given range of the

TABLE III.

Optimum values of c/b for the range $\beta_1 \leq \beta_0 \leq \beta_2$ and for $\alpha = 80°$ and 85°. Wavelength, λ, is calculated under the assumption that the grating constant is 1/600 mm. α is the angle of incidence. β_1 and β_2 are the angles of diffraction corresponding to the shortest and the longest wavelength of a given wavelength range, respectively. b and c are the lengths of the semi-axes of the ellipsoid.

$\alpha = 80°$			
β_1	β_2	Wavelength Range (A)	c/b
−79°	−72°	53- 563	0.21254
	−67°	53-1072	0.23435
	−63°	53-1563	0.25089
	−59°	53-2127	0.26643
$\alpha = 85°$			
β_1	β_2	Wavelength Range (A)	c/b
−83° 30′	−75°	44- 505	0.13439
	−69°	44-1044	0.15702
	−65°	44-1498	0.17038
	−61°	44-2026	0.18265

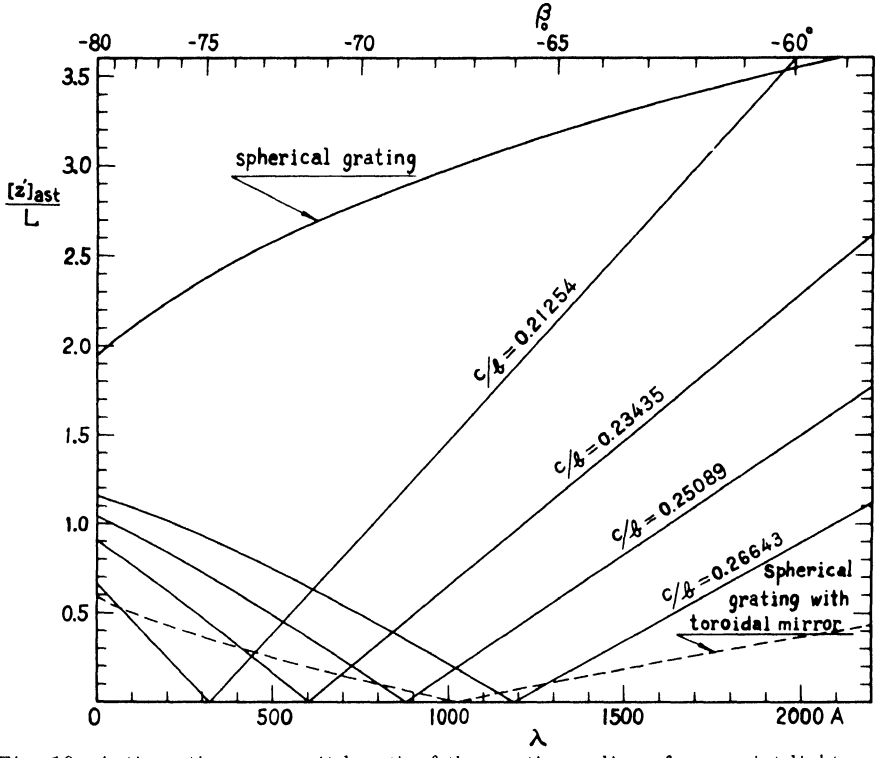


Fig. 19. Astigmatism per unit length of the grating rulings for a point light source, $[z']_{ast}/L$, in the grazing incidence mounting ($\alpha = 80°$). The grating constant of 1/600 mm is assumed. In the figure the amount of astigmatism is plotted for a spherical concave grating, ellipsoidal concave gratings with various values of c/b, as noted, and a combination of a spherical concave grating and a toroidal mirror. λ and β_0 are the wavelength and the angle of diffraction, respectively. b and c are lengths of semi-axes of the ellipsoid.

angle of diffraction, $\beta_1 \leq \beta_0 \leq \beta_2$, is given by minimizing (27) over the given range of β_0:

$$\sin \beta_0^* = A[-1 + (1 + 2A^{-2})^{1/2}]^{1/2}, \tag{28}$$

where

$$A = \frac{2\sqrt{2}\,(\sin^3\beta_2 - \sin^3\beta_1)}{3[2(\beta_2 - \beta_1) + \sin 2\beta_2 - \sin 2\beta_1]}.$$

As examples, (27) is shown graphically by the dashed curves in Figs. 19 and 20 for the cases $\alpha = 80°$, $\beta_1 = -79°$, $\beta_2 = -59°$, $\lambda^* = 1024$ A and $\alpha = 85°$, $\beta_1 = -83° 30'$, $\beta_2 = -61°$, $\lambda^* = 954$ A, where λ^* is the wavelength of the stigmatic image.

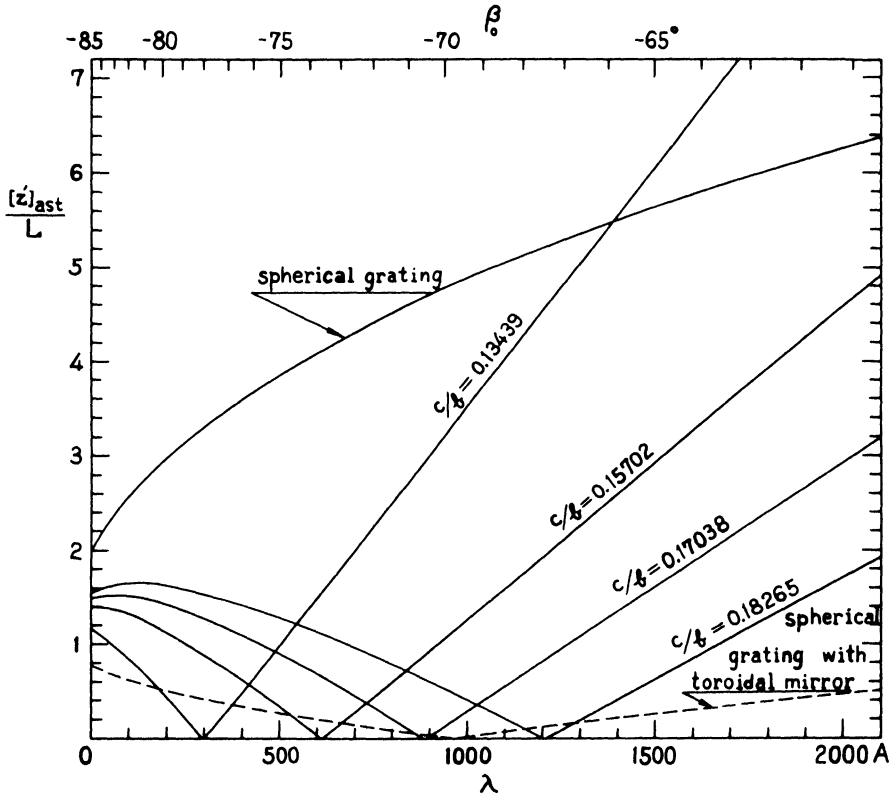


Fig. 20. Astigmatism per unit length of the grating rulings for a point light source, $[z']_{ast}/L$, in the grazing incidence mounting ($\alpha = 85°$). The grating constant of 1/600 mm is assumed. In the figure the amount of astigmatism is plotted for a spherical concave grating, ellipsoidal gratings with various values of c/b, as noted, and a combination of a spherical concave grating and a toroidal mirror.

(8) The Radius Mounting (the Beutler Mounting)

A monochromator action is performed by rotating the grating about the center of the Rowland circle (Fig. 23). In Fig. 24 wavelengths are plotted as a function of the angle of incidence. The optimum grating width and the astigmatism for various wavelengths are shown graphically in Fig. 25. In the calculations the angle made by lines connecting the grating center to the entrance and exit slits is taken 6° and a 1 m grating with 1200 grooves/mm is assumed.

As is easily seen from Fig. 25, this mounting provides fairly wide optimum grating width and small astigmatism over the quite wide wavelength range. However, in this mounting the direction of the line connecting the entrance slit to the grating center changes with wave-

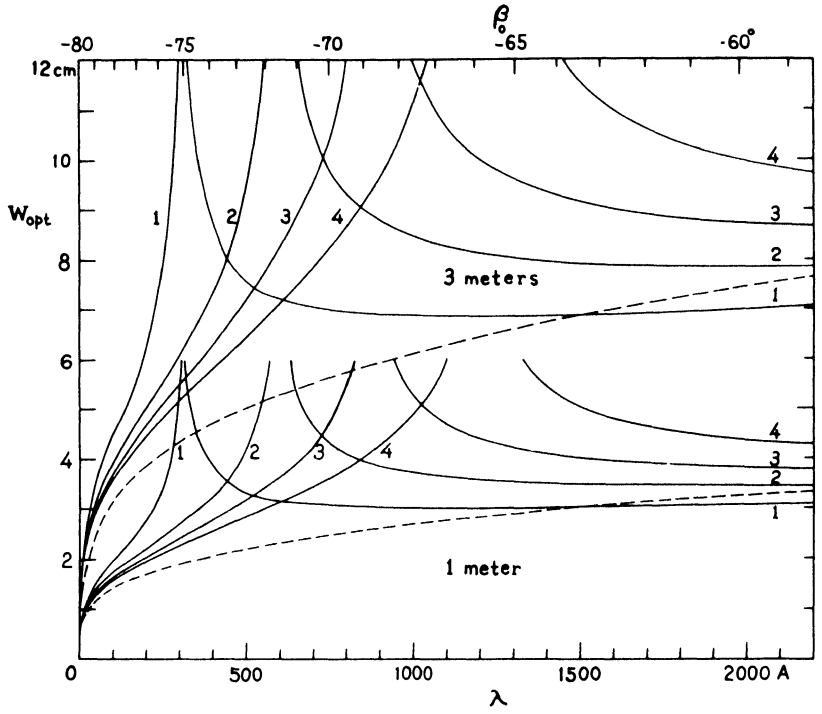


Fig. 21. Optimum grating width, W_{opt}, in the grazing incidence mounting ($\alpha = 80°$). The upper solid curves show W_{opt} of ellipsoidal concave gratings with $b^2/c = 3m$. The lower solid curves are for ellipsoidal concave gratings with $b^2/c = 1m$. The curves 1, 2, 3, and 4 correspond to ellipsoidal concave gratings of $c/b = 0.21254$, 0.23435, 0.25089, and 0.26643, respectively. The upper and lower dashed curves are for spherical concave gratings with R = 3m and R = 1m, respectively, where R is radius of curvature of the grating. For ellipsoidal concave gratings, $a = c \neq b$, where a, b, and c are the lengths of the semi-axes of the ellipsoid.

length. Because of this disadvantage the radius mounting is not suitable to the present purpose, although it looks very nice in its optical properties and scanning mechanism.

(9) The Seya-Namioka Mounting

If we set the entrance and exit slits in such a way that the angle between lines connecting the grating center to the slits is chosen as about 70°, and that the entrance and exit slits are placed at distances of approximately 0.8181 R and 0.8176 R from the grating center, then spectral images are brought into a reasonably sharp focus at the fixed

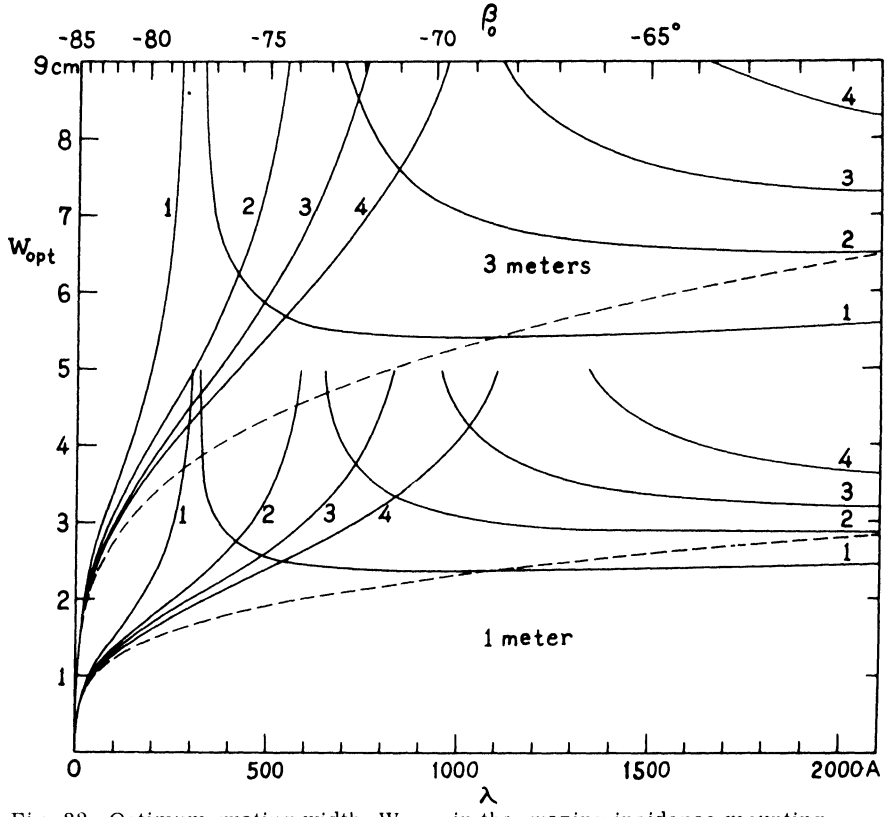


Fig. 22. Optimum grating width, W_{opt}, in the grazing incidence mounting ($\alpha = 85°$). The upper solid curves show W_{opt} of ellipsoidal concave gratings with $b^2/c = 3m$. The lower solid curves are for ellipsoidal concave gratings with $b^2/c = 1m$. The curves 1, 2, 3, and 4 correspond to ellipsoidal concave gratings of $c/b = 0.13439$, 0.15702, 0.17038, and 0.18265, respectively. The upper and lower dashed curves are for spherical concave gratings with $R = 3m$ and $R = 1m$, respectively, where R is the radius of curvature of the grating. For ellipsoidal concave gratings, $a = c \neq b$, where a, b, and c are the lengths of the semi-axes of the ellipsoid.

exit slit by simple rotation of the grating about the vertical axis through its center (Fig. 26, p. 257).

Assuming that the angle made by lines connecting the grating center to the slits is 70° 15′ and the grating constant is 1/1200 mm, wavelengths are plotted against angles of incidence in Fig. 27 (p. 258).

This mounting provides the simplest scanning mechanism among all the possible mountings. However, the detailed analysis of the mounting shows two major disadvantages: (1) The optimum grating width is rather narrow, and (2) astigmatism is large. These effects are easily seen from Figs. 28 and 29. Fig. 28 is the plot of the theo-

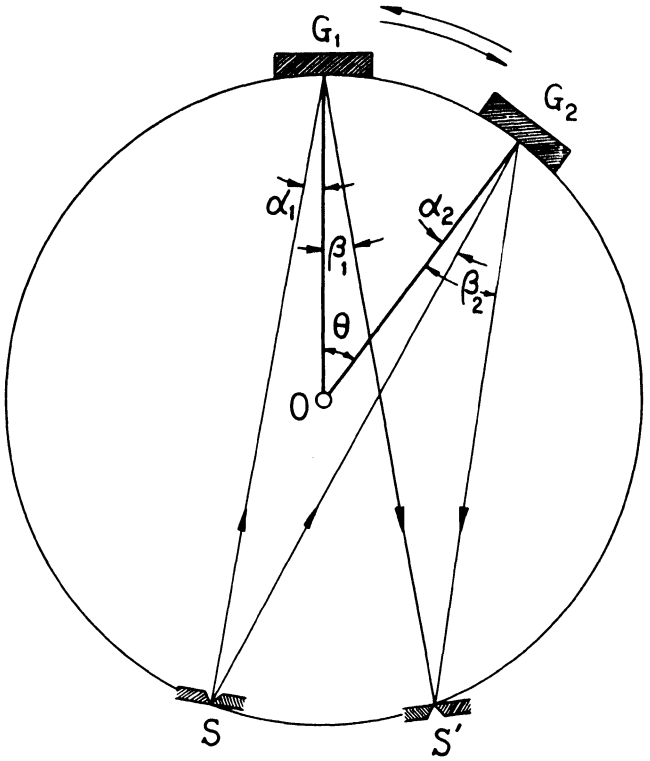


Fig. 23. The radius mounting (the Beutler mounting). The grating moves along its Rowland circle to perform a monochromator action. O is the pivot point for grating rotation and also the center of the Rowland circle; θ, the angle of grating rotation about the pivot point O; S, the fixed entrance slit; S′, the fixed exit slit; G_1 and G_2, various positions of the grating; α_1 and α_2, various angles of incidence; and β_1 and β_2, various angles of diffraction.

retical resolving power as a function of grating width. In Fig. 29 the astigmatism is graphically shown against wavelengths. For these calculations, $\alpha - \beta_0 = 70°15'$, $R/r = 1.2223$, $R/r' = 1.2230$, and $\sigma = 1/600$ mm are assumed, where R is the radius of curvature of the grating, σ is the grating constant, and r and r′ are the distances between the grating center and the entrance and exit slits, respectively.

To eliminate these shortcomings, we may suggest the use of an ellipsoidal concave grating. This solves the problem concerning astigmatism completely and shows slight increase of the optimum width. The instrumental constants for the ellipsoidal concave grating are the same as those for the spherical concave grating, namely, we have

$$\left.\begin{aligned} &\alpha - \beta_0 = 70°15', \\ &\frac{b^2}{ar} = 1.2223 \quad \text{and} \quad \frac{b^2}{ar'} = 1.2230. \end{aligned}\right\} \tag{29}$$

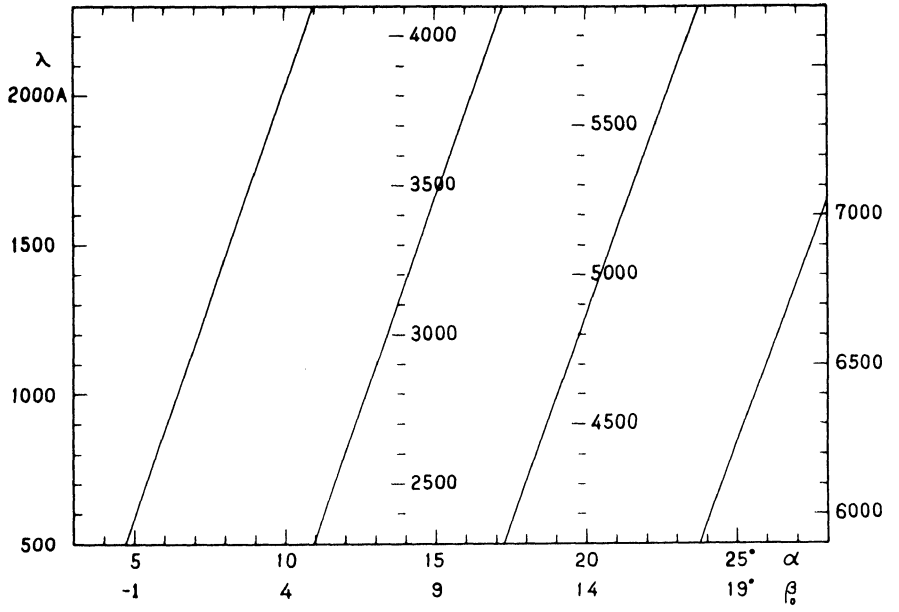


Fig. 24. Wavelength, λ, vs. angles of incidence, α, and of diffraction, β_0, in the radius mounting. 1200 grooves/mm and $\alpha - \beta_0 = 6°$ are assumed.

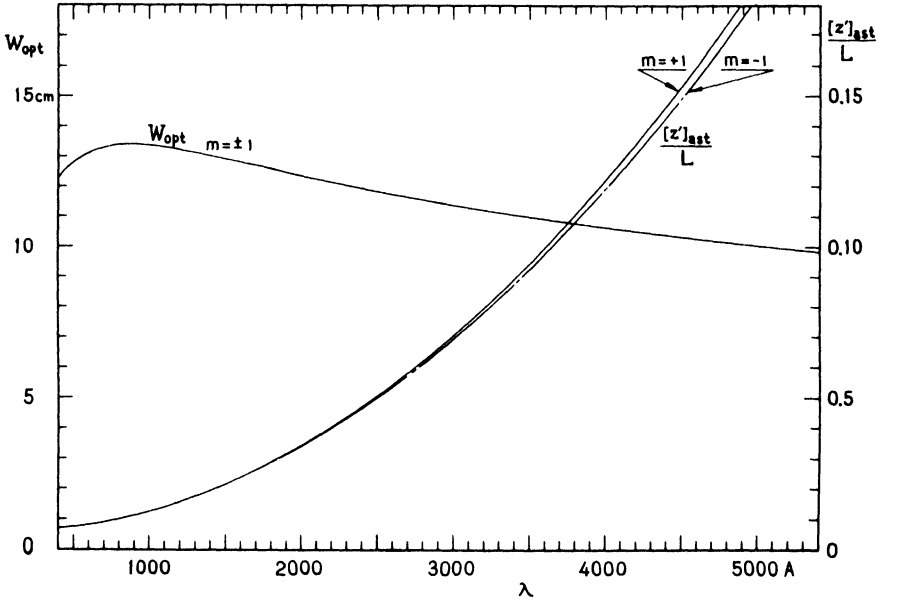


Fig. 25. Optimum grating width, W_{opt}, and astigmatism per unit length of the grating rulings, $[z']_{ast}/L$, in the radius mounting. $\alpha - \beta_0 = 6°$ and a 1m grating having 1200 grooves/mm are assumed, and m is the spectral order.

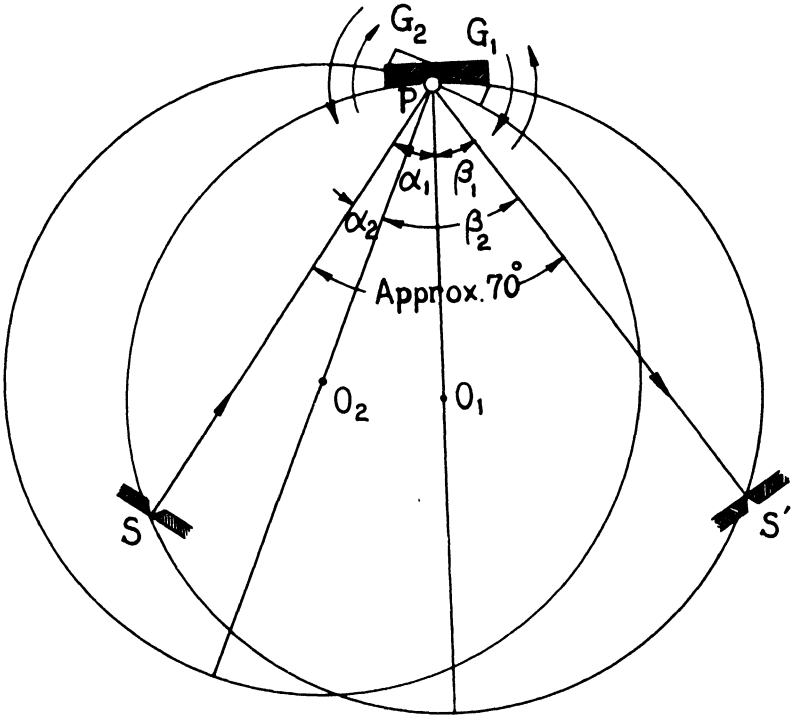


Fig. 26. The Seya-Namioka mounting. Monochromator action is performed by simple rotation of the grating under the conditions that $\angle$ SPS′ = 70°, $\overline{SP}$ = 0.8181R, and $\overline{S'P}$ = 0.8176R, where R is the radius of curvature of the grating. P is the center of grating rotation. S and S′ are the entrance and exit slits, respectively. Both slits are approximately on a Rowland circle when the zero order spectrum is brought into a focus at S′. O_1 and O_2 are various positions of the center of the Rowland circle; G_1 and G_2, various positions of the grating; α_1 and α_2, various angles of incidence; and β_1 and β_2, various angles of diffraction.

The astigmatism of this system is expressed by

$$\frac{[z']_{ast}}{L} = \frac{ar'}{b^2}\left|\frac{b^2}{ar}+\frac{b^2}{ar'}-2\frac{b^2}{c^2}\cos\frac{\alpha-\beta_0}{2}\cos k\right| \tag{30}$$

$$= 0.81766\left|2.4453-0.67583\frac{b^2}{c^2}\cos k\right|, \tag{30'}$$

where $k = -1/2\,(\alpha+\beta_0)$. The optimum value of b^2/c^2 which minimizes the astigmatism in a given range of β_0, $\beta_1 \leq \beta_0 \leq \beta_2$, is given by

$$\frac{c}{b} = 0.40895\left[\frac{2(k_2-k_1)+\sin 2k_2-\sin 2k_1}{\sin k_2-\sin k_1}\right]^{1/2}, \tag{31}$$

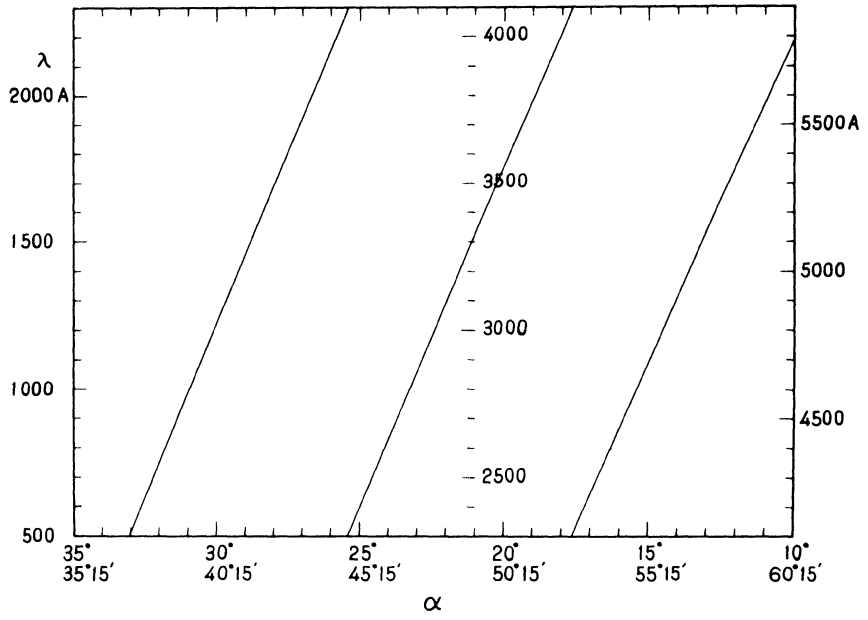


Fig. 27. Wavelength, λ, vs. angle of incidence, α, in the Seya-Namioka mounting. $\alpha - \beta_0 = 70° 15'$ and 1200 grooves/mm are assumed.

where the conditions (29) are considered. For several wavelength ranges optimum values of c/b are listed in Table IV. Fig. 29 (p. 260).

TABLE IV.

The optimum values of c/b in the Seya-Namioka mounting. β_1 and β_2 are the initial and final angles of diffraction in the range, respectively. α is the angle of incidence, λ* the wavelength at which the stigmatic image is formed on the exit slit. b and c are the lengths of the semi-axes of the ellipsoid. The grating constant of 1/600 mm is assumed here for the calculation of wavelengths.

β_1	β_2	α	Wavelength Range (A)	λ* (A)	c/b
	−37° 15′	34° to 33°	535-1011	786	0.81773
	−38° 15′	34° to 32°	535-1486	1049	0.81760
	−39° 15′	34° to 31°	535-1961	1314	0.81742
	−40° 15′	34° to 30°	535-2435	1584	0.81721
	−41° 15′	34° to 29°	535-2909	1852	0.81695
−36° 15′					
	−42° 15′	34° to 28°	535-3382	2125	0.81665
	−43° 15′	34° to 27°	535-3853	2395	0.81631
	−44° 15′	34° to 26°	535-4324	2666	0.81593
	−45° 15′	34° to 25°	535-4793	2936	0.81551
	−46° 15′	34° to 24°	535-5261	3206	0.81505
	−47° 15′	34° to 23°	535-5727	3476	0.81455

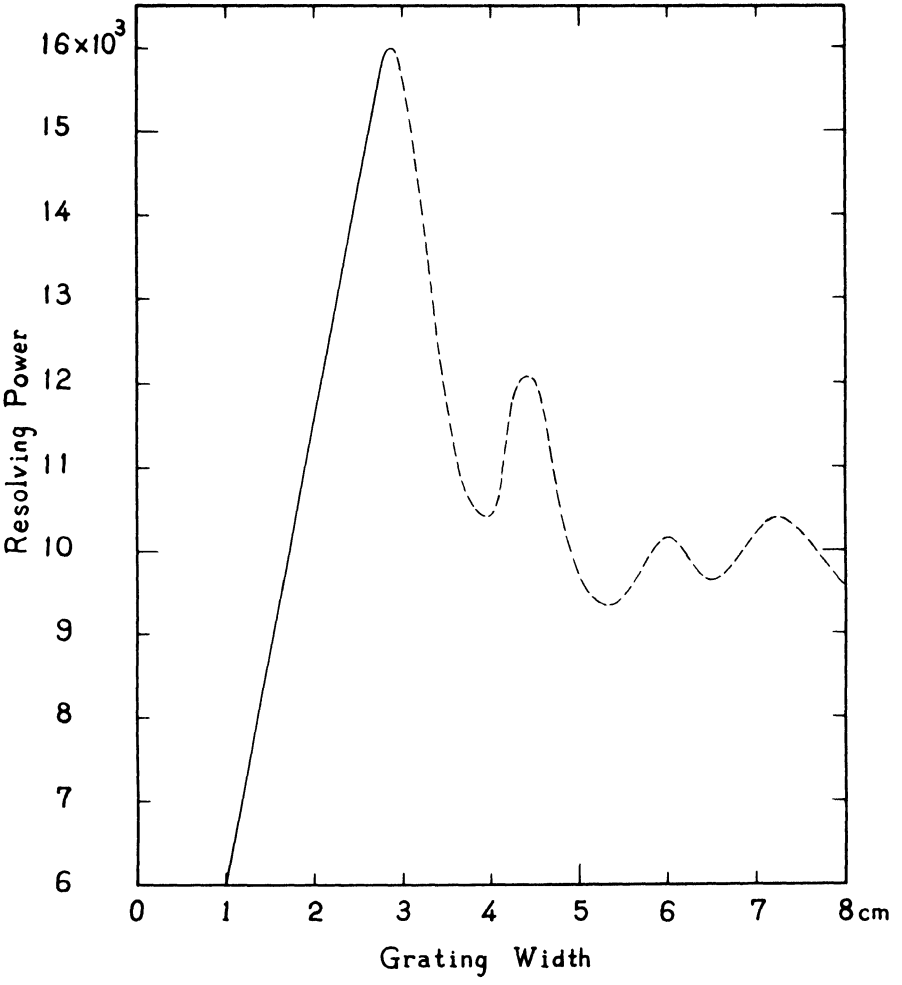


Fig. 28. The resolving power of the grating at 1510A (a 1m grating with 600 grooves/mm is assumed). The solid curve shows the resolving power for which the secondary maxima are not intense enough to be troublesome. The dotted curve is the resolving power obtained by applying a conventional definition of resolving power to the intensity distribution curves having very strong secondary maxima. The resolving power shown here is of the grating itself and does not include any factors due to the finite slit width, Doppler effect, sensitivity of detectors, etc. Therefore, in practice these effects must be taken into consideration, namely, the values of resolving power shown here will be further reduced.

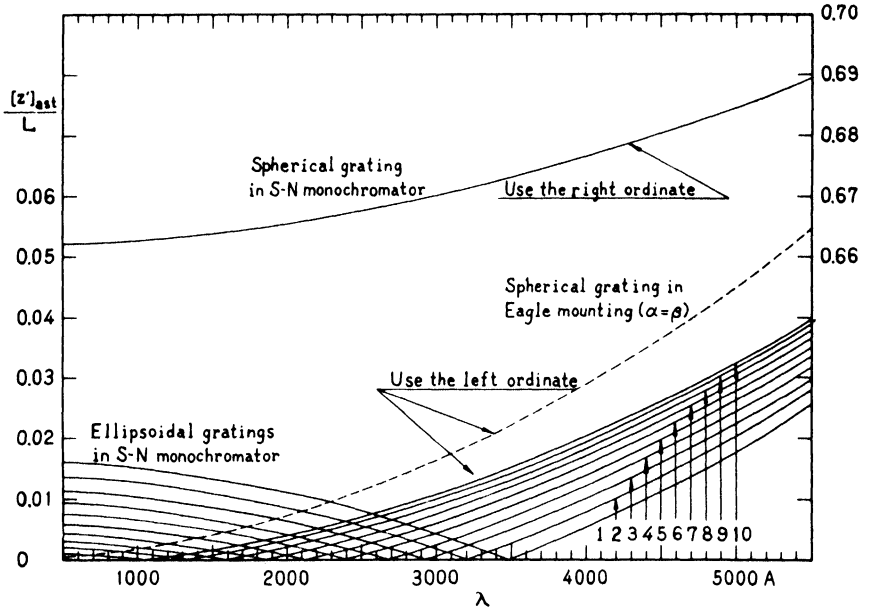


Fig. 29. Astigmatism per unit length of the grating rulings for a point light source, $[z']_{ast}/L$, in the Seya-Namioka mounting. For the computation the following instrumental constants are used: $C = \alpha - \beta_0 = 70°15'$, $R/r = 1.2223$, $R/r' = 1.2230$, and $\sigma = 1/600$ mm, where $R = b^2/a$ is the diameter of the Rowland circle, σ is the grating constant, and r and r′ are distances between the grating center and the entrance slit and the exit slit, respectively. The upper solid curve shows astigmatism of a spherical concave grating. The lower solid curves denoted by 1, 2, ..., 9 and 10 correspond to ellipsoidal concave gratings with c/b = 0.81455, 0.81505, 0.81551, 0.81593, 0.81631, 0.81665, 0.81695, 0.81721, 0.81742, and 0.81760, respectively. As a comparison, astigmatism of a spherical concave grating in the in-plane Eagle mounting ($\alpha = \beta_0$) is also shown. a, b and c are the lengths of the semi-axes of the ellipsoid.

shows the amount of astigmatism per unit length of the ruling for a point light source, $[z']_{ast}/L$, as a function of wavelength for various values of c/b, where the grating constant of 1/600 mm is assumed. It should be noted that the astigmatism of the ellipsoidal concave grating is relatively small and is comparable to that of the in-plane Eagle mounting of the spherical concave grating, the mounting which gives the least astigmatism.

Therefore, if one wants to utilize this mounting in a space telescope, the ellipsoidal concave grating must be used as the dispersing system.

(10) The Johnson-Onaka Mounting

To produce adequately sharp spectral images at the fixed exit slit, the grating is rotated about a vertical axis, which is displaced from

the grating center by a calculated amount d (Fig. 30). The pivot point C is on the line through the grating center G_1 and the point M which is on the Rowland circle midway between the slits.

The optimum length of d is given by

$$d = \frac{R \sin \theta}{1 - 1/2 \tan \phi \ (\tan \alpha_1 - \tan \beta_1)}. \tag{32}$$

For the in-plane Eagle mounting, the best choices of d and $\overline{NC}$ are

$$d = \frac{R\lambda_0}{2\sigma}$$

and

$$\overline{NC} = R + \frac{d^2}{R} - \frac{(\Delta\lambda)^2 R}{32\sigma^2} \tag{33}$$

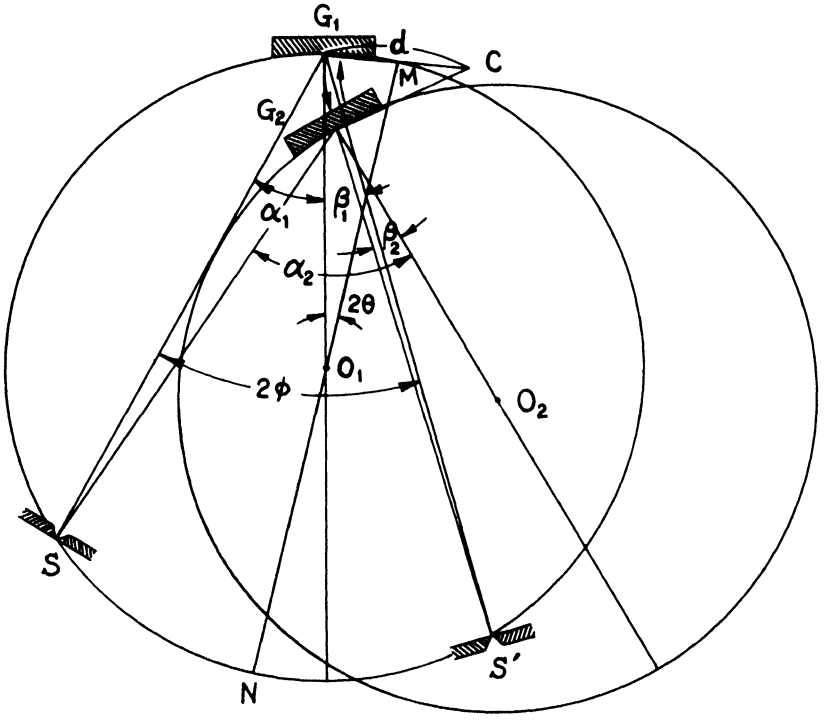


Fig. 30. The Johnson-Onaka mounting. Rotation of the grating about the pivot point C brings images into relatively sharp focus at the fixed exit slit S′. The points M and N are on the Rowland circle, whose center is at O_1, midway between the entrance slit S and the exit slit S′. The pivot point C is on the line through the grating center G_1 and the point M. Suffix 1 indicates the state in which all the optical components lie on the Rowland circle. G_1 and G_2 are various positions of the grating; O_1 and O_2, various positions of the center of the Rowland circle; α_1 and α_2, various angles of incidence; β_1 and β_2, various angles of diffraction; $2\theta = \angle G_1O_1M$; $2\phi = \angle SG_1S'$; and $\ell = G_1C$.

in the wavelength range, $\lambda_1 \leq \lambda \leq \lambda_2$, where $\lambda_0 = 1/2\ (\lambda_1 + \lambda_2)$ and $\Delta\lambda = \lambda_2 - \lambda_1$. In this case, C is on the tangent to the Rowland circles.

Because of near normal incidence, this mounting has relatively small astigmatism but the facts are that usable spectral range is limited to about 1000 A or a little wider and that the direction of the line connecting the entrance slit and the grating center changes with wavelength resulting in disadvantages.

(11) The Ebert-Fastie Mounting

The only difficulty in utilizing a plane grating in the vacuum ultraviolet region has been merely due to poor reflectance of coating materials. With the discovery of the Al-MgF_2 film combination,[61,63] it became possible to construct a plane grating monochromator at wavelengths down to 1200 A. Among plane grating mountings, the Ebert-Fastie mounting has the most desirable characteristics: Good focus is obtained for all wavelengths in a low f-number system with fixed entrance and exit slits, fixed illumination angle, and fixed exit beam angle; its scanning system requires only a simple rotation of the grating about a vertical axis through the grating center; although aberrations in this mounting have not been fully treated theoretically, excellent resolution has been obtained in the visible, and the use of circular slits provides almost stigmatic spectral images.

The Ebert-Fastie mounting shown in Fig. 31 consists of the plane grating G and the spherical concave mirror M. Light from the en-

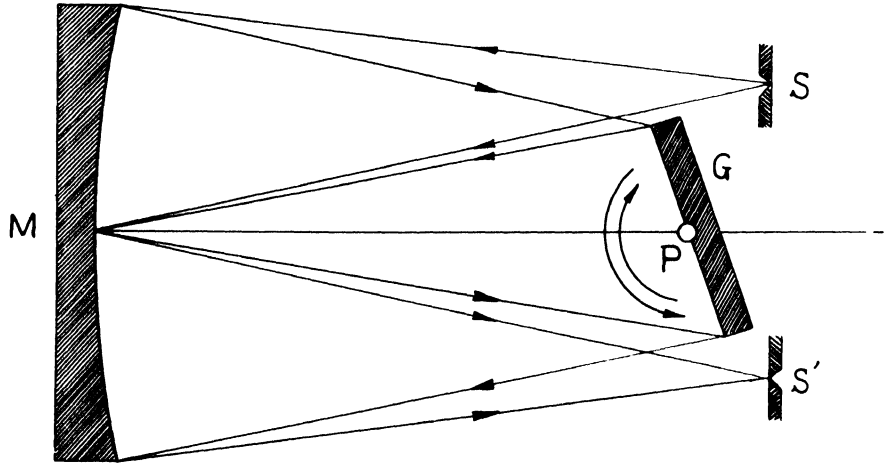


Fig. 31. The Ebert-Fastie Mounting. To perform a monochromator action, the plane grating G is simply rotated about the pivot point P going through the grating center. M is the fixed spherical mirror; S, the fixed entrance slit; and S', the fixed exit slit.

trance slit S, which is in the focal plane of the mirror, strikes the upper half of the mirror, which renders it parallel and sends it to the grating. The diffracted rays go to the lower half of the mirror and focus onto the exit slit S′, which is also in the focal plane of the mirror. Both slits lie on an Ebert circle whose center is located on the line through the center of the grating and the mirror.

IV. SUMMARY

Table V is a summary of some important characteristics of the mountings described in the previous section. The Abney, off-plane Eagle, and radius mountings are definitely not acceptable to our purpose (the reasons are evident in Table V). It is cumbersome to perform adequately precise monochromator action in the Rowland and Wadsworth mountings; therefore, these are not recommended. Because of its small wavelength coverage the Johnson-Onaka mounting is also not sufficient to meet with our present purpose. This leaves us the normal incidence, in-plane Eagle, grazing incidence, Seya-Namioka (with an ellipsoidal concave grating), and Ebert-Fastie mountings.

In the previous section, we considered the grating mountings from the view point of aberrations in the systems and of mechanical complexity to achieve monochromator action. However, for the present purpose intensities of light sources, i.e., stars, cannot be increased as we can do to some extent in laboratories. Under such energy-limited conditions, we must examine the relative efficiency of each mounting. Let us make the following assumptions: (1) The entrance slit will be illuminated with a beam which matches at least with the f-number of the monochromator; (2) the length of the illuminated part of the entrance slit is quite short; (3) the detection system is capable of collecting a beam of a given f-number from the exit slit up to 1.5 cm; (4) the aberration limited resolution is 1 A or less; (5) the grating blazes are made equally effective in all mountings; (6) the length of the grating rulings is 5 cm; and (7) the monochromator is restricted to approximately 1 m in length.

Under these assumptions the relative efficiency of each mounting is determined by the surface reflectance, astigmatic energy loss, and the f-number of the system, that is, the relative efficiency η is given by

$$\eta = \frac{\mathcal{R}\,(100 - \xi)}{f}, \tag{34}$$

where $\mathcal{R}$ is the reflectivity of the system as a whole, ξ is the percentage intensity loss due to astigmatism, and f the f-number of the system. Now, we compute the approximate value of η of each mounting in the wavelength region 1200 to 2000 A by assuming approximate average values of $\mathcal{R}$, ξ, and f over the given wavelengths. The results

TABLE V.

Summary of some characteristics of the grating mountings. A 1 m, 1200 grooves/mm grating is assumed for all mountings except for the grazing incidence (2 m, 600 grooves/mm), Wadsworth (2 m, 1200 grooves/mm), and Ebert-Fastie mountings (plane). In the table the following abbreviations are used: G, grating; S, entrance slit; S′, exit slit; O, center of the Rowland circle; P, vertical axis through the grating center; and C, vertical axis displaced by some distance from the grating center.

	Rowland	Abney	Wadsworth	Normal Incidence	In-Plane Eagle	Off-Plane Eagle
Wavelength coverage with 1A resolution	500 ~ 8000A	500 ~ 8000A	1000 ~ 8000A	500 ~ 8000A	500 ~ 8000A	Not suitable to gratings whose radius of curvature is shorter than 3 meters.
Scanning mechanism	G & S′ move along rails	S rotates about O	G rotates about P; S′ moves along parabola	S′ moves along Rowland circle	G moves along rail & rotates. S′ rotates about S	
Fixed optical elements	Entrance slit	Exit slit, grating	Entrance slit, mirror	Entrance slit, grating	Entrance slit	
Complexity to achieve monochromator action	Medium	Simple	Complex	Simple	Medium	
Angle of incidence, α	Varies	Varies	Varies	Constant, near 0°	$\alpha \cong \beta_0$, varies	
Angle of diffraction, β_0	0°	0°	0°	Varies	$\beta_0 \cong \alpha$, varies	
Direction of diffracted rays	Varies	Constant	Varies	Varies	Varies	
Direction of line connecting entrance slit to grating center	Constant	Varies	Constant	Constant	Constant	
Astigmatism	Small	Small	Zero	Very small for $m = 1$, small or medium for $m = -1$	Very small	
f number with 1A resolution in the vacuum ultraviolet region	7 ~ 9	7 ~ 9	13 ~ 16	7 ~ 10	6 ~ 8	
Numbers of reflecting surfaces	1	1	2	1	1	

TABLE V. (continued)

	Grazing Incidence	Radius	Seya-Namioka	Johnson-Onaka	Ebert-Fastie
Wavelength coverage with 1A resolution	10 (depends on α) ~ 2000A	500 ~ 8000A	500 ~ 6000A	500 ~ 1700A	1200 ~ 8000A
Scanning mechanism	S′ moves along Rowland circle	G moves along Rowland circle	G rotates about P	G rotates about C	G rotates about P
Fixed optical elements	Entrance slit, grating	Entrance slit, exit slit	Entrance slit, exit slit	Entrance slit, exit slit	Entrance slit, exit slit, mirror
Complexity to achieve monochromator action	Medium	Simple	Very simple	Simple	Very simple
Angle of incidence, α	Constant, $\geq 80°$	Varies	$\alpha - \beta_0 \cong 70°$, varies	Varies, near normal	Varies
Angle of diffraction, β_0	Large angles, varies	Varies	$\alpha - \beta_0 \cong 70°$, varies	Small angles, varies	Varies
Direction of diffracted rays	Varies	Varies	Constant	Varies	Constant
Direction of line connecting entrance slit to grating center	Constant	Varies	Constant	Varies	Constant
Astigmatism	Very large (for spherical grating); large (for ellipsoidal grating)	Very small	Large (for spherical grating); very small (for ellipsoidal grating)	Small	Very small
f number with 1A resolution in the vacuum ultraviolet region	30 ~ 60	7 ~ 8	10 ~ 14	11 ~ 13	4 ~ 6
Numbers of reflecting surfaces	1	1	1	1	1

TABLE VI.

Approximate values of the relative efficiencies of the grating mountings, η. $\mathfrak{R}$ is the reflectivity of the system as a whole, ξ is the percentage intensity loss due to astigmatism, and f is the f-number of the system. Here we assumed the range of 1200 to 2000 A and an Al-MgF_2 coating on the grating and mirror.

	Kind of Grating	$\mathfrak{R}$	$100 - \xi$	f	η
Normal Incidence	1 m spherical concave	0.8	100	8	10
In-Plane Eagle	1 m spherical concave	0.8	100	6	13.3
Grazing Incidence	2 m spherical concave	1	5.5	50	0.1
	2 m ellipsoidal concave	1	30	30	1
Seya-Namioka	1 m spherical concave	0.83	40	12	2.8
	1 m ellipsoidal concave	0.83	100	10	8.3
Ebert-Fastie	Plane	0.51	100	5	10.2

are listed in Table VI. These η values are only a measure, but give us enough information about the efficiency of the mounting for the vacuum ultraviolet.

Because of high reflectivity in the wavelength region shorter than 500 A, it is essential to use the grazing incidence regardless of its disadvantages. The other mountings do not give us satisfactory results in this region. If the wavelengths desired are limited to longer than 1200 A, the Ebert-Fastie mounting has the most desirable features among all of the mountings. If it is required to cover the range of 500 to 4000 A by one monochromator, the normal incidence, in-plane Eagle, and Seya-Namioka mountings are almost equally efficient. Among these three, optically the in-plane Eagle mounting is the best, the normal incidence is second, and then the Seya-Namioka mounting (with an ellipsoidal concave grating). Mechanically, on the other hand, the order of preference reverses. The final choice among the three must be made, therefore, in connection with the design of the telescope system and other auxiliary instruments, proposed spectral performance, detecting method, volume and shape of space available for a monochromator in a space telescope system, required mechanical reliability (simplicity), and so forth.

The author is indebted to Mr. D. T. Hoxie for assistance in the numerical calculations.

REFERENCES

[1] H. A. Rowland, Phil. Mag. 13, 469 (1882) and 16, 197, 210 (1883).
[2] H. Kayser, Handbuch der Spectroscopie (Hirzel, Leipzig, 1900), Vol. 1, p. 470.
[3] E. C. C. Baly, Spectroscopy (Longmans, Green and Co., London, 1924).
[4] W. de W. Abney, Phil. Trans. Roy. Soc. (London) 177, 11 and 457 (1886).
[5] F. L. O. Wadsworth, Astrophys. J. 3, 47 (1896).
[6] C. Runge and F. Paschen, Ann. Physik 61, 641 (1897).
[7] W. F. Meggers and K. Burns, Sci. Papers Natl. Bur. Standards (USA) [411], 18, 185 (1922).
[8] R. F. Jarrell, J. Opt. Soc. Am. 32, 666 (1942).
[9] C. Runge and F. Paschen, Abhandl. deut. K. Akad. Wiss. Berlin, Anhang 1 (1902).
[10] G. H. Dieke and H. M. Crosswhite, J. Opt. Soc. Am. 35, 471 (1945).
[11] F. S. Tomkins and M. Fred, Spectrochim. Acta 6, 139 (1954).
[12] Th. J. M. Sluyters and E. De Hass, Rev. Sci. Instr. 29, 597 (1958).
[13] R. A. Sawyer, J. Opt. Soc. Am. 15, 303 (1927).
[14] K. T. Compton and J. C. Boyce, Rev. Sci. Instr. 5, 218 (1934).
[15] A. Eagle, Astrophys. J. 31, 120 (1910).
[16] T. Lyman, Spectroscopy of the Extreme Ultraviolet (Longmans, Green and Co., New York 1928).
[17] E. J. Bair, P. C. Cross, T. L. Dawson, E. A. Wilson, and J. H. Wise, J. Opt. Soc. Am. 43, 681 (1953).
[18] A. Eagle, Proc. Phys. Soc. (London) 23, 233 (1911).
[19] G. R. Harrison, Rev. Sci. Instr. 2, 600 (1931) and 4, 651 (1933).
[20] P. G. Wilkinson, J. Mol. Spectroscopy, 1, 288 (1957).
[21] T. Namioka, J. Opt. Soc. Am. 49, 460 and 961 (1959).
[22] J. B. Hoag, Astrophys. J. 66, 225 (1927).
[23] M. Siegbahn and T. Magnusson, Z. Physik 95, 133 (1935).
[24] P. G. Kruger, Rev. Sci. Instr. 4, 128 (1933).
[25] R. K. Brehm and G. Benzie, Rev. Sci. Instr. 28, 552 (1957).
[26] R. A. Sawyer, Experimental Spectroscopy (Prentice-Hall, Inc., N. Y., 1944), Second Ed., p. 154.
[27] Y. Fujioka and R. Ito, Sci. of Light (Tokyo) 1, 1 (1951).
[28] R. Tousey, F. S. Johnson, J. Richardson, and N. Toran, J. Opt. Soc. Am. 41, 696 (1951).
[29] M. Seya, Sci. of Light (Tokyo) 2, 8 (1952).
[30] T. Namioka, Sci. of Light (Tokyo) 3, 15 (1954); J. Opt. Soc. Am. 49, 951 (1959).
[31] H. Greiner and E. Schäffer, Optik 14, 263 (1957) and 15, 51 (1958).
[32] P. D. Johnson, J. Opt. Soc. Am. 42, 278 (1952); Rev. Sci. Instr. 28, 883 (1957).
[33] R. Onaka, Sci. of Light (Tokyo) 7, 23 (1958).
[34] H. Ebert, Wied. Ann. 38, 489 (1889).
[35] W. G. Fastie, J. Opt. Soc. Am. 42, 641 and 647 (1952), and 43, 1174 (1953).
[36] H. M. Crosswhite and W. G. Fastie, J. Opt. Soc. Am. 46, 110 (1956).
[37] W. G. Fastie, H. M. Crosswhite, and P. Gloersen, J. Opt. Soc. Am. 48, 106 (1958).
[38] D. W. Robinson, J. Opt. Soc. Am. 49, 966 (1959).
[39] R. T. Glazebrook, Phil. Mag. 15, 414 (1883).
[40] E. Mascart, J. Phys. 2, 5 (1883).
[41] W. Baily, Phil. Mag. 22, 47 (1886).

[42] H. Kayser, Handbuch der Spectroscopie (Hirzel, Leipzig, 1900), Vol. 1, pp. 450-470.
[43] C. Runge and K. W. Meissner, Handbuch der Astrophysik (Julius Springer, Berlin, 1933), Vol. 1, pp. 235-257.
[44] J. E. Mack, J. R. Stehn, and B. Edlen, J. Opt. Soc. Am. **22**, 245 (1932).
[45] J. E. Mack and J. R. Stehn, J. Opt. Soc. Am. **23**, 184 (1933).
[46] D. L. MacAdam, J. Opt. Soc. Am. **23**, 178 (1933).
[47] G. H. Dieke, J. Opt. Soc. Am. **23**, 274 (1933).
[48] I. S. Bowen, J. Opt. Soc. Am. **23**, 313 (1933).
[49] F. Zernike, Pieter Zeeman (Martinus Nijhoff, Hague, Netherlands, 1935), pp. 323-335.
[50] R. A. Sawyer, Experimental Spectroscopy (Prentice Hall, Inc., New York, 1944), 2nd Ed., pp. 132-146 and pp. 165-178.
[51] H. G. Beutler, J. Opt. Soc. Am. **35**, 311 (1945).
[52] S. C. Miller, R. Mercure and W. A. Rense, Astrophys. J. **124**, 580 (1956).
[53] A. E. Douglas and G. Herzberg, J. Opt. Soc. Am. **47**, 625 (1957).
[54] W. A. Rense and T. Violett, J. Opt. Soc. Am. **49**, 139 (1959).
[55] Iu. P. Shchepetkin, Optics and Spectroscopy **6**, 538 (1959).
[56] G. R. Rosendal, Ball Brothers Research Corporation Report, (Boulder, Colorado, April 20, 1959).
[57] T. Namioka, J. Opt. Soc. Am. **49**, 446 (1959).
[58] S. C. Miller, Special Report No. 2, Upper Air Laboratory, University of Colorado (1950).
[59] T. Namioka, to be published in J. Opt. Soc. Am.; Space Division Report 002-60 and 003-60 (Kitt Peak National Observatory, 1960).
[60] For theories on aspherical concave gratings, see the following papers: H. Haber, J. Opt. Soc. Am. **40**, 153 (1950) (toroidal grating); Iu. P. Shchepetkin, Optika i Spektroskopiia (USSR) **4**, 383 and 513 (1958) (aspherical grating with one symmetry plane); H. Greiner and E. Schäffer, Optik **16**, 288 and 350 (1959) (toroidal grating).
[61] F. Hall, J. Opt. Soc. Am. **47**, 662 (1957).
[62] G. Hass and R. Tousey, J. Opt. Soc. Am. **49**, 593 (1959).
[63] P. H. Berning, G. Hass, and R. P. Madden, J. Opt. Soc. Am. **50**, 586 (1960).

INDEX

Abney mounting, 236, 238
Aerodynamic torques on satellites, 210
Aeronomy, terrestrial, 74-84
Alpha Virginis nebula, 119, 127-131
Anti-matter, matter annihilation, as a γ-ray source, 106
Astigmatism in grazing incidence spectrograph, 18, 19
(*See also* Grazing incidence mounting)
Astrostat, 185, 192-197
Atmosphere of earth, absorption by, 1-4, 74-84
penetration by solar radiation, 1-3
Atmospheres, planetary, effects of solar ultraviolet on, 88-90
Attitude control, needs for, 205
Aurorae and the solar wind, 166

Background counting rate, suppression of, 63-67
Ball Brothers Research Corporation satellite, 199, 200
Bendix photomultiplier, 53-59
Bent-ogive rocket configuration, 191, 192
Beutler mounting, 252-253

Calibration, spectral, 21-23, 44, 45, 59-62
Camera, Lyman-α solar disc, NRL, 4
University of Colorado, 20, 21
Cassiopeia A as a γ-ray source, 106
Cerenkov detector, 101, 102
Charge equality, electron and proton, 179
Comets, correlation of appearance with solar activity, 154
general description, 153
tails of, accelerations in, 153
direction of, 155
Corona, electron density of, 135, 136, 140-142, 144
expansion of, 157-165
flux from, 110-112
heat conduction of, 134, 140, 141
hydrodynamic model, 160-165
irregularities in, 133, 134, 147, 148
quiet, 134-137
rotation of, 142-144
static model, 158-160
temperature of, 110, 133, 135-137, 139, 144
turbulence in, 137
Corpuscular radiation from sun, 157, 158
(*See also* Solar wind)
Cosmic rays, high-energy, origin of, 184
solar, 151, 152
Counters, photon, 107-109
Crab Nebula as a γ-ray source, 105
Cygnus A as a γ-ray source, 106

Damping, magnetic, of satellite spin, 219-226
(*See also* Torque, magnetic)
de Sitter universe, 180, 181
De-spin, satellite (*see* Damping; Torque)

Eagle mounting, in-plane, 242-245
off-plane, 246-247

Ebert-Fastie mounting, 262-263
Emission lines, solar (*see* Spectrum)
  widths of, 13-15, 24-26
Epsilon Persei, ultraviolet flux from, 132
Expansion of the universe, 179-180
Eyes, photoelectric, for tracking, 188-191

F layer, source of ionization of, 32
Filters for ultraviolet, 107-109
Flares, solar, X-ray and Lyman-α emission from, 114-117
Fraunhofer spectrum in the solar ultraviolet, NRL, 1, 7
  University of Colorado, 30-32

Galaxy, as a γ-ray source, 103-105
  γ-ray sources, possible, 103-106
  γ-ray telescope, 101-103
Geocorona, 118, 119
Geomagnetic field, 165-167
Geomagnetic storms, 151
Grating, concave, ellipsoidal, 233-234
  spherical, 229-233, 230-234
Gravitational torques on satellites, 209, 217, 218
Grazing-incidence mounting, 247-251
Guide telescopes for satellites, 196, 197
Gyroscopic torques on satellites, 213, 214

Hydrogen, molecular, radiation from, 119, 120, 131

Interplanetary magnetic fields, 150-155, 167-169
Interplanetary medium, nature of, 91-95
Interplanetary plasma, 96-98, 150, 153, 155, 156
Ionization of F layer, source of, 32
Ionization chambers, 107-109, 122-125

Johnson-Onaka mounting, 260-262

Kitt Peak National Observatory orbiting telescope, 199, 202

Libration, effects on satellite, 211-213, 219
Limb darkening (and brightening) of sun, 26
Line profiles of solar Lyman-α, 13-15, 25, 26
Line widths, solar emission lines in the ultraviolet, 13-15, 24-26
Lunar atmosphere, 90-91
Lunar coloration, 173-175
Lunar dust, 177
Lunar-dust transport, 175, 176
Lunar erosion, 173
Lunar history, 172, 173
Lunar pointing control, 197
Lunik III, 197, 198
Lyman-α, night-sky radiation, 115-119
  solar, image in light of, 11, 12, 26
    (*See also* Camera)
    intensity of, 11, 114-117
    line profile of, 13-15, 25, 26

Magellanic cloud as a γ-ray source, 105
Magnetic damping of satellite spin, 219-226

Magnetic fields, interplanetary, 150-155, 167-169
Magnetic torques on satellites, 211-213, 219
Matter, anti-matter annihilation, 106
Micrometeorite impact torques on satellites, 210, 211
as a γ-ray source, 106
Monochromator, Hinteregger-AFRD, 48-52, 58
Monochromator measurements, schematic, 40-43
Monochromator mountings, Abney, 236, 238
Beutler, 252-253
Eagle, in-plane, 242-245
off-plane, 246-247
Ebert-Fastie, 262-263
Grazing-incidence, 247-251
Johnson-Onaka, 260-262
Paschen-Runge, 241-242
Radius, 252-253
Rowland, 232, 234-237
Seya-Namioka, 253-260
Wadsworth, 231, 239-241
Moon (*see* entries under Lunar)

Nebular observations, ultraviolet, 119, 120, 126-131
Nebular photometers, ultraviolet, 121-125
Night-sky Lyman-α radiation, 115-119

Observatories, orbiting, attitude control of, 205
Ball Brothers, 199, 200
NASA, 199
Orion nebulosity, ultraviolet radiation from, 119, 126-130

Paschen-Runge mounting, 241-242
Photoelectric effect, 53-55
Photographic detection, disadvantages of, 38
Photometers, stellar and nebular ultraviolet, 121-125
Photomultiplier, windowless, 53-59
Photon counters, 107-109
and ionization chambers, 122-125
Plasma, interplanetary, 96-98, 150, 153, 155, 156
Plasma probe, 98-100
Pointing control, lunar, 197
solar, 187-192
stellar, 196, 197
Predisperser, NRL solar spectrograph, 5
Probe, plasma, 98-100

Radiation-pressure torques on satellites, 209, 210, 218, 219
Radio bursts from sun, 152
Radius mounting, 252-253
Reaction jets, torques from, 208
Reaction torques on satellites, 207-209
Reaction wheels, torques from, 208, 209
Rowland mounting, 232, 234-237

Sail to produce radiation-pressure torque, 219
Satellites, attitude control of, 205
Ball Brothers, 199, 200
Orbiting Astronomical Observatory, NASA, 199
Seya-Namioka mounting, 253-260
Solar cosmic rays, 151, 152
Solar flares, X-ray and Lyman-α, emission from, 114-117
Solar limb darkening (and brightening), 26
Solar monochromator (*see* entries under Monochromator)
Solar pointing control, 187-192
Solar radio bursts, 152
Solar spectrograph (*see* Spectrograph)
Solar spectrum (*see* Spectrum)

Solar wind, 97, 166
density of, 155
flux in, 154, 155
terrestrial effects of, 165-167
velocity of, 155
Spectrograph, solar, NRL, 4, 5
University of Colorado, 18-21
Spectrometer (*see* Monochromator; Spectrum)
Spectrum, solar emission lines, AFRD scans of, 68, 69, 78, 82
NRL observations of, 8-10
solar X-ray, 111, 112
University of Colorado observations of, 23, 24, 27-30
Spica nebula, 119, 127-131
Steady-state universe, 180-182
Stellar observations, ultraviolet, 132
Stellar photometers, ultraviolet, 121-125
Stellar pointing control, 196, 197
Stellar wind, 165
Sun, as a γ-ray source, 105, 106
X-ray photograph of, 112-114

Telemetry, rocket monochromator, 51, 52
Telescope, γ-ray, 101-103
guide, for satellites, 196, 197
Terrestrial effects of solar wind, 165-167
Torque on orbiting structures, aerodynamic, 210
gravitational, 209, 217, 218
Torque on orbiting structures, gyroscopic, 213, 214
magnetic, 211-213, 219
(*See also* Damping)
micrometeorite impact, 210, 211
radiation-pressure, 209, 210, 218, 219
reaction, 207-209

Ultraviolet sources, nighttime, 119, 126-132
Universe, de Sitter, 180, 181
expansion of, 179-180
steady-state, 180-182

Wadsworth mounting, 231, 239-241
Wind, solar (*see* Solar wind)
stellar, 165
Windowless photomultipliers, 53-59
Windows for the ultraviolet, 107-109

X-rays, coronal, 109-114
flare radiation in, 114-117
solar image in, 112-114
solar spectroscopy, 111, 112

Yo-yo, satellite de-spin device, 214-217

Zodiacal light, 145-147, 149, 150